Copper complexes as biomimetic models of catechol oxidase: mechanistic studies

Koval, I.A.

Copper complexes

as biomimetic models of catechol oxidase:

mechanistic studies

PROEFSCHRIFT

ter verkrijging van
de graad van Doctor aan de Universiteit Leiden
op gezag van de Rector Magnificus Dr. D. D. Breimer,
hoogleraar in de faculteit der Wiskunde en
Natuurwetenschappen en die der Geneeskunde,
volgens besluit van het College voor Promoties
te verdedigen op donderdag 2 februari 2006
klokke 16:15 uur

door

Iryna A. Koval

Geboren te Kyiv, Oekraïne in 1979

Samenstelling promotiecomissie

Promotor:	Prof. Dr. J. Reedijk
Co-promotor:	Dr. P. Gamez
Referent:	Dr. C. Belle (Université J. Fourier, Grenoble, Frankrijk)
Overige Leden:	Prof. Dr. J. Brouwer
	Prof. Dr. B. Krebs (Westfälische Wilhelms-Universität Münster, Duitsland)
	Dr. E. Bouwman

The cover of this thesis depicts a painting of Vincent van Gogh "Almond blossom". It was chosen to acknowledge Van Gogh Program, a joined collaborative grant of French Ministry of Research and Foreign Affairs (EGIDE) and NWO which allowed visits and exchange between Leiden University and Université J. Fourier (Grenoble, France) within the framework of research reported in this thesis. This research was further supported by the NRSC Catalysis (a Research School Combination of HRSMC and NIOK).

"A scientist in his laboratory is not a mere technician: he is also a child confronting natural phenomena that impress him as though they were fairy tales."

Marie Sklodowska Curie

"I think, therefore I am"

René Descartes

Table of Contents

1 Introduction[†]

1.1 Copper-containing metalloproteins

Proteins containing copper ions at their active site are usually involved as redox catalysts in a range of biological processes, such as electron transfer or oxidation of various organic substrates. In general, four major functions of such proteins can be distinguished: (i) metal ion uptake, storage and transport; (ii) electron transfer; (iii) dioxygen uptake, storage and transport; (iv) catalysis. Initially, all copper proteins were classified based on their spectroscopic features, which led to the distinguishing of the type-1, type-2 and type-3 active sites. However, recent development of crystallographic and spectroscopic techniques enabled the discovery of other types of copper-containing active sites, and a current classification distinguishes seven different types of active site in the oxidized state of copper-containing proteins; they are briefly outlined below.

Type-1 active site

The copper proteins with the type-1 active site are commonly known as "blue copper proteins" due to their intense blue color. The latter is caused by a strong absorption at *ca.* 600 nm, corresponding to an LMCT transition from a cysteine sulfur to copper(II) ions.[1] These proteins are usually participating in electron transfer processes, and the most well-known representatives of this class include plastocyanin, azurin and amicyanin.[2] The type-1 active site is also found in some multicopper oxidases, which contain more than one copper sites, such as ascorbate oxidase, and in redox enzymes such as nitrite reductase. The coordination sphere around the copper center in the type-1 active site is constituted by two nitrogen donor atoms from two histidine residues, a sulfur atom from a cysteine residue and a weakly coordinated sulfur atom from, in most cases, a methionine residue (Figure 1.1, a). Instead of methionine, a glutamine or a leucine are known to be present in some cases.

[†] This chapter is based on: Koval, I.A., Gamez, P., Belle, C., Selmeczi, K., Reedijk, J., submitted to Chem. Soc. Rev.

Type-2 active site

The copper proteins containing the type-2 active site are also known as "normal" copper proteins, a name historically based on their EPR features which are similar to common Cu^{II} complexes containing an N,O chromophore with tetragonal geometry. The copper coordination sphere in these proteins is constituted by four N and/or O donor atoms in either square-planar or distorted tetrahedral geometry.[3,4] The examples of the proteins with this active site include copper-zinc superoxide dismutase, dopamine-β-hydroxylase, phenylalanine hydroxylase and galactose oxidase (Figure 1.1, b).[5] The proteins of this class are mostly involved in catalysis, such as disproportionation of $O_2^{\bullet-}$ superoxide anion, selective hydroxylation of aromatic substrates, C-H activation of benzylic substrates and primary alcohols oxidation.

Type-3 active site

This class is represented by three proteins, namely hemocyanin, tyrosinase and catechol oxidase. The active site contains a dicopper core, in which both copper ions are surrounded by three nitrogen donor atoms from histidine residues.[3,6] A characteristic feature of the proteins with this active site is their ability to reversibly bind dioxygen at ambient conditions. Hemocyanin (Figure 1.1, c) is responsible for dioxygen transport in certain mollusks and arthropods, whereas tyrosinase and catechol oxidase utilize dioxygen to perform an oxidation of phenolic substrates to catechols (tyrosinase) and subsequently to *o*-quinones (tyrosinase and catechol oxidase), which later on undergo polymerization with the production of the pigment melanin. The copper(II) ions in the *oxy* state of these proteins are strongly antiferromagnetically coupled, leading to EPR-silent behavior. The crystal structures of hemocyanin[7] and catechol oxidase[8] have been solved, whereas the exact structure of tyrosinase still remains unknown.

Type-4 active site

The copper site in these proteins is usually composed of a type-2 and a type-3 active sites, together forming a trinuclear cluster. In some cases, these proteins also contain at least one type-1 site and are in this case addressed as multicopper oxidases, or blue oxidases.[3] The trinuclear cluster and the type-1 site are connected through a Cys-His electron transfer pathway. The representatives of this class are laccase (polyphenol oxidase),[9-11] ascorbate oxidase (Figure 1.1, d)[12] and ceruloplasmin,[13] which catalyze a range of organic oxidation reactions.

Very recently, Lieberman and Rosenzweig[14] reported a 2.8 Å resolution crystal structure of methane monooxygenase, the enzyme encountered in metamophores, which are bacteria catalyzing the methane conversion to methanol. In the crystal structure, three copper centers have been found: a mononuclear center resembling a type-2 active site, and an unusual site, refined as dinuclear, in which two copper ions are located at a very short distance of 2.6 Å (Figure 1.1, e). In contrast to other multicopper oxidases, the dinuclear site is situated 21 Å apart from the mononuclear site. The oxidation states of the three copper ions are not clear, but the mononuclear copper center is believed to

give rise to an EPR signal, typical for the type-2 active sites. However, the presence of some Cu^{I} in the crystal structure was confirmed by X-ray absorption near edge spectra (XANES), which would suggest that at least one or both copper ions in the dinuclear site have +1 oxidation state.

The Cu_A active site

This type of active site is also known as a mixed-valence copper site. It contains a dinuclear copper core, in which both copper ions have a formal oxidation state +1.5 in the oxidized form. Both copper ions have a tetrahedral geometry and are bridged by two thiolate groups of two cysteinyl residues. Each copper ion is also coordinated by a nitrogen atom from a histidine residue. This site exhibits a characteristic seven-line pattern in the EPR spectra and is purple colored. Its function is a long-range electron transfer, and this site can be found, for example, in cytochrome *c* oxidase[15-17] and nitrous oxide reductase (Figure 1.1, f).

The Cu_B active site

This active site was detected close to an iron center in cytochrome *c* oxidase (Figure 1.1, g).[18] In this site, a mononuclear Cu ion is coordinated by three nitrogen atoms from three histidine residues in a trigonal pyramidal geometry. No fourth ligand coordinated to the metal ion was detected. The vacant position in the copper coordination sphere is directed towards the vacant position in the coordination sphere of the heme iron ion. Two metal ions are strongly antiferromagnetically coupled in the oxidized state. A copper-iron distance of 5.3 Å for *Paracoccus denitrificans* and 4.5 Å for bovine heart cytochrome *c* oxidase was found. The function of the Cu_B site is the four-electron reduction of dioxygen to water.

The Cu_Z active site

The Cu_Z active site consists of four copper ions, arranged in a distorted tetrahedron and coordinated by seven histidine residues and one hydroxide anion. This site was detected in nitrous oxide reductase (Figure 1.1, h) and is involved in the reduction of N_2O to N_2. The crystal structures of nitrous oxidase from *Pseudomonas nautica* and *Paracoccus denitrificans* were solved at resolutions of 2.4 Å and 1.6 Å, respectively.[19,20] The copper ions in the tetranuclear cluster are bridged by an inorganic sulfur ion,[21] which until recently was believed to be a hydroxide anion. The metal-metal distances between the Cu2 and Cu4 and Cu2 and Cu3 atoms are very short (*ca.* 2.5-2.6 Å) and can be thus regarded as metal-metal bonds, whereas the distances between the other copper centers are substantially longer (*viz.* 3.0-3.4 Å).[19] Three copper ions are coordinated by two histidine residues, whereas the fourth is coordinated by only one, forming thus a substrate binding site. The oxidation states of the copper ions in the resting state are still unclear, as the EPR spectra of this active site can be explained by two different oxidation schemes, *i.e.* $Cu^{I}_3Cu^{II}$ and $Cu^{I}Cu^{II}_3$, both resulting in four-line spectra.

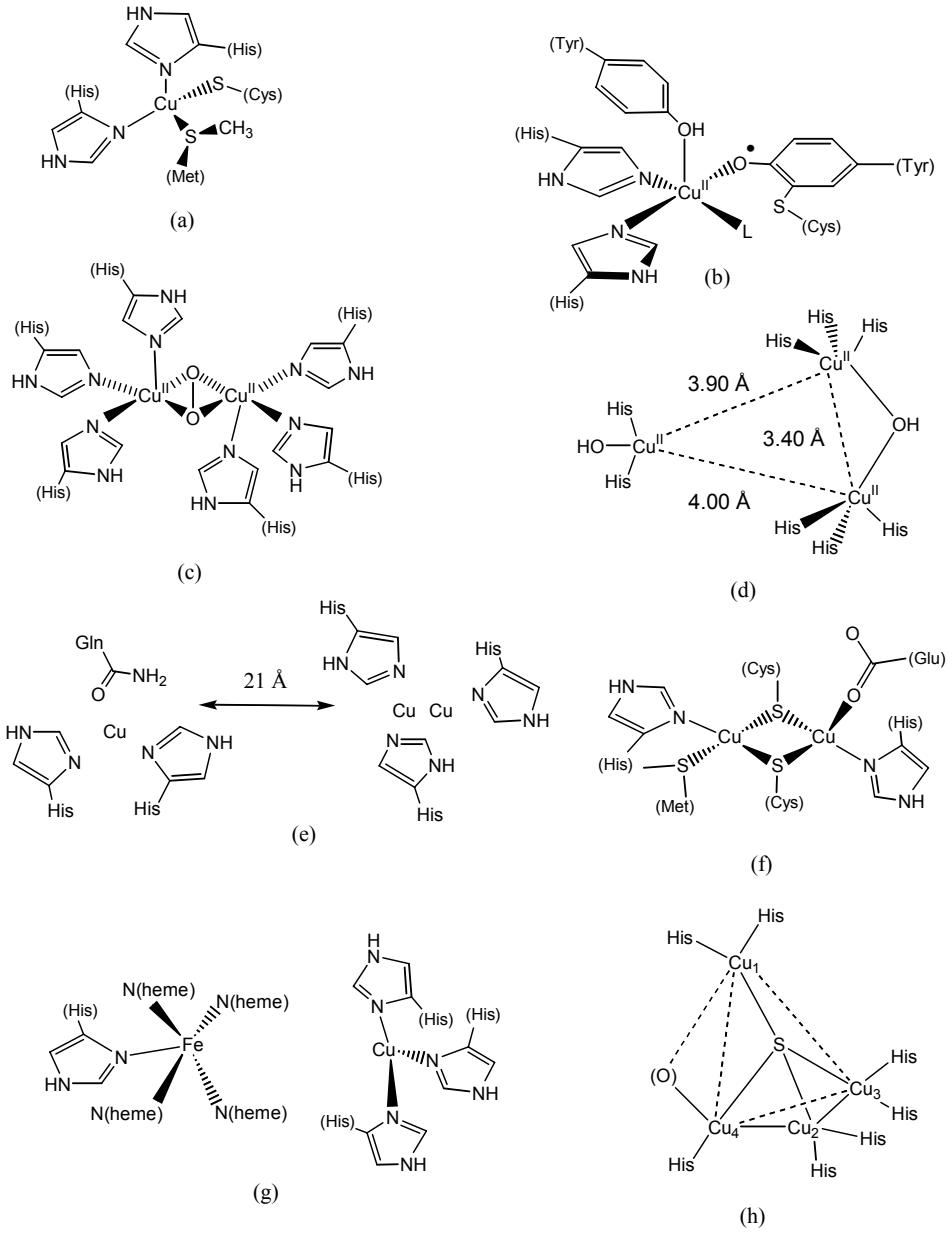

Figure 1.1. Schematic representations of the selected active sites of the copper proteins: plastocyanin[22] (type-1, a), galactose oxidase[23] (type-2, b), *oxy* hemocyanin[7] (type-3, c), ascorbate oxidase[12] (type-4, or multicopper site, d), methane monooxygenase[14] (multicopper site, e), nitrous oxide reductase[24] (Cu_A site, f), cytochrome c oxidase[18] (Cu_B site, g) and nitrous oxide reductase (Cu_Z site, h).[19]

1.2 Catechol oxidase: structure and function

1.2.1 General

Catechol oxidase (COx) is an enzyme containing the type-3 active site that catalyzes the oxidation of a wide range of *o*-diphenols (catechols), such as caffeic acid, to the corresponding quinones in a process known as a catecholase activity. The latter highly reactive compounds undergo an auto-polymerization leading to the formation of a brown polyphenolic pigment, *i.e.* melanin, a process thought to protect a damaged tissue against pathogens or insects.[25] COx's are found in plant tissues and in

crustaceans. The first COx was isolated in 1937.[26] Subsequently, they were purified from a wide range of vegetables and fruits (*e.g.* potato, spinach, apple, grape berry),[26] and more recently, from gypsy wort[27] and litchi fruit.[28] The purity of COx's was not always satisfactory due to a multiplicity of isozymes and forms, but improved purification protocols have been reported,[26] *e.g.* for COx from black poplar.[27]

The molecular weight of COx's varies, depending on the tissue and organism from which it has been extracted. Two ranges of molecular mass can sometimes be found, even in a single source: one in the range of 38-45 kDa, and another in the range of 55-60 kDa. This difference is possibly due to C-terminal processing.[29] Smaller enzymes with a molecular weight of about 30 kDa are also found, but they are generally described as proteolyzed derivatives of the purified mature protein.

In 1998, Krebs and co-authors have reported the crystal structures of the catechol oxidase isolated from *Ipomoea batatas* (sweet potato) in three catalytic states: the native *met* ($Cu^{II}Cu^{II}$) state, the reduced *deoxy* ($Cu^{I}Cu^{I}$) form, and in the complex with the inhibitor phenylthiourea.[8] An isolated monomeric enzyme with a molecular weight of 39 kDa was found to be ellipsoid in shape with dimensions of 55×45×45 $Å^3$. The secondary structure of the enzyme is primarily α-helical with the core of the enzyme formed by a four-helix bundle composed of α-helices α2, α3, α6 and α7. The helical bundle accommodates the catalytic dinuclear copper center and is surrounded by the helices α1 and α4 and several short β-strands. Each of the two copper ions is coordinated by three histidine residues contributed from the four helices of the α-bundle.

1.2.2 The structures of the active site

1.2.2.1 The *met* ($Cu^{II}Cu^{II}$) state

In the native *met* state, two copper ions are 2.9 Å apart. In addition to six histidine residues, a bridging solvent molecule, most likely hydroxide anion was refined in a close proximity to the two metal centers (CuA-O 1.9 Å, CuB-O 1.8 Å), completing the coordination sphere of the copper ions to a trigonal pyramid. These findings are in agreement with EXAFS data for the oxidized COx's from *Lycopus europaeus* and *Ipomoea batatas*, confirming the presence four N/O donor atoms and a $Cu^{II}…Cu^{II}$ distance of 2.9 Å in solution for both enzymes.[30,31] The apical positions are occupied by the His 109 and His 240 residues for CuA and CuB, respectively (Figure 1.2, left). EPR data reveal a strong antiferromagnetic coupling between the copper ions, therefore the presence of a bridging OH^- ligand between the copper(II) ions was proposed for the *met* form of the enzyme.

1.2.2.2 The reduced *deoxy* ($Cu^{I}Cu^{I}$) state

Upon reduction of the copper(II) ions to +1 oxidation state, the distance between them increases to 4.4 Å, while the histidine residues move only slightly, and no

significant change was observed for other residues of the protein.[8] Based on the residual electron density maps, a water molecule was positioned on a distance of 2.2 Å from the CuA atom. Thus, the coordination sphere around CuA ion is a distorted trigonal pyramid, with three nitrogen atoms from the histidine residues forming a basal plane, while the coordination sphere around CuB ion can be best described as square planar with one missing coordination site.

1.2.2.3 The adduct of catechol oxidase with the inhibitor phenylthiourea

Phenylthiourea binds to catechol oxidase by replacing the hydroxo bridge, present in the *met* form. The sulfur atom of phenylthiourea is coordinated to both copper(II) centers, increasing the distance between them to 4.2 Å (Figure 1.2, right). The amide nitrogen is weakly interacting with the CuB center (Cu-N distance of 2.6 Å), completing its square-pyramidal geometry. The dicopper core in catechol oxidase is found in the center of a hydrophobic pocket lined by the side chains of Ile 241, Phe 261, His 244 and Ala 264.[8] Upon phenylthiourea binding, the phenyl ring of Phe 261 and the imidazole ring of His 244 undergo a conformational change to form hydrophobic interactions with the aromatic ring of the inhibitor. These van der Waals interactions further contribute to the high affinity (IC_{50} = 43 μM, K_M = 2.5 mM for catechol substrate[30]) of this inhibitor to the enzyme.

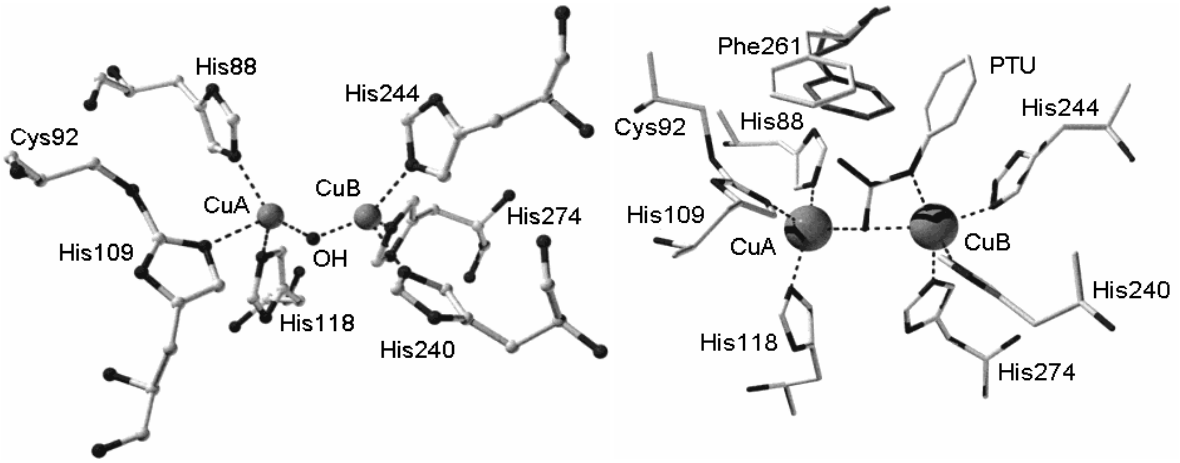

Figure 1.2. Left: coordination sphere of the dinuclear copper(II) center in the *met* state. Right: crystal structure of the inhibitor complex of catechol oxidase with phenylthiourea. Phe 261 is shown additionally in the orientation of native COx (in dark color) to show rotation of Phe 261 in the inhibitor complex (in light color). Redrawn after Krebs and co-workers.[29]

1.2.2.4 The dioxygen binding by the dicopper(I) center: *oxy* state

The *oxy* form of catechol oxidase can be obtained by treating the *met* form of the enzyme with dihydrogen peroxide. Eicken *et al.*[30] reported that the treatment of the 39 kDa catechol oxidase from *Ipomoea batatas* (ibCOx) with H_2O_2 leads to absorption bands at 343 nm (ε = 6500 $M^{-1}cm^{-1}$) and 580 nm (ε = 450 $M^{-1}cm^{-1}$), which reach

maximal development when 6 equivalents of dihydrogen peroxide are added (Figure 1.3). Similar results have been reported for COx's isolated from *Lycopus europaeus and Populus nigra.*[27] This type of UV-Vis spectra is characteristic for a μ-η^2:η^2-peroxo-dicopper(II) core, which was originally reported by Kitajima *et al.*[32] for a synthetic dinuclear copper model complex. The first strong absorption in the range of 335-350 nm is assigned to a peroxo O_2^{2-} (π_σ^*) → Cu^{II} ($d_{x^2-y^2}$) charge transfer, whereas the second weak band around 580 nm corresponds to a peroxo O_2^{2-} (π_v^*) → Cu^{II} ($d_{x^2-y^2}$) CT transition.[4,33]

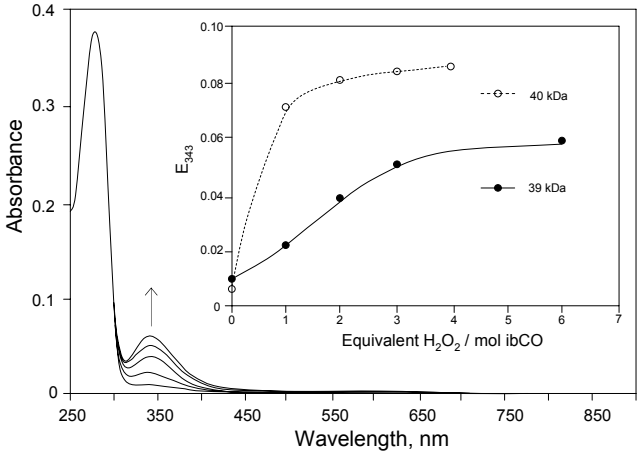

Figure 1.3. Titration of the 39 kDa ibCOx in 0.5 M NaCl, 50 mM sodium phosphate pH = 6.7 with H_2O_2. Insert: absorption at 343 nm without and after addition of one, two, three and six equivalents of H_2O_2. Redrawn after Krebs and co-workers.[30]

1.2.2.5 The covalent cysteine-histidine bond

An interesting feature of the dinuclear copper center in catechol oxidase is the unusual thioether linkage formed between the Cε atom of the histidine His 109, one of the ligands to CuA ion, and the cysteine sulfur atom of Cys 92. It should be noted that a thioether linkage has also been described for the type-2 copper enzyme galactose oxidase. In this structure, a covalent bond formed between the Cε carbon atom of a tyrosinate ligand and the sulfur atom of a cysteine residue was proposed to stabilize the tyrosine radical generated during catalysis.[23] There are also reports of this type of bond for a tyrosinase from *Neurospora crassa*,[34] as well as for several types of hemocyanins.[35-37] The absence of this unit in arthropod hemocyanins and in human tyrosinase does not, however, support its involvement in the electron transfer process. The crystal structure of CO reveals that this covalent bond puts additional structural restraints on the coordination sphere of the CuA ion. In particular, such restrains may help to impose the trigonal-pyramidal geometry (which can be also regarded as a distorted trigonal bipyramid with a vacant apical position) on the CuA ion in +2 oxidation state. This may in turn optimize the redox potential of the metal needed for the oxidation of the catechol substrate and may allow a rapid electron transfer in the

redox processes. Also, this thioether bond may prevent the displacement of His 109 and a didentate binding mode of the substrate to a single Cu^{II} ion.

1.2.3 Enzymatic reaction mechanism

Catechol oxidase catalyzes the oxidation of *o*-diphenols (catechols) to the respective quinones through four-electron reduction of dioxygen to water. Krebs and co-workers proposed a mechanism for the catalytic process, based on biochemical,[3,38] spectroscopic[30] and structural[8] data, as depicted in Figure 1.4. The catalytic cycle begins with the *met* form of catechol oxidase, which is the resting form of the enzyme. Because the *oxy* state of COx could be obtained only after the addition of H_2O_2, this form was excluded as the start situation. The dicopper(II) center of the *met* form reacts with one equivalent of catechol, leading to the formation of quinone and to the reduced *deoxy* dicopper(I) state. This step is supported by the observation that stoichiometric amounts of the quinone product form immediately after the addition of catechol, even in the absence of dioxygen.[8,39] Based on the structure of COx with the bound inhibitor phenylthiourea, the monodentate binding of the substrate to the CuB center has been proposed. Afterwards, dioxygen binds to the dicopper(I) active site replacing the solvent molecule bonded to CuA in the reduced enzyme form. Binding of the catechol substrate to the *deoxy* state prior to dioxygen binding seems less likely, as no substrate binding was observed upon treating the reduced by dithiothreitol enzyme with the high molar excess of catechol, indicating a low binding affinity of the substrate to the dicopper(I) center. UV-Vis spectroscopy and Raman data suggested that dioxygen binds in the bridging side-on μ-η^2:η^2 binding mode with a copper-copper separation of 3.8 Å, as determined by EXAFS spectroscopy.[30] The rotation of the side chain of Phe 261 in the enzyme opens the dicopper center to permit the binding of the catechol substrate. The observed binding mode of phenylthiourea and the modeled catechol-binding mode suggest that a simultaneous binding of catechol and dioxygen is possible. Superposition of the aromatic ring of the modeled catechol substrate and the phenyl ring of phenylthiourea places the coordinated catecholate hydroxylate group close to the coordinated amide nitrogen of the inhibitor and maintains the favorable van der Waals interactions observed in the inhibitor complex.[8] In this model, CuB is six-coordinated with a tetragonal planar coordination by His 240, His 244 and the dioxygen molecule. The CuA site retains the tetragonal pyramidal geometry with dioxygen, His 88 and His 118 in equatorial positions, His 109 in an axial position and a vacant sixth coordination site. In this proposed ternary COx-O_2^{2-}-catechol complex, two electrons can be transferred from the substrate to the peroxide, followed by the cleavage of the O-O bond, loss of water and the formation of the quinone product, together with the restoration of the *met* state, completing the catalytic cycle.

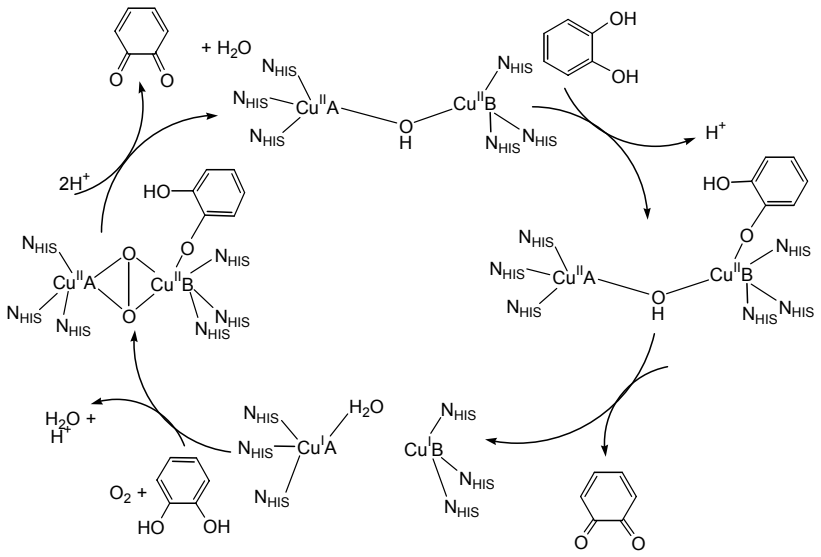

Figure 1.4. Catalytic cycle of catechol oxidase from *Ipomoea batatas*, as proposed on the basis of structural, spectroscopic and biochemical data. Two molecules of catechol (or derivatives thereof) are oxidized, coupled with the reduction of molecular oxygen to water. The ternary $COx\text{-}O_2^{2-}$-catechol complex was modeled, guided by the binding mode observed for the inhibitor phenylthiourea. Redrawn after Krebs and co-workers.[39]

A totally different mechanism of the catalytic cycle, however, was proposed by Siegbahn,[40] who applied a hybrid density functional theory for a quantum chemical study of the catalytic cycle. According to the author, the growing number of theoretical[41] and experimental[42,43] studies suggest that the active site of an enzyme, which is deeply buried in the low dielectric of a protein, as observed in catechol oxidase, should not change its charge during the catalytic cycle. However, in the mechanism, proposed by Krebs *et al.*,[8] the charge of the active site changes from +1 in the peroxo-dicopper(II)-catecholate adduct, to +3 in the met form. According to Siegbahn,[40] this in turn implies the availability of several external nearby bases, which could store protons, released during the cycle. At the same time, the X-ray crystal structure does not reveal the presence of such candidates in the region of the active site. Consequently, a different mechanism[40] was proposed by the author based on the DFT calculations, as depicted in Figure 1.5. The catalytic cycle starts from the deoxy dicopper(I) form. In order to maintain an overall charge + 1 of the active site, the author proposed a presence of a bridging hydroxide ligand between the two copper(I) ions,[44] in contrast to the X-ray crystallographic findings,[8] which suggest a presence of a water molecule, asymmetrically bonded to only one copper center. At the first stage, catechol binds to the deoxy form, transferring the proton to the bridging hydroxide with a consequent generation of the bridging water molecule between the metal centers. Afterwards, dioxygen displaces a water molecule, binding as a superoxide radical anion and resulting in the formation of the mixed-valence dicopper(II,I) species (step a). The superoxide then abstracts a hydrogen atom (a proton and an electron) from the bound

substrate. To release the quinone molecule, an electron is then transferred from the quinone radical to the Cu^{II} ion, leading to the restoration of the dicopper(I) state (steps b and c). The next step involves the cleavage of the O-O bond, which is accompanied by a transfer of two protons from the substrate and two electrons (from one of the Cu^{I} ions and the substrate) to the peroxide moiety (steps d, e). Altogether this leads to a product which can be best described as a $Cu^{II}Cu^{I}$ species with a quinone radical anion. The second electron transfer from the quinone radical to the Cu^{II} center leads to the restoration of the initial hydroxo-bridged dicopper(I) form.

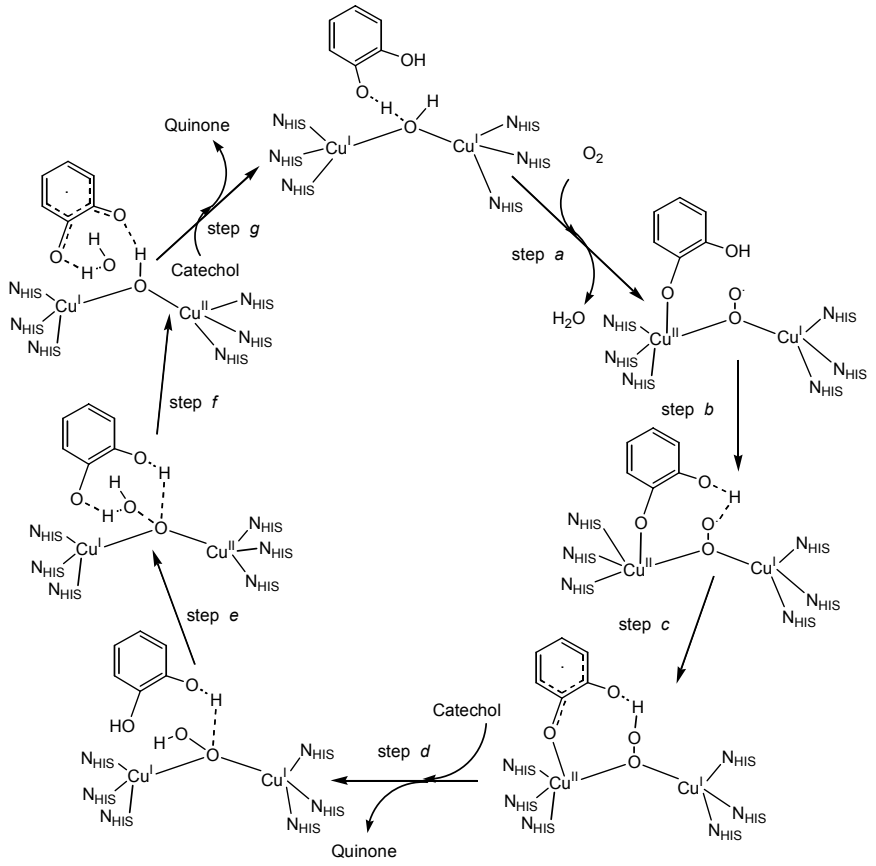

Figure 1.5. The mechanism of the catalytic cycle of catechol oxidase, as proposed by Siegbahn.[40]

However, it should be noted that at the present moment the latter mechanism is not supported by the experimental findings. In particular, an existence of a bridging μ-1,1-superoxide radical anion, the formation of which is proposed by the author, has never been reported in the literature.

1.3 Model systems of catechol oxidase

1.3.1 Historic overview

The ability of the copper complex to oxidize phenols and catechols has been well known for at least 40 years. For example, in 1964 Grinstead reported the oxidation of 3,5-di-*tert*-butylcatechol ($DTBCH_2$) to the respective 3,5-di-*tert*-butyl-*o*-

benzoquinone (DTBQ) with 55% yield in 75% aqueous methanol in the presence of 1% of copper(II) chloride.[45] In 1974, Thuji and Takayanagi reported the oxidative cleavage of catechol, leading to the formation of *cis,cis*-muconic acid, by dioxygen and copper(I) chloride in aqueous solution.[46] Rogić and Demmin have also studied the oxidation of catechol by copper(I) chloride and dioxygen in various solvent mixtures.[47] The reactions were usually carried out in pyridine in the presence of 5 molar equivalents of an alcohol (MeOH, EtOH, *i*-PrOH or *n*-BuOH). Depending on the reaction conditions, either muconic acid or its monoalkyl esters were obtained as products. However, in the presence of dichlorobis(pyridine)copper(II) in pyridine-methanol mixture under dioxygen, 4,5-dimethoxy-1,2-benzoquinone was isolated as the reaction product.

One of the pioneering mechanistic studies on catechol oxidation by copper(II) complexes was presented by Lintvedt and Thuruya.[48] In their study of the kinetics of the reaction of $DTBCH_2$ with dioxygen catalyzed by bis(1-phenyl-1,3,5-hexanetrionato)dicopper(II) complex, the authors showed that the overall reaction was first order in the substrate and second order in Cu^{II}, thus in fact confirming that the active reaction intermediate involved in the rate-determining step was a dicopper-catecholate species. Another interesting early mechanistic studies is the work of Demmin, Swerdloff and Rogić,[49] who emphasized the main steps in the catalytic process: (i) formation of dicopper(II)-catecholate intermediate; (ii) electron transfer from the aromatic ring to two copper(II) centers, resulting in the formation of *o*-benzoquinone and two copper(I) centers; (iii) irreversible reaction of the generated copper(I) species with dioxygen, resulting in copper(II)-dioxygen adduct, and (iv) the reaction of this adduct with catechol, leading to regeneration of the dicopper(II)-catecholate intermediate and formation of water as the byproduct.

Oishi *et al.* have reported the higher activity of dinuclear copper(II) complexes in the oxidation of $DTBCH_2$ in comparison to their mononuclear analogues,[50] thus confirming the earlier hypothesis of Lintvedt and Thuruya about the formation of the dicopper-catecholate intermediate in the catalytic process.[48] Furthermore, the authors reported a stoichiometric oxidation of $DTBCH_2$ in anaerobic conditions to the respective quinone by a number of mononuclear and dinuclear copper(II) complexes, which was consistent with the 1st step of the mechanism proposed by Demmin, Swerdloff and Rogić.[49] They also made an interesting observation that mononuclear planar copper(II) complexes could not be reduced by $DTBCH_2$ and showed very little catecholase activity in comparison to the readily reducible complexes. Thus, the catalytic activity of the complexes appeared to correlate with their reduction potentials. Another interesting conclusion made by these authors was, that the catecholase activity of the dinuclear copper(II) complexes seemed to depend on the metal-metal distance; thus, the complexes for which the copper-copper separation was estimated to be more than 5 Å, showed very little catalytic activity. Therefore, the authors suggested the hypothesis of the catecholase activity being regulated by a steric match between the

dicopper(II) center and the substrate. The higher activity of dinuclear copper(II) complexes in catechol oxidation in comparison to the mononuclear copper(II) complexes has also been pointed out by some other authors, *e.g.* Malachowski[51] and Casellato *et al.*[52]

In 1985, the hypothesis about the formation of the dicopper-catecholate intermediate at the first stage of the catalytic reaction was further supported by Karlin and co-workers[53], who have succeeded in crystallizing the adduct of tetrachlorocatechol (TCC) with the dicopper(II) complex with a phenol-based dinucleating ligand (Figure 1.6, see Section 1.3.2.2.1 for details). However, almost at the same time Thompson and Calabrese[54] proposed that the catalytic reaction proceeds via the one-electron transfer from catechol to the copper(II) ion, resulting in the formation of a semiquinone intermediate species. The authors have prepared and characterized a bis(3,5-di-*tert*-butyl-*o*-semiquinonato)copper(II) complex by reaction of $[Cu_2(py)_4(OCH_3)_2](ClO_4)_2$ with $DTBCH_2$ in anaerobic conditions. Interestingly, they did not observe the simultaneous two-electron transfer yielding DTBQ and two copper(I) centers. The formation of the semiquinone species in the catalytic cycle was later reported by other authors.[55-57]

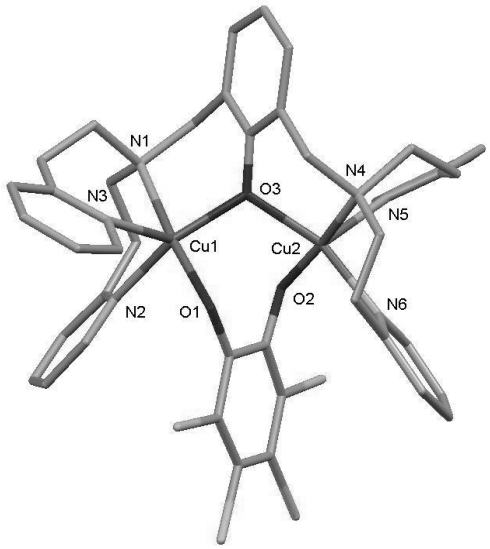

Figure 1.6. Crystal structure of the complex cation of $[Cu_2(L\text{-}O^-)(TCC)]^+$. LOH: 2,6-bis(*N,N*-bis(2-methylpyridyl)aminomethyl)phenol. The Cu…Cu distance is 3.248(2) Å. Redrawn after Karlin and co-workers.[53]

The determination of the structure of hemocyanin, another protein with the type-3 active site, in 1989,[7] and extensive studies on the enzyme tyrosinase, responsible for the conversion of L-tyrosine to L-DOPA, leading to melanin production, prompted the extensive studies on the synthetic models of the type-3 active site and their reactivity. In the early 1990s, a few research groups reported the formation of dihydrogen peroxide instead of water as a dioxygen reduction product in the catalytic oxidation of $DTBCH_2$ by the copper(II) complexes.[58,59] In order to explain their experimental results, Chyn and

Urbach proposed two different mechanisms for the catalytic cycle, as depicted in Scheme 1.1:[58]

(1)

$Cu^{II}...Cu^{II} + DTBCH_2 \longrightarrow Cu^{I}...Cu^{I} + DTBQ + 2H^+$ (fast)

$Cu^{I}...Cu^{I} + O_2 \longrightarrow Cu^{II}(O_2)^{2-}Cu^{II}$ (slow)

$Cu^{II}(O_2)^{2-}Cu^{II} + 2H^+ \longrightarrow Cu^{II}...Cu^{II} + H_2O_2$ (fast)

(2)

Initial step:

$Cu^{II}...Cu^{II} + DTBCH_2 \longrightarrow Cu^{I}...Cu^{I} + DTBQ + 2H^+$

Redox cycle

$Cu^{I}...Cu^{I} + O_2 \underset{k_2}{\overset{k_1}{\rightleftharpoons}} Cu^{II}(O_2)^{2-}Cu^{II}$

$Cu^{II}(O_2)^{2-}Cu^{II} + 2H^+ \longrightarrow Cu^{II}...Cu^{II} + H_2O_2$

Scheme 1.1. Two possible mechanistic pathways resulting in the formation of H_2O_2 as a by-product, as proposed by Chyn and Urbach [58]

Rockcliffe and Martell have published numerous studies on catechol oxidation by dicopper(II) and peroxo-dicopper(II) complexes.[60-66] A rather significant attention has been devoted to the structure-activity relationship of the catalytically active compounds. Very detailed mechanistic studies on the catecholase activity of a series of structurally related dicopper(II) complexes have also been published by Casella and co-workers,[67-70] who reported that the catalytic reaction proceeds via a biphasic mechanism, in which a fast stoichiometric reaction between the dicopper(II) center and the catechol substrate is followed by a slower catalytic reaction. They have also grouped together different mechanisms earlier proposed for the catecholase activity of dicopper(II) complexes, as shown in Scheme 1.2.

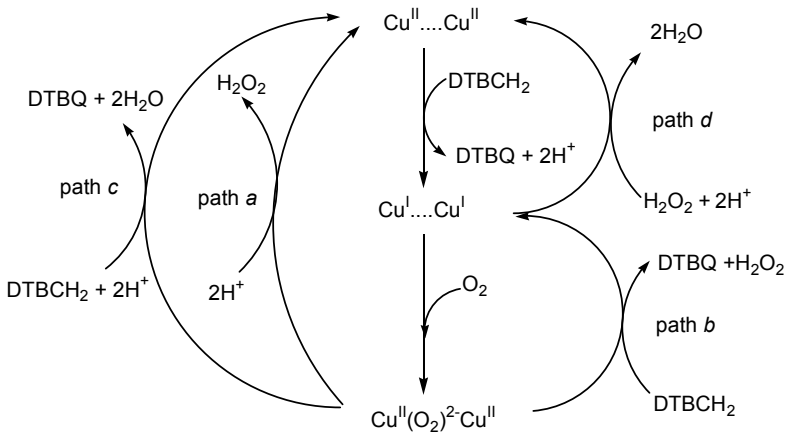

Scheme 1.2. The possible reaction pathways in the catalytic cycle of catechol oxidation by dicopper(II) complexes, as proposed by Casella and co-workers. Redrawn after Casella and co-workers.[68]

However, despite the significant attention received by this topic and the large number of publications on the catalytically active copper(II) complexes, detailed mechanistic studies are unfortunately quite scarce.[58,59,67,68,71-73] As a consequence, the catalytic pathways proposed by different authors are often largely speculative in nature and sometimes controversial. Furthermore, it appears that very different methods to explore the catecholase activity and to study the reaction mechanism were applied by different research groups, which makes the corresponding results difficult to compare. An overview of the different approaches to study the reaction mechanism in respect to earlier reported works will be presented below.

1.3.2 Mechanistic studies: different approaches

1.3.2.1 General

The approaches used by different research groups to study the mechanism of catecholase activity of the copper(II) complexes can be roughly divided into four major groups. The first one is dealing with the substrate binding to the metal centers. This group includes a crystallographic and/or spectroscopic characterization of the adducts of the catechol(ate) or structurally related compounds with the copper complexes and studies on the interaction of the complexes with catechol in anaerobic conditions. The interest in this subject is enhanced by the currently disputed way of the substrate binding to the active site of catechol oxidase. The original assumption of the didentate bridging binding mode of the substrate[3] has been called into question by crystallographic findings for the native enzyme; these suggested an alternative mechanism with monodentate binding of the catechol to only one of the copper ions.[8,39]

The second group includes structure-activity relationship studies. These include the correlation of the catecholase activity of the complexes with the metal-metal distance in the dicopper(II) core, their redox potentials, ligand properties (electronic properties, basicity, sterical demands) and the nature of the bridging ligands between the two metal centers. For the sake of simplicity, pH-dependent studies were also included in this group, as the pH-influenced changes in the catalytic activity of the complexes are usually caused by the structural changes at the dicopper center. The third approach includes the kinetic studies on the catalytic reaction, *e.g.* the influence of the various factors (*e.g.* substrate, catalyst and dioxygen concentration, addition of dihydrogen peroxide *etc.*) on the reaction rates; and the proposals on the reaction mechanism based on these data.

Finally, the fourth group includes the examples of stoichiometric oxidation of catechol substrates by peroxo- or oxo-dicopper complexes, which are almost always proposed as intermediate species in the catalytic oxidation of catechol by copper(II) compounds.[8,64,65,67,68]

1.3.2.2 Substrate-binding studies

1.3.2.2.1 Structural characterization of dicopper-catecholate adducts

The various possible binding modes of catechol to the copper centers are summarized in Figure 1.7.

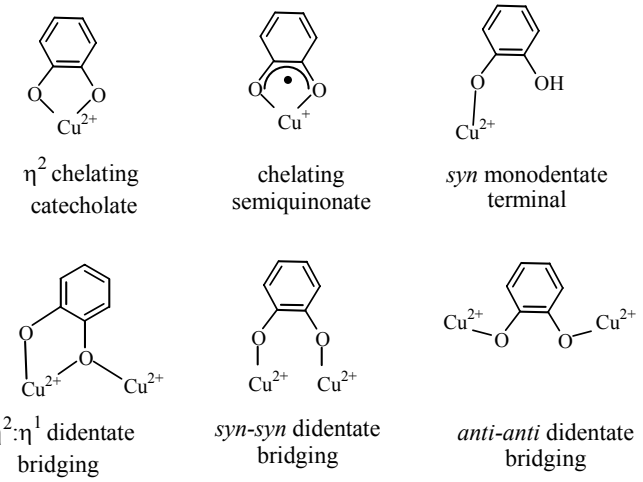

Figure 1.7. Different binding modes of the (deprotonated) catechol substrate to the copper centers.

The first crystallographically characterized adduct of a dicopper(II) complex with tetrachlorocatecholate was reported by Karlin and co-workers.[53] The compound was prepared by reacting tetrachloro-1,2-benzoquinone with the dicopper(I) precursor complex in dichloromethane. The catecholate anion binds as a bridging ligand in a *syn-syn* fashion to both copper(II) ions, resulting in a metal-metal separation of 3.248(2) Å. Both copper(II) ions adopt a square-pyramidal geometry, with the oxygen atoms of the catecholate anion occupying the basal plane, as depicted in Figure 1.6.

Other structurally characterized examples of catechol adducts with dinuclear copper(II) complexes were reported significantly later. Thus, Comba and co-authors[74] have reported the crystal structures of four different copper-tetrachlorocatecholate adducts, with three different modes of substrate coordination to the metal centers (Figure 1.8): as a monodentate, monoprotonated ligand (**1**), as a didentate fully deprotonated chelating ligand (**2** and **4**), and as a bridging deprotonated ligand between the two copper(II) centers (**3**, *anti-anti* binding mode). Interestingly, the authors reported that the highest catecholase activity was observed for the complexes which bound catecholate in a didentate bridging fashion, whereas mononuclear copper(II) complexes were found to be completely inactive.

Meyer and co-workers[75] have reported the structures of three dinuclear Cu^{II} complexes, in which the deprotonated tetrachlorocatecholate is bound to only one of the two copper(II) ions in a didentate chelating fashion (Figure 1.9). It is further linked via one or two hydrogen bridges to water molecules bound to the adjacent metal center. Interestingly, the copper-copper separation in the precursor dicopper(II) complexes

(Figure 1.10, complexes **3**$(ClO_4)_2$ and **4**$(ClO_4)_2$) exceeds 4 Å, which probably precludes the binding of the catecholate to both copper(II) ions.

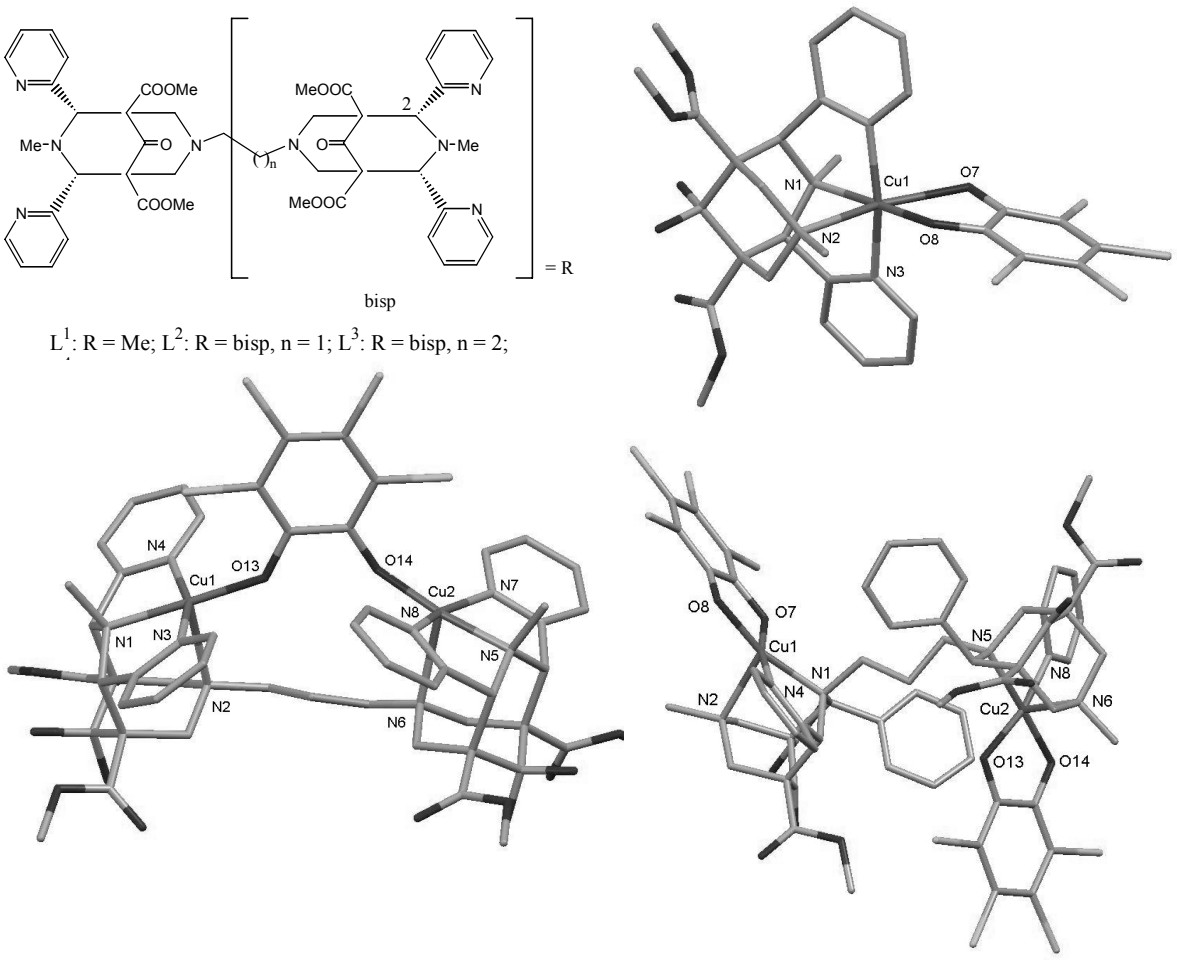

L^1: R = Me; L^2: R = bisp, n = 1; L^3: R = bisp, n = 2;

Figure 1.8. The structures of the bispidine ligands (left) and the X-ray crystal structure projections of $[Cu_2(L^1)(TCC)]$ (**2**, top, right), $[Cu_2(L^3)(TCC)]^{2+}$ (**3**, bottom, left) and $[Cu_2(L^4)(TCC)_2]$ (**4**, bottom, right). Redrawn after Comba and co-workers.[74]

An interesting example of the formation of mononuclear copper(II)-semiquinonate complexes was reported by Tolman and co-workers.[76] The authors reported the oxidation of $DTBCH_2$ and TCC by μ-η^2:η^2 peroxo-dicopper(II) and μ-oxo-dicopper(III) complexes, resulting in the dissociation of the dinuclear core and the formation of mononuclear copper(II)-semiquinonate adducts. Similarly to the earlier reported mononuclear copper-catecholate adducts, the semiquinonate ligand is occupying two places in the coordination sphere or the metal ion, with a ferromagnetic coupling realized between the unpaired electron of the Cu^{II} ion and the organic radical. Thompson and Calabrese[77] have reported the crystal structure of a Cu^{II}-semiquinonate complex, obtained by the interaction of a bis-methanolate-bridged copper(II) dimer with $DTBCH_2$ (see also Section 1.3.1). During this process, the dicopper(II) core undergoes a dissociation into two mononuclear units, with one electron being transferred from the

catecholate substrate to one of the two copper(II) ions, resulting in the formation of the Cu^{II}-semiquinonate and the reduced Cu^{I} mononuclear species.

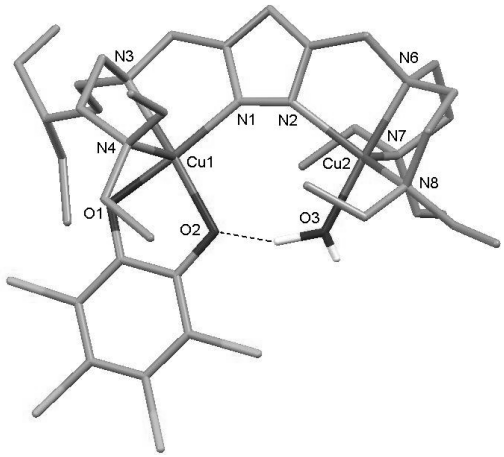

Figure 1.9. X-ray crystal structure of one of the dicopper(II)-catecholate adducts crystallized by Meyer and co-workers. The Cu…Cu distance is 4.4388(8) Å. Redrawn after Meyer and co-workers.[75]

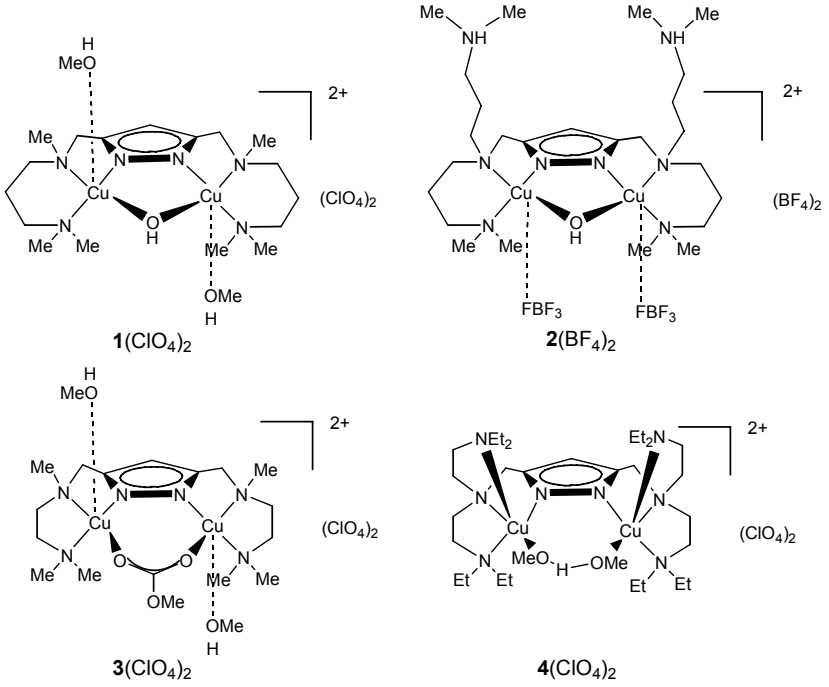

Figure 1.10. Schematic representations of the copper(II) complexes of the various pyrazolate ligands, prepared by Meyer and co-workers[75] (in the case of **1**, the analogous complex **1'**, which bears ethanol instead of methanol ligands, was analyzed crystallographically). The Cu…Cu distance is 3.540(1) Å for **1'**$(ClO_4)_2$, 3.447(2) Å for **2**$(BF_4)_2$, 4.088(1) Å for **3**$(ClO_4)_2$ and 4.553(1) for **4**$(ClO_4)_2$. Redrawn after Meyer and co-workers.[75]

1.3.2.2.2 Substrate binding to the metal centers followed by spectroscopic methods

Attempts to monitor the binding of the catechol substrate to the metal centers by spectroscopic methods, mostly UV-Vis spectroscopy, were undertaken by many authors. Thus, Reim and Krebs[78] titrated solutions of catalytically active and inactive

dicopper(II) complexes with the phenol-based ligands (Figure 1.11) with tetrachlorocatechol and followed the changes spectrophotometrically. Whereas the inactive complexes appeared to be completely indifferent to TCC, the reaction of the active complexes with the substrate was accompanied by the development of new bands in the 400-500 nm range, assigned to the catecholate → Cu^{II} charge transfer, and changes in the positions and extinction coefficients of the Cu^{II} d-d bands. These results indicated the binding of the substrate to the metal centers prior to the catalytic cycle for the active complexes and revealed that the inactive complexes did not interact with the substrate.

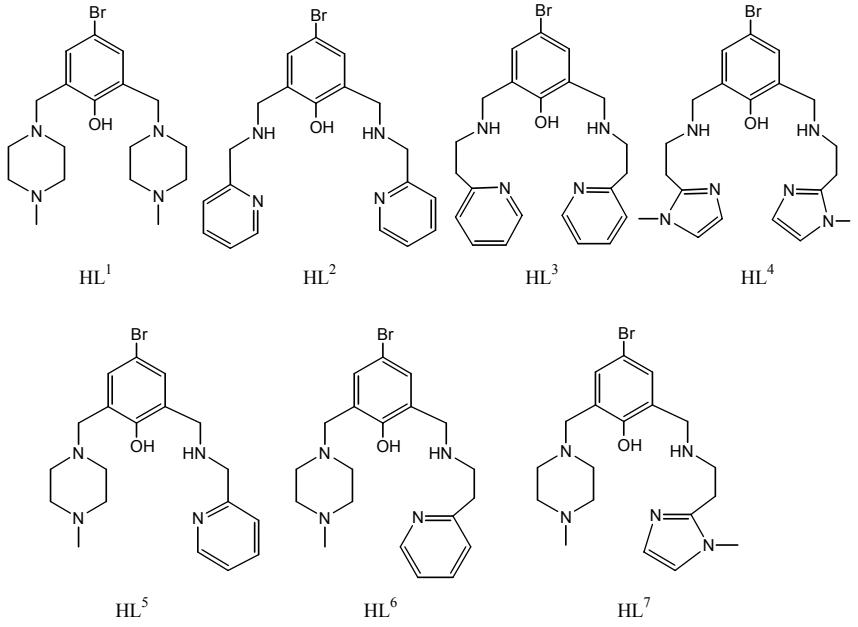

Figure 1.11. Pentadentate dinucleating phenol-based ligands prepared by Reim and Krebs. Only the complexes of the ligands HL^1, HL^5, HL^6 and HL^7 showed catecholase activity. Redrawn from Reim and Krebs.[78]

Jäger and co-authors have also studied the interaction of a series of the copper(II) complexes of aminocarbohydrate *β*-ketoenaminic ligands with TCC.[79] However, in this case both the active and inactive complexes were found to interact with TCC, although the spectra of the active compounds changed to a remarkably higher degree in comparison to the inactive molecules. The observed spectroscopic changes were rather consistent with those reported by Reim and Krebs:[78] the development of a new band at 480 nm along with the decrease of the d-d band of the Cu^{II} ion at 650 nm. Very similar results (a development of a new band in the 400-500 nm range and changes in the position and absorption of the d-d bands of the Cu^{II} ions) during the interaction of TCC with the dicopper(II) complexes of some dinucleating ligands (*e.g.* phenol-based) were also reported by Mukherjee *et al.*[80] Comba and co-workers[74] have reported the titration of the mononuclear and dinuclear complexes $[Cu_2(L^1)(solv)]^{2+}$, $[Cu_2(L^2)(solv)_2]^{4+}$ and $[Cu_2(L^3)(solv)_2]^{4+}$ (see Figure 1.8) with TCC

and showed that in the first case, a strong absorption band appeared at *ca.* 450 nm, whereas for dinuclear complexes, equilibriums between species with absorptions at *ca.* 450 nm and *ca.* 530 nm were established. The authors proposed that catecholate-bridged compounds are formed with $[Cu_2(L^2)(solv)_2]^{4+}$ and $[Cu_2(L^3)(solv)_2]^{4+}$, whereas a mononuclear catecholate complex is formed with $[Cu_2(L^1)(solv)]^{2+}$.

Very detailed studies on the substrate binding to the copper(II) complexes with the phenol-based dinucleating ligands were reported by Belle *et al.*[81] The authors studied the binding of TCC and $DTBCH_2$ (the binding studies of the latter compound were performed in anaerobic conditions) to a catalytically active μ-hydroxo-dicopper(II) complex with the phenol-based ligand HL_{OCH_3} (Scheme 1.3, insert) and its inactive bis-aqua-dicopper(II) analogue. In both cases, a new UV-Vis band at *ca.* 450 nm developed upon addition of TCC to the complexes, reaching its maximum when two molar equivalents of catechol were added to the solution. Thus, in both cases, a first substrate binding occurred, followed by a second one. EPR-spectroscopic measurements showed that in the case of the catalytically active hydroxo complex, the catechol binding results in the cleavage of the hydroxo bridge, leading to the evolution of the EPR-signal, in contrast to the EPR-silent initial complex. The stopped-flow studies allowed the determination of a kinetic constant of the fixation of the second equivalent of TCC by this complex, whereas the fixation of the first molar equivalent was found to be too fast to be determined. In the case of the inactive bis-aqua-dicopper(II) complex, the binding of TCC did not lead to any appreciable changes in the EPR-spectrum, and the fixation of two substrate molecules was too fast to be distinguished. The anaerobic studies on the $DTBCH_2$ binding to the complexes indicated that, in contrast to the natural enzyme, catechol is not oxidized stoichiometrically in the absence of dioxygen. However, electrochemical studies indicated that the binding of $DTBCH_2$ to the active hydroxo complex affects significantly its electrochemical behavior, leading to a complex being made more easily reducible and oxidizable. On the contrary, the electrochemical behavior of the inactive diaqua complex was only weakly affected by the binding of the substrate.

Based on these observations, the authors proposed a mechanism of the substrate binding to the dicopper(II) center, as depicted on Scheme 1.3, which reconciled two earlier proposed modes of the substrate fixation by the natural enzyme: a didentate bridging mode proposed by Solomon for the catecholase activity of tyrosinase,[3] and a monodentate asymmetric coordination, proposed by Krebs.[8] In this mechanism, the substrate first binds to only one copper center along with the concomitant cleavage of the hydroxo bridge. Then, the proton transfer from the second phenol group of catechol to the hydroxyl group bound to the second copper center occurs, resulting in the displacement of a water molecule and the bridging coordination of the catecholate.

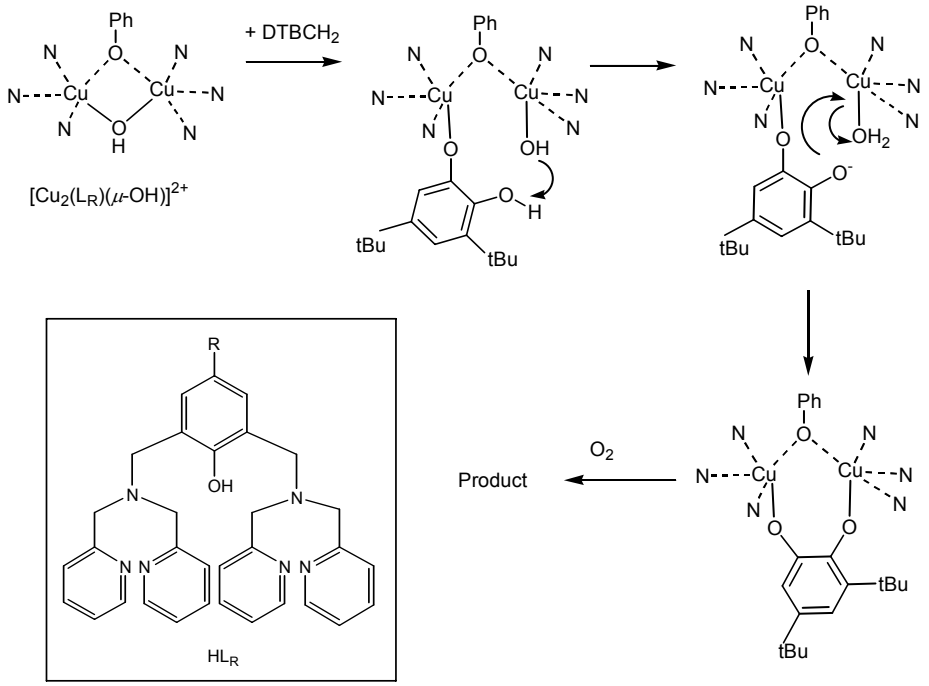

Scheme 1.3. Proposed mechanism for the interaction between the dinuclear μ-hydroxo-copper(II) complexes and $DTBCH_2$. Insert: dinucleating ligands HL_R employed to prepare the copper(II) complexes: R = CH_3 (HL_{CH3}), F (HL_F), CF_3 (HL_{CF3}), and OCH_3 (HL_{OCH3}). Redrawn after Belle and co-workers.[81]

Casella and co-workers[82] have used inactive *p*-nitrocatechol (NCat) to isolate and spectroscopically characterize catecholate adducts of mononuclear and dinuclear copper(II) complexes. The authors prepared the complexes of the composition [Cu(L6)(NCat)] (L6 = *N,N*-bis[2-(1'-methyl-2'-benzimidazolyl)ethyl]amine), $[Cu_2(L66)(NCat)](ClO_4)_2$ (L66 = α,α'-bis{bis[2-(1'-methyl-2'-benzimidazolyl)ethyl]amino}-*m*-xylene, Figure 1.12) and $[Cu_2(L66)(NCat)_2]$ (the latter compound was studied only in solution), and reported their IR, Raman and UV-Vis spectra.

Based on the very similar spectroscopic features of [Cu(L6)(NCat)] and $[Cu_2(L66)(NCat)](ClO_4)_2$ (C-O stretch peak of the coordinated catecholate at 1265±2 cm^{-1} in the IR spectra and in the Raman spectra with the excitation length of 454.5 nm; bands at 293, 350 and 468 nm in the UV-Vis spectra), the authors proposed that in both compounds catecholate is bound in a similar chelating η^2 mode to one copper ion, eventually exhibiting an additional η^1 bridging coordination to a second copper atom in the dicopper(II) complex, as depicted in Figure 1.13. In addition, the second equivalent of catechol could bind to the dicopper complex, forming a bis-catecholate adduct, which also seems to indicate that the substrate is bound to only one metal center. In fact, these results seem to correlate with the observations of Belle *et al.*,[81] who also reported the successive binding of two catechol molecules to dicopper complexes and suggested the asymmetric coordination of the substrate.

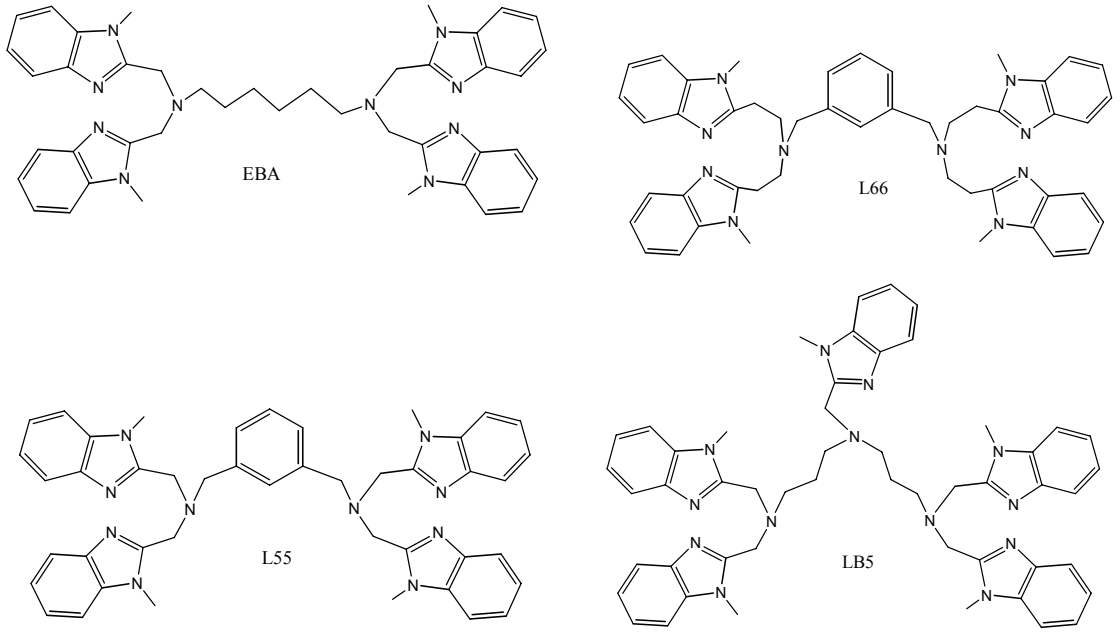

Figure 1.12. Structures of the ligands EBA, L55, L66 and LB5, prepared by Casella and co-workers.[67,68]

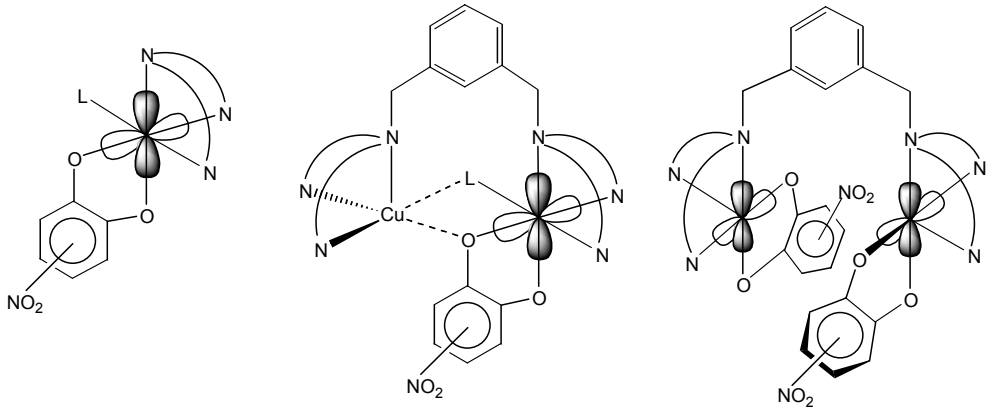

Figure 1.13. Structure proposals for [Cu(L6)(NCat)] (left), $[Cu_2(L66)(NCat)](ClO_4)_2$ (middle) and $[Cu_2(L66)(NCat)_2]$ (right). Redrawn after Casella and co-workers.[82]

1.3.2.2.3 Anaerobic interaction of catechol with copper(II) complexes

The stoichiometric oxidation of the catechol substrate by the dicopper(II) core, leading to the formation of quinone and dicopper(I) species, has often been proposed as the first step in the catalytic cycle.[8,68,79,83] Consequently, some examples of studies on anaerobic interaction of the copper(II) complexes with $DTBCH_2$ have been reported. In most cases, the reduction of the dicopper(II) core along with the release of the quinone molecule was indeed observed, in some cases only in the presence of catechol excess.[69-71,79,84] As an example, the spectroscopic changes observed upon treating the dicopper(II) complex $[Cu_2(L55)]^{2+}$ (L55 = α,α'-bis{bis[1-(1'-methyl-2'-

benzimidazolyl)methyl]amino}-*m*-xylene, Figure 1.12) with $DTBCH_2$, reported by Casella and co-workers,[70] are shown in Figure 1.14.

At -90 °C, the electron transfer from catechol to the dicopper(II) core is prevented, which enabled the authors to spectrophotometrically characterize the catecholate adduct with the complex (curve b, Figure 1.14). Similarly to earlier reported UV-Vis spectra of adducts with electron-poor catechols,[79-81] this species is characterized by weak absorptions at 345 and 440 nm, attributed to LMCT bands. Upon warming the reaction mixture to room temperature, the dicopper(II) core is reduced to the copper(I) state, and the molecule of quinone is released, easily monitored by the absorption at *ca.* 400 nm (curve c, Figure 1.14).

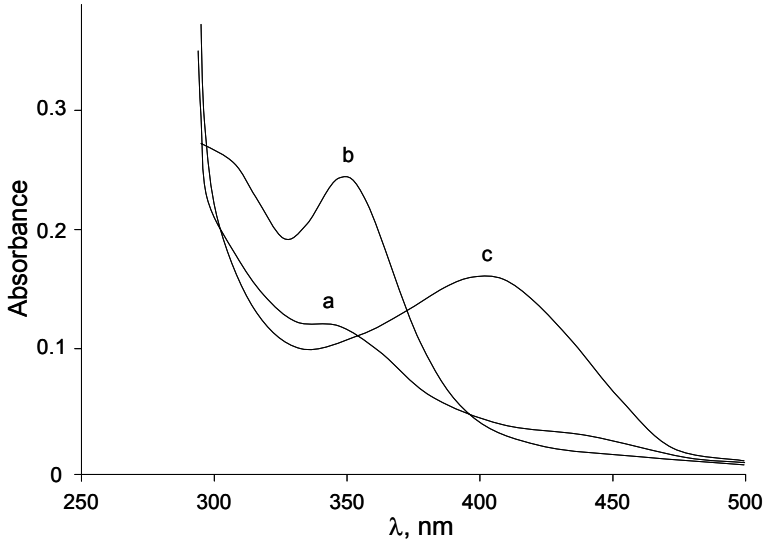

Figure 1.14. Electronic spectra recorded anaerobically in methanol solution at -90 °C of: (a) $[Cu_2(L55)]^{4+}$ (0.2 mM) and (b) its complex with $DTBCH_2$ (1.8 mM). Spectrum (c) shows the stoichiometric formation of DTBQ after warming the solution to room temperature (λ = 396 nm, ε = 1600 $M^{-1}cm^{-1}$). Redrawn after Casella and co-workers.[70]

Some exceptions from this type of behavior, however, have been reported. Thus, μ-hydroxo-dicopper(II) complexes with a series of phenol-based ligands reported by Belle *et al.* (Scheme 1.3, insert) do not oxidize $DTBCH_2$ in anaerobic conditions, but instead bind two equivalents of the substrate in two successive steps.[81] As discussed above, the parent complexes become more easily reducible and oxidizable upon binding of the first molecule of the substrate, whereas the binding of the second molecule hardly affects further the electrochemical behavior. A number of authors have reported that in case of the anaerobic catechol interaction with mononuclear copper(II) complexes, one-electron transfer takes place, leading to the formation of copper(I)-semiquinonate species.[57,85] The reaction of dinuclear copper(II) complexes, formed by the self-assembly of two mononuclear units, with catechol was found to result in the dissociation of the dicopper(II) core.[56,77] As a result, either a mononuclear copper(II)-catecholate adduct,[56,86]

or a copper(II)-semiquinonate product along with the reduced copper(I) co-product,[77] were formed.

It should be noted that some authors have reported the vanishing of the d-d and/or LMCT bands of the copper(II) complexes immediately after the substrate addition along with the appearance of the characteristic quinone absorption at 400 nm in the UV-Vis spectra also in the presence of dioxygen.[79,87,88] These changes were also attributed to the fast stoichiometric reaction between the complex and the substrate, leading to the reduction of the copper(II) centers and the release of one molar equivalent of the quinone, prior to the rest of the catalytic cycle.

1.3.2.3 Structure-activity relationship

1.3.2.3.1 Metal-metal distance vs. catecholase activity

The assumption that a steric match between the dicopper(II) center of a complex and catechol substrate is required for the catecholase activity has been published as early as 1980.[50] Consequently, the majority of the authors use a comparison of the metal-metal distances within a series of structurally related complexes to interpret the difference in their catecholase activities, if their crystal structures are available.[75,80,89] Taking into account that the copper-copper distance in the *met* form of the natural enzyme is very short (2.9 Å only), and comparing this value to that reported by Karlin and co-workers[53] for the *o*-catecholate-bridged dicopper(II) complex (*ca.* 3.25 Å, Figure 1.6), a conclusion can be drawn that the optimal copper-copper distance for the catecholase activity falls in a range of 2.9–3.2 Å. Kao *et al.*[89] have studied the catecholase activities within a series of oxy-bridged dicopper(II) complexes and showed that the complexes with the metal-metal distance, closest to that observed for the *met* form of catechol oxidase, display the best catalytic activity, as depicted in Figure 1.15.

Nevertheless, a large metal-metal separation in dicopper(II) complexes does not necessarily prohibit a catecholase activity. For example, Meyer and co-workers have reported the catalytic oxidation of $DTBCH_2$ by two dicopper(II) complexes with a metal-metal separation of 4.088 Å and 4.553 Å (Figure 1.10, complexes **3**$(ClO_4)_2$ and **4**$(ClO_4)_2$).[75] The catecholase activity of these complexes was found, however, to be significantly lower in comparison to their analogues with the shorter (*ca.* 3.5 Å) copper-copper distance (Figure 1.10, complexes **1**$(ClO_4)_2$ and **2**$(BF_4)_2$). Furthermore, Selmeczi *et al.* reported the catecholase activity of a dicopper(II) complex $[Cu_2(L^1)(CF_3SO_3)_2(H_2O)_4](CF_3SO_3)_2$ (L^1=1,3-bis{*N,N*-bis(2-[2-pyridyl]ethyl)}aminopropane, Figure 1.16), in which a copper-copper distance amounts to 7.840 Å.[71,72]

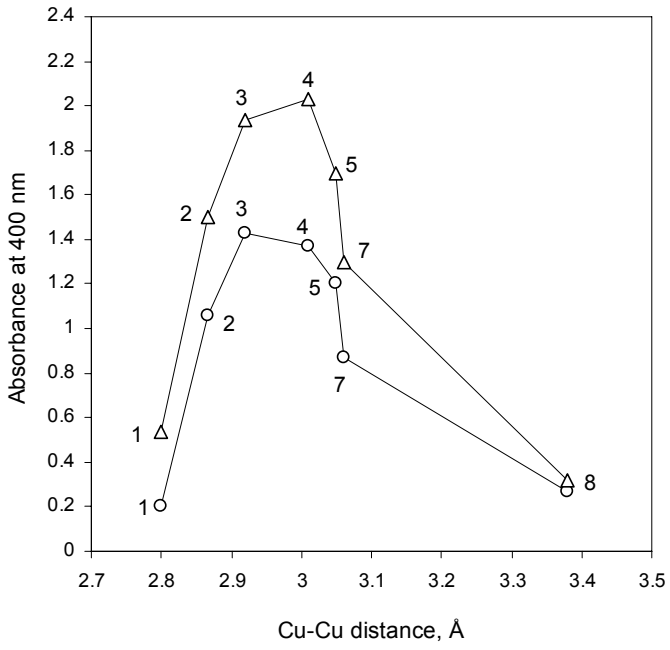

Figure 1.15. Plot of absorption of the quinone band at 400 nm (a) 30 min (– ○ –) and (b) 60 min (– Δ –) after addition of $DTBCH_2$ to the oxy-bridged complexes *vs.* copper-copper distance in these complexes. Redrawn after Kao *et al.*[89]

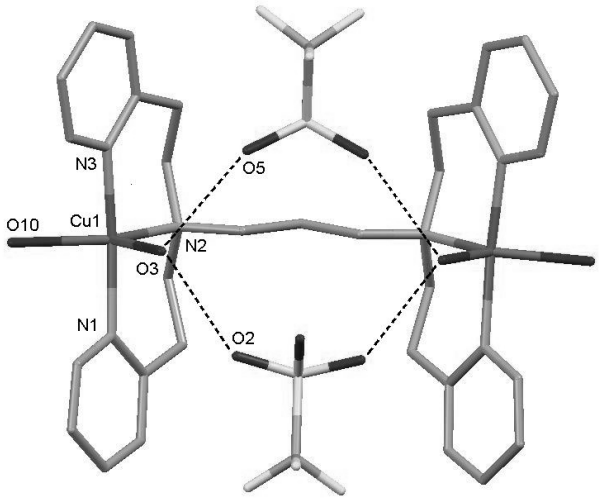

Figure 1.16. X-ray crystal structure of $[Cu_2(L^1)(CF_3SO_3)_2(H_2O)_4]^{2+}$ (L = 1,3-bis{*N*,*N*-bis(2-[2-pyridyl]ethyl)}aminopropane), prepared by Selmeczi *et al.*[71] The Cu…Cu distance is 7.8398(9) Å.

1.3.2.3.2 Electrochemical properties of the complexes vs. catecholase activity

Many research groups have attempted to correlate the redox properties of the copper(II) complexes with their catecholase activity.[67,75,78,80,88,90,91] However, a correlation between the two is not easily established. For example, Torelli *et al.*[91] reported that the inactive bis-aqua-dicopper(II) complex with the HL_{CH3} ligand (Scheme 1.3, insert) could be more easily reduced than its catalytically active μ-hydroxo-bridged analogue. On the other hand, the same authors reported the existence of a correlation between the

first reduction potentials of hydroxo-bridged dicopper(II) complexes with a series of dinucleating compartmental ligands HL_R ligands (Scheme 1.3, insert) and their catecholase activities.[90] The authors have changed the *para*-substituents on the phenol ring of dinucleating compartmental ligands HL_R (Scheme 1.3, insert) and showed that the presence of the strong electron-withdrawing CF_3 group in this position results in a completely inactive dicopper(II) complex. The complexes with *p*-CH_3, *p*-OCH_3 and *p*-F substituents were found to exhibit catecholase activity; furthermore, taking the methyl-substituted complex as a reference, a higher activity was observed in the presence of the electron-donating OCH_3 group, whereas the presence of an electron-withdrawing fluorine atom was found to inhibit the activity to a moderate extent.

Reim and Krebs[78,88] studied the electrochemical behavior of a series of dicopper(II) complexes with dinucleating phenol-based ligands (Figure 1.11) in acetonitrile solution, but observed only irreversible and ill-defined reduction steps. The reduction potentials were found to be very sensitive to the degree of protonation and/or the number of transferred electrons, thus no clear relationship between the redox properties of the complexes and their catecholase activity could be established.

Mukherjee *et al.* also reported the absence of an obvious correlation between the first reduction potentials of the doubly bridged dicopper(II) complexes with various endogenous and exogenous bridges and their catecholase activity.[80] However, Casella and co-workers succeeded in calculating the reaction rates for the two successive steps of the catalytic reaction (a fast stoichiometric reaction between a dicopper(II) complex and catechol and a slower catalytic reaction), and showed a clear dependence of the reaction rate in the first stoichiometric step on the Cu^{II}/Cu^{I} reduction potential.[67] As this step involves the electron transfer from the bound catecholate to the dicopper(II) center, this observation is fully understandable. On the other hand, as overall reaction rates obviously depend on many factors, *i.e.* the rate of the reoxidation of the dicopper(I) species by dioxygen, the rate of the catechol oxidation by the formed peroxo-dicopper intermediate *etc.*, it is hardly surprising that in the majority of cases, no straightforward correlation between the activity and the redox potential of a complex can be established.

1.3.2.3.3 The influence of the exogenous bridging ligands on the catecholase activity of dicopper(II) complexes

The nature of the bridging ligands between the copper centers in a complex plays an important role in its catecholase activity. The small bridging ligands can promote a short copper-copper distance within a dimetal core, required for the catecholate binding in a didentate bridging fashion, which is thought to be beneficial for catecholase activity. On the other hand, the substrate should effectively bind to the copper(II) ions and needs thus to be able to displace a present bridging ligand at the dimetal core. Furthermore, some bridging ligands, *e.g.* OH^- ion, can facilitate the deprotonation of catechol due to their ability to abstract the proton with the subsequent release of a water molecule. In general, it can be stated that such bridging ligands as

hydroxide,[75,80,91] alkoxide or phenoxide[79,80,87,89], imidazolate[92] and carboxylate[75,83,93,94] can be readily displaced by the incoming catecholate and thus promote the catecholase activity. On the other hand, strongly coordinated ligands, such as chloride and bromide, cannot be displaced by the substrate, resulting in catalytically inert compounds.[95,96]

Neves *et al.* studied the catecholase activity of dicopper(II) complexes with acetate bridging ligands in the presence of variable amounts of sodium acetate.[83] The authors reported the decrease of the reaction rates, in accordance with the hypothesis that the acetate competes with the incoming catecholate for a binding site in the copper coordination sphere, leading to inhibition effect. Krebs and co-workers[93] have recently published interesting studies on the catecholase activity of a series of dicopper(II) complexes with phenol-based compartmental ligands and double acetate bridges between the metal centers (Figure 1.17). The authors showed that the presence of the thiomorpholine substituent on the ligand facilitates the displacement of one acetate bridge, leading to higher catalytic activities (see Section 1.3.2.3.4 for details). These results indicate that the easiness of the bridging ligand displacement in general leads to higher catalytic activities, although it is obvious that this factor does not solely control the reactivity.

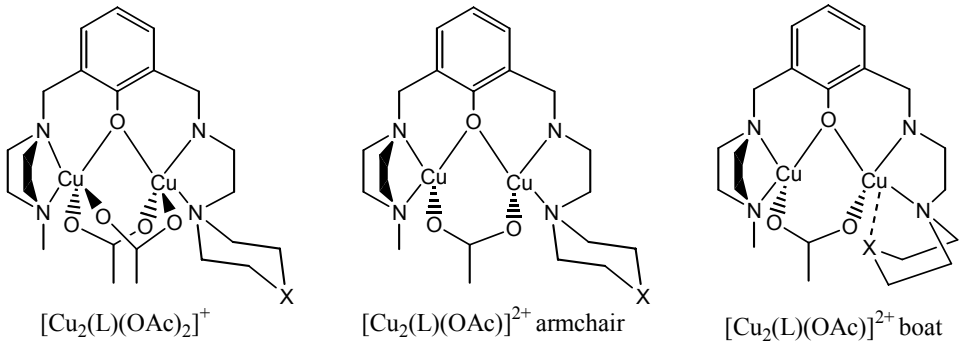

Figure 1.17. Structures of $[Cu_2(L)(OAc)_2]^+$ and the boat and chair conformations of $[Cu_2(L)(OAc)]^{2+}$ (with X = CH_2, O or S). Redrawn after Krebs and co-workers.[93]

On the other hand, Reedijk and co-authors[96] reported the interaction of chloro- and bromo-bridged dicopper(II) complexes of the phenol-based compartmental ligand Hpy2th2s (2,6-bis[*N*-(2-pyridylmethyl)-*N*-(2-thiophenylmethyl)aminomethyl]-4-methylphenol) with catechol substrates (see Chapter 4). In these complexes, both copper ions are pentacoordinated, with three positions in the coordination sphere occupied by the donor atoms of the ligand and the other two by the halogen ions, one bridging and one monocoordinated. Both complexes were found to be inactive in catechol oxidation; however, their titration with TCC indicated that in the chloride complex, one of the monocoordinated chloride anions could be substituted by the catechol substrate. The bridging chloro atom could not be exchanged with the catecholate anion. In the case of the bromide complex, neither monocoordinated nor bridging halogen anions could be substituted by TCC.

A few authors pointed out that the presence of two hydroxide, alkoxide or phenoxide bridges may lead to catalytically inactive complexes. Thus, Mukherjee *et al.* explains the inactivity of the complex $[Cu_2(L^5\text{-}O)_2(ClO_4)_2]$ (L^5-OH = 4-methyl-2,6-bis(pyrazolyl-1-ylmethyl)phenol) by the presence of two phenoxide bridges in its structure.[80] Similarly, Casella and co-workers showed that the active species in the catechol oxidation by the dicopper(II) complex with the ligand L55 (L55 = α,α'-bis{bis[1-1'-methyl-2'-benzimidazolyl)methyl]amino}-*m*-xylene, Figure 1.12) is a monohydroxo-bridged dicopper(II) species, whereas the bis(μ-hydroxo) species is essentially inactive.[70] However, these observations are not conclusive, as the examples of the catalytically active complexes with the double hydroxo,[56,80] alkoxo[79,87,89] and phenoxo[89] bridges have also been reported.

An interesting possible function of the bridging hydroxo group in the catecholase activity of a complex has been proposed by Reim and Krebs.[78] The authors investigated the catecholase activities of a series of dicopper(II) complexes with phenol-based compartmental ligands (Figure 1.11) and reported that the complex containing the exogenous μ-hydroxo bridge exhibits the highest catalytic activity. This appears to be caused by the fact that the bridging hydroxide group enforces the complex to adopt a very strained geometry, which makes it willing to exchange the μ-hydroxo bridged structural motif in favor of the bridging catechol coordination. In the presence of alternative bridging ligands with a larger bite distance, a more relaxed conformation is adopted, which in turn leads to a lower activity.[78]

1.3.2.3.4 The influence of the ligand structure on the catecholase activity of dicopper(II) complexes

Although many authors refer to the ligand properties to explain the results of the catecholase activity studies on the copper complexes, only a few detailed studies on changes in the ligand structure and their influence on the catecholase activity have been reported so far.

Krebs and co-workers[93] have prepared three asymmetric phenol-based compartmental ligands, one arm of which contained piperidine (L1), morpholine (L2) or thiomorpholine (L3) heterocycles (Figure 1.17), and studied the catecholase activity of their dicopper(II) complexes with two acetate bridges between the metal centers. The authors have found that the complex with the thiomorpholine substituent shows the highest catecholase activity, probably because the sulfur atom can displace one of the bridging acetate ligands and yield a free coordination site for the substrate binding. This hypothesis was confirmed by DFT calculations,[93] which were performed to determine the different reaction energies ($[LCu_2(OAc)_2]^+ \rightarrow [LCu_2(OAc)]^{2+} + OAc^-$) for all three monocation conversions into the corresponding monoacetate-bridged dications in their boat and armchair conformations (Figure 1.17). For the thiomorpholine system, the isomer with a boat conformation of the subunit was found to be 5.5 kcal mol^{-1} more stable than the corresponding armchair conformer, whereas for the morpholine system,

the energy difference was only 1.4 kcal mol^{-1}, and for the piperidine system, the armchair conformation was found to be significantly more stabilized. Furthermore, the thiomorpholine-containing structure was found to possess a Cu-S bond (R_{Cu-S} = 2.42 Å). These results indicate the ability of the sulfur atom in the ligand to displace a bridging ligand between the copper(II) centers, which in turn leads to higher catecholase activity of the system in question.

The ligand flexibility also plays a role in the activity of the resulting copper(II) complexes. Kandaswamy and co-workers have studied the catecholase activities of a series of copper(II) complexes with lateral macrodicyclic compartmental ligands (Figure 1.18) and reported the enhancement of the activity with the increase of the macrocyclic ring size.[97] The increase in ring size makes the system more flexible and favors the catalysis phenomenon.

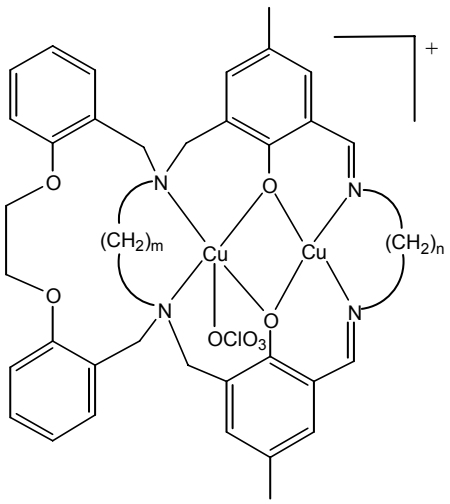

Figure 1.18. General structure of dicopper(II) complexes with macrodicyclic ligands. Redrawn after Kandaswamy and co-workers.[97]

On the other hand, the studies of Reim and Krebs on the catecholase activity of the dicopper(II) complexes with phenol-based compartmental ligands (see Figure 1.11) showed that only the complexes containing piperazine unit within their ligand framework exhibited catecholase activity.[78] This is perhaps related to the fact that the square-pyramidal coordination spheres of the copper(II) ions in these complexes are strongly distorted due to the coordination of the piperazine group. Thus, the presence of a certain substituent in a ligand framework can have a strong influence on the catalytic behavior of the corresponding copper complexes.

1.3.2.3.5 The influence of pH on the catecholase activity of dicopper(II) complexes

The natural enzyme exhibits catecholase activity only in a limited pH range (pH 5-8), with an optimum activity at pH 8, and an irreversible loss of activity below pH 4.0 and above 10.0.[27] Some authors have studied the influence of pH on the catecholase

activity of model copper complexes.[67,70,83,91,94] It should be noted that the changes in pH are often accompanied by the changes in the structure of a complex, leading to different catalytic behavior. Thus, Torelli *et al.*[90,91] have studied the pH-driven interconversions of dicopper(II) complexes with a series of phenol-based compartmental ligands (Scheme 1.3, insert) and found that the μ-phenoxo-μ-hydroxo-dicopper(II) complexes, which are stable at neutral pH values, can reversibly interconvert into the μ-phenoxo-bis-aqua-dicopper(II) and μ-phenoxo-bis(hydroxo)dicopper(II) species at lower and higher pH levels, respectively, as shown in Figure 1.19. Of these species, only the μ-hydroxo-dicopper(II) complexes exhibit catecholase activity. The possible reasons for that could be a short metal-metal distance (2.89 Å) in these complexes and the ability of the bridging hydroxo group to assist in the deprotonation of the incoming catechol substrate, facilitating its binding to the dicopper(II) center, as discussed above (Scheme 1.3).

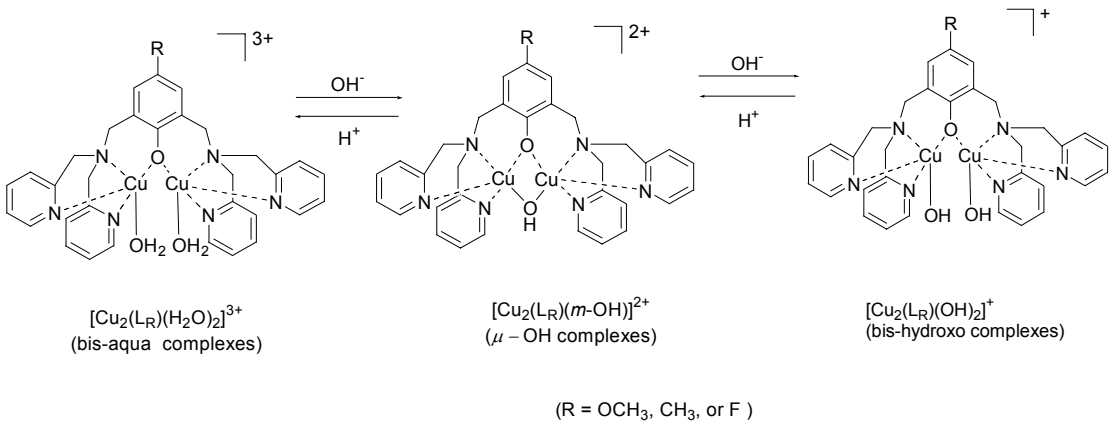

Figure 1.19. pH-driven interconversions of dicopper(II) complexes with phenol-based ligands HL_R. Redrawn after Belle and co-workers.[91]

Fernandez *et al.* have studied the catecholase activity of the dicopper(II) complex with the asymmetric ligand HTPPNOL (*N*,*N*,*N*'-tris-(2-pyridylmethyl)-1,3-diaminopropan-2-ol) at different pH values.[94] The pH-titrations indicated that above pH 8.0, the water molecule, coordinated to one of the two copper(II) ions in solution, undergoes a deprotonation with the formation of a hydroxide group (Figure 1.20). An increase of the activity was observed at pH 8.05, *e.g.* when the hydroxide-containing species is present in solution. The authors have also suggested that the hydroxide moiety assists in the deprotonation of the substrate, facilitating its binding to the dicopper(II) core. This assumption is consistent with the proposal of Belle *et al.*,[81] although the apical coordination of the hydroxide anion was proposed by Fernandez *et al.*, in contrast to the bridging coordination, as determined by the latter authors.

Casella and co-workers[68] have studied the catecholase activity of the dicopper(II) complexes $[Cu_2(LB5)]^{4+}$, $[Cu_2(L55)]^{4+}$ and $[Cu_2(L66)]^{4+}$ (Figure 1.12) in methanol solution and found that at neutral pH values, the complexes oxidized $DTBCH_2$ either

stoichiometrically, or with extremely low catalytic efficiency. Thus, the catalytic reactions were performed at pH 5.1, in the presence of a small amount of an aqueous buffer. At this pH, the contribution of the non-catalytic oxidation of $DTBCH_2$ was found to be negligible. A year later, the authors reported[67] the catecholase activity studies on the dicopper(II) complex $[Cu_2(EBA)]^{2+}$ (Figure 1.12) and the influence of pH on the catalytic behavior. The authors analyzed only the acidic pH range in order to prevent the possible substrate autoxidation and to increase the pH sensitivity. The studies were performed at two different substrate concentrations: the one that gave the highest reaction rate, and the one-fourth of this substrate concentration. While at lower catechol concentration the pH influence was negligible, at high substrate concentration the reaction rate in both phases (see above for the biphasic mechanism proposed by Casella and co-workers) increased with the pH with a saturation behavior (Figure 1.21).

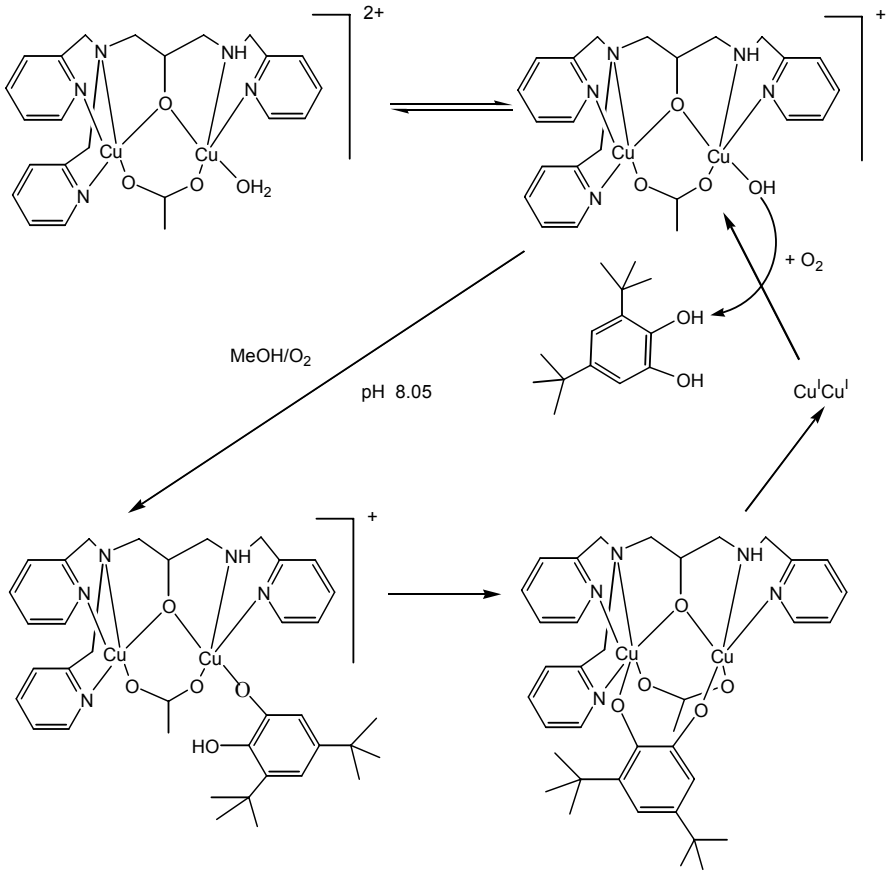

Figure 1.20. Mechanism of the interaction between the dinuclear copper(II) complex with the asymmetric ligand HTPPNOL and 3,5-di-*tert*-butylcatechol, as proposed by Fernandes *et al.*[94]

Later, Casella and co-workers[70] have reported the studies on the catecholase activity of the dicopper(II) complex with the ligand L55 in a mixed solvent of 75% methanol/glycerol (7/1 v.v.) and 25% (v/v) aqueous 50 mM Hepes buffer, which allowed to keep the pH of the solution close to neutral values. The studies on the pH influence on the catalytic reaction rates showed that the maximal rate was observed

around pH 7, whereas it dropped drastically above pH 7.5 (Figure 1.22, left). Earlier studies on the pH-driven interconversions[98] of this complex indicate that rate profile parallels the distribution curve of the monohydroxo species $[Cu_2(L55)(H_2O)(OH)]^{3+}$, while the bis($\mu$-hydroxo) species $[Cu_2(L55)(OH)_2]^{2+}$, which is dominant above pH 6.5, is catalytically inactive (Figure 1.22, right).

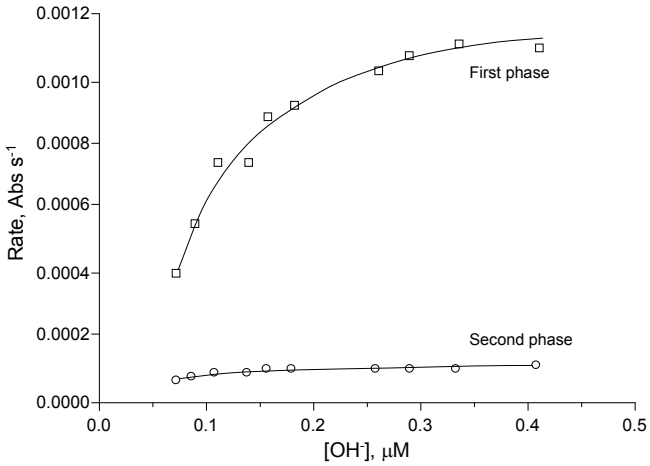

Figure 1.21. Dependence of the rate (as absorbance change at 396 nm *vs.* time) of the first and second phases of catalytic oxidation of $DTBCH_2$ by $[Cu_2(EBA)]^{4+}$ (14 μM) on the solution pH, as reported by Casella and co-workers.[67] The concentration of 3,5-di-*tert*-butylcatechol was 6 mM in all experiments. The reactions were performed in 30:1 mixture of methanol/aqueous phosphate buffer, the pH of which was varied from 3.4 to 5.3. Redrawn after Casella *et al.* [67]

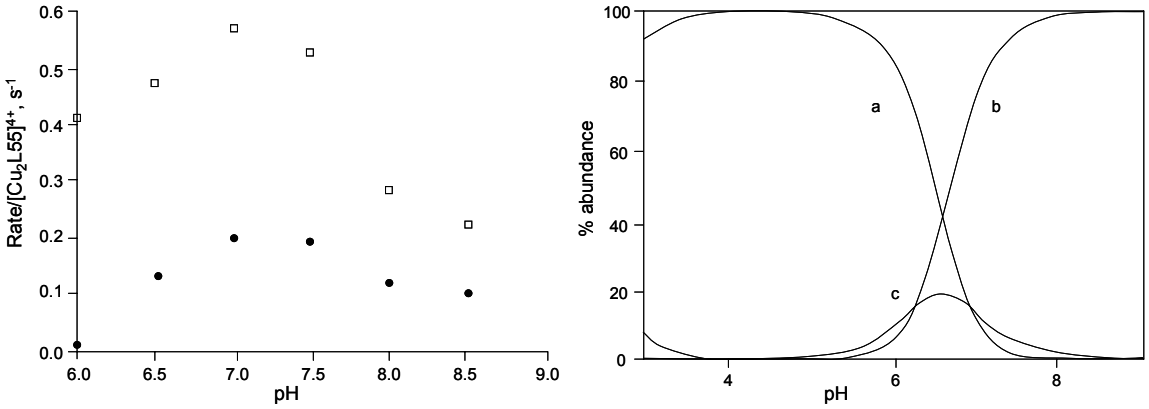

Figure 1.22. Left: rate dependence for the first (open squares) and second (solid circles) steps of the oxidation of $DTBCH_2$ (2 mM) catalyzed by $[Cu_2(L55)]^{4+}$ (6 μM) on the pH in the mixed solvent of 75% methanol/glycerol (7:1) and 25% (v/v) Hepes buffer (50 mM). Redrawn after Casella and co-workers.[70] Right: species distribution in the 2Cu/L55 system as a function of pH in acetonitrile/water solution: a) $[Cu_2(L55)(H_2O)_2]^{4+}$; b) $[Cu_2(L55)(H_2O)(OH)]^{3+}$; $[Cu_2(L55)(OH)_2]^{2+}$. Redrawn after Casella and co-workers.[98]

Thus, it appears that all authors have reached a similar conclusion: in case of pH-driven interconversions of (bis)aqua-, monohydroxo- and bis(hydroxo)-dicopper(II) species, the monohydroxo derivatives usually exhibit the highest catecholase activity, likely to be caused by the short metal-metal distance enforced by the bridging hydroxide anion, and its function in the substrate deprotonation, facilitating its binding to the catalytic core.

1.3.2.4 Kinetic studies

1.3.2.4.1 Dependence of the reaction rates on the complex and catechol concentration

Almost all reports on the catecholase activity of copper(II) complexes include the kinetic studies, *e.g.* the dependence of the reaction rates on the concentration of the substrate, catalyst, dioxygen and some additives, *e.g.* dihydrogen peroxide or kojic acid. It appears that in most cases, a simple Michaelis-Menten model is sufficient to describe the behavior or the catalytic system. This kinetic model, initially proposed for the enzymatic catalysis by Leonor Michaelis and Maud Menten in 1913, is based on the assumption that the catalyst and substrate reversibly react with each other to form an intermediate species prior to the substrate conversion, according to Scheme 1.4.

$$E + S \underset{k_{-1}}{\overset{k_1}{\rightleftharpoons}} ES \xrightarrow{k_2} E + P$$

Scheme 1.4. The mechanism of the interaction of the enzyme (E) with the substrate (S), leading to the formation of the product P, according to the Michaelis-Menten model.

The reaction rate for this model is determined by the equation (1.1), also called Michaelis-Menten equation:

$$V = \frac{V_{max}[S]}{K_M + [S]} \tag{1.1}$$

In this equation, V_{max} corresponds to the limiting reaction rate, reached at a very high substrate concentration. Thus, a characteristic of a Michaelis-Menten system is the substrate saturation behavior, upon which the reaction rate asymptotically approaches a certain value with the substrate concentration increase, but never reaches it. K_M is a Michaelis constant, which corresponds to the substrate concentration at which the reaction rate is equal to one half of the maximal value, and is defined as $(k_2+k_{-1})/k_1$ (Figure 1.23).

A rearrangement of the equation (1.1) leads to the equation (1.2), from which a linear dependence of the reciprocal reaction rates on the reciprocal substrate concentration becomes obvious. By building a plot of 1/V *vs.* 1/[S], also known as a double reciprocal, or Lineweaver-Burk plot, and taking into account that $V_{max} = k_2$ [E],

the kinetic constants k_2 and K_M can be determined (Figure 1.23, right). The constant k_2 in this case corresponds to the turnover frequency, determined in s^{-1}.

$$\frac{1}{V} = \frac{[S] + K_M}{V_{max}[S]} = \frac{[S]}{V_{max}[S]} + \frac{K_M}{V_{max}[S]} = \frac{1}{V_{max}} + \frac{K_M}{V_{max}} \cdot \frac{1}{[S]} \qquad (1.2)$$

Most of the studies on the catecholase activity of copper(II) model compounds, performed by the method of the initial reaction rates, showed that the catalytic reaction indeed shows a saturation behavior *vs.* the substrate (=catechol) concentration, making a Michaelis-Menten model applicable.[68,69,75,78-80,83,91,93,94] The observed Michaelis constants usually vary in a range of 10^{-4}-10^{-3} M, and k_2 values fall in a range of 10^{-2}-10^{-1} s^{-1}. Less studies report the dependence of the reaction rates on the catalyst (=complex) concentration.[68,78,80] Usually, a linear dependence is found, indicating that the reaction shows a first-order dependence on the catalyst.

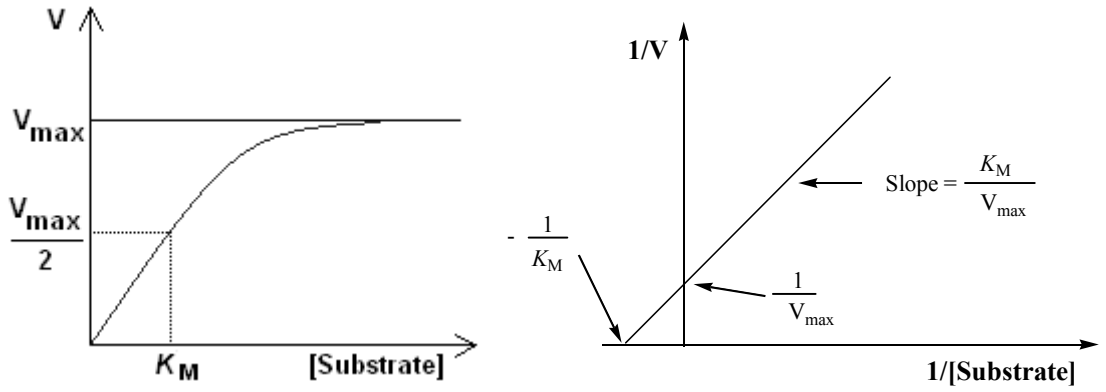

Figure 1.23. Left: the plot of the reaction rates *vs.* the substrate concentration according to the Michaelis-Menten model. Right: an example of a Lineweaver-Burk plot.

A few exceptions from a general trend have also been reported. Thus, in some cases the reaction rates were found to be independent on the substrate concentration.[68,71,75] This behavior can be explained by the presence of another rate-determining step in the overall catalytic cycle, for example, a reoxidation of the dicopper(I) species by molecular dioxygen, as proposed by Casella and co-workers.[68] In this case, the reaction rates are expected to depend on the concentration of molecular dioxygen. Unfortunately, the influence of dioxygen concentration on the reaction rates has been only studied in a few cases, but the works of Casella and co-workers[68] and Speier and co-workers[71] proved indeed that a strong dependence of the reaction rates on dioxygen concentration exists for the catalytic systems, showing a zero-order dependence on the catechol. For example, a three-fold increase in the reaction rate was reported by Casella for the complex $[Cu_2L66]^{4+}$, for which the reaction rates were found to be independent on the substrate concentration, when the solution was saturated with pure dioxygen instead of air.[68] The studies of Speier and co-workers[71] showed a clear

dioxygen saturation behavior for the complex $[Cu_2(L^1)(CF_3SO_3)_2(H_2O)_4](CF_3SO_3)_2$ (L^1=1,3-bis{*N,N*-bis(2-[2-pyridylethyl)}aminopropane, Figure 1.16), for which a zero-order dependence on the substrate has been reported (Figure 1.24).

Casella and co-workers,[67] who proposed a biphasic mechanism for the oxidation of catechol by dicopper(II) complexes (a fast stoichiometric oxidation of catechol by dicopper(II) core, followed by a slower catalytic reaction), have derived a kinetic equation for two consecutive steps in the catalytic cycle (equation 1.3), which allows to determine the reaction rate constants k_1 and k_2 of the first and the second phases. [DTBQ] and [Cat] correspond to the concentrations of DTBQ and the catalyst, respectively.

$$[3,5\text{-DTBQ}] = \frac{k_1[\text{Cat}]}{k_1 + k_2}\left\{2\,k_1 t - \frac{k_1 - k_2}{k_1 + k_2}\left[1 - \exp\left[-(k_1 + k_2) \times t\right]\right]\right\} \quad (1.3)$$

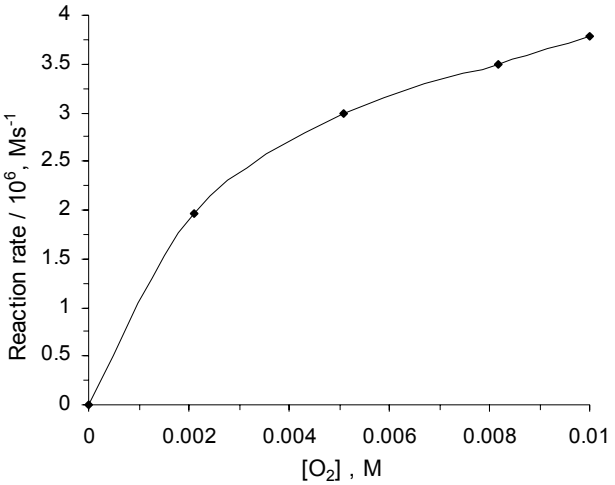

Figure 1.24. The dependence of the oxidation rate of $DTBCH_2$ catalyzed by $[Cu_2(L^1)(CF_3SO_3)_2(H_2O)_4](CF_3SO_3)_2$ on the dioxygen concentration. Conditions: $[[Cu_2(L^1)(CF_3SO_3)_2(H_2O)_4](CF_3SO_3)_2]$=0.125 mM, $[DTBCH_2]$=4.16 mM at 25 °C in MeOH. Redrawn after Speier and co-workers.[71]

Very recently, the same authors reported that in the case of catechol oxidation by the complex $[Cu_2(L55)]^{4+}$ (Figure 1.12), two steps of the catalytic cycle could be separated.[70] The use of stopped-flow technique allowed the determination of the reaction rate in the first stiochiometric phase, whereas the rate of the second step was studied in a time interval of 5-20 s after the beginning of the reaction. In order to prove the reliability of this method, the authors have also calculated the rates of the first and the second phases by fitting the development of the quinone absorbance with time to equation 1.3. In spite of the differences in the two methods of analysis, the results obtained were identical.

1.3.2.4.2 Dihydrogen peroxide formation during the catalytic reaction

The overall catalytic mechanism, reported by Casella and co-workers in 1998 (Scheme 1.2),[68] indicates that either water or dihydrogen peroxide can form as a side product in the catalytic oxidation of catechol by copper(II) complexes. The formation of dihydrogen peroxide in the reaction mixture has indeed been reported in a few cases;[58,59,71,75,83] however, it should be noted that the reports containing the studies aimed to definitely establish the mode of the dioxygen reduction to either water or dihydrogen peroxide are quite scarce. The exact way of dihydrogen peroxide formation is not fully understood. Curiously, in some cases the formation of dihydrogen peroxide is correlated with the detection of the semiquinone intermediate species in the catalytic reaction.[56,57,99] It is indeed plausible that the dihydrogen peroxide may form as a product of the oxidation of the copper(I)-semiquinone intermediate, as proposed by Kodera *et al.*[56] (Scheme 1.5). This mechanism can be rationalized as follows. In case of dicopper(II) complexes, the simultaneous reduction of two copper(II) centers to the copper(I) state results in the oxidation of one equivalent of catechol, leading to the release of one quinone molecule. In case of mononuclear copper(II) complexes (or dinuclear complexes, formed by self-assembly of two mononuclear units), only one electron transfer may occur, resulting in the formation of copper(I)-semiquinonate intermediate species. The reaction of such species with dioxygen may result in the two-electrons reduction of the latter, leading to the reoxidation of the copper(I) ion, a release of the quinone molecule and dihydrogen peroxide formation. Thus, only one molecule of catechol is being oxidized per such catalytic cycle, in contrast to the mechanism proposed for the natural enzyme[8] and for dicopper(II) complexes.[68]

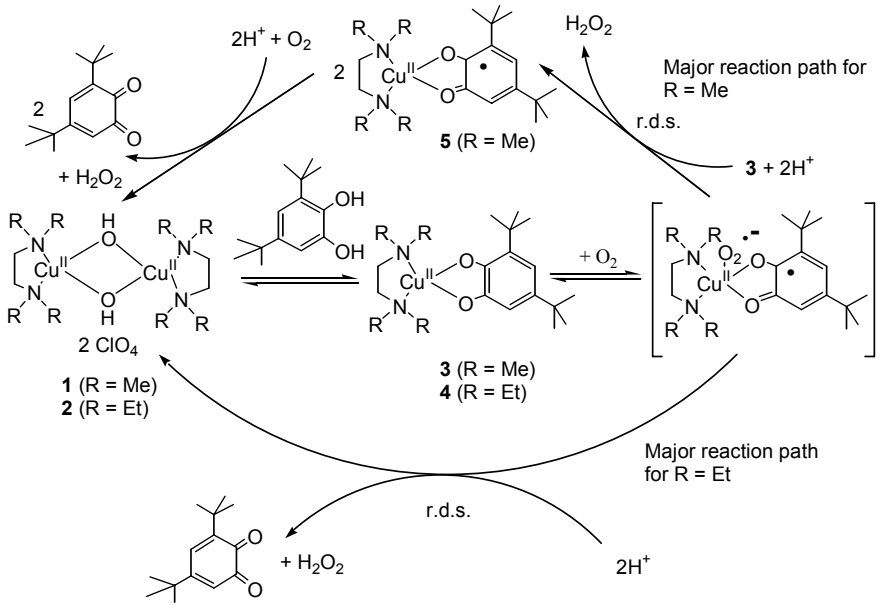

Scheme 1.5. The proposed mechanism of the catechol oxidation, leading to dihydrogen peroxide formation as a byproduct, as proposed by Kodera *et al.* Redrawn after Kodera and co-workers.[56]

It is, however, not clear how dihydrogen peroxide can form upon catechol oxidation by dinuclear copper(II) complexes. According to the overall mechanism proposed by Casella, it may form either via the path a, or the path b (Scheme 1.2).[68] The studies of Ackermann *et al.*[75] showed that upon consumption of one mole of dioxygen, one molar equivalent of quinone was formed, which allowed the authors to propose that the catalytic cycle proceeds via the mechanism including the path a (the protonation of the dicopper(II)-peroxo species, leading to the dihydrogen peroxide release). On the contrast, the path b has been proposed by Selmeczi *et al.*[71] Although both paths are liable, another possibility can though exist. The studies of Ackermann[75] and Casella[82] on dicopper(II)-catecholate adducts indicate that the doubly deprotonated catecholate can bind to only one of the two copper(II) ions instead of the dinuclear bridging coordination, especially when the metal-metal distance is long. It is logical to assume that in this case, only one-electron transfer can occur, resulting in the formation of a mixed-valence $Cu^{I}Cu^{II}$-semiquinonate species. Its interaction with dioxygen may further proceed via the mechanism proposed by Kodera *et al.*[56] It is thus plausible that only one of the two copper ions plays a part in the electron transfer, whereas another has only a structural role. This is certainly an interesting possibility, as the examples of the enzymes containing two or more metal ions, only one of which plays a role in catalysis, are widely known in nature. Unfortunately, very limited information available on this subject does not allow accepting or discarding this option.

1.3.2.4.3 The influence of dihydrogen peroxide on the reaction rates

The studies on the influence of dihydrogen peroxide on the catalytic behavior have only been reported in a few cases.[67,68] In general, dihydrogen peroxide can participate in the catalytic cycle by reoxidizing the reduced dicopper(I) species to the copper(II) oxidation state, thus competing in this with dioxygen. Respectively, its influence is to a large extent defined by the sensitivity of the formed dicopper(I) intermediate to dioxygen. In case of slow reoxidation of this species by dioxygen, dihydrogen peroxide enhances the reaction rates, as the reduced species prefers to react with it instead of dioxygen. On the contrary, when the reoxidation proceeds very fast, the reaction rates are not significantly affected by dihydrogen peroxide addition. In fact, even a slight decrease of the reaction rates may be observed, perhaps caused by the conversion of the active dicopper(II) complex into a less reactive peroxide intermediate, according to the following reaction:

$$Cu^{II}\ldots Cu^{II} + H_2O_2 \rightarrow Cu^{II}(O_2)^{2-}Cu^{II} + 2H^{+}$$

Furthermore, the saturation behavior in dihydrogen peroxide can be observed.[68] This can be related to the fact that presence of dihydrogen peroxide changes the rate-determining step in the reaction. At low H_2O_2 concentration, a normal reoxidation of dicopper(I) species by dioxygen takes place. At higher concentrations, the copper(I)

species can be oxidized by both dioxygen and dihydrogen peroxide, whereas above a certain H_2O_2 concentration, only the latter reaction takes place.

1.3.2.4.4 The influence of the inhibitor kojic acid on the reaction rates

The only example of the studies on the influence of inhibitors on the catecholase activity of model copper complexes has been published by Casella and co-workers, who reported the inhibiting effect of kojic acid on the catecholase activity of dicopper(II) complexes with the ligands L55, L66 and EBA (Figure 1.12).[73] The inhibitor strongly binds to the dicopper(II) complex in the first stoichiometric step of the reaction and to the dicopper(II)-dioxygen adduct in the second step, preventing in both cases the binding of the catechol substrate. The inhibition was found to be of a competitive type. The latter means that in the presence of an inhibitor, a higher substrate concentration is required to achieve the same reaction rates that were reached in its absence resulting in a higher K_M. In case of a non-competitive inhibitor, the binding of the inhibitor to the catalyst molecule makes it inactive. The differences in Lineweaver-Burk plots for a competitive and a non-competitive inhibition mechanisms are shown in Figure 1.25.

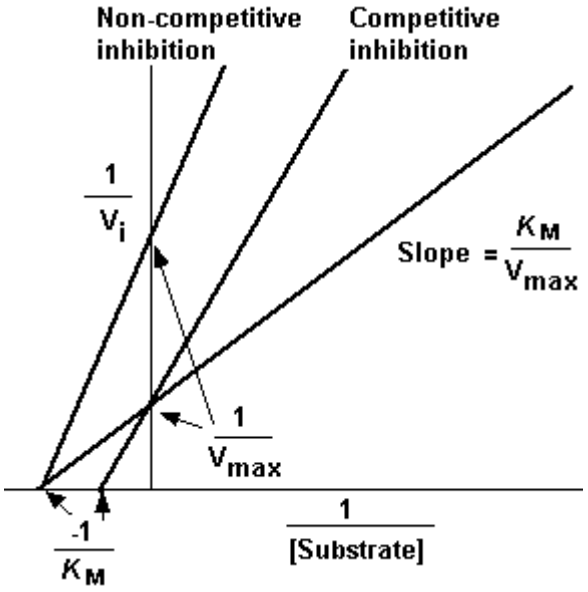

Figure 1.25. An example of Lineweaver-Burk plots for a competitive and a non-competitive inhibition.

Fitting the rate data considering a simple linear competitive inhibition mechanism according to the equation (1.4), the authors could determine the K_I parameter, characterizing the inhibition behavior:

(1.4)

$$V = \frac{\frac{k_{cat}}{K_M}\,[\text{complex}]\;\varepsilon_{DTBQ}\,[\text{DTBC}]}{1 + \frac{1}{K_I}\,[\text{I}] + \frac{[\text{DTBC}]}{K_M}}$$

In this equation, [*I*] corresponds to the concentration of kojic acid, whereas K_M and k_{cat} are Michaelis constant and a turnover frequency determined in the absence of the inhibitor. The value $1/K_I$ corresponds in this case to the formation constants of the catalyst-inhibitor complexes. The inhibition mechanism, proposed by Casella and co-workers, is depicted in Scheme 1.6.

1.3.2.5 Stoichiometric oxidation of catechol by (per)oxo-dicopper complexes

The formation of peroxo-dicopper species as a result of dioxygen binding to a reduced dicopper(I) intermediate and a subsequent oxidation of catechol by them has often been proposed[61,62,64,67,68,71,75] as a second (catalytic) stage of the catechol oxidation by model copper complexes. However, relatively few examples of the interaction of such species with catechol substrates are described in the literature. A schematic representation of the structures of previously reported dicopper-dioxygen cores is shown in Figure 1.26. Kitajima *et al.* reported the oxidative coupling of $DTBCH_2$ by a μ-η^2:η^2 peroxo complex $[Cu_2(HB(3,5\text{-}Me_2pz)_3](O_2)$ ($HB(3,5\text{-}Me_2pz)$ = tris(3,5-dimethylpyrazolyl)borate), leading to the formation of the C-C-coupled products.[100] Interestingly, no formation of *o*-benzoquinone was observed, unless exogenous dioxygen was introduced into the reaction mixture.

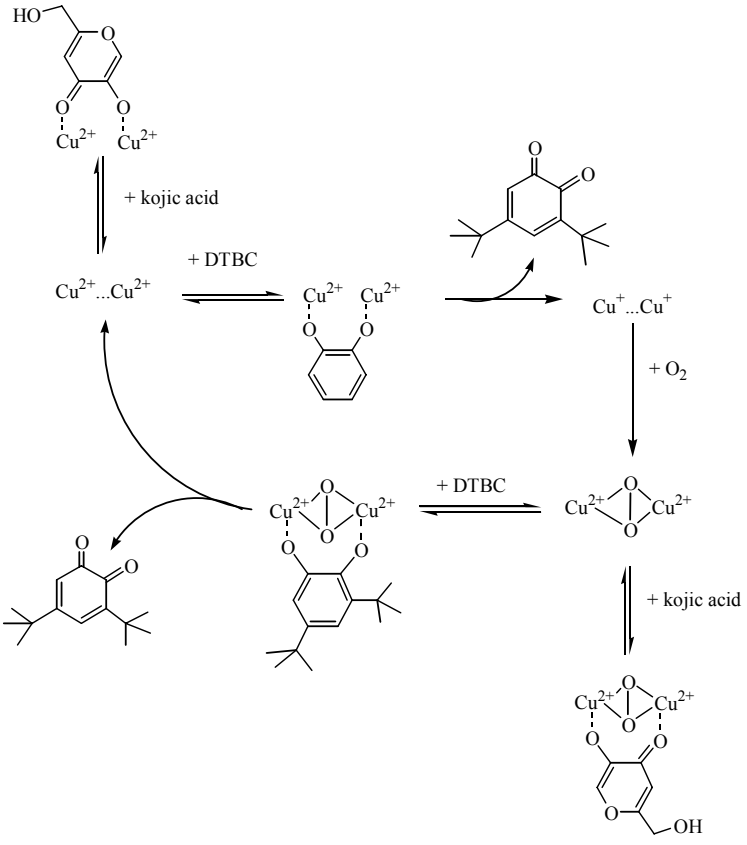

Scheme 1.6. The mechanism of model dicopper(II) complexes inhibition by kojic acid. Redrawn after Casella and co-workers.[73]

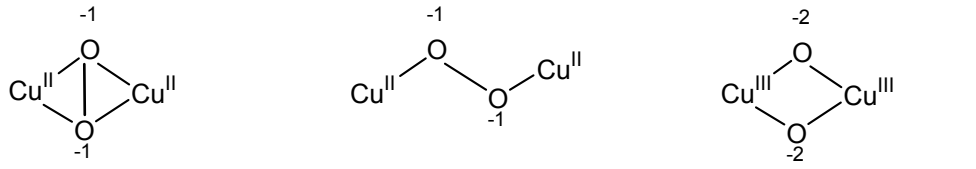

μ–η^2:η^2-peroxo -dicopper(II)

trans-μ–1,2-peroxo-dicopper(II)

bis-μ-oxo-dicopper(III)

Figure 1.26. Schematic representation of dicopper-dioxygen cores, reported in the literature.

Casella and co-workers reported a stoichiometric oxidation of $DTBCH_2$ to DTBQ by a μ-η^2:η^2 peroxo-dicopper complex with the ligand L66 (Figure 1.12).[101] The same type of reactivity was observed by Stack and co-workers for a bis μ-oxo-dicopper complex $[(L_{TMCHD})_2Cu^{III}{}_2(O)_2]^{2+}$ (TMCHD = *N,N,N′,N′*-tetramethyl-(*1R,2R*)-cyclohexanediamine).[102] The oxidation of $DTBCH_2$ by μ-η^2:η^2 and bis μ-oxo-dicopper complexes was also reported by Tolman and co-workers[76] with isolation of mononuclear copper(II)-semiquinonate complexes as a sole product of the reaction, the (per)oxo-dicopper species being generated by reaction of two essentially mononuclear Cu^I molecules with dioxygen. Rockcliffe and Martell also reported a number of examples on the stoichiometric oxidation of catechols to the respective quinones or dicarboxylic acids involving various dicopper-dioxygen complexes.[61,64-66] Unfortunately, these authors did not provide detailed information concerning the structure of the peroxo species. Although the end-on dioxygen-binding mode was proposed based on the results of molecular modeling,[63] the UV-Vis spectroscopic data,[63,66] reported by the authors, as well as the overall reactivity of the described peroxo species[62,65] suggest that dioxygen is bound in the μ-η^2:η^2 mode.

Very recently, Reedijk and co-workers[103] reported a stoichiometric oxidation of $DTBCH_2$ by the trans-μ-1,2-peroxo-dicopper(II) complex with the macrocyclic ligand [22]py4pz (= 9,22-bis(2-pyridylmethyl)-1,4,9,14,17,22,27,28,29,30-decaazapentacyclo-[22.2.1.$1^{4,7}$.$1^{11,14}$.$1^{17,20}$] triacontane-5,7(28),11(29),12,18,20(30),24(27),25-octaene) (Chapter 7). The stoichiometric oxidation was found to proceed in two steps through the formation of the intermediate species, characterized by the intensive absorption at 342 nm (ε =3960 $M^{-1}\cdot cm^{-1}$) in the UV-vis spectrum (Chapter 7). Based on the resonance Raman spectroscopic studies and the kinetic isotopic effect measurements, the authors proposed that the first step involves the proton transfer from the substrate to the nucleophilic peroxo core, resulting in the formation of μ-1,1-hydroperoxo-dicopper(II)-catecholate species, while the second step involves the oxidation of the bound substrate.

1.4 The scope of this thesis

This thesis is devoted to the studies on the model compounds of the type-3 active site copper proteins, in particular catechol oxidase. Chapter 1 presents a general overview of the copper proteins, the structure and properties of catechol oxidase, the copper enzyme with the type-3 active site, and discusses earlier reported model

compounds of this enzyme and the mechanistic studies, aimed to elucidate the mechanism of catechol oxidation by the natural enzyme and by model complexes. Chapter 2 deals with the development of the strategy of the synthesis of dinucleating asymmetric ligands to model the asymmetry of the dicopper core, found in the natural enzyme,[8] and reports the crystal structure and properties of the asymmetric complex $[Cu_2(py3asym)(H_2O)_{1.5}(NO_3)_{2.5}](NO_3)_{0.5}$ (Hpy3asym = 2-[*N,N*-bis(2-pyridylmethyl)aminomethyl]-4-methyl-6-[(2-pyridylmethyl)aminomethyl]phenol. In Chapter 3 the crystal structures and properties of a number of Cu^{II}, Mn^{II} and Co^{II} complexes with the ligand Hpy2ald (Hpy2ald = 3-[*N,N*-di(2-pyridylmethyl)aminomethyl]-5-methylsalicylaldehyde), which has been prepared as an intermediate in the synthesis of the asymmetric ligand Hpy3asym are reported. In Chapter 4 the synthesis of the symmetric phenol-based ligand Hpy2th2s (Hpy2th2s = 2,6-bis[*N*-(2-pyridylmethyl)-*N*-(2-thiophenylmethyl)aminomethyl]-4-methylphenol), bearing thiophene and pyridine substituents, as well as the properties of its two dicopper(II) complexes and their interaction with catechol model substrates are described. This ligand was designed to model an unusual thioether bond, discovered in a close proximity to one of the copper ions in the active site of catechol oxidase.[8] In Chapter 5, the synthesis of the asymmetric phenol-based ligand Hpy2th1as (Hpy2th1as = 2-[*N,N*-bis(2-pyridylmethyl)aminomethyl]-4-methyl-6-[2-thiophenylmethyl)-aminomethyl]phenol), containing a tertiary amine arm with two pyridine substituents in the 2 position of the phenol ring, and a secondary amine arm bearing a thiophene ring in the 6 position of the phenol ring, is reported. Two copper(II) complexes, obtained with this ligand, have been crystallographically and spectroscopically characterized, and their structural properties are discussed.

In Chapter 6 the paramagnetic ^1H NMR spectroscopy on the monohydroxo-bridged dicopper(II) complex $[Cu_2[22]py4pz)(\mu\text{-}OH)](ClO_4)_3\cdot H_2O$ (**1**) with the macrocyclic N-donor ligand [22]py4pz (9,22-bis(2-pyridylmethyl)-1,4,9,14,17,22,27,28,29,30-decaazapentacyclo-[22.2.1.1^{4,7}.1^{11,4}.1^{17,20}]triacontane-5,7(28),11(29),12,18,20(30),24(27),25-octaene) and its magnetic properties are reported. The catecholase activity of this dicopper(II) complex, as well as the synthesis and characterization of its reduced dicopper(I) analogue $[Cu_2([22]py4pz)](ClO_4)_2\cdot 2CH_3OH$ (**2**) and the trans-μ-1,2-peroxo-dicopper(II) adduct (**3**), including 3D structure of **2**, are discussed in Chapter 7. These three compounds represent models of the three states of the catechol oxidase active site: *met*, *deoxy* (reduced) and *oxy*. The dicopper(II) complex **1** catalyzes the oxidation of catechol model substrates in aerobic conditions, while in the absence of dioxygen a stoichiometric oxidation takes place, leading to the formation of quinone and the respective dicopper(I) complex. The dicopper(I) complex binds molecular dioxygen at low temperature, forming a trans-μ-1,2-peroxo-dicopper adduct, which was characterized by UV-Vis and resonance Raman spectroscopy, and electrochemically.

This peroxo complex stoichiometrically oxidizes a second molecule of catechol in the absence of dioxygen. A catalytic mechanism of catechol oxidation by **1** is proposed, and its relevance to the mechanisms earlier proposed for the natural enzyme and other copper complexes is discussed.

In Chapter 8 the mechanism of catechol oxidation by a copper(II) complex with the macrocyclic ligand [22]pr4pz (9,22-dipropyl-1,4,9,14,17,22,27,28,29,30-decaazapentacyclo [22.2.1.1^{4,7}.1^{11,14}.1^{17,20}]triacontane-5,7(28),11(29),12,18,20(30),24(27),25-octaene), containing a carbonate bridge between the copper(II) ions, is discussed. The complex has a tetranuclear structure in the solid state, with one macrocyclic unit accommodating two carbonate-bridged copper(II) ions, and two copper(II) ions of two different macrocyclic units being further doubly bridged by two oxygen atoms of the two carbonate anions. This tetranuclear cluster was found dissociate into two dinuclear units in solution at the concentration range, used for the catecholase activity studies. The dinuclear complex catalyzes the oxidation of $DTBCH_2$ to the respective quinone in methanol by two different mechanisms, one proceeding via the formation of a semiquinone intermediate species with the subsequent production of dihydrogen peroxide as a by-product, and another proceeding via the two electrons reduction of the dicopper(II) center by the substrate, with two molecules of quinone and one molecule of water generated per one catalytic cycle. Chapter 9 presents general conclusions and an overview of the perspectives for further research.

Chapters 1-8 of this thesis have either been published[96,103-107] or submitted for publication.[108-110]

1.5 References

(1) Guckert, J. A.; Lowery, M. D.; Solomon, E. I. *J. Am. Chem. Soc.* **1995**, *117*, 2817-2844.
(2) Gray, H. B.; Malmström, B. G.; Williams, R. J. P. *J. Biol. Inorg. Chem.* **2000**, *5*, 551-559.
(3) Solomon, E. I.; Sundaram, U. M.; Machonkin, T. E. *Chem. Rev.* **1996**, *96*, 2563-2605.
(4) Solomon, E. I.; Baldwin, M. J.; Lowery, M. D. *Chem. Rev.* **1992**, *92*, 521-542.
(5) Ettinger, M. J. *Biochemistry* **1974**, *13*, 1242 - 1247.
(6) Solomon, E. I.; Hemming, B. L.; Root, D. E. *Bioinorganic Chemistry of Copper* **1993**, 3-20.
(7) Volbeda, A.; Hol, W. G. *J. Mol. Biol.* **1989**, *209*, 249-279.
(8) Klabunde, T.; Eicken, C.; Sacchettini, J. C.; Krebs, B. *Nat. Struct. Biol.* **1998**, *5*, 1084-1090.
(9) Piontec, K.; Antorini, M.; Choinowski, T. *J. Biol. Chem.* **2002**, *277*, 37663-37669.
(10) Claus, H. *Micron* **2004**, *35*, 93-96.
(11) Bertrand, T.; Jolivalt, C.; Briozzo, P.; Caminade, E.; Joly, N.; Madzak, C.; Mougin, C. *Biochemistry* **2002**, *41*, 7325-7333.
(12) Messerschmidt, A.; Rossi, A.; Ladenstein, R.; Huber, R.; Bolognesi, M.; Gatti, G.; Machesini, A.; Petruzzelli, R.; Finazzi-Agró, A. *J. Mol. Biol.* **1989**, *206*, 513-529.
(13) Musci, G. *Prot. Pept. Lett.* **2001**, *8*, 156-169.
(14) Lieberman, R. L.; Rosenzweig, A. C. *Nature* **2005**, *434*, 177-182.
(15) Itawa, S.; Ostermeier, C.; Ludwig, B.; Michel, H. *Nature* **1995**, *376*, 660-669.
(16) Tsukihara, T.; Aoyama, H.; Yamashita, E.; Tomizaki, T.; Yamaguchi, H.; Shinzawa-Itoh, R.; Nakashima, R.; Yaono, R.; Yoshikawa, S. *Science* **1995**, *269*, 1069-1074.
(17) Wilmanns, M.; Lappalainen, P.; Kelly, M.; Sauer-Eriksson, E.; Saraste, M. *Proc. Natl. Acad. Sci. USA* **1995**, *92*, 11955-11959.
(18) Kadenbach, B. *Angew. Chem. Int. Ed. Engl.* **1995**, *34*, 2635-2637.
(19) Brown, K.; Djinovic-Carugo, K.; Haltia, T.; Cabrito, I.; Saraste, M.; Moura, J. J. G.; Moura, I.; Tegoni, M.; Cambillau, C. *J. Biol. Chem.* **2000**, *275*, 41133-41136.
(20) Haltia, T.; Brown, K.; Tegoni, M.; Cambillau, C.; Saraste, M.; Mattila, K.; Djinovic-Carugo, K. *Biochem. J.* **2003**, *369*, 77-88.

(21) Brown, K.; Dijnovic-Carugo, K.; Haltia, T.; Cabrito, I.; Saraste, M.; Moura, J. J.; Moura, I.; Tegoni, M.; Cambillau, C. *J. Biol. Chem.* **2000**, *275*, 41133-41136.
(22) Colman, P. M.; Freeman, H. C.; Guss, J. M.; Murata, M.; Norris, V. A.; Ramshaw, J. A. M.; Venkatappa, M. P. *Nature* **1978**, *272*, 319-324.
(23) Ito, N.; Phillips, S.; Stevens, C.; Ogel, Z. B.; McPherson, M. J.; Keen, J. N.; Yadav, K. D. S.; Knowles, P. F. *Nature* **1991**, *350*, 87-90.
(24) Prudêncio, M.; Pereira, A. S.; Tavares, P.; Besson, S.; Cabrito, I.; Brown, K.; Samyn, B.; Devreese, B.; Cambillau, C.; Moura, I. *Biochemistry* **2000**, *39*, 3899-3907.
(25) Dervall, B. J. *Nature* **1961**, *189*, 311.
(26) Mayer, A. M.; Harel, E. *Phytochem.* **1979**, *18*, 193-215.
(27) Rompel, A.; Fischer, H.; Meiwes, D.; Buldt Karentsopoulos, K.; Dillinger, R.; Tuczek, F.; Witzel, H.; Krebs, B. *J. Biol. Inorg. Chem.* **1999**, *4*, 56-63.
(28) Jiang, Y. M.; Fu, J. r.; Zauberman, G.; Fuchs, Y. *J. Sci. Food Agric.* **1999**, *79*, 950-954.
(29) Gerdemann, C.; Eicken, C.; Krebs, B. *Acc. Chem. Res.* **2002**, *35*, 183-191.
(30) Eicken, C.; Zippel, F.; Büldt-Karentzopoulos, K.; Krebs, B. *FEBS Lett.* **1998**, *436*, 293-299.
(31) Rompel, A.; Fischer, H.; Büldt-Karentzopoulos, K.; Meiwes, D.; Zippel, F.; Nolting, H.-F.; Hermes, C.; Krebs, B.; Witzel, H. *J. Inorg. Biochem.* **1995**, *59*, 715.
(32) Kitajima, N.; Fujisawa, K.; Moro-oka, Y.; Toriumi, K. *J. Am. Chem. Soc.* **1989**, *111*, 8975-8976.
(33) Solomon, E. I.; Tuczek, F.; Root, D. E.; Brown, C. A. *Chem. Rev.* **1994**, *94*, 827-856.
(34) Lerch, K. *J. Biol. Chem.* **1982**, *257*, 6414-6419.
(35) Gielens, C.; de Geest, N.; Xin, X. Q.; Devreese, B.; van Beeumen, J.; Preaux, G. *Eur. J. Biochem.* **1997**, *248*, 879-888.
(36) Miller, K. I.; Cuff, M. E.; Lang, W. F.; Varga-Weisz, P.; Field, K. G.; van Holde, K. E. *J. Mol. Biol.* **1998**, *278*, 827-842.
(37) Cuff, M. E.; Miller, K. I.; van Holde, K. E.; Hendrickson, W. A. *J. Mol. Biol.* **1998**, *278*, 855-870.
(38) Wilcox, D. E.; Porras, A. G.; Hwang, Y. T.; Lerch, K.; Winkler, M. E.; Solomon, E. I. *J. Am. Chem. Soc.* **1985**, *107*, 4015-4027.
(39) Eicken, C.; Krebs, B.; Sacchettini, J. C. *Curr. Opin. Struct. Biol.* **1999**, *9*, 677-683.
(40) Siegbahn, P. E. M. *J. Biol. Inorg. Chem.* **2004**, *9*, 577-590.
(41) Siegbahn, P. E. M. *Q. Rev. Biophys.* **2003**, *36*, 91-145.
(42) Orville, A. M.; Lipscomb, J. D.; Ohlendorf, D. H. *Biochemistry* **1997**, *36*, 10052-10066.
(43) Lee, S.-K.; Lipscomb, J. D. *Biochemistry* **1999**, *38*, 4423-4432.
(44) Siegbahn, P. E. M. *J. Biol. Inorg. Chem.* **2003**, *8*, 567-576.
(45) Grinstead, R. R. *Biochemistry* **1964**, *3*, 1308-1314.
(46) Thuji, J.; Takayanagi, H. *J. Am. Chem. Soc.* **1974**, *96*, 7349-7350.
(47) Rogic, M. M.; Demmin, T. R. *J. Am. Chem. Soc.* **1978**, *98*, 7441-7443.
(48) Thuruya, S.; Lintvedt, R. L. 176th National Meeting of the American Chemical Society, Miami, Sept. 1978, 1978.
(49) Demmin, T. R.; Swerdloff, M. D.; Rogic, M. M. *J. Am. Chem. Soc.* **1991**, *103*, 5795-5804.
(50) Oishi, N.; Nishida, Y.; Ida, K.; Kida, S. *Bull. Chem. Soc. Jpn.* **1980**, *53*, 2847-2850.
(51) Malachowski, M. R. *Inorg. Chim. Acta* **1989**, *162*, 199-204.
(52) Casellato, U.; Tamburini, S.; Vigato, P. A.; de Stefani, A.; Vidali, M.; Fenton, D. E. *Inorg. Chim. Acta* **1983**, *69*, 45-51.
(53) Karlin, K. D.; Gultneh, Y.; Nicholson, T.; Zubieta, J. *Inorg. Chem.* **1985**, *24*, 3725-3727.
(54) Thompson, J. S.; Calabrese, J. C. *J. Am. Chem. Soc.* **1986**, *108*, 1903-1907.
(55) Speier, G. *New J. Chem.* **1994**, *18*, 143-147.
(56) Kodera, M.; Kawata, T.; Kano, K.; Tachi, Y.; Itoh, S.; Kojo, S. *Bull. Chem. Soc. Jpn.* **2003**, *76*, 1957-1964.
(57) Kaizer, J.; Pap, J.; Speier, G.; Parkanyi, L.; Korecz, L.; Rockenbauer, A. *J. Inorg. Biochem.* **2002**, *91*, 190-198.
(58) Chyn, J.-P.; Urbach, F. L. *Inorg. Chim. Acta* **1991**, *189*, 157-163.
(59) Balla, J.; Kiss, T.; Jameson, R. F. *Inorg. Chem.* **1992**, *31*, 58-62.
(60) Martell, A. E.; Motekaitis, R. J.; Menif, R.; Rockcliffe, D. A.; Llobet, A. *J. Mol. Cat. A* **1997**, *117*, 205-213.
(61) Rockcliffe, D. A.; Martell, A. E. *J. Chem. Soc., Chem. Commun.* **1992**, 1758-1760.
(62) Rockcliffe, D. A.; Martell, A. E. *Inorg. Chem.* **1993**, *32*, 3143-3152.
(63) Rockcliffe, D. A.; Martell, A. E. *J. Mol. Catal. A* **1995**, *99*, 87-99.
(64) Rockcliffe, D. A.; Martell, A. E. *J. Mol. Catal. A* **1995**, *99*, 101-114.
(65) Rockcliffe, D. A.; Martell, A. E. *J. Mol. Cat. A* **1996**, *106*, 211-221.
(66) Rockcliffe, D. A.; Martell, A. E.; Reibenspies, J. H. *J. Chem. Soc., Dalton Trans.* **1996**, 167-175.
(67) Monzani, E.; Battaini, G.; Perotti, A.; Casella, L.; Gullotti, M.; Santagostini, L.; Nardin, G.; Randaccio, L.; Geremia, S.; Zanello, P.; Opromolla, G. *Inorg. Chem.* **1999**, *38*, 5359-5369.

(68) Monzani, E.; Quinti, L.; Perotti, A.; Casella, L.; Gulotti, M.; Randaccio, L.; Geremia, S.; Nardin, G.; Faleschini, P.; Tabbi, G. *Inorg. Chem.* **1998**, *37*, 553-562.
(69) Monzani, E.; Casella, L.; Zoppellaro, G.; Gullotti, M.; Pagliarin, R.; Bonomo, R.; Tabbi, G.; Nardin, G.; Randaccio, L. *Inorg. Chim. Acta* **1998**, *282*, 180-192.
(70) Granata, A.; Monzani, E.; Casella, L. *J. Biol. Inorg. Chem.* **2004**, *9*, 903-913.
(71) Selmeczi, K.; Reglier, M.; Giorgi, M.; Speier, G. *Coord. Chem. Rev.* **2003**, *245*, 191-201.
(72) Selmeczi, K.; Reglier, M.; Speier, G.; Peintler, G. *React. Kinet. Catal. Lett.* **2004**, *81*, 143-151.
(73) Battaini, G.; Monzani, E.; Casella, L.; Santagostini, L.; Pagliarin, R. *J. Biol. Inorg. Chem.* **2000**, *5*, 262-268.
(74) Börzel, H.; Comba, P.; Pritzkow, H. *Chem. Commun.* **2001**, 97-98.
(75) Ackermann, J.; Meyer, F.; Kaifer, E.; Pritzkow, H. *Chem. Eur. J.* **2002**, *8*, 247-258.
(76) Berreau, L. M.; Mahapatra, S.; Halfen, J. A.; Houser, R. P.; Young, V. G.; Tolman, W. B. *Angew. Chem. Int. Ed. Engl.* **1999**, *38*, 207-210.
(77) Thompson, J. S.; Calabrese, J. C. *Inorg. Chem.* **1985**, *24*, 3167-3171.
(78) Reim, J.; Krebs, B. *J. Chem. Soc., Dalton Trans.* **1997**, 3793-3804.
(79) Wegner, R.; Gottschaldt, M.; Görls, H.; Jäger, E.-G.; Klemm, D. *Chem. Eur. J.* **2001**, *7*, 2143-2157.
(80) Mukherjee, J.; Mukherjee, R. *Inorg. Chim. Acta* **2002**, *337*, 429-438.
(81) Torelli, S.; Belle, C.; Hamman, S.; Pierre, J. L.; Saint-Aman, E. *Inorg. Chem.* **2002**, *41*, 3983-3989.
(82) Plenge, T.; Dillinger, R.; Santagostini, L.; Casella, L.; Tuczek, F. *Z. Anorg. Allg. Chem.* **2003**, *629*, 2258-2265.
(83) Neves, A.; Rossi, L. M.; Bortoluzzi, A. J.; Szpoganicz, B.; Wiezbicki, C.; Schwingel, E.; Haase, W.; Ostrovsky, S. *Inorg. Chem.* **2002**, *41*, 1788-1794.
(84) Gupta, M.; Mathur, P.; Butcher, R. J. *Inorg. Chem.* **2001**, *40*, 878-885.
(85) Speier, G.; Tisza, S.; Tyeklár, Z.; Lange, C. W.; Pierpont, C. G. *Inorg. Chem.* **1994**, *33*, 2041-2045.
(86) Benelli, C.; Dei, A.; Gatteschi, D.; Pardi, L. *Inorg. Chem.* **1990**, *29*, 3409-3415.
(87) Zippel, F.; Ahlers, F.; Werner, R.; Haase, W.; Nolting, H.-F.; Krebs, B. *Inorg. Chem.* **1996**, *35*, 3409-3419.
(88) Than, R.; Feldmann, A. A.; Krebs, B. *Coord. Chem. Rev.* **1999**, *182*, 211-241.
(89) Kao, C.-H.; Wei, H.-H.; Liu, Y.-H.; Lee, G.-H.; Wang, Y.; lee, C.-J. *J. Inorg. Biochem.* **2001**, *84*, 171-178.
(90) Belle, C.; Beguin, C.; Gautier-Luneau, I.; Hamman, S.; Philouze, C.; Pierre, J. L.; Thomas, F.; Torelli, S.; Saint-Aman, E.; Bonin, M. *Inorg. Chem.* **2002**, 479-491.
(91) Torelli, S.; Belle, C.; Gautier-Luneau, I.; Pierre, J. L.; Saint-Aman, E.; Latour, J. M.; Le Pape, L.; Luneau, D. *Inorg. Chem.* **2000**, *39*, 3526-3536.
(92) Gao, J.; Reibenspies, J. H.; Martell, A. E. *Inorg. Chim. Acta* **2003**, *346*, 67-75.
(93) Merkel, M.; Möller, N.; Piacenza, M.; Grimme, S.; Rompel, A.; Krebs, B. *Chem. Eur. J.* **2005**, *11*, 1201-1209.
(94) Fernandes, C.; Neves, A.; Bortoluzzi, A. J.; Mangrich, A. S.; Rentschler, E.; Szpoganicz, B.; Schwingel, E. *Inorg. Chim. Acta* **2001**, *320*, 12-21.
(95) Gentschev, P.; Feldmann, A. A.; Lüken, M.; Möller, N.; Sirges, H.; Krebs, B. *Inorg. Chem. Comm.* **2002**, *5*, 64-66.
(96) Koval, I. A.; Huisman, M.; Stassen, A. F.; Gamez, P.; Roubeau, O.; Belle, C.; Pierre, J. L.; Saint-Aman, E.; Luken, M.; Krebs, B.; Lutz, M.; Spek, A. L.; Reedijk, J. *Eur. J. Inorg. Chem.* **2004**, 4036-4045.
(97) Thirumavalavan, M.; Akilan, P.; Kandaswamy, M.; Kandaswamy Chinnakali; Senthil Kumar, G.; Fun, H. K. *Inorg. Chem.* **2003**, *42*, 3308-3317.
(98) Battaini, G.; Casella, L.; Gullotti, M.; Monzani, E.; Nardin, G.; Perotti, A.; Randaccio, L.; Santagostini, L.; Heinemann, F. W.; Schindler, S. *Eur. J. Inorg. Chem.* **2003**, 1197-1205.
(99) Speier, G.; Tyeklar, Z.; Tóth, P.; Speier, G.; Tisza, S.; Rockenbauer, A.; Whalen, A. M.; Alkire, N.; Pierpont, C. G. *Inorg. Chem.* **2001**, *40*, 5653-5659.
(100) Kitajima, N.; Koda, T.; Iwata, Y.; Moro-oka, Y. *J. Am. Chem. Soc.* **1990**, *112*, 8833-8839.
(101) Santagostini, L.; Gulotti, M.; Monzani, E.; Casella, L.; Dillinger, R.; Tuczek, F. *Chem. Eur. J.* **2000**, *6*, 519-522.
(102) Mahadevan, V.; Dubois, L.; Hedman, B.; Hodgson, K. O.; Stack, T. D. *J. Am. Chem. Soc.* **1999**, *121*, 5583-5584.
(103) Koval, I. A.; Belle, C.; Selmeczi, K.; Philouze, C.; Saint-Aman, E.; Schuitema, A. M.; Gamez, P.; Pierre, J.-L.; Reedijk, J. *J. Biol. Inorg. Chem.* **2005**, *10*, 739-750.
(104) Koval, I. A.; Pursche, D.; Stassen, A. F.; Gamez, P.; Krebs, B.; Reedijk, J. *Eur. J. Inorg. Chem.* **2003**, 1669-1674.

(105) Koval, I. A.; Huisman, M.; Stassen, A. F.; Gamez, P.; Lutz, M.; Spek, A. L.; Reedijk, J. *Eur. J. Inorg. Chem.* **2004**, 591-600.
(106) Koval, I. A.; Huisman, M.; Stassen, A. F.; Gamez, P.; Lutz, M.; Spek, A. L.; Pursche, D.; Krebs, B.; Reedijk, J. *Inorg. Chim. Acta* **2004**, *357*, 294-300.
(107) Koval, I. A.; van der Schilden, K.; Schuitema, A. M.; Gamez, P.; Belle, C.; Pierre, J.-L.; Luken, M.; Krebs, B.; Roubeau, O.; Reedijk, J. *Inorg. Chem.* **2005**, *44*, 4372-4382.
(108) Koval, I. A.; Gamez, P.; Belle, C.; Selmeczi, K. *Chem. Soc. Rev.*, submitted for publication.
(109) Koval, I. A.; Selmeczi, K.; Belle, C.; Philouze, C.; Saint-Aman, E.; Gautier-Luneau, I.; Schuitema, A. M.; van Vliet, M.; Gamez, P.; Roubeau, O.; Lüken, M.; Krebs, B.; Lutz, M.; Spek, A. L.; Pierre, J.-L.; Reedijk, J. *Chem. Eur. J.*, submitted for publication.
(110) Koval, I. A.; Sgobba, M.; Huisman, M.; Lüken, M.; Saint-Aman, E.; Gamez, P.; Krebs, B.; Reedijk, J. *New J. Chem*, submitted for publication.

2 Synthetic route to novel asymmetric dinucleating ligands. Crystal structure and properties of the complex $[Cu_2(py3asym)(H_2O)_{1.5}(NO_3)_{2.5}](NO_3)_{0.5}$ †

In this chapter the synthesis of the new asymmetric ligand 2-[*N,N*-bis(2-pyridylmethyl)aminomethyl]-4-methyl-6-[(2-pyridylmethyl)aminomethyl]phenol (Hpy3asym), which was conceived to model the asymmetry in the active site of catechol oxidase, is reported. This phenol-based "end-off" compartmental ligand holds one tridentate and one didentate arm attached to the 2 and 6 positions of the phenolic ring. A dinuclear copper(II) nitrate complex with this ligand $[Cu_2(py3asym)(H_2O)_{1.5}(NO_3)_{2.5}](NO_3)_{0.5}$ has been obtained and structurally characterized. In this complex both copper ions have a distorted octahedral geometry and are endogenously bridged by the phenolic oxygen atom of the deprotonated ligand. The complex shows a donor-atom asymmetry that consists of a N_3O_3 donor set for the Cu1 ion and a N_2O_4 donor set for the Cu2 ion. The spectral properties of the complex, as well as its electrochemical and magnetic behavior, are discussed.

---

†This chapter is based on: Koval, I. A., Pursche, D., Stassen, A. F., Gamez, P., Krebs, B. and Reedijk, J., Eur. J. Inorg. Chem., 2003, 1669-1674

2.1 Introduction

The term "dinucleating ligands" was first introduced in 1970 by Robson[1] to describe a class of polydentate chelating ligands, able to bind simultaneously two metal ions. Since then, a very large number of such ligands were designed, and their coordination compounds were thoroughly investigated. The possible applications of the complexes with this type of ligands vary from modeling the active sites of many metalloenzymes,[2-4] to hosting and carrying small molecules[5-7] or homogeneous catalysis.[8,9]

Among many different types of dinucleating ligands, the phenol-based compartmental ligands attracted particularly wide attention of scientists. The term "compartmental" was introduced to indicate a ligand containing two adjacent, but dissimilar coordination sites.[2] Particular interest in this type of ligands resulted from the recent recognition of the asymmetric nature of a number of dimetallic biosites.[10,11] The understanding of the ability of individual metal ions to play possibly different functions in dinuclear sites in metalloenzymes led to the design of a large number of asymmetric ligands where two compartments would provide a different coordination surrounding for the two metal ions.

As stated in Chapter 1, the active site of catechol oxidase is asymmetric, which led to the proposal that during the catalytic cycle, the binding of the substrate occurs to only one of the metal centers (CuB). Taking the inspiration from the natural molecule, the attention has been turned to the deliberate design of novel model systems of the type-3 active site, where the two copper ions would have distinctly different coordination surroundings. The site specificity of the copper ions may help to answer an important question concerning the binding of the substrate in the natural enzyme, *e.g.* is the catechol substrate forming a bridge between the two copper(II) centers rather than binding to only one of them?

In this chapter, the synthesis of the novel phenol-based ligand 2-[*N,N*-bis(2-pyridylmethyl)aminomethyl]-4-methyl-6-[(2-pyridylmethyl)aminomethyl]phenol, Hpy3asym, is described. In this ligand, the 2 and the 6 positions of the phenol-ring are substituted by a tridentate and a didentate arm containing nitrogen donor atoms, providing two copper ions with different coordination surroundings. The crystal structure, spectroscopy, electrochemical and magnetic behavior of a new asymmetric dicopper(II) complex with this ligand are reported.

2.2 Results and Discussion

2.2.1 Synthesis

The ligand Hpy3asym has been synthesized in four steps (Figure 2.1) from commercially available 5-methylsalicylaldehyde. The first step includes the introduction of a methylene chloride group in the 3' position of the phenol ring. The chloride atom is

subsequently substituted by di-(2-picolyl)amine. Finally, the reductive amination of the aldehyde group by 2-aminomethylpyridine and sodium borohydride leads to the desired ligand.

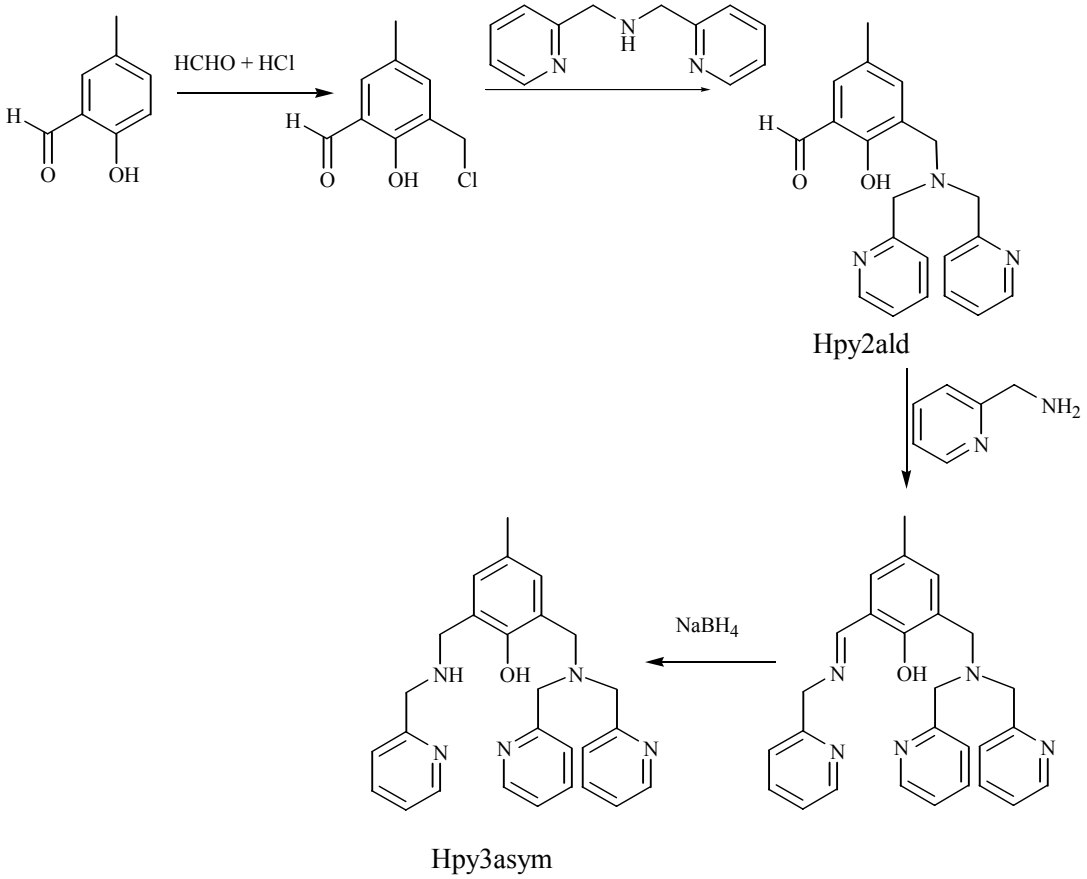

Figure 2.1. The reaction scheme of the synthesis of the phenol-based compartmental "end-off" ligand Hpy3asym

The straightforward synthetic pathway, developed for the synthesis of Hpy3asym, can also be successfully applied for the preparation of other dinucleating asymmetric ligands, with variations in the number and type of the donor atoms, as reported elsewhere.[12]

The dicopper(II) complex $[Cu_2(py3asym)(H_2O)_{1.5}(NO_3)_{2.5}](NO_3)_{0.5}$ (**1**) has been prepared by mixing one molar equivalent of the ligand with two equivalents of copper(II) nitrate in an acetonitrile/water mixture. The evaporation of the solvent and washing of the residue with small amounts of acetone resulted in the pure compound.

2.2.2 Crystal structure description

Very small green rectangular crystals of **1** have been obtained by slow evaporation of an acetonitrile solution of the complex. An ORTEP projection of the complex is depicted in Figure 2.2 (left), selected bond lengths and bond angles are given in Table 2.1. The compound crystallizes in the space group $P2_1/n$. Both copper ions have specifically different coordination surroundings, showing a donor-atom

asymmetry. An endogenous phenolato bridge is present in the dinuclear core, but no exogenous bridge is present. The N_3O_3 coordination sphere around the Cu1 ion can be regarded as a very distorted octahedron. The equatorial plane is formed by the tertiary amine nitrogen atom N1 at a distance of 2.0182(18) Å, two *trans* located nitrogen atoms N2 and N3 from two pyridine rings at a distance of 1.9860(17) Å and 1.9760(18) Å, respectively, and the oxygen atom O2 from a water molecule at a distance of 1.9701(16) Å. One of the axial positions is occupied by the bridging phenolate oxygen atom O1 at a relatively long distance of 2.3070(13) Å. The second apical position has a weak O-donor ligand, which was refined for 50% to be water and for 50% a disordered nitrate anion. The oxygen atom O20 (occupancy 0.4886) from the water molecule is at a distance of 2.535(3) Å. The loosely bound oxygen atom O10 (occupancy 0.5114) from the disordered nitrate counter anion (the Cu1-O10a distance is 3.007(6) Å) is at a much larger distance, which, however, still matches the range of bond lengths observed for copper-oxygen bonds along the Jahn-Teller axis.[13-16] The in-plane *cis* angles around the Cu1 ion vary in quite a broad range, *viz.* 83.92(8)º for the N1-Cu1-N3 angle and 96.92(7)º for the O2-Cu1-N2 angle. Their sum amounts to 357.76º. The O-Cu1-O angle along the Jahn-Teller axis is equal to 173.85(8)º for the O1-Cu1-O20 angle and 165.46(10)º for the O1-Cu1-O10 angle, thus indicating a significant distortion from the regular octahedral geometry.

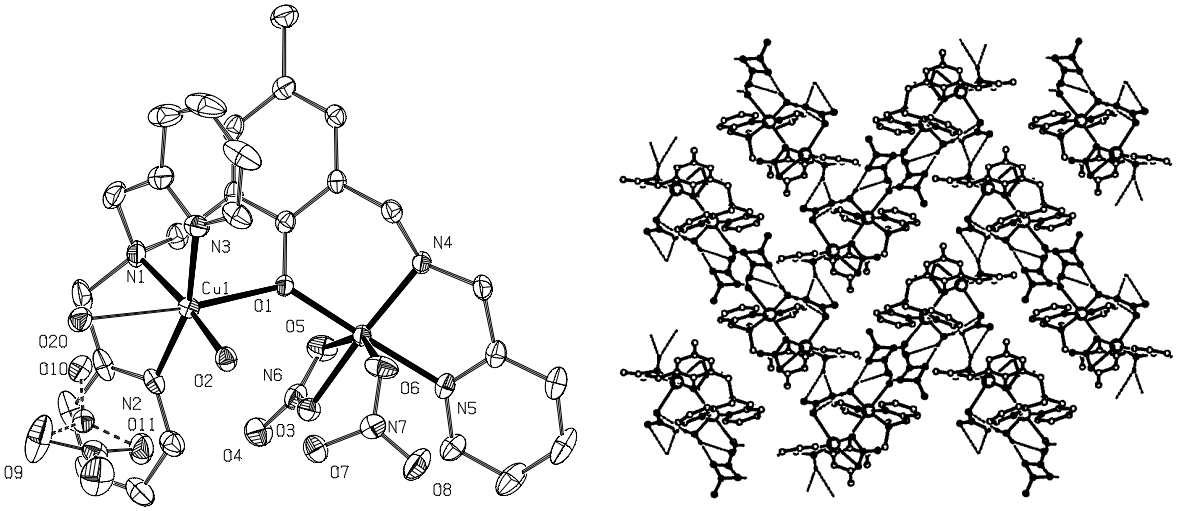

Figure 2.2. Left: ORTEP projection of $[Cu_2(py3asym)(H_2O)_{1.5}(NO_3)_{2.5}](NO_3)_{0.5}$ (**1**). The hydrogen atoms are omitted for clarity. The second axial position at Cu1 ion has a O-donor ligand, which was found in 50% to be water and in 50% a disordered nitrate anion (see text for further details). Right: PLATON[17] projection of a "herring-bone" packing arrangement along the crystallographic *a* axis. All hydrogen atoms, besides those participating in hydrogen bonding, are omitted.

The absence of an exogenous bridge between the two copper ions promotes the large copper-copper separation of 3.9003 Å, which is significantly longer than the distances observed for the similar complexes with two types of bridges between the copper ions.[5,9,18,19] It is interesting to notice that potentially bridging nitrate anions are

present in the complex; however, they fail to bridge the two copper ions, instead being coordinated as monodentate and didentate chelating ligands. The distribution of charged and neutral ligands in the complex is also remarkable: one neutral water molecule is coordinated to the Cu1 ion, whereas two charged nitrate anions are coordinated to the Cu2 ion.

Table 2.1. Selected bond distances and bond angles for **1**

Bond lengths (Å)			
Cu1 – O2	1.9700(16)	Cu2 – N4	1.9841(17)
Cu1 – N3	1.9767(19)	Cu2 – N3	1.9907(15)
Cu1 – N2	1.9866(18)	Cu2 – N5	2.0167(17)
Cu1 - O1	2.3069(14)	Cu2 – O5	2.5438(16)
Cu1 – O20	2.548(3)	Cu2 – O6	2.5985(17)
Cu1 – O10	3.010(3)	Cu2 – O1	1.9357(14)

Bond angles (º)			
Cu1 – O21 – Cu2	133.49(7)		
O2 – Cu1 – N2	96.92 (7)	O1 – Cu2 – N4	94.66(6)
N3 – Cu1 – N2	163.36(8)	O1 – Cu2 – O3	90.71(6)
O2 – Cu1 – N1	84.46(8)	N4 – Cu2 – O3	170.49(7)
N2 – Cu1 – N1	83.88(8)	O1 – Cu2 – N5	172.59(7)
O2 – Cu1 – O1	96.90(6)	N4 – Cu2 – N5	82.45(7)
N3 – Cu1 – O1	90.21(6)	O3 – Cu2 – O5	93.13(7)
N2 – Cu1 – O1	102.18(6)	O1 – Cu2 – O5	87.36(6)
N1 – Cu1 – O1	92.85(6)	N4 – Cu2 – O5	116.56(7)
O2 – Cu1 – O20	87.70(9)	O1 – Cu2 – O6	95.52(6)
N2 – Cu1 – O20	81.22(9)	N4 – Cu2 – O6	85.63(6)
O1 – Cu1 – O20	173.85(8)	O3 – Cu2 – O6	101.68(5)
O2 – Cu1 – O10	71.82(8)	N5 – Cu2 – O6	77.49(6)
N3 – Cu1 – O10	98.72(8)	O5 – Cu2 – O6	157.38(5)
N1 – Cu1 – O20	82.36(9)		
N3 – Cu1 – O20	85.50(9)		
N3 – Cu1 – O10	98.72(8)		
N2 – Cu1 – O10	71.50(8)		
N1 – Cu1 – O10	98.97(8)		
O1 – Cu1 – O10	165.78(7)		
O20 – Cu1 – O10	20.35(8)		

The coordination sphere around the second copper ion Cu2 can also be described as a distorted octahedron, but with a N_2O_4 donor set. The equatorial plane around the Cu2 ion is formed by two *cis* located nitrogen atoms N4 from the secondary amine (the Cu2-N4 distance is 1.9838(17) Å) and N5 from the pyridine ring (the Cu2-N5 distance is 2.0181(17) Å), and two *cis* oxygen atoms, O1 from the bridging phenolate (the Cu2-O1 distance is 1.9353(14) Å) and O3 from the chelating nitrate

anion (the Cu2-O3 distance is 1.9910(14) Å). The second oxygen atom O5 from the chelating nitrate anion and the oxygen atom O6 from the monocoordinated nitrate anion occupy the axial positions, thus adjusting the coordination sphere around the copper ion to a very distorted octahedron (the distances Cu2-O5 and Cu2-O6 are equal to 2.5431(16) Å and 2.5982(16) Å, respectively). The in-plane *cis* angles vary in the range 87.36º-94.64º. The angle O5-Cu2-O6, which should be equal to 180º in the regular octahedron, is only 157.37(5)º, indicating an even greater distortion from the regular octahedron geometry than observed in the case of the Cu1 ion.

The crystal packing is stabilized by an extensive net of intra- and intermolecular hydrogen bonds (see Table 2.2). In particular, a bifurcated intramolecular hydrogen bonding is realized between the proton H2b of the water molecule coordinated to the Cu1 ion and the two oxygen atoms O6 and O7 of the monodentate nitrate anion coordinated to the Cu2 ion, giving an impression of exogenous pseudo-bridge between the two copper ions. Furthermore, each formula unit is connected via intermolecular hydrogen bonds to three neighboring units. The PLATON[17] projection of the crystal packing along the crystallographic *a* axis is shown in Figure 2.2 (right). As can be seen, the molecules are assembled by means of hydrogen bonds to form a "herring-bone" pattern.

Table 2.2. Hydrogen bonds (D-H…A) with the distance H…A < r(A) + 2.000 Å and the angle DHA > 110°.

Donor - H.....Acceptor	*D – H (Å)*	*H...A (Å)*	*D...A (Å)*	*D - H...A (º)*
O2 - H2a...O11	0.736	1.971	2.704	174.09
O2 - H2a...O10	0.736	2.518	3.026	127.91
O2 - H2b...O7	0.915	1.802	2.657	154.44
O2 - H2b...O6	0.915	2.448	3.245	145.50
N4 - H4...O7 [x-1/2,-y+1/2,z-1/2]	0.930	2.119	2.917	143.16
O20 - H20a...O9 [-x,-y,-z+1]	0.759	2.087	2.821	163.07
O20 - H20b...O9	0.999	2.010	2.985	164.96
O20 - H20b...O11	0.999	2.486	3.191	127.27

2.2.3 Physical characterization

Besides the crystal structure determination, the complex has been spectroscopically and magnetically characterized. Electrospray mass spectra (ESI-MS) of the complex performed in acetonitrile reveal one major peak at *m/z* 688, corresponding to $[Cu_2(py3asym)(NO_3)_2]^+$. The theoretical isotopic pattern calculated for the empirical formula $C_{27}H_{28}Cu_2N_7O_7$ is in agreement with the experimentally found one. Thus, the 1.5 water molecules coordinated to the Cu1 ion, observed in the solid state, are lost during the measurement. The UV-Vis spectrum of the solid exhibits two

peaks at 456 and 640 nm. The first peak is assigned to a LMCT transition between the bridging phenoxo group and copper ions,[9] whereas the second one is characteristic for Cu^{II} d-d transitions.[20] The positions of these bands do not significantly change when the spectrum of the complex is taken in acetonitrile solution, suggesting no important modifications in the copper-ligand chromophores.

A cyclic voltammogram of the complex recorded in acetonitrile, when scanning towards the negative region of potentials, shows two successive one-electron electrochemical signals. The first one at -0.13 V *vs.* Ag/AgCl is assigned to the $Cu^{II,II}{}_2/Cu^{II,I}{}_2$ redox-couple. The second one at -0.33 V is attributed to the formation of $Cu^{I,I}{}_2$ species. They both appear to be irreversible. In addition, a very broad peak at ca. -0.7 V suggests the reduction of both copper ions to Cu^0 and the deposit of the free metal on the electrode surface. On the reverse scan, an additional sharp anodic peak is observed at -0.27 V. This is the so-called stripping peak, caused by the redissolution of the metallic copper. This peak is absent if the potential sweep is reversed at ca. -0.5 V, before the reduction to Cu^0 could take place. The anodic part of the cyclic voltammogram is characterized by three successive fully irreversible oxidation waves at 1.16, 1.48 and 1.68 V, apparently corresponding to the oxidation of the ligand and/or water molecules.

2.2.4 Magnetic properties

In Figure 2.3, the magnetic susceptibility of **1** is shown, plotted as both χ^{-1} and χ versus the temperature. The compound displays a weak ferromagnetic coupling with a Curie temperature θ of 0.87 K and a Curie-Weiss constant C of 0.39 cm^3 K mol^{-1}. The value for μ is 1.10 B.M.

The magnetic properties of this dinuclear copper(II) complex have been interpreted in terms of the Bleaney-Bowers equation (2.1),[21] where g is the magnetic field splitting factor, J is the exchange integral of magnetic theory and TIP is a Temperature Independent Paramagnetism term of 1 mole of copper(II) ions.

$$\chi_M = \frac{2g^2N\beta^2}{kT\,[3 + exp\,(-J/kT)]} + TIP \qquad (2.1)$$

The fit was accomplished by minimization of the reliability factor, defined as $R = \Sigma(\chi_m T_{calc} - \chi_m T_{obs})^2/(\chi_m T_{obs})^2$, by a least-squares procedure. The best fit was obtained for the exchange integral J = -4.6 cm^{-1}, the magnetic field splitting factor g = 2.02 and $R = 2.9\times10^{-3}$.

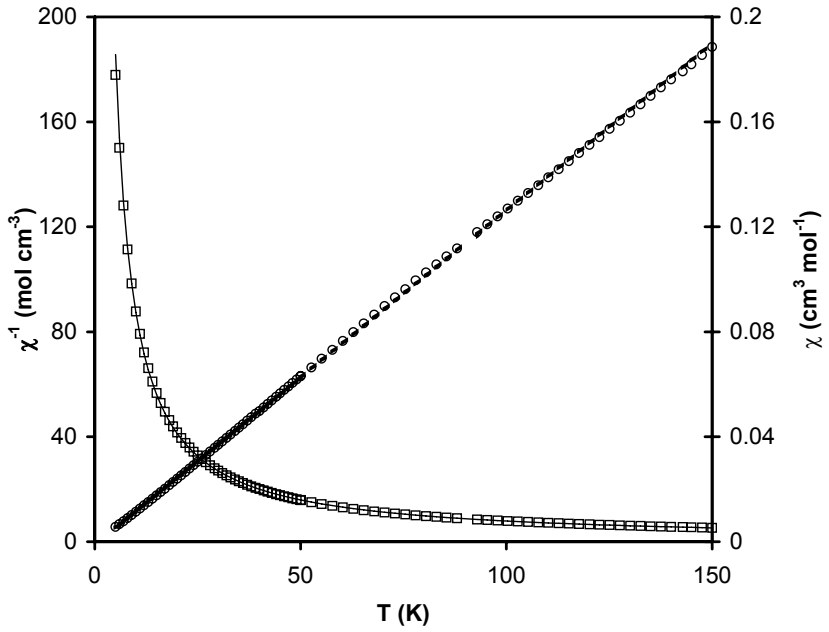

Figure 2.3. Magnetic susceptibility plotted as χ^{-1} versus *T;* (O) and as χ versus T; (□). The dashed line is the Curie-Weiss plot from near field theory, the solid line is the theoretical curve according to the Bleaney-Bowers equation.

2.2.5 Relevance to the active site of catechol oxidase

Similarly to the *met* state of natural enzyme, the dicopper(II) core in the complex comprises a single bridging oxygen atom, provided by the deprotonated phenolate moiety of the ligand. However, the two metal ions are being held on a long distance of 3.9003 Å, which is significantly larger than 2.9 Å, the Cu…Cu distance reported for the *met* form of catechol oxidase.[10] In addition, although the ligand has been designed to yield a coordination number asymmetry at the dimetal core, with its two pendant arms providing, respectively, three and two nitrogen donor atoms for coordination, it can be seen that each copper ion is coordinated by six donor atoms, with the coordination sphere being completed to a distorted octahedral surrounding by counter ions and solvent molecules. The complex shows thus a donor atom asymmetry instead, and its structure only vaguely resembles that of the natural enzyme, in which both copper ions have a distorted trigonal pyramidal coordination sphere with an N_3O donor set (see Chapter 1). However, the developed synthetic pathway for the synthesis of this ligand and other asymmetric dinucleating compartmental ligands opens new possibilities for the design of new model systems and allows easy variations in the number and the type of donor atoms surrounding each metal ion (Chapters 3-5). It should also be noted that the presence of other potentially bridging ligands, *e.g.* hydroxide anions, may lead to a significantly shorter metal-metal distances in the dicopper core, making the respective complexes promising functional models of catechol oxidase.

2.3 Experimental Section

2.3.1 Materials and Methods

Most of the synthetic work was carried out using standard Schlenk techniques. All chemicals were commercially available and used without further purification. 5-methylsalicylaldehyde was purchased from Fluka, 2-(aminomethyl)pyridine from Acros, and di-(2-picolyl)amine from Aldrich. 3-chloromethyl-5-methylsalicylaldehyde was prepared according to the procedure described by Lock.[22] Tetrahydrofuran and methanol were dried by reflux over sodium. C,H,N determinations were performed on a Perkin Elmer 2400 Series II analyzer. NMR spectra were recorded on a JEOL FX-200 (200MHz) FT-NMR spectrometer. Solid-state ligand field spectra (300-2000 nm, diffuse reflectance) and in solution were taken on a Perkin-Elmer 330 spectrophotometer equipped with a data station. IR spectra were recorded as pure solid on a Perkin Elmer FT-IR Paragon 1000 spectrophotometer with a Specac single-reflection diamond ATR P/N 10500, using the diffuse reflectance technique (4000-300 cm^{-1}, res. 4 cm^{-1}). Electrospray mass spectra (ESI-MS) were recorded on the Thermo Finnigan AQA apparatus. Cyclic voltammetry measurements were performed with an Autolab PGSTAT 10 cyclic voltammeter, using a Pt working electrode and a Ag/AgCl reference electrode in acetonitrile (10^{-3} M), with tetrabutylammonium perchlorate as supporting electrolyte, at a scan rate of 0.1 V/s. DC magnetic susceptibility measurements (5-150 K) were carried out at 0.1 Tesla using a Quantum Design MPMS-5 5T SQUID magnetometer. Data were corrected for magnetisation of the sample holder and for diamagnetic contributions, which were estimated from the Pascal constants.

2.3.2 Ligand synthesis

3-[*N,N*-bis(2-pyridylmethyl)aminomethyl]-5-methylsalicylaldehyde (Hpy2ald): A solution of di-(2-picolyl)amine (1.08 g, 5.4 mmol) and triethylamine (1.09 g, 10.8 mmol) in 50 ml of dry THF was added dropwise upon stirring to a solution of 3-chloromethyl-5-methylsalicylaldehyde (1 g, 5.4 mmol) in 250 ml of dry THF under Ar atmosphere. After completion of the addition, the resulting white suspension was refluxed for two hours and cooled to room temperature. After the removal of the triethylamine hydrochloride salt by filtration, the resulting solution was evaporated under reduced pressure, yielding a yellow oil, from which the product crystallized within a few minutes. The recrystallization from methanol-diethyl ester mixture gave slightly yellowish crystals of the pure compound. Yield: 1.55 g, 4.5 mmol (82%). ^{1}H-NMR ($CDCl_3$, 200 MHz, ppm): δ = 10.42 (s, 1H, aldehyde proton), 8.56 (d, 2H, 6'py-H); 7.63 (td, 2H, 4'py-H); 7.40 (td, 2H, 5'py-H); 7.21(s, 1H, 6'phenol-H); 7.18 (d, 2H, 3'py-H); 7.13 (s, 1H, 4'phenol-H); 3.89 (s, 4H, N-(CH_2py)$_2$); 3.80 (s, 2H, phenol-CH_2-N); 2.23 (s, 3H, CH_3) .

2-(bis(2-pyridylmethyl)aminomethyl)-4-methyl-6-[(2-pyridylmethyl)iminomethyl]phenol: A solution of 2-pyridylmethylamine (0.39 g, 3.6 mmol) in 50 ml of dry methanol was added dropwise upon stirring to a solution of Hpy2ald (1.26 g, 3.6 mmol) in 250 ml of dry methanol under argon. After the addition was complete, the resulting bright yellow solution was heated for two hours at 50 °C. The successful formation of the imine derivative was verified by NMR. ^{1}H NMR ($CDCl_3$, 200 MHz, ppm): δ = 8.51 (d, 3H, 6'py-H); 8.34 (s, 1H, CH=N); 7.62 (td, 3H, 4'py-H); 7.33 (t, 3H, 5'py-H); 7.26(d, 2H, 3'py-H); 7.09 (s, 1H, 3'phenol-H); 7.03 (2, 1H, 5'phenol-H); 4.92 (s, 2H, CH=N-CH_2) 3.88 (s, 4H, N-(CH_2py), 3.80 (s, 2H, phenol-CH_2-N); 2.29 (s, 3H, CH_3).

2-[bis(2-pyridylmethyl)aminomethyl]-4-methyl-6-[(2-pyridylmethyl)aminomethyl]phenol (Hpy3asym): 0.41 g (10.9 mmol, 3 eq/1CH=N) of $NaBH_4$ were added *in situ* to a solution of 2-(bis(2-pyridylmethyl)aminomethyl-4-methyl-6-[(2-pyridylmethyl)iminomethyl]phenol in methanol. After the hydrogen evolution stopped, the resulting colorless solution was refluxed for two hours and evaporated under reduced pressure. The residue was dissolved in acidified water and washed three times with dichloromethane. The water layer was made alkaline (pH~9) by addition of concentrated ammonia. The resulting white suspension was extracted three times with dichloromethane. The organic layers were collected and dried over Na_2SO_4. After evaporation under reduced pressure, the pure compound was obtained as clear yellow oil. Yield: 1.54 g, 3.5 mmol (96%). ^{1}H NMR ($CDCl_3$, 200 MHz, ppm): δ = 8.55 (d, 3H, 6'py-H); 7.59 (td, 3H, 4'py-H); 7.36 (d, 3H, 3'py-H); 7.14 (t, 3H, 5'py-H); 6.93 (s, 1H, 3'phenol-H); 6.84 (s, 1H, 5'phenol-H); 3.95 (s, 2H, NH-CH_2-py); 3.91 (s, 2H, phenol-CH_2-NH); 3.85 (s, 4H, N-(CH_2-py)$_2$); 3.75 (s, 2H, phenol-N-CH_2); 2.22 (s, 3H, CH_3). ^{13}C NMR ($CDCl_3$, 200 MHz, ppm): δ = 159.35; 154.80; 147.32; 136.17; 128.35; 126.35; 124.00; 123.11; 122.85; 121.67; 59.06; 56.12; 54.65; 50.95; 26.22.

2.3.3 Synthesis of $[Cu_2(py3asym)(H_2O)_{1.5}(NO_3)_{2.5}](NO_3)_{0.5}$ (1)

The bulk sample was prepared by dissolving 0.076 g (0.17 mmol) of Hpy3asym and 0.09 g (0.37 mmol) of $Cu(NO_3)_2{\cdot}3H_2O$ in 10 ml of an acetonitrile-water mixture (1:1). The resulting solution was stirred for one hour at room temperature and evaporated till dryness under reduced pressure. After washing with a small amount of acetone, 0.08 g (0.1 mmol, 59% yield) of the pure compound was obtained as a dark green powder. Elemental analysis, % found (calc.) for $[Cu_2(py3asym)(H_2O)_{1.5}(NO_3)_{2.5}](NO_3)_{0.5}$ (=$C_{27}H_{31}Cu_2N_8O_{11.5}$): C, 41.3 (41.7); H, 4.0 (3.9); N, 14,4 (14.7). MS(ESI): *m/z* 688 ($[Cu_2(py3asym)(NO_3)_2]^+$). IR: 3600-3200, broad band (H_2O, asymmetric and symmetric OH stretching), 3184 (N-H stretching), 1613 (HOH bending), 1484 (chelating didentate NO_3^-, N=O stretching), 1396 (monodentate NO_3^-, NO_2 asymmetric stretching), 1290 (monodentate NO_3^-, symmetric NO_2 stretching, and chelating didentate NO_3^-, asymmetric NO_2 stretching).[23]

Single crystals of the complex, suitable for X-ray crystal structure determination, were obtained by slow evaporation of an acetonitrile solution containing stoichiometric amounts of $Cu(NO_3)_2 \cdot 3H_2O$ and the ligand.

2.3.4 X-ray crystallographic measurements

A single crystal of $[Cu_2(py3asym)(H_2O)_{1.5}(NO_3)_{2.5}](NO_3)_{0.5}$ was mounted at 100 K on a Bruker AXS SMART 6000 diffractometer equipped with Cu-Kα radiation (λ = 1.54184 Å). $C_{27}H_{31}Cu_2N_8O_{11.5}$, Fw = 778.68 g mol^{-1}, rectangular green needles, 0.17×0.08×0.07 mm^3, a = 10.3731(2) Å, b = 22.1430(4) Å, c = 14.2325(2) Å, β =105.709(10)°, Z = 4, V = 3146.98(9) $Å^3$, $\rho_{calc.}$ = 1.644 g cm^{-3}, μ = 2.322 cm^{-1}, absorption correction: SADABS,[24] monoclinic, space group $P2_1/n$ (no. 14), reflections collected: 18421, independent reflections: 5871 (R_{int} = 0.0314). The structure was solved by direct methods and refined using the SHELX program package.[25,26] All hydrogen atoms were placed on idealized positions riding on the carrier atom, with isotropic thermal parameters, except two hydrogen atoms connected to O20. They were assigned to rest electron density on the electron density map. The final cycle refinement, including 475 parameters, converged to *R1* = 0.0312 (*R1* = 0.0388 all data) and *wR2* = 0.0800 (*wR2* = 0.0826 all data) with a maximum (minimum) residual electron density of 0.463 (–0.293) e $Å^{-3}$.

Crystallographic data (without structure factors) for the structure of the complex have been deposited with the Cambridge Crystallographic Data Centre as supplementary publication no. CCDC 197305. Copies of the data can be obtained free of charge from the CCDC (12 Union Road, Cambridge CB2 1EZ, UK; tel: (+44) 1223-336-408; fax: (+44) 1223-336-003).

2.4 References

(1) Robson, R. *Inorg. Nucl. Chem. Lett.* **1970**, *6*, 125-128.
(2) Fenton, D. E. *Inorg. Chem. Comm.* **2002**, *5*, 537-547.
(3) Karlin, K. D.; Hayes, J. C.; Gultneh, Y.; Cruse, R. W.; McKown, J. W.; Hutchinson, J. P.; Zubieta, J. *J. Am. Chem. Soc.* **1984**, *106*, 2121-2128.
(4) Lambert, E.; Chabut, B.; Chardon-Noblat, S.; Deronzier, A.; Chottard, G.; Bousseksou, A.; Tuchagues, J.-P.; Laugier, J.; Bardet, M.; Latour, J.-M. *J. Am. Chem. Soc.* **1997**, *119*, 9424-9437.
(5) Murthy, N. N.; Mahroof-Tahir, M.; Karlin, K. D. *Inorg. Chem.* **2001**, *40*, 628-635.
(6) Meyer, F.; Rutsch, P. *Chem. Comm.* **1998**, 1037-1038.
(7) Suzuki, M.; Kanatomi, H.; Murase, I. *Chem. Lett.* **1981**, 1745-1748.
(8) Gamez, P.; von Harras, J.; Roubeau, O.; Driessen, W. L.; Reedijk, J. *Inorg. Chim. Acta* **2001**, *324*, 27-34.
(9) Torelli, S.; Belle, C.; Gautier-Luneau, I.; Pierre, J. L.; Saint-Aman, E.; Latour, J. M.; Le Pape, L.; Luneau, D. *Inorg. Chem.* **2000**, *39*, 3526-3536.
(10) Klabunde, T.; Eicken, C.; Sacchettini, J. C.; Krebs, B. *Nat. Struct. Biol.* **1998**, *5*, 1084-1090.
(11) Solomon, E. I.; Sundaram, U. M.; Machonkin, T. E. *Chem. Rev.* **1996**, *96*, 2563-2605.
(12) Huisman, M.; Koval, I. A.; Gamez, P.; Reedijk, J. *Inorg. Chim. Acta* **2005**, in press.
(13) *Comprehensive Coordination Chemistry*; Wilkinson, G., Ed.; Pergamon Press: Toronto, 1987; Vol. 5.
(14) Barszcz, B.; Glowiak, T.; Jezierska, J. *Polyhedron* **1999**, *18*, 3713-3721.
(15) Rizzi, A. C.; Piro, O. E.; Castellano, E. E.; Nascimento, O. R.; Brondino, C. D. *Inorg. Chim. Acta* **2000**, *305*, 19-25.

(16) Manikandan, P.; Muthukuraman, R.; Thomas, K. R.; Varghese, B.; Chandramouli, G. V. R.; Manoharan, P. T. *Inorg. Chem.* **2001**, *40*, 2378-2389.
(17) Spek, A. L. *J. Appl. Cryst.* **2003**, *36*, 7-13.
(18) Belle, C.; Beguin, C.; Gautier-Luneau, I.; Hamman, S.; Philouze, C.; Pierre, J. L.; Thomas, F.; Torelli, S.; Saint-Aman, E.; Bonin, M. *Inorg. Chem.* **2002**, 479-491.
(19) Uozumi, S.; Ohba, M.; Okawa, H.; Fenton, D. E. *Chem. Lett.* **1997**, 673-674.
(20) Lever, A. B. P. *Inorganic Electronic Spectroscopy*; 2 ed.; Elsevier: Amsterdam, 1984.
(21) Kahn, O. *Molecular Magnetism*; Wiley-VCH: New York, 1993.
(22) Lock, G. *Chem. Ber.* **1930**, *63*, 551-559.
(23) Nakamoto, K. *Infrared and Raman Spectra of Inorganic and Coordination Compounds*; 4 ed.; John Wiley & Sons: New York, 1986.
(24) Bruker AXS Inc., Madison, WI, 1999.
(25) Sheldrick, G. M.; *SHELXTL PLUS*. University of Göttingen, Germany, 1990
(26) Sheldrick, G. M.; *SHELXL-97, Program for the refinement of crystal structures*. University of Göttingen, Germany, 1997

3 | Structural diversity in Cu^{II}, Co^{II} and Mn^{II} complexes of a phenol-based ligand containing amine, pyridine and formyl functions: 3D structures and solution studies.[†]

The phenol-based ligand Hpy2ald, prepared as an intermediate in the synthesis of the ligand Hpy3asym, described in Chapter 2, contains formyl, amine and pyridine functions. Its reaction with Cu^{II}, Mn^{II} and Co^{II} salts leads to complexes with very different structural features and different nuclearities. Depending on the counter ion, the carbonyl group of the ligand can be either bound to a metal ion, or remain non-coordinated, fully changing the ligand coordination behavior. In this chapter the 3D structures, solution and magnetic properties of six different complexes: $[Co_2(py2ald)_2](ClO_4)_2 \cdot 0.7CH_3OH$ (**1**), $[Co_2(py2ald)_2](BF_4)_2 \cdot CH_3OH$ (**2**), $[Mn_2(py2ald)_2](ClO_4)_2 \cdot C_4H_{10}O$ (**3**), $[Cu(Hpy2ald)Br_2] \cdot 0.5H_2O$ (**4**), $[Mn(Hpy2ald)Cl_2]$ (**5**) and $[Cu_2(py2ald)(\mu\text{-}NO_3)(NO_3)_2] \cdot CH_3CN$ (**6**) are reported. In the first three complexes, two metal ions are doubly bridged by two deprotonated phenolate groups of two ligands, resulting in dinuclear structures, with the oxygen atom of the carbonyl group occupying one position in the metal coordination sphere. In the latter three complexes, the coordinating counter ions Br^-, Cl^- and NO_3^- prevent a binding of the weaker donor (carbonyl group) to the metal centers, leading to complexes with a metal to ligand ratio of 2:2, 1:1, and 2:1, respectively. In the first two complexes, the phenol group of the ligand remains protonated and fails to bridge two metal ions, instead being semi-coordinated to only one metal ion.

[†]This chapter is based on: Koval, I. A.; Huisman, M.; Stassen, A. F.; Gamez, P.; Lutz, M.; Spek, A. L. Pursche, D.; Krebs, B. and Reedijk, J., Inorg. Chim. Acta, 2004, 357, 294-300, and Koval, I. A.; Huisman, M.; Stassen, A. F.; Gamez, P.; Lutz, M.; Spek, A. L.; and Reedijk, J. Eur. J. Inorg. Chem., 2004, 591-600

3.1 Introduction

Some time ago, Adams *et al.* reported[1,2] an unexpected nickel-induced hydrolysis of unsymmetrical Schiff base compartmental ligands, which resulted in the transformation of the imino group of the ligands into a formyl moiety. As this hydrolysis only occurred when nickel(II) salts with non- or weakly coordinating anions were used, it was suggested that the presence of such anions, as well as of nickel ions is crucial.[2] All dinuclear complexes, which were obtained with these *in situ* generated ligands, were found to have very similar crystal structures, comprised of a dimetal core with two bridging phenolato groups from two ligands. In all cases the metal to ligand ratio was found to be 2:2. The coordination environment around each metal ion was completed to a distorted octahedron by three nitrogen donor atoms from an amino arm of the ligand and an oxygen atom of the formyl group formed due to the hydrolysis.

In this chapter, six novel complexes of the phenol-based compartmental ligand Hpy2ald (Figure 3.1), containing formyl, amino and pyridine functions, with copper(II), cobalt(II) and manganese(II) ions are reported. The ligand Hpy2ald was prepared as an intermediate in the synthesis of the asymmetric dinucleating ligand Hpy3asym (Chapter 2).[3] Three of the reported complexes ($[Co_2(py2ald)_2](ClO_4)_2 \cdot 0.7CH_3OH$ (**1**), $[Co_2(py2ald)_2](BF_4)_2 \cdot CH_3OH$ (**2**) and $[Mn_2(py2ald)_2](ClO_4)_2 \cdot C_4H_{10}O$ (**3**)) possess a structure very similar to those reported by Adams *et al.*,[1,2] whereas the other three complexes, namely $[Cu(Hpy2ald)Br_2] \cdot 0.5H_2O$ (**4**), $[Mn(Hpy2ald)Cl_2]$ (**5**) and $[Cu_2(py2ald)(\mu\text{-}NO_3)(NO_3)_2] \cdot CH_3CN$ (**6**), exhibit completely different structural features. The crystal structures, spectroscopic and magnetic properties of all six complexes are reported.

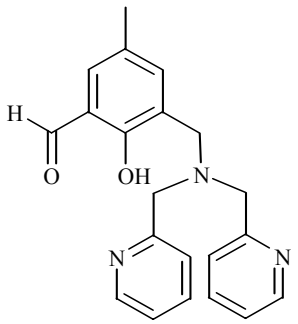

Figure 3.1. The phenol-based ligand Hpy2ald.

3.2 Results and Discussion

3.2.1 Crystal structure descriptions

$[Co_2(py2ald)_2](ClO_4)_2 \cdot 0.7CH_3OH$ (1)

Pink rectangular blocks of the compound were obtained by diethyl ether diffusion into the methanol solution of the reactants. An ORTEP projection of the

complex cation $[Co_2(py2ald)_2]^{2+}$ is shown in Figure 3.2. Selected bond lengths and angles are presented in Table 3.1. The compound crystallizes in the space group *Fdd2*, with sixteen formula units present per unit cell. The complex cation is constituted by two deprotonated ligands and two Co^{II} ions, resulting in a dimeric structure with a Co…Co separation of 3.2031(6) Å. Two cobalt ions are bridged by two μ-phenoxy bridges from two deprotonated cresolates, resulting in an almost ideal parallelogram formed by two *trans*-located cobalt ions Co1 and Co2 and two *trans*-located oxygen atoms O31 and O71. The distances Co1-O71 and Co2-O31 are approximately equal (2.0323(19) Å and 2.0344(19) Å, respectively), as well as the distances Co1-O31 and Co2-O71 (2.100(2) Å and 2.101(2) Å, respectively). The interior angles of the parallelogram are 78.32(7) and 78.25(8)° for O-Co-O and 101.57(8) and 101.55(9)° for Co-O-Co, and their sum amounts to 359.7°, which is very close to the planar value of 360°.

Both cobalt ions have a significantly distorted octahedral surrounding, accomplished by a N_3O_3 donor set. The coordination sphere of each ion is completed by two nitrogen atoms from two pyridine rings, a nitrogen donor from a tertiary amine group and an oxygen from the carbonyl group. For both ions, the oxygen atom from the deprotonated cresolate and the nitrogen atom from the tertiary amine group are occupying the axial positions, whereas two pyridine rings lie in the equatorial plane on either side of the ligand plane and thus are *trans*-located to each other.

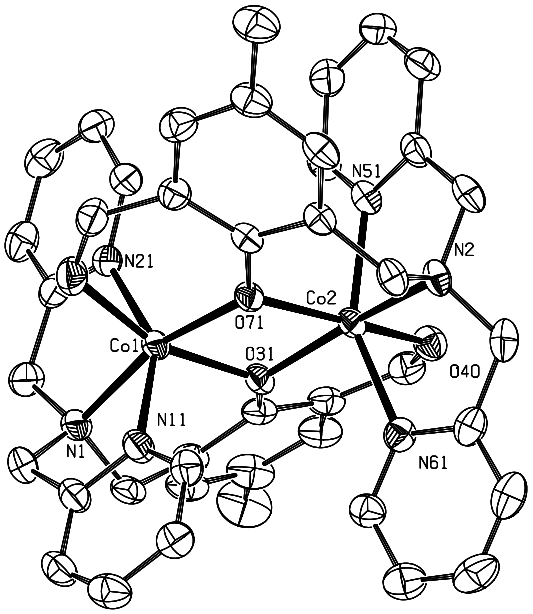

Figure 3.2. ORTEP projection of the dinuclear cation $[Co_2(py2ald)_2]^{2+}$. Hydrogen atoms are omitted for clarity.

The doubly positive charge of the complex cation is compensated by perchlorate anions. One perchlorate is on a general position and two independent perchlorates are located on twofold axes. Additionally, 0.7 molecule of non-coordinated methanol is refined per formula unit.

$[Co_2(py2ald)_2](BF_4)_2 \cdot CH_3OH$ (2)

Pink hexagonal crystals of the complex were obtained by slow diethyl ether diffusion into a methanol solution of the ligand and cobalt(II) tetrafluoroborate. As the complex unit was found to be isomorphous to its perchlorate analogue, its projection is not depicted. Selected bond lengths and bond angles of compound **2** are presented in Table 3.1.

Table 3.1. Selected bond lengths and bond angles for $[Co_2(py2ald)_2](ClO_4)_2 \cdot 0.7CH_3OH$ (**1**) and $[Co_2(py2ald)_2](BF_4)_2 \cdot CH_3OH$ (**2**)

Bond lengths (Å)	**1**	**2**		**1**	**2**
Co1 - N11	2.118(2)	2.112(3)	Co2 - N51	2.111(2)	2.099(3)
Co1 - N21	2.121(2)	2.124(3)	Co2 - N61	2.111(2)	2.105(3)
Co1 - N1	2.171(2)	2.174(3)	Co2 - N2	2.168(2)	2.168(3)
Co1 - O31	2.100(2)	2.100(3)	Co2 - O31	2.0343(18)	2.033(2)
Co1 - O71	2.0325(18)	2.033(2)	Co2 - O71	2.101(2)	2.094(2)
Co1 - O80	2.157(2)	2.161(3)	Co2 - O40	2.141(2)	2.146(2)

Bond angles (°)	**1**	**2**		**1**	**2**
O31 - Co1 - O71	78.32(7)	78.36(9)	O31 - Co2 - O40	87.97(8)	87.95(10)
O31 - Co1 - O80	162.24(7)	162.39(9)	O31 - Co2 - O71	78.25(8)	78.51(9)
O31 - Co1 - N1	91.61(9)	91.67(10)	O31 - Co2 - N2	166.29(8)	166.60(10)
O31 - Co1 - N11	103.97(8)	104.09(10)	O31 - Co2 - N51	111.58(8)	111.20(10)
O31 - Co1 - N21	95.94(9)	95.79(10)	O31 - Co2 - N61	94.43(8)	94.33(11)
O71 - Co1 - O80	87.41(8)	87.49(9)	O40 - Co2 - O71	162.73(7)	162.87(8)
O71 - Co1 - N1	165.10(8)	165.03(10)	O40 - Co2 - N2	102.95(8)	102.82(10)
O71 - Co1 - N11	93.04(8)	92.80(10)	O40 - Co2 - N51	82.18(9)	82.10(10)
O71 - Co1 - N21	113.45(8)	113.50(9)	O40 - Co2 - N61	86.69(9)	86.69(11)
O80 - Co1 - N1	104.30(9)	104.13(11)	O71 - Co2 - N2	92.30(8)	92.18(9)
O80 - Co1 - N11	87.14(9)	86.86(11)	O71 - Co2 - N51	93.16(8)	92.96(10)
O80 - Co1 - N21	79.97(10)	80.17(11)	O71 - Co2 - N61	104.54(8)	104.60(10)
N1 - Co1 - N11	78.62(9)	78.68(11)	N2 - Co2 - N51	78.52(9)	78.59(11)
N1 - Co1 - N21	78.20(8)	78.30(10)	N2 - Co2 - N61	78.20(9)	78.57(11)
N11 - Co1 - N21	149.70(9)	149.86(11)	N51 - Co2 - N61	151.16(9)	151.57(11)

$[Mn_2(py2ald)_2](ClO_4)_2 \cdot C_4H_{10}O$ (3)

Bright-yellow rod-shaped crystals of the complex were obtained by slow diffusion of diethyl ether into a methanol solution of the ligand and manganese(II) perchlorate. An ORTEP projection of the complex is shown in Figure 3.3. The selected bond lengths and angles are presented in Table 3.2. The complex crystallizes in the

space group $P\overline{1}$ (no. 2). The unit cell includes one doubly charged complex cation, two perchlorate anions and one disordered molecule of diethyl ether. As in the case of the cobalt(II) complexes, two manganese ions are bridged by two oxygen atoms of deprotonated cresolate moieties, with a Mn1…Mn2 separation of 3.4013(10) Å. Each manganese(II) ion is further coordinated by two nitrogen donor atoms of two pyridine rings, the nitrogen atom of the tertiary amino group and the oxygen atom of the aldehyde group. The coordination spheres around both manganese ions can best be described as a trigonal prism, with torsion angles of 9.4°, 19.5° and 27.6° for the Mn1 ion, and 7.9°, 2.8° and 1.9° for the Mn2 ion. Two trigonal faces of the prism around the Mn1 ion are formed by the atoms N11, N1 and O31, and the atoms O80, O71 and N21. For the Mn2 ion, the two trigonal faces are formed by the atoms O31, O40 and N61, and the atoms N51, N2, O71. All Mn-N and Mn-O distances are in a normal range for high-spin (S = 5/2) manganese(II) complexes.[4] In contrast to both cobalt complexes, non-coordinated counter ions do not exhibit any disorder.

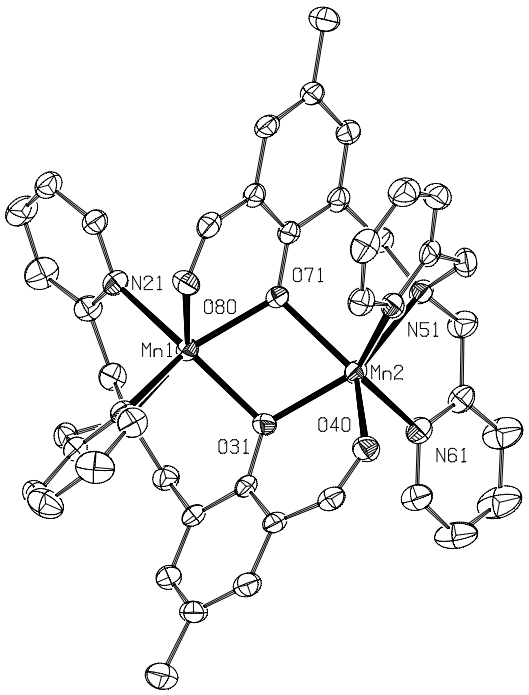

Figure 3.3. ORTEP projection of the complex cation $[Mn_2(py2ald)_2]^{2+}$

$[Cu(Hpy2ald)Br_2]\cdot 0.5H_2O$ (4)

A molecular plot of the complex is shown in Figure 3.4. Selected bond lengths and angles are presented in Table 3.3. As can be evidenced from the picture, the unit cell encloses two mononuclear formula units and one water molecule, which appears to be disordered over two positions with an occupancy factor of 0.50. These uncoordinated water molecules act as hydrogen bond donors with coordinated bromide anions as acceptors (see Table 3.5), thus resulting in the formation of centrosymmetric dimers with the formal composition $[Cu(Hpy2ald)Br_2]_2\cdot H_2O$.

Table 3.2. Selected bond lengths and bond angles for $[Mn_2(py2ald)_2](ClO_4)_2 \cdot C_4H_{10}O$ (**3**)

Bond lengths (Å)			
Mn1 - N11	2.227(3)	Mn2 - N51	2.214(3)
Mn1 - N21	2.262(3)	Mn2 - N61	2.201(3)
Mn1 - N1	2.330(3)	Mn2 - N2	2.374(3)
Mn1 - O31	2.169(2)	Mn2 - O31	2.121(2)
Mn1 - O71	2.112(2)	Mn2 - O71	2.194(2)
Mn1 - O80	2.231(2)	Mn2 - O40	2.220(3)

Bond angles (°)			
O31 - Mn1 - O71	73.50(9)	O31 - Mn2 - O40	80.18(9)
O31 - Mn1 - O80	121.77(10)	O31 - Mn2 - O71	72.82(9)
O31 - Mn1 - N1	82.96(10)	O31 - Mn2 - N2	138.56(10)
O31 - Mn1 - N11	95.70(10)	O31 - Mn2 - N51	132.57(10)
O31 - Mn1 - N21	142.89(10)	O31 - Mn2 - N61	98.95(10)
O71 - Mn1 - O80	80.21(9)	O40 - Mn2 - O71	129.86(9)
O71 - Mn1 - N1	128.93(10)	O40 - Mn2 - N2	139.74(10)
O71 - Mn1 - N11	149.93(11)	O40 - Mn2 - N51	82.39(10)
O71 - Mn1 - N21	99.95(10)	O40 - Mn2 - N61	91.11(10)
O80 - Mn1 - N1	148.40(10)	O71 - Mn2 - N2	82.32(9)
O80 - Mn1 - N11	82.27(10)	O71 - Mn2 - N51	85.84(10)
O80 - Mn1 - N21	91.79(10)	O71 - Mn2 - N61	133.75(10)
N1 - Mn1 - N11	75.40(11)	N2 - Mn2 - N51	76.04(11)
N1 - Mn1 - N21	73.08(11)	N2 - Mn2 - N61	74.93(11)
N11 - Mn1 - N21	104.86(11)	N51 - Mn2 - N61	125.22(11)

The coordination environment around the copper(II) ion can be best described as either a very distorted octahedron with a Br_2N_3O donor set, or a square pyramid with a Br_2N_3 donor set and loosely bound phenol group. The phenol group of the cresol ring remains protonated, which disables it to form a bridge between two copper ions. This in turn results in the formation of the mononuclear complex. The oxygen atom O1 from the phenol group thus can be best regarded as only semi-coordinated to the Cu1 ion, with a very long Cu-O distance of 2.932(2) Å. It lies in one of the apical positions of an imaginary octahedron, with the second apical position being occupied by one of the bromide anions at a distance Cu1-Br1 of 2.7278(4) Å. The O1-Cu1-Br1 angle is 170.75(4)˚. The equatorial plane is formed by the second bromide anion Br2, the nitrogen atom N1 from the tertiary amine group, and two nitrogen atoms N11 and N21 from the pyridine rings. The pyridine rings are located on either side of the ligand plane, thus being "*trans*" to each other. The interior angles N1-Cu1-N11 and N1-Cu1-N21 are

smaller than 90˚ (81.03(8)˚ and 81.05(8)˚, respectively), due to the constrains imposed by the three-bond ligand-bite.

Besides the intermolecular hydrogen bonding, an intramolecular hydrogen bond is realized between the cresolic proton and the oxygen atom from the formyl group (the O1…O10 distance of 2.645 Å, see also Table 3.5).

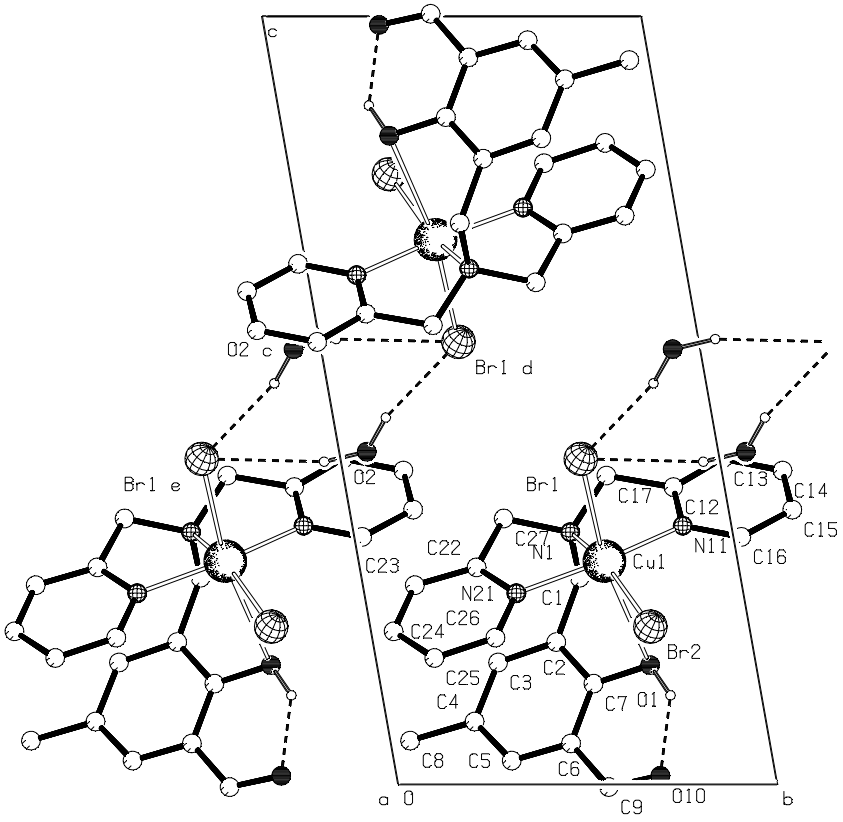

Figure 3.4. PLATON[5] projection of the crystal structure of $[Cu(Hpy2ald)Br_2]\cdot 0.5H_2O$ (**4**). The occupancy factor of each water molecule is 0.50. Only the hydrogen atoms participating in hydrogen bonding are shown.

[Mn(Hpy2ald)Cl$_2$] (5)

An ORTEP projection of the complex is shown in Figure 3.5. Selected bond lengths and angles are presented in Table 3.4. The structure of the complex looks very similar to that of complex **4**. However, in this case no intermolecular hydrogen bonding is present between the formula units. The coordination environment around the Mn1 ion can be described as a very distorted octahedron. The chloride anion Cl2 and the oxygen atom O31 from the cresol group are occupying the axial positions. Although the Mn1-O31 distance of 2.793(2) Å is shorter than the respective distance in complex **4** (2.932(2) Å), the oxygen atom can still be best regarded as only semi-coordinated to manganese ion.

Table 3.3. Selected bond lengths and bond angles for $[Cu(Hpy2ald)Br_2]\cdot 0.5H_2O$ (**4**).

Bond lengths (Å)			
Cu1 - Br1	2.7278(4)	Cu1 - N1	2.0815(19)
Cu1 - Br2	2.4299(4)	Cu1 - N11	2.0170(19)
Cu1 - O1	2.932(2)	Cu1 - N21	2.0246(19)

Bond angles (º)			
Br1 - Cu1 - Br2	99.197(12)	Br2 - Cu1 - N21	97.42(6)
Br1 - Cu1 - O1	170.75(4)	O1 - Cu1 - N1	82.40(7)
Br1 - Cu1 - N1	100.65(5)	O1 - Cu1 - N11	78.43(7)
Br1 - Cu1 - N11	93.34(6)	O1 - Cu1 - N21	95.50(7)
Br1 - Cu1 - N21	93.63(5)	N1 - Cu1 - N11	81.03(8)
Br2 - Cu1 - O1	78.04(5)	N1 - Cu1 - N21	81.05(8)
Br2 - Cu1 - N1	160.15(5)	N11 - Cu1 - N21	161.69(8)
Br2 - Cu1 - N11	98.15(6)		

Similarly to the copper(II) bromide complex, the OH group of the cresolic moiety remains protonated. The Cl2-Mn1-O31 angle is 175.64(5) º. The basal plane of the octahedron is formed by two nitrogen atoms N11 and N21 from two pyridine rings, the nitrogen atom N1 from the tertiary amine group and the chloride anion Cl1 (the Mn-N distances vary in a range of 2.217(2)-2.360(2) Å, the Mn1-Cl1 distance is 2.3737(9) Å). Also in this compound an intramolecular hydrogen bond is realized between the hydrogen atom of the cresolic group and the oxygen atom from the formyl group, with an O31…O40 distance of 2.660 Å (see Table 3.5).

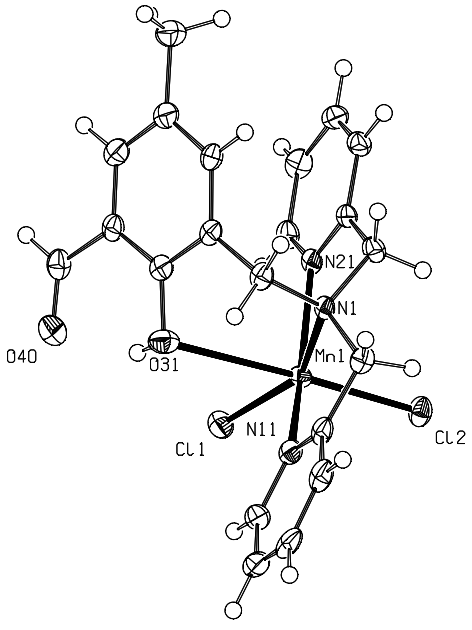

Figure 3.5. ORTEP projection of the crystal structure of $[Mn(Hpy2ald)Cl_2]$ (**5**)

Table 3.4. Selected bond lengths and angles for [Mn(Hpy2ald)Cl_2] (**5**)

Bond lengths (Å)			
Mn1 - Cl1	2.3737(9)	Mn1 - N1	2.360(2)
Mn1 - Cl2	2.4078(8)	Mn1 - N11	2.217(2)
Mn1 - O31	2.793(2)	Mn1 - N21	2.223(2)

Bond angles (º)			
Cl1 - Mn1 - Cl2	106.07(3)	Cl2 - Mn1 - N21	94.92(6)
Cl1 - Mn1 - O31	76.21(5)	O31 - Mn1 - N1	75.92(7)
Cl1 - Mn1 - N1	151.89(5)	O31 - Mn1 - N11	78.07(7)
Cl1 - Mn1 - N11	104.33(6)	O31 - Mn1 - N21	88.15(7)
Cl1 - Mn1 - N21	102.28(6)	N1 - Mn1 - N11	73.27(8)
Cl2 - Mn1 - O31	175.64(5)	N1 - Mn1 - N21	73.22(7)
Cl2 - Mn1 - N1	101.98(5)	N11 - Mn1 - N21	145.95(8)
Cl2 - Mn1 - N11	97.70(6)		

Table 3.5. Hydrogen bonds D - H…A for [Cu(Hpy2ald)Br_2]$_2$·H_2O (**4**) and [Mn(Hpy2ald)Cl_2] (**5**)

	Donor - H....Acceptor	*D – H (Å)*	*H...A (Å)*	*D...A (Å)*	*D - H...A (º)*
	O1 - H10 .. O10	1.00(5)	1.82(5)	2.645(3)	137(4)
[Cu(Hpy2ald)Br_2]·0.5H_2O	O2 - H20 .. Br1^{i}	0.99	2.44	3.405(4)	164.2
	O2 - H30 .. Br1	0.95	2.70	3.592(4)	155.3
[Mn(Hpy2ald)Cl_2]	O31 - H10 ... O40	0.72(3)	2.01(3)	2.660(3)	151(4)

i = 2-x, 1-y, 1-z
ii = x, 1-y, z

[Cu_2(py2ald)(μ-NO_3)(NO_3)$_2$]·CH_3CN (6)

An ORTEP projection of [Cu_2(py2ald)(μ-NO_3)(NO_3)$_2$]·CH_3CN is shown in Figure 3.6. Selected bond lengths and angles are given in Table 3.6. The dinuclear core is constituted by two copper ions (Cu...Cu distance 3.0652(6) Å) bridged on one side by an endogenous (μ-phenoxo) bridge and on the other side by an exogenous didentate nitrate anion. The complex shows both coordination number and donor-atom asymmetry. Cu1 is five coordinated with an almost ideal square pyramidal geometry (the parameter τ, which is used to describe the percentage of trigonal distortion from square pyramidal geometry, is 0.07 for the Cu1 ion; τ is 0 for an ideal square pyramid and 1 for an ideal trigonal bipyramid),[6] and an N_3O_2 donor set. The basal plane is constituted by two *cis*-located oxygen atoms, O1 from the deprotonated cresolate and O32 from the bridging nitrate anion, and two *cis*-located nitrogen atoms, N1 of the

tertiary amine group and N20 of the pyridine ring. The nitrogen atom N10 from the other pyridine ring is occupying the apical position. The interior angles of the basal plane vary in a range of 82.07(9)-93.06(8)°. The distance Cu1…O41 is 3.031(3) Å and is perhaps too long to consider the O41 atom as a sixth ligand for the Cu1 ion.

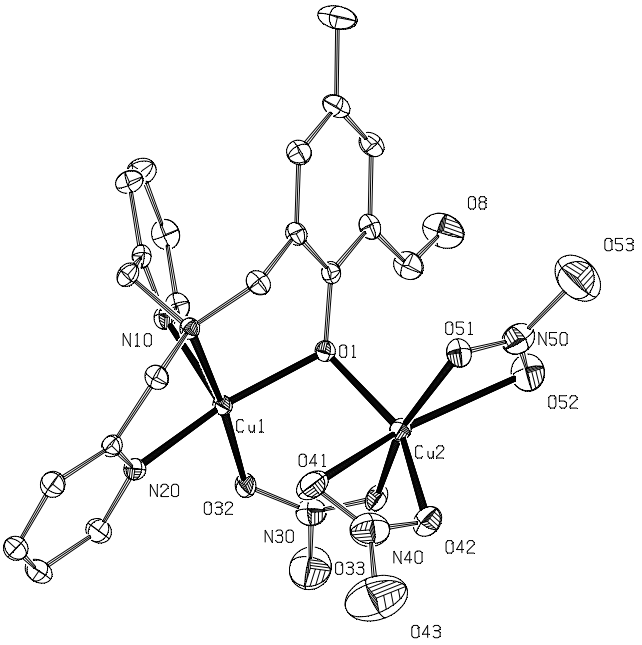

Figure 3.6. ORTEP projection of the crystal structure of $[Cu_2(py2ald)(\mu\text{-}NO_3)(NO_3)_2]\cdot CH_3CN$ (**6**). Hydrogen atoms and non-coordinated acetonitrile molecule are omitted for clarity.

The Cu2 ion is six coordinated with a very distorted octahedral geometry and an O_6 donor set. Only one of the oxygen atoms belongs to the ligand, whereas the five others are from three different nitrate anions. Two oxygen atoms O41 and O52 from two didentate chelating nitrate ions are occupying the axial positions, with long Cu-O bonds of 2.585(3) Å and 2.479(3) Å, respectively. The angle O41-Cu2-O52 is only 149.42(9)°, indicating a very large distortion from the regular octahedral geometry, apparently imposed by the small bite angle of the nitrate anions. The oxygen atoms O42 and O51 of two didentate chelating nitrate anions, the oxygen atom O1 of the deprotonated cresolate and the oxygen atom O31 of the didentate bridging nitrate anion lie in the equatorial plane, with Cu-O distances of 1.945(2)-1.978(2) Å. The interior angles of the equatorial plane are somewhat larger than 90˚, *viz.* 90.26(10)-95.55(10)°. One non-coordinated molecule of acetonitrile is present in the crystal lattice.

3.2.2 Physical characterization

3.2.2.1 Mass-spectroscopy

Electrospray mass-spectra (ESI-MS) of both cobalt(II) complexes recorded in a methanol solution reveal one major peak at *m/z* 405, corresponding to $[Co_2(py2ald)_2]^{2+}$ (z = 2). The experimentally observed isotopic pattern is in agreement with the

theoretically calculated one for $C_{42}H_{40}Co_2N_6O_4$. Similarly, in the ESI-MS spectrum of $[Mn_2(py2ald)_2](ClO_4)_2$ recorded in a methanol solution, a *m/z* 401 peak, corresponding to $[Mn_2(py2ad)_2]^{2+}$ (z = 2), can be found.

Table 3.6. Selected bond lengths and angles for $[Cu_2(py2ald)(\mu\text{-}NO_3)(NO_3)_2]\cdot CH_3CN$ (**6**)

Bond lengths (Å)			
Cu1 – O1	1.9918(19)	Cu2 – O2	1.959(2)
Cu1 - O32	1.937(2)	Cu2 - O31	1.945(2)
Cu1 – N1	2.041(2)	Cu2 – O41	2.585(3)
Cu1 - N10	2.199(2)	Cu2 - O42	1.946(2)
Cu1 - N20	1.999(2)	Cu2 - O51	1.978(2)
Cu1…O41	3.031(3)	Cu2 - O52	2.479(3)

Bond angles (º)			
O1 – Cu1 – O32	92.46(8)	O1 – Cu2 – O31	90.63(9)
O1 - Cu1 - N1	93.06(8)	O1 - Cu2 - O41	96.70(8)
O1 - Cu1 - N10	89.20(8)	O1 - Cu2 - O42	151.99(9)
O1 - Cu1 - N20	163.73(9)	O1 - Cu2 - O51	93.75(9)
O32 - Cu1 - N1	174.17(9)	O51 - Cu2 - O52	57.90(8)
O32 - Cu1 - N10	99.34(9)	O1 - Cu2 - O52	101.69(8)
O32 - Cu1 - N20	92.11(9)	O31 - Cu2 - O41	103.36(8)
N1 - Cu1 - N10	82.59(9)	O31 - Cu2 - O42	90.26(10)
N1 - Cu1 - N20	82.07(9)	O31 - Cu2 - O51	158.59(9)
N10 - Cu1 - N20	105.44(9)	O31 - Cu2 - O52	100.68(8)
Cu1 - O1 - Cu2	101.75(9)	O41 - Cu2 - O42	55.99(10)
		O41 - Cu2 - O51	96.94(8)
		O41 - Cu2 - O52	149.42(9)
		O42 - Cu2 - O51	95.55(10)
		O42 - Cu2 - O52	105.63(10)

The mass spectra of $[Cu(Hpy2ald)Br_2]\cdot H_2O$ and $[Mn(Hpy2ald)Cl_2]$, both recorded in methanol, are characterized by one major peak corresponding to the moiety $[M(Hpy2ald)X]^+$ (*m/z* 491 for M = Cu and m/z 437 for M = Mn). These results are as expected and indicate that the solid-state structures of both complexes are retained in solution. It is also interesting to note that both Mn^{II} complexes are quite stable towards dioxygen in solution and can be easily isolated and recrystallized without undergoing the oxidation to Mn^{III} derivatives.

The mass spectra of $[Cu_2(py2ald)(\mu\text{-}NO_3)(NO_3)_2]$ were recorded for comparison in two different solvents (acetonitrile and methanol). The spectrum of the complex in acetonitrile solution shows two major peaks. The most intense one at *m/z* 596

corresponds to the fragment $[Cu_2(py2ald)(NO_3)_2]^+$, in agreement with the solid-state structure of the complex. However, the second peak in the spectrum with only a slightly lower intensity (relative abundance 95%) at *m/z* 472, corresponds to the mononuclear fragment $[Cu(Hpy2ald)NO_3]^+$. The discrimination between mononuclear and dinuclear fragments is unambiguous from the difference observed in the isotopic patterns, caused by the presence of one or two copper ions. The structure of the latter complex can be expected to look in general similar to the structure of the copper bromide complex, with the phenol group of the ligand being still protonated. The same two peaks are observed when the spectrum is recorded in methanol solution, thus it appears that the dinuclear complex with the deprotonated ligand exists in equilibrium with the mononuclear complex with the protonated ligand.

3.2.2.2 Ligand field spectroscopy

In the diffuse reflectance spectra of the powdered solids, for both cobalt complexes two major peaks are clearly visible. One of them, at approximately 420 nm, is a LMCT transition between the bridging phenoxo group and the metal ions and is typical for dinuclear complexes with phenol-based deprotonated ligands.[7,8] The second peak, located at 1051 nm for the perchlorate complex and 1042 nm for the tetrafluoroborate complex corresponds to the $^4T_{2g} \leftarrow {}^4T_{1g}(F)$ d-d transitions. In addition, in the spectra of both complexes another peak is observed at approximately 520 nm, as a shoulder of the LMCT transition band, which corresponds to the $^4T_{1g}(P) \leftarrow {}^4T_{1g}(F)$ transition. The latter two bands are typical for d-d transitions in octahedrally surrounded Co^{II} ions.[9] The positions of the bands are not significantly changing if the spectra are recorded in methanol, suggesting the absence of any significant modifications in the metal coordination sphere in solution. The diffuse reflectance spectrum of **3** is characterized by only one rather broad peak at 377 nm. It appears that the d-d transition band in octahedrally surrounded Mn^{II} is hidden by the LMCT band from the bridging phenoxo groups to the metal ions, which is usually observed around 400 nm.[9] As in the case of both cobalt complexes, no significant changes were observed when the electronic spectrum was recorded in methanol.

In the diffuse reflectance spectrum of complex **4,** a fairly broad peak corresponding to a d-d transition of the Cu^{II} ions is observed at 750 nm with the shoulder around 940 nm. As shown previously, such spectroscopic behavior (high-energy absorption band in the visible region with a low-energy shoulder) is typical for square-pyramidal copper(II) complexes.[10] Thus, the coordination sphere around the metal center can be indeed best described as square pyramidal. Another intensive band is observed at 378 nm. Taking into account that the OH group of the ligand is only semi-coordinated to the copper ion, and thus the LMCT band from the OH group to the metal ions is unlikely to be visible, this band has been assigned to the charge transfer from the bromide anions to the copper ions. Similarly, in the diffuse reflectance

spectrum of complex **5** a band is observed at 356 nm, which has been assigned to the charge transfer band from the chloride anions to the manganese ions. The d-d transition band in octahedrally surrounded Mn^{II} is known to be very weak, and must be hidden by the tail of the LMCT band, which is not uncommon.[9] The diffuse reflectance spectrum of complex **6** is characterized by two major peaks. The first one, at 418 nm, corresponds to the LMCT transition of phenolate group to the copper ions.[8] The second peak at 640 nm is in a normal range for d-d transitions of Cu^{II} ions.[9]

When the spectrum of complex **4** is taken in methanol solution, the position of the d-d band shifts somewhat towards the UV region (near 700 nm). Possible reasons for this shift can be additional solvation of the copper ions or the partial ligand exchange of the bromide anions with methanol molecules. The spectrum of $[Mn(Hpy2ald)Cl_2]$ (**5**) remains unchanged if recorded in methanol.

For comparison, the spectrum of complex **6** was recorded in two different solvents: acetonitrile and methanol. When the spectrum is recorded in an acetonitrile solution, the position of the d-d transition band shifts to 672 nm ("red shift"). In methanol, this shift is even bigger (from 640 nm to 719 nm). These results suggest a change of the coordination sphere around the copper(II) ions in solution, presumably towards a square-pyramidal geometry.[4] This observation appears to be in agreement with the results of mass-spectroscopic measurements, which also suggest the presence of significant amounts of mononuclear copper(II) species. As can be noticed, the position of the d-d band in the spectrum of complex **6** in a methanol solution is quite close to the position of the d-d band for complex **4**, which can be regarded as an additional evidence for the presence of mononuclear species similar in structure to complex **4**.

3.2.2.3 EPR spectroscopy on Cu^{II} complexes 4 and 6.

The EPR spectrum of complex **4** in the solid state has a rhombic character, with $g_x = 2.05$, $g_y = 2.10$ and $g_z = 2.25$, suggesting a $d_{x^2-y^2}$ ground state. When the spectrum is recorded in a methanol glass, a hyperfine splitting becomes obvious. Three of four lines are easily observed (Figure 3.7, left, solid line), whereas the fourth is partially hidden in the $g_{x,y}$ region. The spectrum was simulated[11] (Figure 3.7, left, dashed line) using the parameters $g_x = 2.04$, $g_y = 2.06$, $g_z = 2.24$, $A_x \approx A_y \approx 0$ and $A_z = 18.4$ mT (192×10^{-4} cm^{-1}). These data suggest a distorted square-pyramidal surrounding for the Cu^{II} ions,[12] in agreement with the crystal structure of the complex.

One can also notice an additional peak at high field (approximately 330 mT), with a *g*-value below 2, in the spectrum of the complex. The appearance of this signal may indicate the presence of small amount of dinuclear copper(II) species in solution. Although the solid-state structure of the complex is essentially mononuclear, the partial formation of dinuclear species in solution due to the presence of potentially bridging bromide anions can be imagined. In this case, this absorption should originate from a

$\Delta M_s = \pm 1$ transition of the triplet spectrum.[8] No signal corresponding to a $\Delta M_s = \pm 2$ transition could though be detected. As the structure of these presumably dinuclear species is unknown, the presence of this high-field signal was neglected during the simulation of the spectrum.

The EPR spectrum of compound **6**, recorded in the solid state at room temperature, exhibits one fairly broad isotropic signal with $g = 2.15$. No hyperfine splitting is resolved and no triplet signal is detected. The resolution does not improve upon cooling to liquid nitrogen temperature. A very similar spectrum is observed when the measurement is performed in a frozen acetonitrile solution. These data suggest an interaction between two copper(II) centers at relatively close positions, leading to exchange narrowing. However, when the spectrum is recorded in a methanol glass, it becomes much more complicated (Figure 3.7, right, solid line). The spectrum obviously indicates the presence of two different species in solution, and can be best regarded as an overlapping superposition of two rhombic spectra. In both cases, the ^{63,65}Cu hyperfine splitting in the g_z region can be observed, although some lines are partially hidden either due to the overlapping of two spectra with each other, or in the $g_{x,y}$ region. The resulting spectrum was satisfactory simulated[11] (Figure 3.7, right, dashed line) considering two non-interacting Cu^{II}-containing species in an approximate ratio 1:1. For the species X, the simulating parameters are $g_x \approx g_y = 2.10$, $g_z = 2.44$, $A_x = 1.1$ mT (10.1×10^{-4} cm^{-1}), $A_y = 0$, $A_z = 10.9$ mT (124.3×10^{-4} cm^{-1}), and for the species Y, $g_x \approx g_y = 2.14$, $g_z = 2.26$, $A_x = 0$, $A_y = 0.43$ mT (4.3×10^{-4} cm^{-1}), and $A_z = 17.2$ mT (181.5×10^{-4} cm^{-1}).

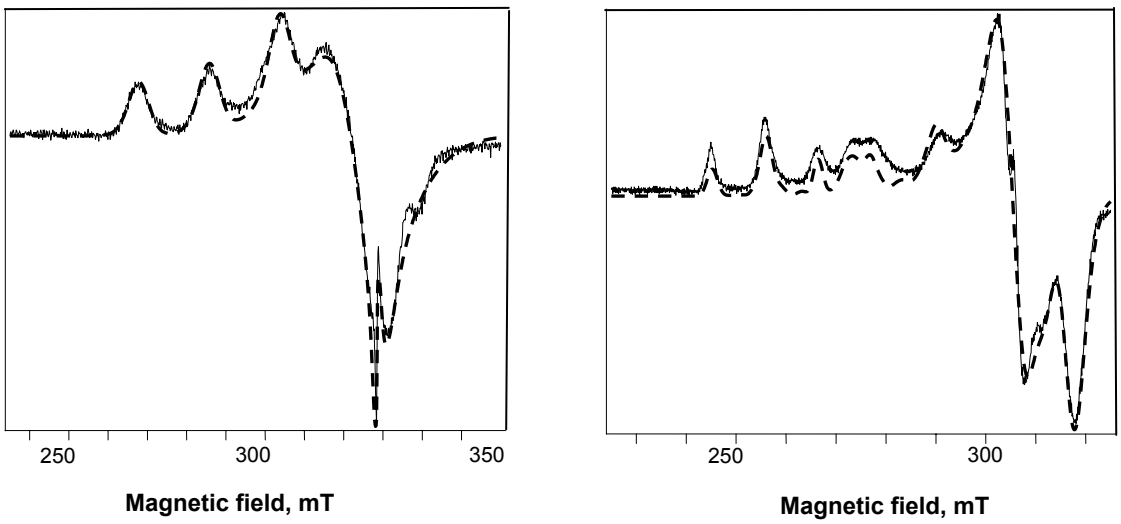

Figure 3.7. Left: X-band EPR spectrum of **4** (frozen methanol solution, 77 K, solid line) and the simulated curve[11] (dashed line). The sharp signal corresponds to the reference DPPH (g = 2.0036). Right: X-band EPR spectrum of **6** (frozen methanol solution, 77 K, solid line) and simulated curve[11] (dashed line).

Although the exact interpretation proved to be difficult, these parameters suggest a $d_{x^2-y^2}$ ground state for both species X and species Y. The simulation parameters for the species X are characteristic for elongated rhombic octahedral CuO_6 chromophores,[4] and are very close to the values typical for Cu^{II} ions in methanol glass. The origin of this species can be Cu^{II} ions, coordinated by nitrate anions and/or, at least partially, by methanol molecules. The simulation parameters for the species Y are close to those for square-planar CuN_2O_2 chromophores. Thus, these results are in a good agreement with the presence in solution of a mononuclear species $[Cu(Hpy2ald)NO_3]^+$, as suggested by mass and ligand field spectroscopy. However, it should be noticed that neither EPR, nor ligand field measurements provide any direct evidence confirming the presence of dinuclear species in solution as well. Thus, although the presence of dinuclear species was evidenced during the mass spectroscopic measurements, it can not be directly deduced from other spectroscopic techniques. Therefore another possibility, *i.e.* the complete dissociation of the dinuclear complex into mononuclear units of composition $[Cu(Hpy2ald)NO_3]^+$ in methanol solution, can also not be excluded.

3.2.2.4 Magnetic susceptibility

Magnetic susceptibility measurements have been performed on crystals of **1** (*m* = 16.99 mg) and **2** (*m* = 46.28 mg) at 0.1 Tesla in the temperature range of 5 - 300 K. The plot of the χ^{-1} and χT versus the temperature (with χ being the magnetization per cobalt(II) ion) is shown in Figure 3.8. Because the magnetic behavior of the two compounds is almost identical, only the susceptibility curve of compound **1** is given.

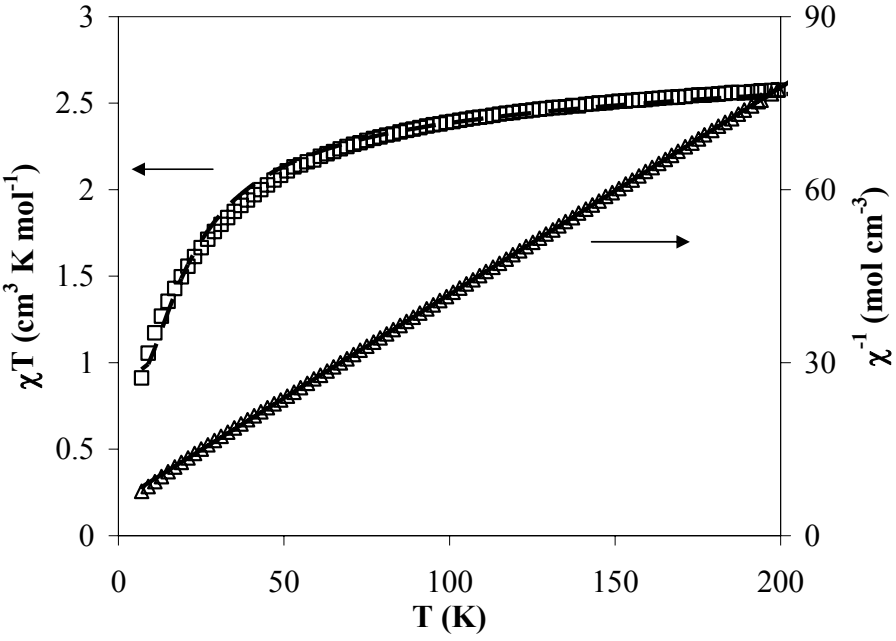

Figure 3.8. χT *vs.* T (□) and χ^{-1} *vs.* T (Δ) curves of **1**. The solid line represents the linear fitting according the Curie-Weiss law, the dashed line represent the calculated lines for the parameters $g_1 = 2.31$, $-J_1 = 3.56$ cm^{-1} and $\theta_1 = 3.0$ K, with $R_1 < 7.9 \cdot 10^{-4}$.

At 300 K, $\chi_1 T$ = 2.59 cm^3 K mol^{-1}, which is close to the expected value for a single, uncoupled cobalt(II) ion. The value of $\chi_1 T$ decreases upon cooling, going to zero at very low temperatures. The same behavior is observed for **2**, with a value for $\chi_1 T$ = 2.58 cm^3 K mol^{-1} at 300 K.

Fitting the linear part of the χ^{-1} *vs. T* curve (between 50 and 300 K) results in the Curie constants C_1 = 2.63 cm^3 K mol^{-1} and C_2 = 2.78 cm^3 K mol^{-1} and Curie-Weiss temperatures of θ_1 = -18.7 K with $R_1 < 4.5 \cdot 10^{-6}$ and θ_2 = -16.5 K with $R_2 < 8.7 \cdot 10^{-7}$ (the reliability factor R is defined as $R = n^{-1}[\Sigma(\chi_{obs}-\chi_{cal})^2/(\chi_{cal})^2]$, where n = number of data points). The Curie constants correspond to *g* values of 2.36 for compound **1** and 2.43 for compound **2**.

The susceptibilities of **1** and **2** have been simulated over the entire temperature range using a modified Van Vleck equation (3.1)[13,14] for a pair of coupled S = 3/2 spins (see Figure 3.8), where $x = \exp(-J/kT)$ and N, k and β have their normal values.[15]

$$\chi_M = \frac{g^2 N\beta^2}{k(T-\theta)} \times \frac{14 + 5x^6 + x^{10}}{7 + 5x^6 + 3x^{10} + x^{12}} + TIP \qquad (3.1)$$

The observed and calculated susceptibilities are in agreement over the entire temperature range, applying the constants g_1 = 2.31, $-J_1$ = 3.56 cm^{-1} and θ_1 = 3.0 K, with $R_1 < 7.9 \cdot 10^{-4}$, for compound **1**, and the constants g_2 = 2.32, $-J_2$ = 3.30 cm^{-1} and θ_2 = 4.2 K, with $R_2 < 2.6 \cdot 10^{-4}$ for compound **2.**

The magnetic susceptibility of crystals of **3** (13.18 mg) has been measured between 5 and 250 K, with an external field of 0.1 Tesla. The plot of χ^{-1} and χT versus the temperature (with χ being the magnetization per manganese(II) ion) is shown in Figure 3.9. Also in this compound a decrease in magnetic susceptibility is observed with decreasing temperatures, from a value of χT = 4.29 cm^3 K mol^{-1} at 250 K, to 1.4 cm^3 K mol^{-1} at 5 K. A Curie-Weiss behavior above 30 K results in a Curie constant C_3 = 4.38 cm^3 K mol^{-1}, which corresponds to a *g* value of g_3 = 2.00.

The magnetic susceptibility fit for the dinuclear manganese(II) system based on the isotropic Heisenberg model $H = 2J \cdot S1 \cdot S2$ ($S1$=$S2$=5/2) is expressed by equation 3.2,[16] where $x = \exp(-J/kT)$, and the other symbols have their usual meanings.[15] The cryomagnetic properties of **3** are simulated well by equation 3.2, using the magnetic parameters g_3 = 1.99, J_3 = 0.57 cm^{-1} and TIP= 0. The reliability factor $R = 1.3 \cdot 10^{-5}$.

$$\chi_M = \frac{g^2 N\beta^2}{kT} \times \frac{x^{28} + 5x^{24} + 14x^{18} + 30x^{10} + 55}{x^{30} + 3x^{28} + 5x^{24} + 7x^{18} + 9x^{10} + 11} + TIP \qquad (3.2)$$

Magnetic susceptibility measurements on powdered crystals of **4** (m = 50.20 mg), **5** (19. 04 mg) and **6** (m = 29.11 mg) have also been performed at 0.1 Tesla. Values for χ in the copper(II) complexes have been calculated for dinuclear species.

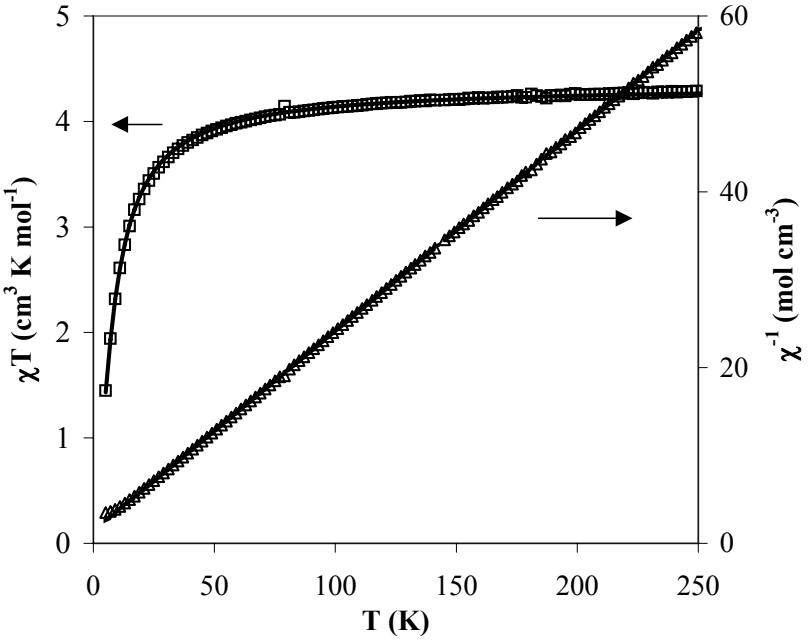

Figure 3.9. χT *vs.* T (□) and χ^{-1} *vs.* T (Δ) curves of **3**. The solid line represents the linear fitting according the Curie-Weiss law, the dashed line represent the calculated lines for the parameters $g_3 = 1.99$, $J_3 = 0.57$ cm^{-1}, TIP = 0 and $R = 1.3\times10^{-5}$.

At 300 K, the χT for complex **4** is 0.84 cm^3 K mol^{-1}. This value remains almost constant, as the compound shows a Curie-Weiss behavior over the entire temperature region. The Curie constant $C_2 = 0.42$ cm^3 K mol^{-1} indicates a *g*-value of 2.12. The Curie temperature θ_2 is 0 K, as expected. Thus, no magnetic coupling is present between two mononuclear fragments coupled by the disordered water molecule.

For complex **5**, χT is 4.40 cm^3 K mol^{-1} at 300 K, corresponding to a magnetic moment of 5.93 μ_B. This value is in perfect agreement with the theoretically expected one for a high-spin Mn^{II} ion (S = 5/2). It remains unchanged over the entire temperature range, indicating a paramagnetic behavior of the complex, as could be predicted from its crystal structure. The Curie temperature θ is 0 K, as expected.

The plot of χ^{-1} and χT versus the temperature for complex **6** between 5 and 150 K (with χ being the magnetization per dinuclear complex) is shown in Figure 3.10. From the increase of the magnetic susceptibility at low temperature (from $\chi_6 T = 0.89$ cm^3 K mol^{-1} at 150 K to $\chi_6 T = 1.05$ cm^3 K mol^{-1} at 5 K) ferromagnetic behavior is evidenced. By linear regression, the Curie constant has been determined to be $C = 0.45$ cm^3 K mol^{-1}, which results in a *g* value of 2.18. This value is in a very good agreement with the one determined from EPR measurements in the solid state ($g = 2.15$).

A ferromagnetic interaction is usually observed, when the magnetic orbitals of two closely located metal ions have a negligible overlap, whereas the antiferromagnetic exchange is found when the magnetic orbitals are pointing towards each other in such a way that the overlap integral is reasonably large.[17,18] In compound **6**, two unpaired

electrons from the Cu1 and Cu2 ions are both occupying $d_{x^2-y^2}$ orbitals. In a symmetrical complex, a bridging phenoxo group with an angle of 101.75(9)° between the copper centers would normally result in an antiferromagnetic interaction. However, due to the asymmetry of the penta- and hexacoordinated copper(II) ions, induced by the ligand Hpy2ald and the nitrate anions, an overlapping of two $d_{x^2-y^2}$ orbitals can be expected to be very insignificant. In this case, a weak ferromagnetic exchange can be expected.

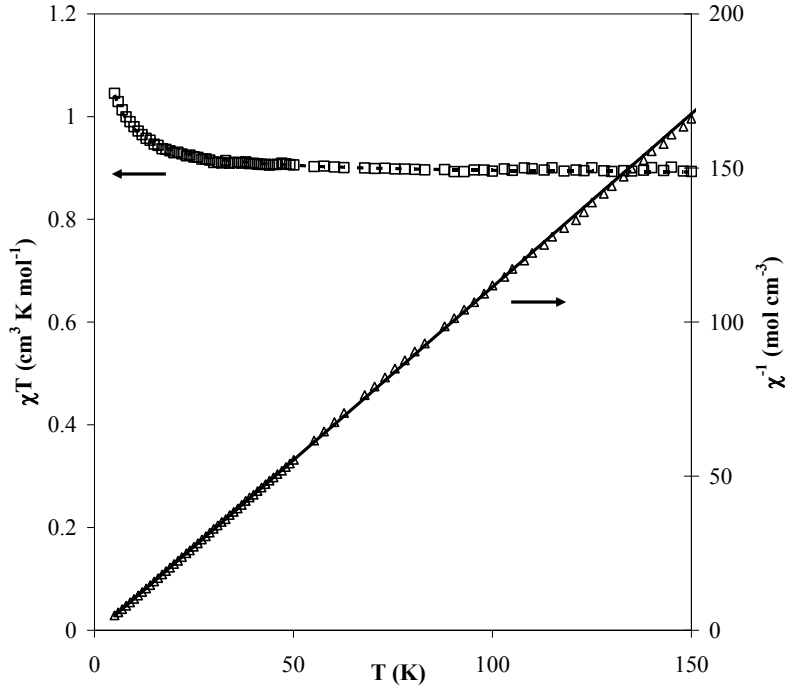

Figure 3.10. $\chi_1 T$ *vs.* T (□) and χ_1^{-1} (Δ) *vs.* T curves of **6**. The solid line represents the linear fitting according to the Curie-Weiss law, the dashed line represent the calculated lines for the parameters J_6 = 3.2 cm^{-1}, g_6 = 2.17 and $R = 1.24 \cdot 10^{-5}$.

The magnetic behavior has been simulated using the Bleaney-Bowers equation (3.3),[15,19] in which $-J$ is the magnetic exchange parameter and all constants have their usual value.[15]

$$\chi_M = \frac{2g^2N\beta^2}{kT\,[3 + exp\,(-J/kT)]} + TIP \qquad (3.3)$$

The best simulation is obtained with the values J_6 = 3.2 cm^{-1} and g_6 = 2.17. The reliability factor R is $1.24 \cdot 10^{-5}$.

3.3 Concluding remarks

The phenol-based ligand Hpy2ald contains a tridentate arm and a carbonyl group in two *ortho* positions with respect to the phenol group. Quite similar ligands and their Ni^{II} coordination compounds were previously described by Adams *et al.*[1] In the overwhelming majority of cases, the ligands reported by Adams were formed *in situ* by

the hydrolysis of an imino arm of the initially dinucleating phenol-based ligands.[1] The structures of the previously described complexes with this type of ligands include dinuclear metal cores, where two metals are doubly bridged by two phenolato groups. In all cases, the C=O group of the ligand is coordinated to the metal ion.[1]

In the present chapter, six new cobalt(II), copper(II) and manganese(II) complexes with the ligand Hpy2ald are reported. Three of them (namely complexes **1**, **2** and **3**) possess structural features very similar to those reported by Adams *et al.*,[1] but the structures of the other three compounds are quite different. Thus, the reaction of Hpy2ald with copper(II) nitrate yields the asymmetric dinuclear complex $[Cu_2(py2ald)(\mu\text{-}NO_3)(NO_3)_2]\cdot CH_3CN$ (**6**), in which the two metal ions are doubly bridged by a deprotonated cresolate anion and a didentate nitrate anion. The metal to ligand ratio in this complex is 2:1, and the octahedral coordination environment of one of the copper ions is completed by chelating nitrate anions. The aldehyde group of the ligand remains non-coordinated.

The reaction of Hpy2ald with $CuBr_2$ yields the mononuclear complex of formal composition $[Cu(Hpy2ald)Br_2]\cdot 0.5H_2O$ (**4**). In the crystal, the copper complexes form dimers by hydrogen bonding with lattice water molecules as hydrogen bond donors and coordinated bromides as acceptors. The metal-to-ligand ratio within a mononuclear fragment is 1:1. In this complex, the phenol group of the ligand remains protonated, failing to bridge two metal ions and instead being only semi-coordinated to one metal. As in the case of the nitrate complex, the aldehyde group is non-coordinated, but hydrogen bonded to the protonated phenol. The octahedral coordination environment around the metal ion is completed by nitrogen donor atoms of the tridentate arm from the ligand and two bromide anions.

Finally, the reaction of Hpy2ald with manganese(II) chloride yields the complex $[Mn(Hpy2ald)Cl_2]$ (**5**). The molecular structure of this complex is very similar to the structure of the copper(II) bromide complex with intramolecular hydrogen bonding, but in this crystal lattice no intermolecular hydrogen bonding is present.

These unusual structural features of the latter three complexes open the possibility to speculate that the structure of complexes with carbonyl-containing phenol-based ligands is largely determined by the donor properties of the anion. Due to the presence of a very weak donor carbonyl group in the ligand, the counter ions present in the solution may compete with the oxygen atom of the carbonyl group for a place in the coordination sphere of the metal ion. Thus, the dinuclear core comprised of two metal ions and two ligands, in which the carbonyl group is coordinated to the metal ions, can only be formed if non-coordinating, or very weakly coordinating anions are present in the solution, as evident from the structures of the complexes **1**, **2** and **3**, containing perchlorate and tetrafluoroborate counter ions. At the same time, the presence of stronger donors, *e.g.* nitrate and halogen anions, prevents a weaker donor, *i.e.* the

carbonyl group, from coordinating to the metal ion. In addition, in all cases, changing the initial ratio of the reactants did not influence the structure of the formed complexes.

3.4 Experimental Section

3.4.1 Materials and Methods

All starting materials were commercially available and used as purchased. The synthesis of the ligand Hpy2ald is reported in Chapter 2. The infrared spectra of the complexes in the 4000-300 cm^{-1} range were recorded on a Bruker 330V IR spectrophotometer equipped with a Golden Gate Diamond. The ligand field spectra of the solids (300-2000 cm^{-1}, diffuse reflectance) and in solution were taken on a Perkin-Elmer 330 spectrophotometer equipped with a data station. Electrospray mass spectra (ESI-MS) in acetonitrile or methanol solution were recorded on a Thermo Finnigan AQA apparatus. X-band electron paramagnetic resonance (EPR) measurements were performed at room temperature and at 77 K in the solid state, or at 77 K as methanol frozen solutions on a Jeol RE2x electron spin resonance spectrometer, using DPPH (g = 2.0036) as a standard. Bulk magnetizations of polycrystalline samples were measured in the range 5-300 K with a Quantum Design MPMS-5S SQUID magnetometer, in a 1 kG applied field. The data were corrected for the experimentally determined contribution of the sample holder. Corrections for the diamagnetic responses of the complexes, as estimated from Pascal's constants, were applied.[20]

3.4.2 Syntheses of the coordination compounds

$[Co_2(py2ald)_2](ClO_4)_2 \cdot 0.7CH_3OH$ (1): 20 ml of a methanol solution of cobalt(II) perchlorate (146 mg, 0.4 mmol) were added to 20 ml of a methanol solution of the ligand (69 mg, 0.2 mmol). Slow evaporation of the solvent yielded pink rectangular crystals suitable for X-ray crystal structure determination. Elemental analysis, % found (calc.) for $[Co_2(py2ald)_2](ClO_4)_2 \cdot 0.7CH_3OH$ ($=C_{42.7}H_{42.8}Cl_2Co_2N_6O_{12.7}$): C, 49.3 (49.7); H, 4.0 (4.2); N, 8.1 (8.0). IR, cm^{-1}: 3567 (O-H stretching); 2898 (C-H stretching); 1635 (C=O stretching); 1606, 1557 (C=N arom., C=C arom.), 1080 (ClO_4^-)

$[Co_2(py2ald)_2](BF_4)_2 \cdot CH_3OH$ (2): 20 ml of a methanol solution of cobalt(II) tetrafluoroborate (136 mg, 0.4 mmol) were added to 20 ml of a methanol solution of the ligand (69 mg, 0.2 mmol). Slow ether diffusion into the resulting pink solution yielded small pink hexagonal crystals of the complex which were found to be suitable for X-ray crystal structure determination. Elemental analysis, % found (calc.) for $[Co_2(py2ald)_2](BF_4)_2 \cdot CH_3OH$ ($=C_{43}H_{43}B_2Co_2F_8N_6O_3$): C, 50.6 (50.8); H, 4.4 (4.4); N, 8.5 (8.3). IR, cm^{-1}: 2916 (C-H stretching); 1635 (C=O stretching); 1607, 1558 (C=N arom., C=C arom.); 1032 (BF_4^-).

$[Mn_2(py2ald)_2](ClO_4)_2 \cdot C_4H_{10}O$ (3): A solution of manganese(II) perchlorate (245 mg, 0.4 mmol) in 20 ml of methanol was added to a solution of the ligand (69 mg, 0.2 mmol) in 20 ml of methanol. Ether diffusion into the resulting bright-yellow solution led to the appearance of yellow rod-shaped crystals which were found suitable for X-ray crystal structure determination. Crystals were found to deteriorate rapidly when taken out of the mother solution, due to the loss of ether molecules from the crystal lattice. Elemental analysis, % found (calc.) for $[Mn_2(py2ald)_2](ClO_4)_2$ (= $C_{42}H_{40}Cl_2Mn_2N_6O_{12}$): C, 50.1 (50.4); H, 4.0 (4.0), N, 8.4 (8.4). IR, cm^{-1}: 2924 (C-H stretching); 1643 (C=O stretching); 1602, 1554 (C=N arom., C=H arom.), 1079 (ClO_4^-).

$[Cu(Hpy2ald)Br_2] \cdot 0.5H_2O$ (4): 20 ml of a methanol solution of the ligand (56 mg, 0.16 mmol) were added to an equal volume of a copper(II) bromide solution (72 mg, 0.32 mmol) in methanol. Green rectangular crystals appeared when the solvent was almost completely evaporated. Their quality was found to be suitable for X-ray diffraction analysis. Elemental analysis, % found (calc.) for $[Cu(Hpy2ald)Br_2]$ (=$C_{21}H_{22}Br_2CuN_3O_{2.5}$): C, 43.9 (43.5); H, 3.8 (3.8); N, 7.5 (7.3). IR, cm^{-1}: ~3600, broad band (H_2O, asymmetric and symmetric OH stretching); 2980 (C-H stretching); 1654 (C=O stretching); 1608 (C=C arom., C=N arom.).

$[Mn(Hpy2ald)Cl_2]$ (5): 20 ml of a methanol solution containing 129 mg (0.8 mmol) of manganese(II) chloride dihydrate were added to an equal volume of a methanol solution of the ligand (56 mg, 0.16 mmol). Slow evaporation of the resulting bright-yellow solution resulted in appearance of colorless crystals of the product. These crystals were found to be of sufficient quality for X-ray crystal structure determination. Elemental analysis, % found (calc.) for $[Mn(Hpy2ald)Cl_2]$ (=$C_{21}H_{21}Cl_2MnN_3O_2$): C, 52.9 (53.3); H, 4.9 (4.5); N, 8.9 (8.9). IR, cm^{-1}: 2968 (C-H stretching); 1655 (C=O stretching); 1604 (C=C arom., C=N arom.)

$[Cu_2(py2ald)(\mu\text{-}NO_3)(NO_3)_2] \cdot CH_3CN$ (6): 20 ml of an acetonitrile solution of the ligand (56mg, 0.16 mmol) were added to an equal volume of a copper(II) nitrate solution (77 mg, 32 mmol) in acetonitrile. Slow evaporation of the solvent led to the appearance of green rectangular crystals, which were of sufficient quality for X-ray structure determination. The crystals were found to deteriorate rapidly when taken out of the mother liquor, due to the loss of acetonitrile. Elemental analysis, % found (calc) for $[Cu_2(py2ald)(\mu\text{-}NO_3)(NO_3)_2$ (=$C_{21}H_{20}Cu_2N_6O_{11}$): C, 37.9 (38.2); H, 3.4 (3.1); N, 12.8 (12.7). IR, cm^{-1}: 3047 (C-H stretching); 1610 (C=O stretching); 1550 (C=C arom., C=N arom.); 1436 (chelating didentate NO_3^-, N=O stretching); 1283 (bridging didentate NO_3^-, $\nu_a(NO_2)$); 998 (bridging didentate NO_3^-, $\nu_s(NO_2)$).

3.4.3 X-ray crystallographic measurements

$[Co_2(py2ald)_2](ClO_4)_2 \cdot 0.7CH_3OH$ (1): $(C_{42}H_{40}Co_2N_6O_4)(ClO_4)_2 \cdot 0.7(CH_4O)$, Fw = 1031.99, red-brown block, 0.30×0.25×0.18 mm^3, orthorhombic, *Fdd2* (no. 43), a = 27.0312(2) Å, b = 34.1008(2) Å, c =18.9101(1) Å, V = 17431.05(19) $Å^3$, Z = 16, $\rho_{calc.}$

= 1.573 g/cm^3. 66127 reflections were measured on a Nonius KappaCCD diffractometer with rotating anode (λ = 0.71073 Å) at a temperature of 150(2) K up to a resolution of $(\sin\theta/\lambda)_{max}$ = 0.61 Å^{-1}; 8090 reflections were unique (R_{int} = 0.040). The structure was solved with Patterson methods (DIRDIF-97)[21]and refined with SHELXL-97[22] against F^2 of all reflections. Non-hydrogen atoms were refined freely with anisotropic displacement parameters. One perchlorate anion was refined with a disorder model. H atoms were refined as rigid groups; methanol H atoms were kept fixed. 634 refined parameters, 52 restraints. Flack x-parameter:[23] 0.005(9). *R* [I > 2σ(I)]: *R1*= 0.0285, *wR2* = 0.0784. *R* [all refl.]: *R1*= 0.0318, wR2 = 0.0806. GoF = 1.040. Residual electron density between –0.36 and 0.46 e/Å^3. Molecular illustration, structure checking and calculations were performed with the PLATON package.[5]

$[Co_2(py2ald)_2](BF_4)_2\cdot CH_3OH$ (2): $(C_{42}H_{40}Co_2N_6O_4)(BF_4)_2(CH_4O)$, Fw = 1016.32, brown block, 0.21×0.15×0.09 mm^3, orthorhombic, *Fdd2* (no. 43), *a* = 26.8533(2) Å, *b* = 33.8399(3) Å, *c* =18.8585(1) Å, *V* = 17137.0(2) Å^3, *Z* = 16, $\rho_{calc.}$ = 1.576 g/cm^3. 55275 reflections were measured on a Nonius KappaCCD diffractometer with rotating anode (λ=0.71073 Å) at a temperature of 150(2) K up to a resolution of $(\sin\theta/\lambda)_{max}$ = 0.59 Å^{-1}; 7384 reflections were unique (R_{int} = 0.053). An absorption correction based on multiple measured reflections was applied (μ = 0.863 mm^{-1}, 0.85-0.92 transmission). Coordinates of compound **1** were taken as starting model and refined with SHELXL-97[22] against F^2 of all reflections. Non-hydrogen atoms were refined freely with anisotropic displacement parameters. One BF_4 anion was refined with a disorder model. H atoms were refined as rigid groups. 608 refined parameters, 40 restraints. Flack x-parameter [23]: -0.026(11). *R* [I > 2σ(I)]: *R1*= 0.0335, *wR2* = 0.0790. *R* [all refl.]: *R1*= 0.0411, *wR2* = 0.0828. GoF = 1.017. Residual electron density was between –0.44 and 0.71 e/Å^3. Molecular illustration, structure checking and calculations were performed with the PLATON package.[5]

$[Mn_2(py2ald)_2](ClO_4)_2\cdot C_4H_{10}O$ (3): $(C_{42}H_{40}Mn_2N_6O_4)(ClO_4)_2(C_4H_{10}O)$, Fw = 1075.20, yellow block, 0.1×0.1×0.04 mm^3, triclinic, $P\overline{1}$ (no. 2), *a* = 12.6517(3) Å, *b* = 12.7867(3) Å, *c* = 16.7288(4) Å, α = 85.068(2)°, β = 75.6270(10)°, γ = 65.4720(10)°, *V* = 2384.55(10) Å^3, *Z* = 2, $\rho_{calc.}$ = 1.497 g/cm^3. 14022 reflections were collected on a Bruker AXS Smart 6000 CCD diffraction system using Cu radiation (λ = 1.54178 Å) at a temperature of 153 K; 8009 reflections were unique (R_{int} = 0.0390). The structure was solved by direct methods using the program SHELXL-97.[22] The final position of all non-hydrogen atoms were taken from a series of full-matrix least-squares refinement cycles based on F² with the SHELXL-97 program followed by difference Fourier synthesis.[22] All non-hydrogen atoms, the counter ions and the ether solvent molecule were refined anisotropically. All hydrogen atoms were placed on calculated positions and allowed to ride on their corresponding atoms. The isotropic thermal parameters for the methyl protons were refined with 1.5 times and for all other hydrogen atoms with 1.2 times of the U_{eq} value of the bonding atom. 624 refined parameters, 0 restraints. *R* [I

> 2σ(I)]: *R1*= 0.0516, *wR2* = 0.1307. *R* [all refl.]: *R1* = 0.0706, *wR2* = 0.1379. GoF = 0.959. Residual electron density was between –0.67 and 0.91 e/Å^3. Illustrations, structure calculations, and structure checking were performed with the PLATON package.[5]

[Cu(Hpy2ald)Br$_2$]·0.5H$_2$O (4): ($C_{21}H_{21}Br_2CuN_3O_2$)(H_2O)$_{0.5}$, Fw = 579.78, green block, 0.24×0.18×0.06 mm^3, triclinic, $P\bar{1}$ (no. 2), a = 7.7651(1) Å, b = 8.8800(1) Å, c = 16.9099(2) Å, α = 98.0365(6)°, β = 93.0171(7)°, γ = 112.7805(6)°, V = 1057.19(2) Å^3, Z = 2, $\rho_{calc.}$ = 1.821 g/cm^3. X-ray intensities were collected on a Nonius KappaCCD diffractometer with rotating anode (λ = 0.71073 Å, graphite monochromator) at a temperature of 150(2) K up to a resolution of $(\sin\theta/\lambda)_{max}$ = 0.65 Å^{-1}. 14345 reflections were collected; 4758 reflections were unique. The structure was solved by automated Patterson methods (DIRDIF99)[24] and refined with SHELXL97[22] against F^2 of all reflections. Non hydrogen atoms were refined freely with anisotropic displacement parameters. The phenolic hydrogen was located in the difference Fourier map and refined freely with isotropic displacement parameters. The water hydrogen atoms were located in the difference Fourier map and kept fixed in these positions. All other hydrogen atoms were refined as rigid groups by direct methods using the program SHELXL-97.[22] *R* [I > 2σ(I)]: *R1*= 0.0260, *wR2* = 0.0595. *R* [all refl.]: *R1*= 0.0325, *wR2* = 0.0625. GoF = 1.036. Illustrations, structure calculations, and structure checking were performed with the PLATON package.[5]

[Mn(Hpy2ald)Cl$_2$] (5): ($C_{21}H_{21}Cl_2MnN_3O_2$), Fw = 473.25, yellow block, 0.56×0.15×0.03 mm^3, triclinic, $P\bar{1}$ (no. 2), a = 7.6829(14) Å, b = 8.8364(11) Å, c = 16.329(2) Å, α = 95.936(11)°, β = 92.005(14)°, γ = 111.789(13)°, V = 1020.6(3) Å^3, Z = 2, $\rho_{calc.}$ = 1.540 g/cm^3. 16182 reflections were collected on a Nonius KappaCCD diffractometer with rotating anode (λ = 0.71073 Å, graphite monochromator) at a temperature of 150(2) K up to a resolution of $(\sin\theta/\lambda)_{max}$ = 0.65 Å^{-1}, of which 4640 reflections were unique. The structure was solved by automated Patterson methods (DIRDIF99)[24] and refined with SHELXL97[22] against F^2 of all reflections. Non hydrogen atoms were refined freely with anisotropic displacement parameters. The phenolic hydrogen was located in the difference Fourier map and refined freely with isotropic displacement parameters. The water hydrogen atoms were located in the difference Fourier map and kept fixed in these positions. All other hydrogen atoms were refined as rigid groups by direct methods using the program SHELXL-97.[22] *R* [I > 2σ(I)]: *R1*= 0.0467, *wR2* = 0.1098. *R* [all refl.]: *R1*= 0.0755, *wR2* = 0.1225. GoF = 1.037. Illustrations, structure calculations, and structure checking were performed with the PLATON package.[5]

[Cu$_2$(py2ald)(μ-NO$_3$)(NO$_3$)$_2$]·CH$_3$CN (6): ($C_{21}H_{20}Cu_2N_6O_{11}$)·($C_2H_3N$), Fw = 700.56, dark green block, 0.48×0.24×0.18 mm^3, monoclinic, $P2_1/c$ (no. 14), a = 8.6632(7) Å, b = 17.3510(10) Å, c = 19.5299(17) Å, α = 90°, β = 97.203(7)°, γ = 90°, V = 2912.5(4) Å^3, Z = 4, $\rho_{calc.}$ = 1.598 g/cm^3. 51234 were collected on a Nonius

KappaCCD diffractometer with rotating anode (λ = 0.71073 Å, graphite monochromator) at a temperature of 150(2) K up to a resolution of $(\sin\theta/\lambda)_{max}$ = 0.65 $Å^{-1}$; 6695 reflections were unique. The structure was solved with direct methods (SHELXS97)[25]and refined with SHELXL97[22] against F^2 of all reflections. Non hydrogen atoms were refined freely with anisotropic displacement parameters. Hydrogen atoms were refined as rigid groups by direct methods using the program SHELXL-97.[22] *R* [I > 2σ(I)]: *R1*= 0.0408, *wR2* = 0.1091. *R* [all refl.]: *R1*= 0.0532, *wR2* = 0.1172. GoF = 1.043. Illustrations, structure calculations, and structure checking were performed with the PLATON package.[5]

Crystallographic data for the structures of the complexes have been deposited with the Cambridge Crystallographic Data Centre as supplementary publication no. CCDC-216684 (compound **1**), 216685 (compound **2**), 216686 (compound **3**), 212531 (compound **4**), 212532 (compound **5**) and 212530 (compound **6**). Copies of the data can be obtained free of charge from the CCDC (12 Union Road, Cambridge CB2 1EZ, UK; tel: (+44) 1223-336-408; fax: (+44) 1223-336-003).

3.5 References

(1) Adams, H.; Fenton, D. E.; Haque, S. R.; Health, S. L.; Ohba, M.; Okawa, H.; Spey, S. E. *J. Chem. Soc., Dalton Trans.* **2000**, 1849-1856.
(2) Adams, H.; Clunas, S.; Fenton, D. E. *Inorg. Chem. Comm.* **2001**, *4*, 667-670.
(3) Koval, I. A.; Pursche, D.; Stassen, A. F.; Gamez, P.; Krebs, B.; Reedijk, J. *Eur. J. Inorg. Chem.* **2003**, 1669-1674.
(4) *Comprehensive Coordination Chemistry*; Wilkinson, G., Ed.; Pergamon Press: Toronto, 1987; Vol. 5.
(5) Spek, A. L. *J. Appl. Cryst.* **2003**, *36*, 7-13.
(6) Addison, A. W.; Rao, T. N.; Reedijk, J.; van Rijn, J.; Verschoor, G. C. *J. Chem. Soc., Dalton Trans.* **1984**, 1349-1356.
(7) Gamez, P.; von Harras, J.; Roubeau, O.; Driessen, W. L.; Reedijk, J. *Inorg. Chim. Acta* **2001**, *324*, 27-34.
(8) Torelli, S.; Belle, C.; Gautier-Luneau, I.; Pierre, J. L.; Saint-Aman, E.; Latour, J. M.; Le Pape, L.; Luneau, D. *Inorg. Chem.* **2000**, *39*, 3526-3536.
(9) Lever, A. B. P. *Inorganic Electronic Spectroscopy*; 2 ed.; Elsevier: Amsterdam, 1984.
(10) Rajendran, U.; Viswanathan, R.; Palaniandavas, M.; Laskiminaraya, N. *J. Chem . Soc., Dalton Trans.* **1994**, 1219-1226.
(11) Neese, F.; *The program EPR, a modeling approach, Version 1.0*. University of Konstanz, 1993
(12) Hathaway, B. J., Billing, D. E. *Coordin. Chem. Rev.* **1970**, *5*, 143-207.
(13) Emori, S.; Nakashima, H.; Mori, W. *Bull. Chem. Soc. Jpn.* **2000**, *73*, 81-84.
(14) Earnshow, A. *Introduction to Magnetochemistry*; Acad. Press: London, 1968.
(15) Kahn, O. *Molecular Magnetism*; Wiley-VCH: New York, 1993.
(16) Sakiyama, H.; Sugawara, A.; Sakamoto, M.; Unoura, K.; Inoue, K.; Yamasaki, M. *Inorg. Chim. Acta* **2000**, *310*, 163-168.
(17) Hay, P. J.; Thibeault, J. C.; Hoffmann, R. *J. Am. Chem. Soc.* **1975**, *97*, 4884-4899.
(18) Kahn, O. *Angew. Chem. Int. Ed. Engl.* **1985**, *24*, 834-850.
(19) Bleaney, B.; Bowers, K. D. *Proc. R. Soc. London Ser. A* **1952**, *214*, 451-465.
(20) Kolthoff, I. M.; Elving, P. J. *Treatise on Analytical Chemistry*; Interscience Encyclopedia, Inc.: New York, 1963.
(21) Beurskens, P. T.; Admiraal, G.; Beurskens, G.; Bosman, W. P.; Garcia-Granda, S.; Gould, R. O.; Smits, J. M. M.; Smykalla, C. *The DIRDIF97 program system, Technical Report of the Crystallography Laboratory, University of Nijmegen, The Netherlands.* **1997**.
(22) Sheldrick, G. M.; *SHELXL-97, Program for the refinement of crystal structures*. University of Göttingen, Germany, 1997
(23) Flack, H. D. *Acta Cryst.* **1983**, *A39*, 876.

(24) Beurskens, P. T.; Admiraal, G.; Beurskens, G.; Bosman, W. P.; Garcia-Granda, S.; Gould, R. O.; Smits, J. M. M.; Smykalla, C. *The DIRDIF99 program system, Technical Report of the Crystallography Laboratory, University of Nijmegen, The Netherlands* **1999**.
(25) Sheldrick, G. M.; *SHELXS-97, Program for crystal structure solution*. University of Göttingen, Germany, 1997

4 | Dinuclear Cu^{II} complexes with the new phenol-based ligand bearing pyridine and thiophene substituents: synthesis, characterization and interaction with catechol substrates.[†]

The reaction of the phenol-based ligand 2,6-bis[*N*-(2-pyridylmethyl)-*N*-(2-thiophenylmethyl)aminomethyl]-4-methylphenol (Hpy2th2s), containing pyridine and thiophene substituents, with copper(II) chloride and bromide yields two new dinuclear complexes of composition $[Cu_2(py2th2s)(\mu\text{-}X)X_2]$, where X = Cl or Br. In both complexes, the copper(II) ions are pentacoordinated and bridged by the deprotonated phenolate anion and by one halogen anion. Both complexes exhibit geometric asymmetry, as the coordination environment around one of the two copper ions is square-pyramidal, whereas the other can be best described as a distorted trigonal bipyramid. The complexes were characterized by means of X-ray single-crystal diffraction, ligand field, EPR and mass spectroscopy and electrochemistry. Magnetic susceptibility measurements indicate an antiferromagnetic coupling between two metal centers ($2J \approx -200$ cm^{-1}). The interaction of the complexes with model substrates 3,5-di-*tert*-butylcatechol and tetrachlorocatechol is reported.

[†]This chapter is based on: Koval, I. A., Huisman, M., Stassen, A. F., Gamez, P., Roubeau, O., Belle, C., Pierre, J. L., Saint-Aman, E., Luken, M., Krebs, B., Lutz, M., Spek, A. L., Reedijk, J., Eur. J. Inorg. Chem., 2004, 4036-4045

4.1 Introduction

As discussed in Chapter 1, an interesting structural feature encountered in the active site of catechol oxidase from sweet potatoes (*Ipomoea batatas*)[1] is an unusual thioether bond between a carbon atom of one of the histidine ligands and the sulfur atom of a nearby cysteine residue from the protein backbone. This structural moiety is thought to impose additional structural restraints on the coordination sphere of one of the copper ions, which may in turn optimize the redox potential of the metal needed for the oxidation of the catechol substrate and may allow a rapid electron transfer in the redox processes. Although a very large number of synthetic models of the type-3 active site appeared in literature in the past few decades, relatively little attention has been paid to this thioether bond.[2] In an attempt to mimic this quite unusual structural feature a new dinucleating phenol-based ligand 2,6-bis[*N*-(2-pyridylmethyl)-*N*-(2-thiophenylmethyl)aminomethyl]-4-methylphenol (abbreviated as Hpy2th2s) with two pendant arms, containing pyridine and thiophene residues, was prepared.

Recent studies on the copper complexes of HL_R ligands, published by Belle *et al.*[3] (see Chapter 1), allowed to propose a new catalytic mechanism for catechol oxidation, emphasizing the role of the μ-hydroxo bridge between the two metal centers. It includes the monodentate coordination of the substrate to one of the metal centers with the concomitant cleavage of the OH bridge, and the subsequent proton transfer from the second OH group of the catechol substrate to the hydroxyl group bound to the second copper center.[3] The release of a water molecule results in a bridging coordination of the catecholate, which undergoes an oxidation to quinone. In order to further demonstrate the importance of the μ-hydroxo bridge on the catalytic cycle, two dinuclear copper(II) complexes with Hpy2th2s have been synthesized, and their structural, spectroscopic, magnetic and electrochemical properties along with their interaction with the model substrates, 3,5-di-*tert*-butylcatechol ($DTBCH_2$) and tetrachlorocatechol (TCC), have been investigated. In these complexes, the two metal ions are doubly bridged by the oxygen atom of the phenolate group and a halogen anion. The influence of the bridging ligands (*e.g.* a halogen *vs.* the hydroxyl anion) on the catecholase activity of dicopper(II) complexes is discussed.

4.2 Results and Discussion

4.2.1 Synthesis

The synthesis of this ligand is depicted in Figure 4.1. The starting compound for the ligand synthesis, *N*-(2-pyridilmethyl)-*N*-(2-thiophenylmethyl)amine, was prepared by reacting the commercially available 2-formylthiophene and 2-methylpyridilamine followed by the reduction of the *in situ* generated imine by $NaBH_4$. The starting compound 2,6-bis(chloromethyl)-4-methylphenol was prepared as previously described.[4] The reaction of 2,6-bis(chloromethyl)-4-methylphenol with a stoichiometric

amount of *N*-(2-pyridilmethyl)-*N*-(2-thiophenylmethyl)amine, in the presence of an excess of NEt_3, resulted in the formation of the ligand, which was isolated as a transparent light-yellow oil. The reaction of Hpy2th2s with copper(II) chloride and bromide led to the formation of two new dinuclear copper complexes, which were isolated as a dark-brown and dark-purple crystals, respectively.

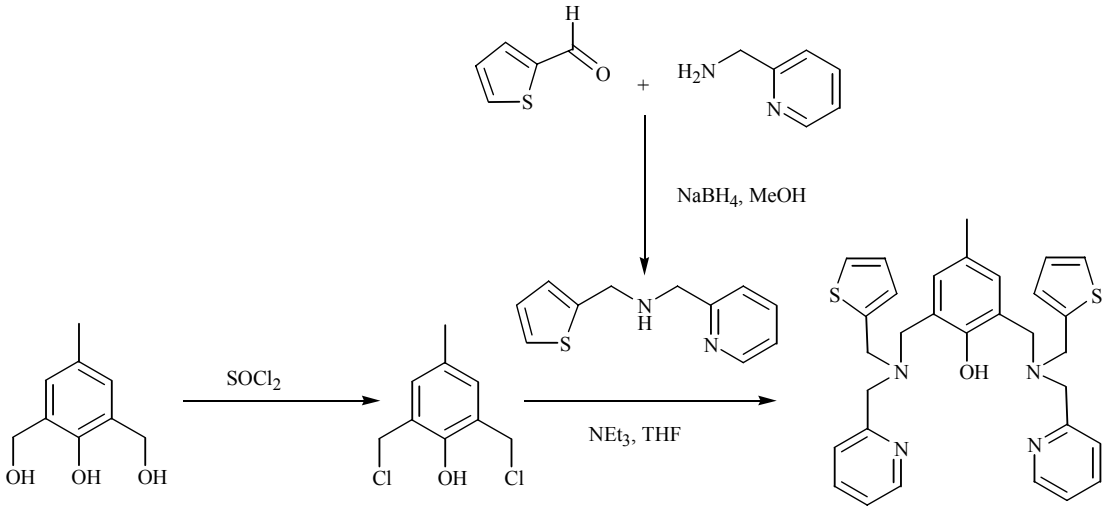

Figure 4.1. The reaction scheme of the synthesis of Hpy2th2s

4.2.2 Crystal structure descriptions

$[Cu_2(py2th2s)(\mu\text{-}Cl)Cl_2]\cdot CH_3OH$ (1)

Rectangular reddish-brown crystals of the complex **1** were obtained by diethyl ether diffusion into a methanol solution containing stoichiometric amounts of copper(II) chloride and the ligand. An ORTEP projection of the crystal structure of the complex is shown in Figure 4.2. Selected bond lengths and angles are presented in Table 4.1.

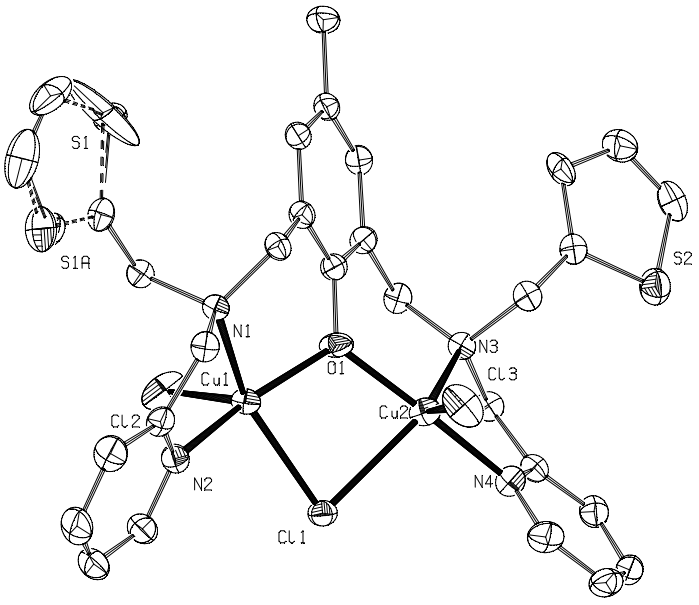

Figure 4.2. ORTEP projection of the complex $[Cu_2(py2th2s)(\mu\text{-}Cl)Cl_2]\cdot CH_3OH$ (**1**). Hydrogen atoms and a non-coordinated methanol molecule are omitted for clarity.

Table 4.1. Selected bond lengths and bond angles of the complex $[Cu_2(py2th2s)(\mu\text{-}Cl)Cl_2]\cdot CH_3OH$ (**1**)

Bond lengths (Å)			
Cu1 - O1	1.9209(19)	Cu2 - O1	1.911(2)
Cu1 - N2	1.975(2)	Cu2 - N4	1.972(2)
Cu1 - N1	2.103(2)	Cu2 - N3	2.083(2)
Cu - Cl1	2.3922(8)	Cu2 - Cl1	2.4717(9)
Cu1 - Cl2	2.3931(10)	Cu2 - Cl3	2.3636(10)
Cu1 - Cu2	3.185(1)		
Bond angles (°)			
O1 - Cu1 - N2	159.33(9)	O1 - Cu2 - N4	168.80(9)
O1 - Cu1 - N1	90.47(8)	O1 - Cu2 - N3	90.59(8)
N2 - Cu1 - N1	81.53(9)	N4 - Cu2 - N3	82.01(9)
O1 - Cu1 - Cl1	82.70(6)	O1 - Cu2 - Cl1	80.76(6)
N2 - Cu1 - Cl1	95.90(7)	N4 - Cu2 - Cl1	97.76(7)
N1 - Cu1 - Cl1	153.25(6)	N3 - Cu2 - Cl1	131.18(6)
O1 - Cu1 - Cl2	100.79(7)	O1 - Cu2 - Cl3	94.77(7)
N2 - Cu1 - Cl2	99.74(7)	N4 - Cu2 - Cl3	96.43(7)
N1 - Cu1 - Cl2	106.18(6)	N3 - Cu2 - Cl3	130.53(6)
Cl1 - Cu1 - Cl2	100.50(3)	Cl1 - Cu2 - Cl3	98.17(4)

The complex crystallizes as methanol solvate in space group $P2_1/n$, with four formula units present per unit cell. The dinuclear core is constituted by two copper(II) ions, bridged on the one side by the endogenous cresolato bridge and on the other side by the chloride anion. The Cu…Cu separation in the complex is 3.185(1) Å. Both copper(II) ions are pentacoordinated with the identical N_2OCl_2 donor sets. However, the complex possesses geometrical asymmetry, as the coordination geometry around Cu1 is almost a regular square pyramid ($\tau = 0.10$),[5] whereas the coordination environment around the Cu2 ion can be best described as a heavily distorted trigonal bipyramid ($\tau = 0.63$).[5] The basal plane of the square pyramid around the Cu1 ion is constituted by the nitrogen atom N1 of the tertiary amine group, the N2 atom of the pyridine ring, the oxygen atom O1 of the cresolate moiety, and the bridging chloride atom Cl1, whereas another chloride anion Cl2 occupies the apical position. In the case of the Cu2 ion, the nitrogen atom N3 of the tertiary amine group, the bridging chloride atom Cl1 and the chloride atom Cl3 form the equatorial plane of the trigonal bipyramid. The axial positions are occupied by the nitrogen atom N4 of the pyridine ring and the oxygen atom O1 of the cresolate group. The thiophene rings of the ligand remain non-coordinated; the Cu…S separations are > 5 Å. One of the thiophene rings shows disorder, with the sulfur atom being refined on two independent positions, with

occupancy factors of 78% (S1) and 22% (S1a). One non-coordinated disordered methanol molecule is present per formula unit, which is hydrogen-bonded to the chloride atom Cl3 (the distance Cl3…O2 = 3.077 Å, the distance Cl3…O2a = 3.179 Å).

$[Cu_2(py2th2s)(\mu\text{-}Br)Br_2]$ (2)

Very dark purple needles of the complex **2** were obtained by slow evaporation of an acetonitrile solution containing stoichiometric amounts of copper(II) bromide and the ligand. An ORTEP projection of the crystal structure is shown in Figure 4.3. Selected bond lengths and angles are presented in Table 4.2.

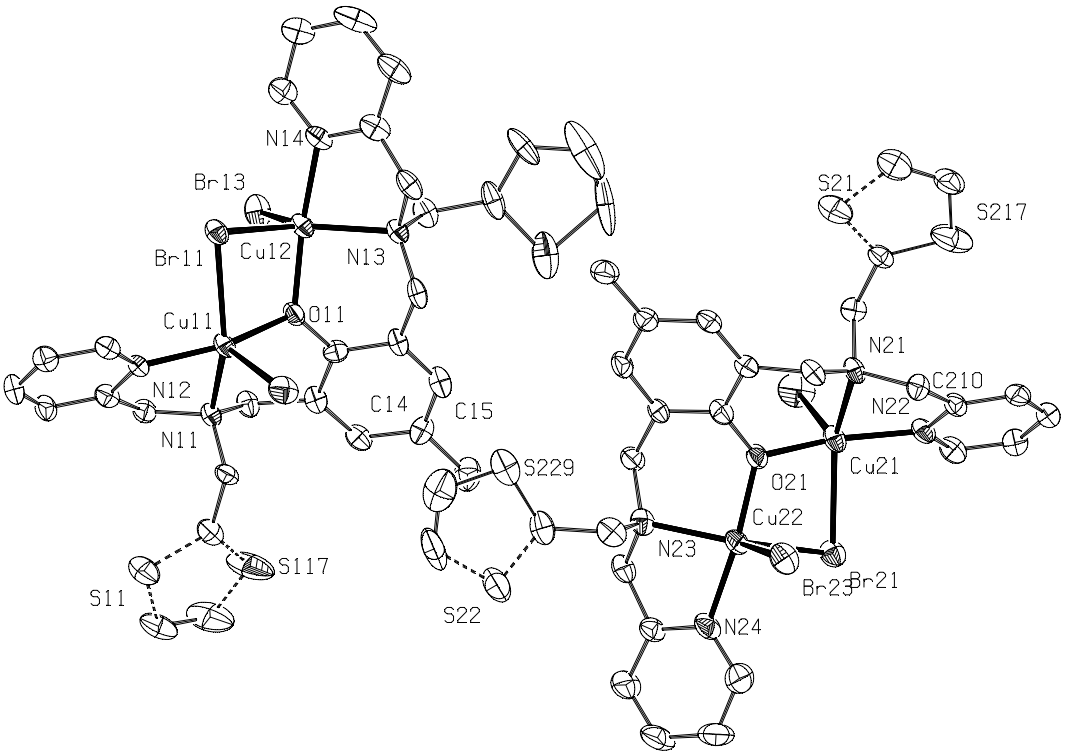

Figure 4.3. ORTEP projection of the two independent formula units of $[Cu_2(py2th2s)(\mu\text{-}Br)Br_2]$ (**2**). Hydrogen atoms are omitted for clarity. Three of the thiophene rings are rotationally disordered.

The complex crystallizes in space group $P\overline{1}$. The asymmetric unit consists of two independent formula units. As in the case of the chloride complex **1**, two copper(II) ions are doubly bridged by the oxygen atom of the cresolate moiety and the halogen anion. The Cu…Cu distances are 3.2710(10) and 3.2394(10) Å, respectively. Both copper ions are pentacoordinated, with N_2OBr_2 donor sets. One of the two independent formula units (Cu11, Cu12) possesses geometrical asymmetry. The geometry around the Cu11 ion is a slightly distorted square pyramid (τ = 0.17),[5] whereas the geometry around the Cu12 ion is a significantly distorted trigonal bipyramid (τ = 0.58).[5]

Table 4.2. Selected bond lengths and bond angles of the complex $[Cu_2(py2th2s)(\mu\text{-}Br)Br_2]$ (**2**).

Bond distances (Å)			
Cu11 - O11	1.925(3)	Cu12 - O11	1.931(4)
Cu11 - N12	1.977(4)	Cu12 - N14	1.986(5)
Cu11 - N11	2.099(4)	Cu12 - N13	2.096(4)
Cu11 - Br11	2.5620(9)	Cu12 - Br11	2.5226(8)
Cu11 - Br12	2.5314(8)	Cu12 - Br13	2.4870(9)
Cu21 - O21	1.931(3)	Cu22 - O21	1.918(4)
Cu21 - N22	1.968(4)	Cu22 - N24	1.981(5)
Cu21 - N21	2.112(4)	Cu22 - N23	2.113(4)
Cu21 - Br21	2.5535(10)	Cu22 - Br21	2.5666(9)
Cu21 - Br22	2.5166(9)	Cu22 - Br23	2.4953(9)
Cu11 - Cu12	3.2710(10)	Cu21 - Cu22	3.2394(10)

Bond angles (°)			
O11 - Cu11 - N12	159.37(17)	O11 - Cu12 - N14	165.93(17)
O11 - Cu11 - N11	91.14(16)	O11 - Cu12 - N13	91.70(17)
N11 - Cu11 - N12	81.55(17)	N13 - Cu12 - N14	81.61(19)
Br11 - Cu11 - O11	81.00(11)	Br11 - Cu12 - O11	81.95(10)
Br11 - Cu11 - N12	95.53(13)	Br11 - Cu12 - N14	93.07(13)
Br11 - Cu11 - N11	149.47(13)	Br11 - Cu12 - N13	130.96(12)
Br12 - Cu11 - O11	97.77(11)	Br13 - Cu12 - O11	96.52(11)
Br12 - Cu11 - N12	102.84(12)	Br13 - Cu12 - N14	97.54(13)
Br12 - Cu11 - N11	108.72(13)	Br13 - Cu12 - N13	119.60(12)
Br11 - Cu11 - Br12	101.58(3)	Br11 - Cu12 - Br13	109.44(3)
O21 - Cu21 - N22	162.14(18)	O21 - Cu22 - N24	164.78(18)
O21 - Cu21 - N21	91.15(16)	O21 - Cu22 - N23	90.99(17)
N21 - Cu21 - N22	81.54(17)	N23 - Cu22 - N24	81.71(19)
Br21 - Cu21 - O21	83.16(12)	Br21 - Cu22 - O21	83.04(11)
Br21 - Cu21 - N22	93.90(14)	Br21 - Cu22 - N24	93.39(15)
Br21 - Cu21 - N21	146.37(13)	Br21 - Cu22 - N23	137.81(12)
Br22 - Cu21 - O21	99.57(12)	Br23 - Cu22 - O21	95.20(11)
Br22 - Cu21 - N22	98.26(13)	Br23 - Cu22 - N24	99.98(14)
Br22 - Cu21 - N21	110.29(13)	Br23 - Cu22 - N23	122.65(12)
Br21 - Cu21 - Br22	103.34(3)	Br21 - Cu22 - Br23	99.51(3)
Cu11 - O11 - Cu12	116.04(18)	Cu21 - O21 - Cu22	114.63(19)
Cu11 - Br11 - Cu12	80.08(3)	Cu21 - Br21 - Cu22	78.50(3)

The nitrogen atom N11 of the tertiary amine group, the nitrogen atom N12 of the pyridine ring, the bridging oxygen atom O11 and the bridging bromide anion Br11 are forming the basal plane of the square pyramid around the Cu11 ion, whereas the monocoordinated bromide anion Br12 is occupying the axial position. The equatorial plane of the trigonal bipyramid around the Cu12 ion is formed by the nitrogen atom N13 of the tertiary amine group and the bromide atoms Br11 and Br13. The axial positions of the bipyramid are occupied by the bridging oxygen atom of the cresolate group and the nitrogen atom N14 of the pyridine ring. One of the non-coordinated thiophene rings is rotationally disordered. Thus, the first orientation has an occupancy factor of 85%, while the 180º rotated orientation has an occupancy factor of 15%. In the second independent formula unit, both copper(II) ions (Cu21 and Cu22) have a significantly distorted square pyramidal geometry (τ = 0.26 for the Cu21 ion and 0.45 for the Cu22 ion)[5]. The basal plane around the Cu21 ion is constituted, similarly to the Cu11 ion, by the two nitrogen atoms N21 and N22, the oxygen atom O21 of the cresolate group and the bridging halogen atom Br21, whereas the bromide anion Br22 occupies the apical position. For the Cu22 ion, the nitrogen atom N23 of the tertiary amine group, the nitrogen atom N24, the bridging oxygen atom O21 and the bridging bromide atom Br21 are forming the basal plane of the square pyramid, with its apical position being occupied by the Br23 atom. Thus, two square pyramids share one side through the atoms O21 and Br21, with their apical positions *trans* located to each other. Both thiophene rings of the ligand remain non-coordinated (Cu…S separations are > 5 Å) and exhibit rotational disorder. Thus, the thiophene ring at S21 was refined on two orientations with occupancies of 0.72 and 0.28, respectively, and the thiophene ring at S22 with occupancies of 0.55 and 0.45, respectively.

4.2.3 Physical characterization

4.2.3.1 Ligand field spectroscopy

The ligand field spectra of both complexes, recorded in the solid state (diffuse reflectance), exhibit almost identical features. Both spectra are characterized by the presence of the charge transfer band from the phenolate moiety to the copper ions[6] around 500 nm (483 nm for complex **1** and 521 nm for complex **2**), and the d-d transition band of the copper(II) ions. The latter band, observed at 774 nm for the chloride complex and at 806 nm for the bromide complex, is in both cases asymmetric, with a shoulder observed at higher wavelengths. As shown previously, such spectroscopic behavior (high-energy absorption band in the visible region with a low-energy shoulder) is typical for square-pyramidal copper(II) complexes.[7] In acetonitrile solution, the charge transfer band is observed at 472 nm for complex **1** (ε = 1851 $M^{-1}cm^{-1}$) and at 500 nm for complex **2** (ε = 1812 $M^{-1}cm^{-1}$). The d-d band is located at 771 nm (ε = 464 $M^{-1}cm^{-1}$) for complex **1** and 791 nm (ε = 534 $M^{-1}cm^{-1}$) for complex **2**.

A small shift of the d-d bands upon dissolution of the complexes in acetonitrile may suggest the coordination of the solvent to the metal centers. However, the partial dissociation of the complexes due to the exchange of the halide anions with acetonitrile molecules can also not be excluded.

4.2.3.2 EPR and magnetic susceptibility studies

Both complexes **1** and **2** are EPR silent in the solid state and in a frozen acetonitrile solution at 100 K, suggesting an antiferromagnetic coupling between the copper ions. Such a behavior is confirmed by the temperature dependence of the molar magnetic susceptibility χ_M depicted in Figure 4.4, which is typical for complexes of antiferromagnetically coupled copper(II) dimers. Indeed the χ_M *vs.* T curves present a broad maximum centered around 160 and 190 K for **1** and **2** respectively, while the values of χ_M at high temperatures (2.10×10^{-3} and 1.85×10^{-3} cm^3 mol^{-1} at 300 K respectively) are slightly lower than expected for two uncoupled copper(II) ions (2.5×10^{-3} cm^3 mol^{-1} for g = 2). Below 40 K, a Curie tail ascribed to paramagnetic impurities is observed, which is usual in such copper(II) complexes. These experimental data were reproduced correctly using the modified Bleaney-Bowers equation (4.1) where χ_M is the magnetic susceptibility per dimer.

$$\chi_M = (1-\rho)\frac{2N_A\beta^2 g^2}{k_B T}\left[3+\exp(-2J/k_B T)\right]^{-1} + 2\rho\left(\frac{N_A\beta^2}{k_B T}\right) + TIP \qquad (4.1)$$

In this equation, $2J$ corresponds to the singlet-triplet energy gap, ρ the fraction of paramagnetic impurity and TIP a term to account for temperature independent paramagnetism, while N_A, β, k_B and g have their usual meaning. The paramagnetic impurity was assumed to be a mononuclear copper(II) species and g was fixed to 2. The best fit parameters were then obtained as $2J$ = –177(2) cm^{-1}, ρ = 1.8(1)% and TIP = $2.9(1)\times10^{-4}$ cm^3mol^{-1} for complex **1** and $2J$ = –219(1) cm^{-1}, ρ = 0.6(1)% and TIP = $2.0(1)\times10^{-4}$ cm^3mol^{-1} for complex **2**. These medium antiferromagnetic couplings should be correlated to a significant overlap between the two magnetic orbitals of the two copper(II) ions in complexes **1** and **2**, through both the halide and phenolate bridges. The short Cu-O bonds and the large Cu-O-Cu angles of the phenolate bridge in **1** and **2**, compared to the long Cu-X bonds, point at a dominant coupling through the phenolate bridge. The coordination sphere around one of the two copper ions is intermediate between a square pyramid and a trigonal bipyramid, while the other has a square pyramidal environment. In the former case, the unpaired electron of copper(II) occupies either the d_z^2 or the $d_{x^2-y^2}$ orbital, which would both point along the Cu-O(phenolate) bond. Short Cu-O bonds and large Cu-O-Cu angles in square pyramidal phenolate bridged Cu dimers result in a strong overlap of $d_{x^2-y^2}$ orbitals and thus produce strong to very strong antiferromagnetic couplings.[8] On the other hand, if one of the copper ions in

such dimers has a trigonal bipyramidal environment, a weaker overlap is expected, and even a weak ferromagnetic coupling has been observed in some cases.[9,10] Therefore, the smaller singlet-triplet energy gap in **1** can be related either to a smaller Cu-O-Cu angle in **1** (*ca.* 112º), compared to **2** (on average over the two dimeric units *ca.* 115.3º), but also to a more distorted trigonal bipyramid coordination sphere in **2** (τ = 0.58, Cu12) than in **1** (τ = 0.63, Cu2). Most likely the difference in the singlet-triplet energy gap is resulting from both structural differences.

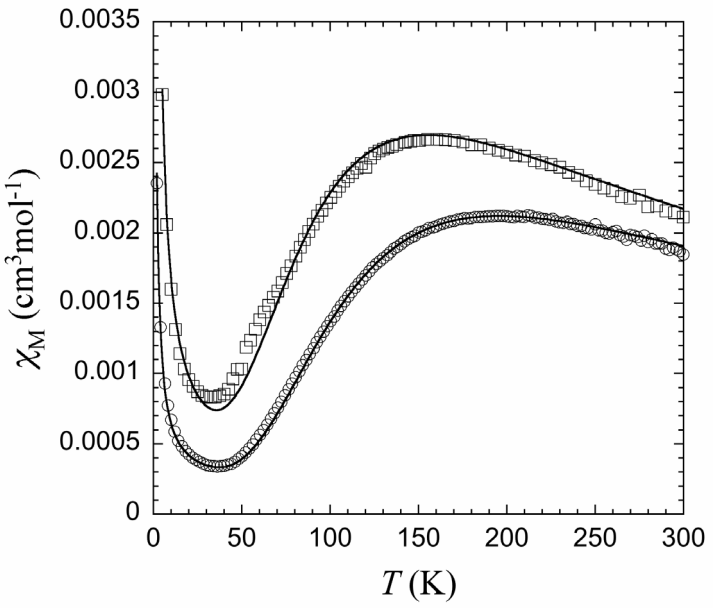

Figure 4.4. χ_M *vs. T* curve for complexes **1** (□) and **2** (○).

4.2.3.3 Electrochemistry

The electrochemical behavior of both complexes was investigated by cyclic voltammetry (CV) and rotating disk electrode voltammetry (RDE) in acetonitrile solution, with tetra-*n*-butylammonium perchlorate (TBAP) as supporting electrolyte (0.1 M). The potentials are referred to an Ag/10mM $AgNO_3$ + CH_3CN + 0.1 M TBAP reference electrode.

When scanning towards the negative region of potentials, the CV curve for both complexes **1** and **2** is characterized by three successive electrochemical signals (Figures 4.5 and 4.6). While the first one for **1**, at E_{pc} = -0.52 V, is irreversible, re-oxidation of the reduced species being seen on the reverse scan at +0.23 V (Figure 4.5, curve a), for **2** it appears to be quasi reversible with $E_{1/2}$ = -0.34 V (ΔE_p = 0.12 V, Figure 4.6, curve a). Coulometric titrations give n = 1 exchanged electron per complex, allowing to attribute this electrochemical system to the complexed $Cu^{II,II}{}_2/Cu^{II,I}{}_2$ redox couple. The UV-Vis spectra of the one-electron reduced complexes exhibit one very broad band around 680 nm. The lack of reversibility of the first electrochemical reduction of **1** and **2** suggests a change in the coordination sphere around the metal center upon reduction, likely a partial dissociation of the exogenous halide ligand and a change in the geometry

of the coordination sphere. Additional electrochemical measurements performed at -40 °C showed that the course of these coupled chemical reaction is not prevented at low temperature. The second electrochemical signal, quasi reversible with $E_{1/2}$ = -0.78 V for **1** and at $E_{1/2}$ = -0.72 V for **2**, corresponds as well to a one-electron process, leading to the complexed $Cu^{II,I}{}_2/Cu^{I,I}{}_2$ redox couple. Finally, the third electrochemical signal at E_{pc}= -1.45 V for **1** and -1.04 V for **2** corresponds to a two-electron process, suggesting the reduction of Cu^{I} ions to the Cu^{0} state and the deposition of metallic copper on the electrode surface. Accordingly, an additional sharp anodic peak is observed on the reverse scan, caused by the redissolution of the metallic copper.

The anodic behavior of complexes **1** and **2** differs. The anodic part of the CV curve for **1** (Figure 4.5, b) is characterized by two electrochemical signals, whereas three signals are observed on the CV curve for **2** (Figure 4.6, b). For **1**, the first one at $E_{1/2}$ = 0.64 V (ΔE_p = 0.26 V) corresponds to a one-electron quasi-reversible oxidation of the complex. The electron transfer is likely to be centered on the phenolate bridge, as previously shown for other phenolate-bridged dinuclear copper(II) complexes.[6,11] This process is followed by the oxidation of the chloride anions which is seen as a shoulder at the negative foot of the over-oxidation wave of the complex (free chloride anions are reversibly oxidized at 0.72 V under the current experimental conditions).

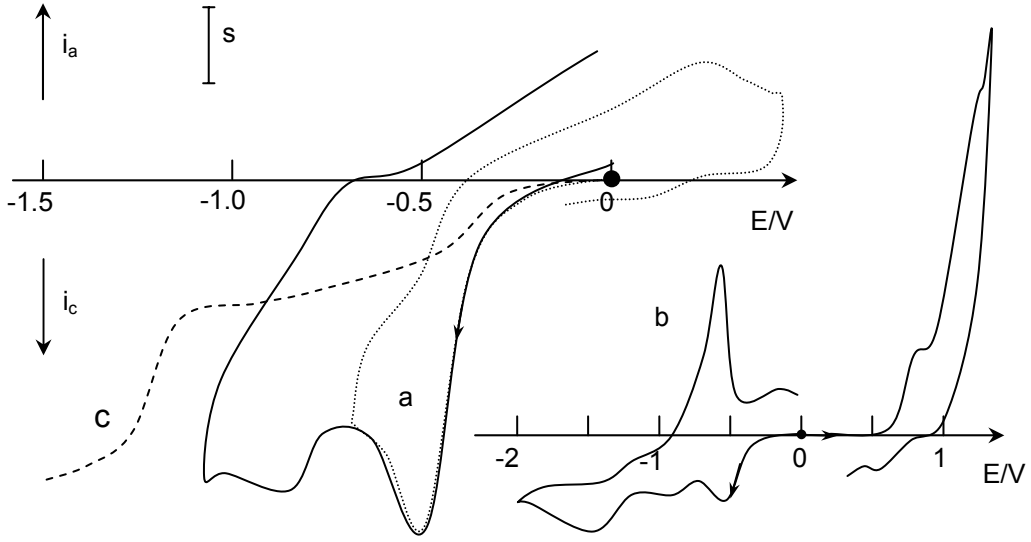

Figure 4.5. Electrochemical curves recorded in a 0.67 mM solution of **1** in CH_3CN + TBAP 0.1 M on a Pt disc (∅ = 5 (a, b) or 3 (c) mm); curves a, b: CV curves, v = 0.1 V s^{-1}; curve c: RDE curve, N = 600 rpm; V *vs* $Ag/AgNO_3$ mM + CH_3CN + TBAP 0.1 M. Scale s = 20 µA (curve a), 120 µA (curve b) or 10 µA (curve c)

The CV curve recorded in a solution of **2** shows an additional fully irreversible one-electron system at E_{pa} = 0.47 V. It is assumed to be due to the one-electron oxidation of bromide anions, free bromide anions being irreversibly oxidized at E_{pa} = 0.39 V under the current experimental conditions. The one-electron, phenolate-based,

oxidation of the complex **2**, similarly to **1**, is observed as a quasi-reversible pair of peaks at $E_{1/2}$ = 0.76 V (ΔE_p = 0.18 V) and is followed at higher potentials by the over-oxidation of the complex.

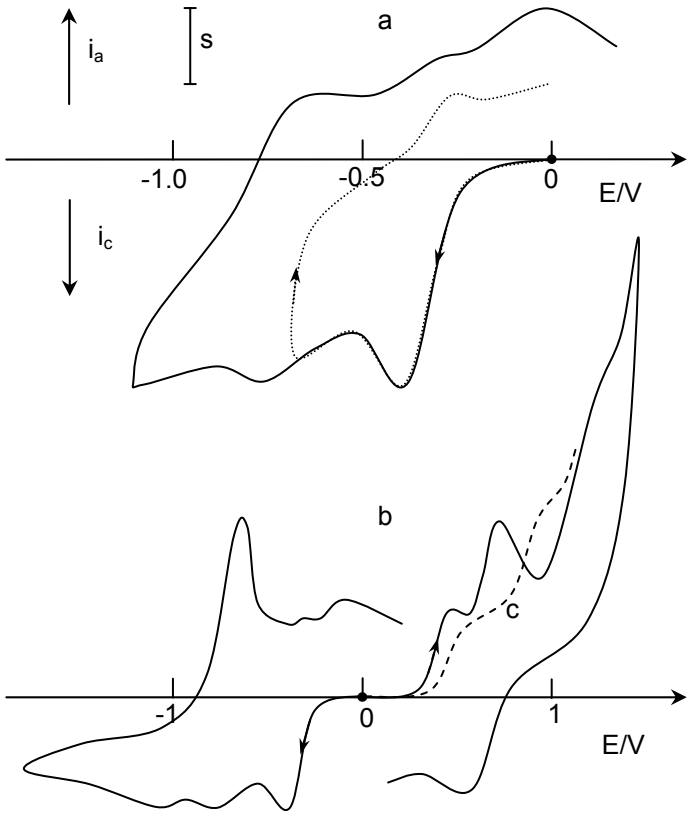

Figure 4.6. Electrochemical curves recorded in a 0.67mM solution of **2** in CH_3CN + TBAP 0.1 M on a Pt disc (∅ = 5 (a, b) or 3 (c) mm); curves a, b: CV curves, v = 0.1 V s^{-1}; curve c: RDE curve, N = 600 rpm; V *vs* $Ag/AgNO_3$ mM + CH_3CN + TBAP 0.1 M. Scale s = 20 μA (curve a), 40 μA (curve b, c).

These results have been confirmed by rotating disk electrode (RDE) voltammetry experiments (Figures 4.5 and 4.6, dashed lines). The RDE curves display one anodic wave at $E_{1/2}$ = 0.84 V for **1** and two successive well-behaved anodic waves at $E_{1/2}$ = 0.42 V and 0.82 V (Figure 4.6, curve c) for **2**. For both complexes, three successive cathodic waves are seen. For **1** and **2**, the first one at $E_{1/2}$ = -0.42 V and -0.40 V, respectively, is followed by a second ill-behaved wave at $E_{1/2}$ = -0.78 V and -0.80 V respectively. The third cathodic wave corresponding to the deposition of metallic copper onto the electrode surface is observed at $E_{1/2}$ = -1.22 V and –1.20 V, respectively.

4.2.3.4 Conductivity measurements

The conductivity measurements of the complexes **1** and **2** were performed on 0.5 mM solutions of the complexes in acetonitrile. The calculated values for equivalent conductivities of both compounds are roughly the same and are equal to 52 $cm^2 \cdot mol^{-1} \cdot Ohm^{-1}$ for complex **1** and 55 $cm^2 \cdot mol^{-1} \cdot Ohm^{-1}$ for complex **2**. Previously, the conductivity range for complexes corresponding to 1:1 type electrolytes was

suggested to lie between 120 and 160 $cm^2 \cdot mol^{-1} \cdot Ohm^{-1}$, if acetonitrile was utilized as a solvent.[12] Although values as low as 90 $cm^2 \cdot mol^{-1} \cdot Ohm^{-1}$ were also reported in some cases, the observed conductivities of both complexes **1** and **2** are still too low to address them as 1:1 electrolytes. As shown previously,[13] such small conductivity values are often found in acetonitrile for non-electrolytes, due to coordinating and solvating properties of this solvent. Some authors[13] argue that they may indicate a partial exchange of counter anions with solvent molecules. Small changes in the positions of the UV-Vis-NIR d-d bands of the complexes upon their dissolution in acetonitrile, observed in the present case, appear to sustain this assumption.

4.2.4 Interaction of the complexes with the model substrates

4.2.4.1 Catecholase activity measurements

To evaluate the ability of the complexes to behave as functional models of catechol oxidase, they were tested as catalysts in the oxidation of 3,5-di-*tert*-butylcatechol ($DTBCH_2$), a widely used model substrate, to the respective quinone. Both complexes exhibit only negligible catecholase activity (TON < 1 after 30 min), making a detailed kinetic analysis dispensable. These results are as expected, confirming that the substitution of the μ-hydroxo bridge by a halogen anion precludes the catecholase activity. However, these results do not provide information whether or not the binding of the substrate to the metal centers ***at all*** takes place. Reim *et al.*[14] have previously shown that, in the case of essentially inactive complexes, no interaction between the dimetal core and the substrate occurred (see Chapter 1). To evaluate whether or not the first step of the catalytic cycle, *e.g.* the binding of catechol to the metal centers, takes place, the interaction of the complexes with tetrachlorocatechol (TCC) was studied. The latter catechol has a very high oxidation potential due to its electron-withdrawing substituents, and is not oxidized by copper complexes.

4.2.4.2 TCC binding studies

The titration of $5 \cdot 10^{-4}$ M solutions of the complexes in acetonitrile with TCC was followed by means of UV-Vis and EPR spectroscopy. The changes observed in UV-Vis spectra of complex **1** upon addition of TCC (up to 4 equivalents) are depicted in Figure 4.7, left. Quite significant changes in the spectrum of the original complex indicate the interaction between the substrate and the metal centers. The presence of two isosbestic points at 570 nm and 724 nm shows the occurrence of only two absorbing species in solution. The Cu^{II} d-d transition band shifts gradually from 789 nm to 718 nm, whereas its absorption decreases to *ca.* 50% of its initial value. Also, the extinction coefficient of the LMCT band decreases from 1851 to *ca.* 1600 $M^{-1}cm^{-1}$ (Figure 4.7).

Whereas the chloride complex obviously reacts with TCC, no changes in the UV-Vis spectrum were observed upon addition of TCC to the bromide complex. Taking

into account a very large structural similarity between the two complexes, it seems reasonable to suggest that the difference in their behavior is caused by the different halogen anions, coordinated to the copper ions. The Cu-Cl bond has a more ionic character in comparison with the Cu-Br bond, which therefore facilitates the substitution of (at least one of) the chloride anions by catechol, whereas no exchange of Br anions with TCC occurs.

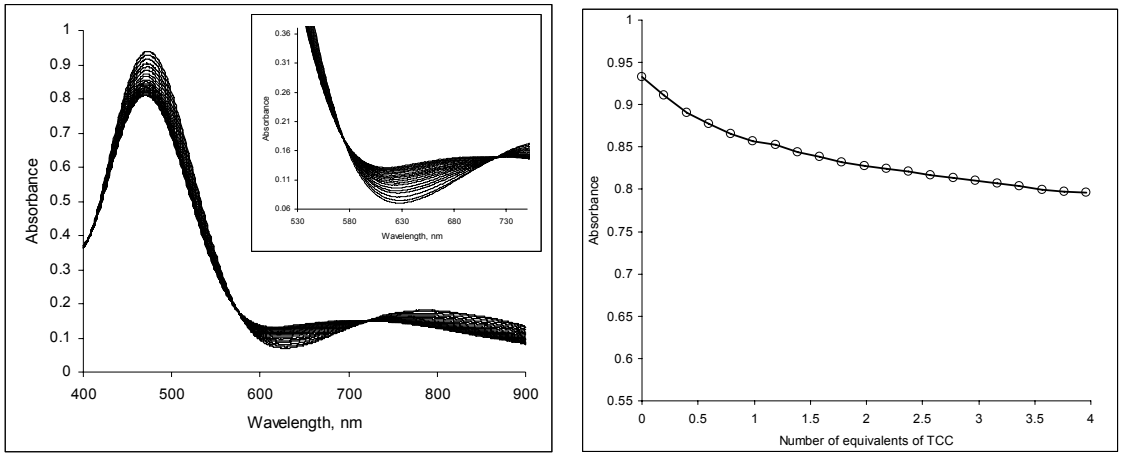

Figure 4.7. Left: UV-Vis titration of the complex **1** (0.5 mM solution in acetonitrile) with TCC (from 0 to 4 equivalents). The insert shows the enlargement of the spectroscopic curves in the range 530-780 nm. Right: decrease of the LMCT band (474 nm) upon titration of the solution of **1** (0.5 mM) in acetonitrile with TCC.

A titration of complex **1** with TCC, followed by X-band EPR spectroscopy, revealed that no evolution of the EPR signal is observed upon addition of TCC. This indicates that the two copper ions are strongly antiferromagnetically coupled, suggesting that they probably remain doubly bridged by the phenolate group and the chloride anion. Although a few structures of copper(II) complexes with a bridging catecholate were previously described,[15,16] no magnetic properties of these compounds have been reported. However, it can be proposed that the cleavage of the halide bridge would lead to the decrease in strength of the magnetic coupling, similarly to the behavior of previously reported μ-hydroxo complexes with phenol-based ligands[3] after the cleavage of the hydroxo bridge. Thus, the reaction of TCC with the chloride complex results probably in the substitution of at least one of the apical chloride anions. In order to further confirm this hypothesis the conductivity of complex **1** in acetonitrile solution before and after an addition of TCC was studied. The equivalent conductivity of TCC itself in CH_3CN is negligible.

The values of the equivalent conductance, observed after addition of 1-4 equivalents of TCC to a 0.5 mM solution of complex **1** are listed in Table 4.3. As can be seen, a substantial increase in conductivity is observed after one equivalent of TCC has been added. Further addition of TCC leads to a slight increase of conductivity, till a

final value of 118 $cm^2 \cdot mol^{-1} \cdot Ohm^{-1}$ is reached. This value fits perfectly in the range suggested for 1:1 electrolytes in acetonitrile.[12] The interaction of **1** with TCC leads to the release of one chloride anion in solution, the complete release being reached in the presence of an excess of TCC as shown by the slight increase of the conductivity above one molar equivalent added. The reversible character of this process is further confirmed from UV-Vis titration experiments that showed that the maximal perturbation in the UV-Vis spectra was reached in the presence of at least 3 equivalents of TCC (Figure 4.7).

Not surprisingly, additions of TCC to the bromide complex do not lead to an increase in conductivity, which is in complete agreement with the hypothesis that no substitution of Br^- anions with TCC is possible.

Table 4.3. Changes in the equivalent conductivity of a 0.5 mM solution of **1** in acetonitrile upon treatment with TCC

Number of equivalents of TCC	*Equivalent conductivity ($cm^2 mol^{-1} Ohm^{-1}$)*
0	52
1	100
2	110
3	117
4	118

4.2.5 General discussion

Many attempts to establish a correlation between the structural parameters of the complexes and their catalytic activity in the oxidation of catechols have been described in literature. Three most important criteria influencing the catalytic properties of the complexes can now be distinguished: (i) the distance between the metal centers;[6,17,18] (ii) the nature of the bridging group between the metal ions;[19,20] (iii) the electronic properties of the complexes.[11] Some other factors, *e.g.* the imposed strain in the complex, due to the rigidity of either the ligand and/or the bridging group, may also play a role.[14] Results published by Reim *et al.*[14] (see Chapter 1) indicate that complexes with strained structures show catalytic activity, whereas complexes present in relaxed, energetically favored conformation are essentially inactive towards catechol oxidation. In the chloride and bromide complexes **1** and **2**, the metal-metal distance and the redox potentials of the metal ions are comparable with the values previously determined for catalytically active complexes;[6,14,19] thus, the absence of catalytic activity is not likely to be due to these two factors. Also, the coordination spheres around the copper ions in both complexes exhibit quite a large distortion from a regular square-pyramidal geometry, resulting in relatively

strained structures. Thus, the main reason for the absence of catalytic activity must originate from the nature of the bridging groups between the two copper ions in the complexes. As discussed above, the crucial steps of the mechanism earlier proposed[3] is the cleavage of the OH bridge between the two metal ions and the subsequent proton transfer from the catechol substrate to the hydroxyl anion, leading to the release of one water molecule. It has been shown that the reaction of catechol with the complexes **1** and **2** does not result in a cleavage of the bridge, although the binding of the substrate to the chloride complex undoubtedly takes place. These results thus emphasize the influence of the bridging group between the copper centers on the catecholase activity of the complexes and underline the importance of the exogenous hydroxo bridge for the catalytic mechanism. This hydroxo ligand appears to be the key factor to achieve the complete deprotonation of catechol, leading to a bridging catecholate prior to the electron transfer. Upon substitution of the hydroxo bridge by a halogen anion, no proton transfer can occur, precluding the binding of catecholate in a didentate bridging fashion, and thus the subsequent catalytic cycle.

4.3 Experimental Section

4.3.1 Materials and Methods

All starting materials were commercially available and used as purchased. 2,6-bis(chloromethyl)-4-methylphenol was prepared as previously described.[4] The NMR spectra were recorded on a JEOL FX-200 (200 MHz) FT-NMR spectrometer. The ligand field spectra of the solids (300-2000 cm^{-1}, diffuse reflectance) were taken on a Perkin-Elmer 330 spectrophotometer equipped with a data station. The ligand field spectra in solution were recorded on a Varian Cary 50 Scan UV-Vis spectrophotometer. Electrospray mass spectra (ESI-MS) in acetonitrile solutions were recorded on a Thermo Finnigan AQA apparatus. X-band electron paramagnetic resonance (EPR) measurements were performed at 77 K in the solid state on a Jeol RE2x electron spin resonance spectrometer, using DPPH ($g = 2.0036$) as a standard, and at 100 K as acetonitrile frozen solutions on a Bruker ESP 300E spectrometer operating at 9.4 GHz (X-band). The conductivity measurements were performed using a Philips PW9526 digital conductivity meter and a PW 9552/60 measuring cell with 0.5 mM solutions of the complexes in acetonitrile. The electrochemical behavior of the complexes was investigated in a 0.1 M solution of tetra-*n*-butylammonium perchlorate (TBAP) in acetonitrile using a EGG 273 potentionstat coupled with a Kipp&Zonen x-y recorder. The experiments were performed at room temperature or at -40 °C in a three-compartment cell. Potentials are referred to an Ag/10 mM $AgNO_3$ + CH_3CN + 0.1 M TBAP reference electrode. The working electrode was a platinum disk of 5 mm diameter for the cyclic voltammetry (CV, 0.1 V/s) experiments or 3 mm diameter for the rotating disk electrode (RDE, 600 rpm) voltammetry experiments. The working

electrode was polished with 1 μm diamond paste prior to each recording. Bulk magnetizations of polycrystalline samples were performed on the crystals of the complexes **1** (11.11 mg) and **2** (16.88 mg) in the temperature range 5-400 K with a Quantum Design MPMS-5S SQUID magnetometer, in a 1 kG applied field. The data were corrected for the experimentally determined contribution of the sample holder. Corrections for the diamagnetic responses of the complexes, as estimated from Pascal's constants, were applied.[21]

4.3.2 Catecholase activity study

The catecholase activity of the complexes was evaluated by reaction with 3,5-di-*tert*-butylcatechol at 25 ºC. The absorption at 400 nm, characteristic of the formed quinone, was measured as a function of time. The experiments were run under 1 atm of dioxygen. 3 ml of a $2.5 \cdot 10^{-4}$ M solution of complex in acetonitrile were placed in a 1 cm path-length cell, and 75 μl of a 1 M solution of the substrate in the same solvent were added. After thorough shaking, the changes in UV-Vis spectra were recorded during 30 min.

The titration of the complexes with tetrachlorocatechol (TCC) was carried out by adding 3 μl aliquots of a 0.1 M solution of TCC (corresponding to 0.198 eq of TCC/1 eq of the complex) to 3 ml of a $5 \cdot 10^{-4}$ M solution of complex in acetonitrile.

4.3.3 Ligand synthesis

***N*-(2-pyridylmethyl)-*N*-(2-thiophenylmethyl)amine:** A solution of 2.00 g (18.5 mmol) of 2-pyridilmethylamine was added dropwise upon stirring to a solution of 2.08 g (18.5 mmol) of 2-formylthiophene in MeOH. The resulting solution was stirred overnight at room temperature. Afterwards, 2.1 g (56 mmol, 3 eq per 1 CH=N) of $NaBH_4$ were added slowly, and the resulting solution was heated three hours at 50 ºC. After evaporation of the solvent, the obtained oil was redissolved in a mixture of dichloromethane and water. The organic and aqueous layers were separated, and the water layer was washed twice with a small amount of dichloromethane. After drying the dichloromethane layer over Na_2SO_4 and evaporation under reduced pressure, the pure product was obtained as light yellow oil. The product is light-sensitive and should be preferably stored in the dark at low temperatures. Yield: 95%. ^{1}H NMR ($CDCl_3$, 200 MHz, ppm): δ = 2.28 (s, 1 H, NH); 3.95 (s, 2H, NHCH_2th); 4.03 (s, 2H, NHCH_2py); 6.93 (d, 1H, 3'th); 6.96 (s, 1H, 4'th); 7.20 (d, 1H, 5'th); 7.15 (t, 1H, 5'py); 7.30 (d, 1H, 3'py); 7.62 (t, 1H, 4'py); 8.55 (d, 1H, 6'py).

2,6-bis[*N*-(2-pyridylmethyl)-*N*-(2-thiophenylmethyl)aminomethyl]-4-methylphenol (Hpy2th2s): A solution of 0.7 g (3.4 mmol) of *N*-(2-pyridylmethyl)-*N*-(2-thiophenylmethyl)amine and 0.7 g (7 mmol) of Et_3N in THF was added dropwise upon stirring to a solution of 0.35 g (1.7 mmol) of 2,6-bis(chloromethyl)-4-methylphenol in THF. After refluxing for 2 hours, the solution was cooled to room

temperature. The filtration of the triethylammonium salt and the subsequent evaporation of the solvent resulted in an oil, which was dissolved in acidified water and washed with dichloromethane. The water layer was made alkaline by adding a concentrated aqueous solution of NH_3, and the resulting suspension was extracted three times with dichloromethane. The organic layer was dried over Na_2SO_4 and evaporated under reduced pressure. The resulting oil was found to be the pure product. Yield: 84%. ^{1}H NMR ($CDCl_3$, 200 MHz, ppm): δ = 2.28 (s, 3H, C<u>H</u>$_3$); 3.82 (s, 4H, NC<u>H</u>$_2$th); 3.85 (s, 4H, phC<u>H</u>$_2$N); 3.89 (s, 4H, NC<u>H</u>$_2$py); 6.95 (m, 4H, 3'th + 4'th), 7.04 (s, 2H, 3'ph + 5'ph); 7.15 (t, 2H, 5'th); 7.24 (d, 2H, 3'py); 7.53 (d, 2H, 5'th); 7.66 (t, 2H, 4'py); 8.56 (d, 2H, 6'py); 10.40 (1H, O<u>H</u>). ESI-MS: m/z 541 ($M + H^+$)

4.3.4 Syntheses of the coordination compounds

[Cu$_2$(py2th2s)(*μ*-Cl)Cl$_2$]·CH$_3$OH (1): 0.15 g (0.28 mmol) of ligand Hpy2th2s and 0.10 g (0.54 mmol) of copper chloride were dissolved in 10 ml of methanol. Addition of 20 ml of diethyl ether resulted in the precipitation of the complex as a dark brown powder. Yield: 46% (102 mg). Single crystals of the complex were obtained by slow diffusion of diethyl ether into a 0.01 M solution of the complex. Elemental analysis, % found (calc.) for [Cu$_2$(py2th2s)(*μ*-Cl)Cl$_2$]·CH$_3$OH (= $C_{32}H_{36}Cl_3Cu_2N_4O_2S_2$): C, 45.73 (47.73), H, 4.14 (4.38), N, 7.25 (6.96), S, 7.91 (7.96). ESI-MS: m/z 737 ([Cu$_2$(py2th2s)Cl$_2$]$^+$)

[Cu$_2$(py2th2s)(*μ*-Br)Br$_2$] (2): 0.15 g (0.28 mmol) of ligand Hpy2th2s and 0.12 g (0.54 mmol) of copper bromide were dissolved in 10 ml of methanol. After addition of diethyl ether to the resulting solution, the complex precipitated as a dark-purple crystalline powder. Yield: 64% (155 mg). Crystals suitable for X-ray diffraction were obtained by slow diffusion of diethyl ether into a 0.01 M solution of the complex in acetonitrile. Elemental analysis, % found (calc.) for [Cu$_2$(py2th2s)(*μ*-Br)Br$_2$] (=$C_{31}H_{32}Br_3Cu_2N_4OS_2$): C, 39.76 (40.95), H, 3.42 (3.76), N, 6.07 (5.97), S, 6.50 (6.83). ESI-MS: m/z 827 ([Cu$_2$(py2th2s)Br$_2$]$^+$)

4.3.5 X-ray crystallographic measurements

[Cu$_2$(py2th2s)(*μ*-Cl)Cl$_2$]·CH$_3$OH (1): A single crystal of [Cu$_2$(py2th2s)(*μ*-Cl)Cl$_2$]·CH$_3$OH (**1**) was mounted at 150 K on a Bruker AXS SMART 6000 diffractometer equipped with Cu-Kα radiation (λ = 1.54184 Å). $C_{32}H_{36}Cu_2N_4O_2S_2Cl_3$, Fw= 802.17, rectangular reddish-brown plates, 0.23×0.21×0.05 mm, a = 7.984(2), b = 34.589(7), c = 12.554(3) Å, β = 94.31(3)°, Z = 4, V = 3457(2) Å^3, monoclinic, space group $P2_1/n$ (no. 14), $\rho_{calc.}$ = 1.541 g cm^{-3}, μ = 5.068 mm^{-1}, absorption correction: SADABS,[22] reflections collected: 19864, independent reflections: 6317 (R_{int} = 0.0386). The structure was solved by direct methods and refined using the SHELX program package.[23,24] All hydrogen atoms were placed on idealized positions riding on the carrier atom, with isotropic displacement parameters. The final cycle of full-matrix least-

squares refinement, including 438 parameters, converted to *R1* = 0.0352 (*R1* = 0.0430 all data) and *wR2* = 0.1009 (*wR2* = 0.1038 all data) with a maximum (minimum) residual electron density of 0.535 (–0.466) e Å^{-3}.

[Cu$_2$(py2th2s)(μ-Br)Br$_2$] (2): $C_{31}H_{31}Br_3Cu_2N_4OS_2$ + solvent, Fw = 906.53, red needle, 0.60×0.06×0.03 mm^3, triclinic, $P\overline{1}$ (no. 2), a = 8.4207(2), b = 17.9812(4), c = 24.2238(6) Å, α = 71.2709(9), β = 81.2708(7), γ = 80.6146(11)°, V = 3407.66(14) Å^3, Z = 4, $\rho_{calc.}$ = 1.767 g cm^{-3}, 43713 measured reflections, 12061 unique reflections (R_{int} = 0.0734), 8080 observed reflections [I > 2σ(I)]. 775 refined parameters, no restraints. *R* (obs. refl.): *R1* = 0.0461, *wR2* = 0.1121. *R* (all data): *R1*= 0.0776, *wR2* = 0.1286. S = 1.085. Residual electron density between –1.08 and 1.17 e/Å^3. Intensities were measured on a Nonius KappaCCD diffractometer with rotating anode (Mo-Kα, λ = 0.71073 Å) at a temperature of 150 K. An absorption correction based on multiple measured reflections was applied (μ = 4.920 mm^{-1}, 0.59-0.86 transmission). The structure was solved with direct methods using the program SHELXS97,[25] and refined with the program SHELXL97[24] against F^2 of all reflections up to a resolution of (sin $\vartheta/\lambda)_{max}$ = 0.60 Å^{-1}. Non-hydrogen atoms were refined freely with anisotropic displacement parameters. Hydrogen atoms were refined as rigid groups. Three of the thiophene rings were rotationally disordered and refined with occupancies of 0.85:0.15, 0.72:0.28, and 0.55:0.45, respectively. The crystal structure contains large voids (150.9 Å^3/unit cell) filled with disordered solvent molecules. Their contribution to the structure factors was secured by back-Fourier transformation (program PLATON,[26] CALC SQUEEZE, 22 e$^-$/unit cell). The drawings, structure calculations, and checking for higher symmetry was performed with the program PLATON.[26]

CCDC-230014 (compound **1**) and 230015 (compound **2**) contain the supplementary crystallographic data for this chapter. These data can be obtained free of charge at www.ccdc.cam.ac.uk/conts/retrieving.html [or from the Cambridge Crystallographic Data Centre, 12, Union Road, Cambridge CB2 1EZ, UK; fax: (internat.) +44-1223/336-033; E-mail: deposit@ccdc.cam.ac.uk].

4.4 References

(1) Klabunde, T.; Eicken, C.; Sacchettini, J. C.; Krebs, B. *Nat. Struct. Biol.* **1998**, *5*, 1084-1090.
(2) Merkel, M.; Möller, N.; Piacenza, M.; Grimme, S.; Rompel, A.; Krebs, B. *Chem. Eur. J.* **2005**, *11*, 1201-1209.
(3) Torelli, S.; Belle, C.; Hamman, S.; Pierre, J. L.; Saint-Aman, E. *Inorg. Chem.* **2002**, *41*, 3983-3989.
(4) Borovik, A. S.; Papaefthymiou, V.; Taylor, L. F.; Anderson, O. P.; Que, L. *J. Am. Chem. Soc.* **1989**, *111*, 6183-6195.
(5) Addison, A. W.; Rao, T. N.; Reedijk, J.; van Rijn, J.; Verschoor, G. C. *J. Chem. Soc., Dalton Trans.* **1984**, 1349-1356.
(6) Torelli, S.; Belle, C.; Gautier-Luneau, I.; Pierre, J. L.; Saint-Aman, E.; Latour, J. M.; Le Pape, L.; Luneau, D. *Inorg. Chem.* **2000**, *39*, 3526-3536.
(7) Rajendran, U.; Viswanathan, R.; Palaniandavas, M.; Laskiminaraya, N. *J. Chem . Soc., Dalton Trans.* **1994**, 1219-1226.
(8) Ruiz, E.; Alemany, P.; Alvarez, S.; Cano, J. *J. Am. Chem. Soc.* **1997**, *119*, 1297-1303.
(9) Bertoncello, K.; Fallon, G. D.; Hodgkin, J. H.; Murray, K. S. *Inorg. Chem.* **1988**, *27*, 4750-4758.

(10) Sorrel, T. N.; O'Connor, C. J.; Anderson, O. P.; Reibenspies, J. H. *J. Am. Chem. Soc.* **1985**, *107*, 4199-4206.
(11) Belle, C.; Beguin, C.; Gautier-Luneau, I.; Hamman, S.; Philouze, C.; Pierre, J. L.; Thomas, F.; Torelli, S.; Saint-Aman, E.; Bonin, M. *Inorg. Chem.* **2002**, 479-491.
(12) Geary, W. J. *Coord. Chem. Rev.* **1971**, *7*, 81-122.
(13) Walton, R. A. *Quart. Rev.* **1965**, *19*, 126-143.
(14) Reim, J.; Krebs, B. *J. Chem. Soc., Dalton Trans.* **1997**, 3793-3804.
(15) Börzel, H.; Comba, P.; Pritzkow, H. *Chem. Commun.* **2001**, 97-98.
(16) Karlin, K. D.; Gultneh, Y.; Nicholson, T.; Zubieta, J. *Inorg. Chem.* **1985**, *24*, 3725-3727.
(17) Fernandes, C.; Neves, A.; Bortoluzzi, A. J.; Mangrich, A. S.; Rentschler, E.; Szpoganicz, B.; Schwingel, E. *Inorg. Chim. Acta* **2001**, *320*, 12-21.
(18) Kao, C.-H.; Wei, H.-H.; Liu, Y.-H.; Lee, G.-H.; Wang, Y.; lee, C.-J. *J. Inorg. Biochem.* **2001**, *84*, 171-178.
(19) Neves, A.; Rossi, L. M.; Bortoluzzi, A. J.; Szpoganicz, B.; Wiezbicki, C.; Schwingel, E.; Haase, W.; Ostrovsky, S. *Inorg. Chem.* **2002**, *41*, 1788-1794.
(20) Mukherjee, J.; Mukherjee, R. *Inorg. Chim. Acta* **2002**, *337*, 429-438.
(21) Kolthoff, I. M.; Elving, P. J. *Treatise on Analytical Chemistry*; Interscience Encyclopedia, Inc.: New York, 1963.
(22) Bruker AXS Inc., Madison, WI, 1999.
(23) Sheldrick, G. M.; *SHELXTL PLUS*. University of Göttingen, Germany, 1990
(24) Sheldrick, G. M.; *SHELXL-97, Program for the refinement of crystal structures*. University of Göttingen, Germany, 1997
(25) Sheldrick, G. M.; *SHELXS-97, Program for crystal structure solution*. University of Göttingen, Germany, 1997
(26) Spek, A. L. *J. Appl. Cryst.* **2003**, *36*, 7-13.

5 | X-ray 3D structures and properties of two copper(II) complexes with an asymmetric phenol-based N,O,S-ligand. Influence of the counter ion on the crystal packing[†]

The new asymmetric phenol-based N,O,S-ligand Hpy2th1as (2-[*N,N*-bis(2-pyridylmethyl)aminomethyl]-4-methyl-6-[2-thiophenylmethyl)aminomethyl]phenol) was prepared by the straightforward reductive amination of 3-[*N,N*-bis(2-pyridylmethyl)aminomethyl]-5-methylsalicylaldehyde (= Hpy2ald, Chapter 3) with 2-thiophenylmethylamine. This ligand was designed to bind two copper(II) ions, providing different steric accessibility for each of them, and to mimic the unusual thioether bond in a close proximity to the metal centers, present in the active site of catechol oxidase. The reaction of Hpy2th1as with copper(II) chloride in methanol results in the formation of the complex $[Cu_2(H_2py2th1as)_2Cl_2](CuCl_4)_2$. During the crystallization, the ligand undergoes a protonation of the secondary amine group, which results in the ligand coordination to only one copper(II) ion. Two mononuclear units are further doubly bridged by two chloride anions, and the positive charge is compensated by two tetrachlorocuprate anions, formed during the crystallization. The complex with a very similar structure of the composition $[Cu_2(H_2py2th1as)_2Cl_2](ClO_4)_4 \cdot 6CH_3OH$ was prepared by reaction of the ligand with copper(II) perchlorate in the presence of the chloride ions. Although the two coordination compounds exhibit virtually identical complex cations, the crystal packings of both molecules are significantly different, apparently induced by the distinct but geometrically related anions, namely tetrachlorocuprate(II) and perchlorate.

[†] This chapter is based on: Koval, I. A., Sgobba, M., Huisman, M., Lüken, M., Saint-Aman, E., Gamez, P., Krebs, B, Reedijk, J., New J. Chem., 2005, submitted for publication

5.1 Introduction

As discussed in Chapters 2-4 of this thesis, phenol-based compartmental ligands of the ‘‘end-off’’ type have often been used for modeling bimetallic biosites,[1-4] in particular catechol oxidase.[5] In Chapter 2 the strategy of the synthesis of dinucleating asymmetric ligands has been discussed,[6] whereas in Chapter 4, the synthesis of the symmetric sulfur-containing phenol-based ligand Hpy2th2s, designed to mimic the presence of a thioether bond in the active site of the enzyme, has been reported.[7] In the present chapter, the two approaches were combined to prepare the asymmetric phenol-based ligand Hpy2th1as, designed to model the two peculiarities of the active site of the enzyme: (i) the asymmetric surrounding of the two metal centers, and (ii) the presence of a sulfur atom in a close proximity to one of them. Similarly to the ligand Hpy3asym, reported in Chapter 2, this ligand contains two dissimilar chelating arms in the 2 and 6 positions of the aromatic ring, designed to provide a different number of donor atoms for the binding of two copper ions. Furthermore, one of these arms contains a thiophene ring, the very weak donor properties of which are expected to prevent its coordination to the metal ions. The reaction scheme of the ligand synthesis is depicted in Figure 5.1. The reaction of the ligand with copper(II) chloride in methanol led to the isolation of the complex $[Cu_2(H_2py2th1as)_2Cl_2](CuCl_4)_2$. Unexpectedly, the secondary amine group of the ligand was found to undergo a protonation during the crystallization, which prevented it from binding to a copper ion. The crystallization of the ligand with copper(II) perchlorate in the presence of chloride anions led to the formation of the complex $[Cu_2(H_2py2th1as)_2Cl_2](ClO_4)_4 \cdot 6CH_3OH$ with a very similar structure of the complex cation. In this chapter, the single-crystal X-ray structures and solution properties of both complexes are discussed in detail.

5.2 Results and Discussion

5.2.1 Ligand synthesis

The ligand Hpy2th1as (2-[*N,N*-bis(2-pyridylmethyl)aminomethyl]-4-methyl-6-[2-thiophenylmethyl)aminomethyl]phenol) was prepared by the condensation of 3-[*N,N*-bis(2-pyridylmethyl)aminomethyl]-5-methylsalicylaldehyde (Hpy2ald, see Chapter 3) with 2-thiophenylmethylamine, followed by the reduction of the imine formed using sodium borohydride (Figure 5.1). This afforded Hpy2th1as as a light yellow oil in 95% yield.

5.2.2 Synthesis of the coordination compounds

The reaction of Hpy2th1as with copper(II) chloride in a 1:2 ratio resulted in the formation of a green crystalline complex **1** in 49% yield. Single crystals of **1** suitable for X-ray structure determination were obtained by diffusion of diethyl ether into a 0.01 M

methanolic solution of the complex. The X-ray analysis revealed that in the complex two copper(II) ions are coordinated by two ligands and are doubly bridged by the chloride anions, resulting in the complex of the formula $[Cu_2(H_2py2th1as)_2Cl_2](CuCl_4)_2$ (Figure 5.2).

In order to avoid the spontaneous formation of the tetrachlorocuprate(II) anions, which would undoubtedly mislead the interpretation of the results of the catecholase activity studies on **1**, and to facilitate the interpretation of the chemical and physical properties of **1**, a complex with a very similar structure, but with perchlorate counter ions, has also been prepared. It has been synthesized by reaction of Hpy2th1as with copper(II) perchlorate in the presence of an external source of chloride ions, which yielded two different reaction products, namely **1** and **2**. Redissolution of both compounds in methanol, followed by the addition of diethyl ether, resulted in the precipitation of **1**, and single crystals of **2** could be obtained upon slow evaporation of the filtrate (see Experimental Section). These crystals were characterized by X-ray crystallography, which showed compound **2** to be structurally closely related to **1** (Figure 5.3), the main differences being the distinct non-coordinated anions and the presence of hydrogen-bonded methanol molecules in the crystal lattice. It should be noted that the best results were achieved, surprisingly, by using hydroxylammonium hydrochloride as a source of Cl^- due to its high solubility in methanol, whereas in case of tetraalkylammonium salts (*e.g.* tetramethyl- and tetraethylammonium chloride), their insoluble perchlorate salts precipitated from the reaction mixture.

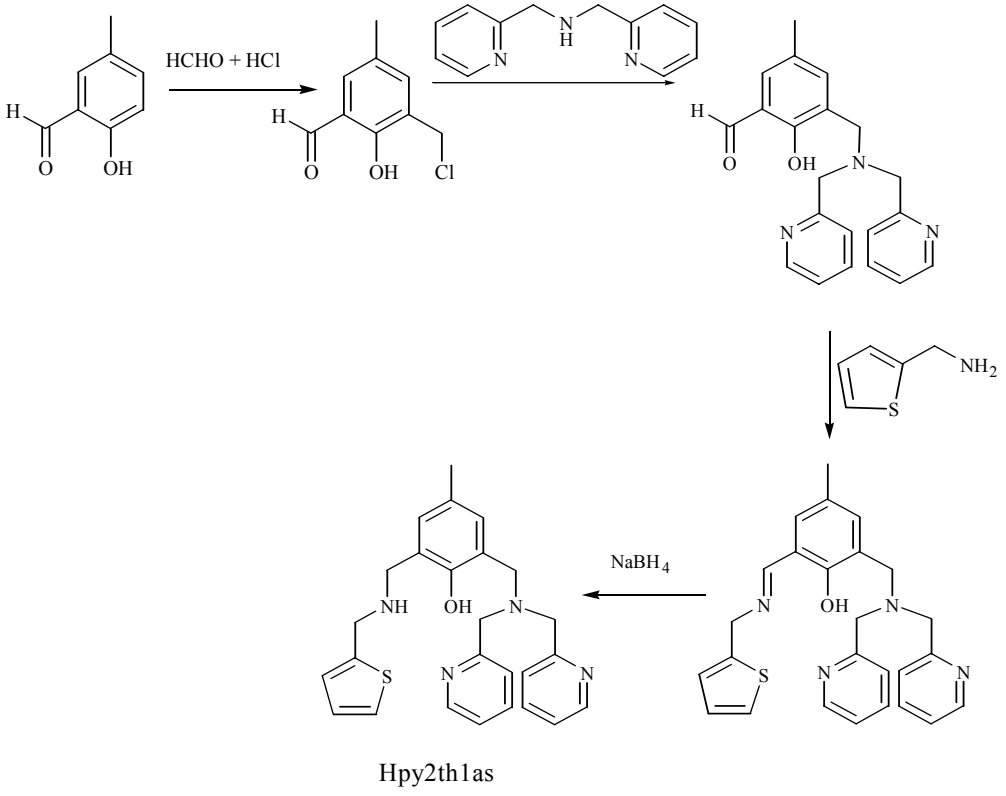

Figure 5.1. The reaction scheme of the synthesis of the ligand Hpy2th1as.

5.2.3 Crystal structure descriptions

$[Cu_2(H_2py2th1as)_2Cl_2](CuCl_4)_2$ (1)

A representation of the crystal structure of the complex is shown in Figure 5.2. Selected bond lengths and bond angles are reported in Table 5.1.

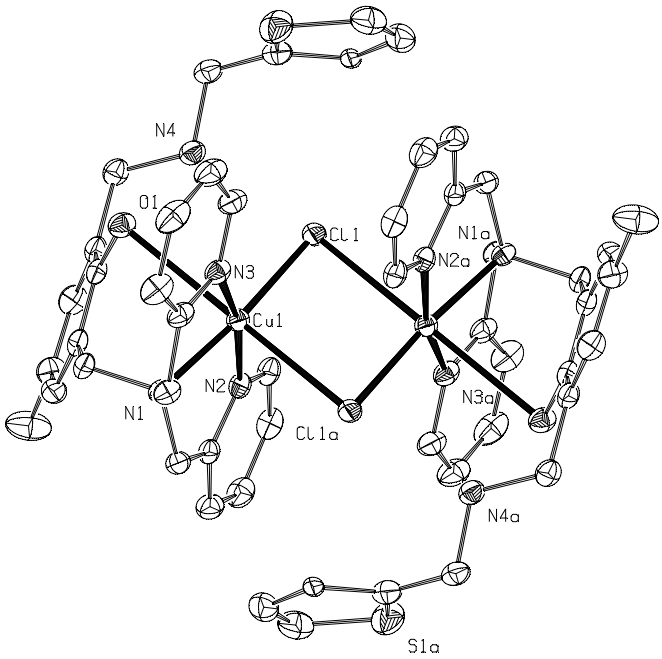

Figure 5.2. ORTEP projection of the complex cation $[Cu_2(H_2py2th1as)_2Cl_2]^{4+}$ in **1**. The hydrogen atoms and the non-coordinated tetrachlorocuprate(II) anions are omitted for clarity.

Table 5.1. Selected bond lengths and bond angles for $[Cu_2(H_2py2th1as)_2Cl_2](CuCl_4)_2$ (**1**)

Bond lengths (Å)			
Cu1…Cu2	3.4387(10)		
Cu1 - N1	2.020(3)	Cu1 - O1	2.784(2)
Cu1 - N2	1.983(2)	Cu1 - Cl1	2.2535(9)
Cu1 - N3	1.996(4)	Cu1 - Cl1a	2.8280(10)

Bond angles (°)			
Cl1 - Cu1 - O1	88.11(6)	Cu1- Cl1 - Cu2	89.32(4)
Cl1 - Cu1 - N1	173.30(8)	O1 - Cu1 - Cl1a	169.31(6)
Cl1 - Cu1 - N2	96.25(8)	N1 - Cu1 - N2	83.51(10)
Cl1 - Cu1 - N3	97.76(8)	N1 - Cu1 - N3	82.43(10)
Cl1 - Cu1 - Cl1a	95.53(4)	N1 - Cu1 - Cl1a	90.63(8)
O1 - Cu1 - N1	85.84(9)	N2 - Cu1 - N3	165.94(11)
O1 - Cu1 - N2	103.68(9)	N2 - Cu1 - Cl1a	85.90(8)
O1 - Cu1 - N3	75.65(9)	N3 - Cu1 - Cl1a	93.90(8)

The complex crystallizes in the space group $P2_1/n$. Similarly to complexes reported earlier with the structurally related ligand Hpy2ald[8] (Chapter 3), the phenol group of the ligand remains protonated and therefore does not act as a bridging ligand connecting two copper ions, instead being only weakly coordinated to one metal center. Furthermore, the secondary amine nitrogen atom N4 is also protonated, resulting in an ammonium moiety which cannot bind to a metal ion. Two mononuclear units are then doubly bridged by two chloride anions, which hold two copper ions at a distance of 3.4387(10) Å. The coordination sphere around the copper ion can be best described as a distorted elongated octahedron with the atoms N1, N2, N3 and Cl1 at the equatorial positions, and the atoms Cl1a and O1 occupying the Jahn-Teller axis. All Cu–N bond lengths are approximately equal, with average Cu–N distances of 2.0 Å. The Cu–Cl1 bond is slightly longer with a value of 2.2535(9) Å. The Cl1a and O1 atoms are located at longer distances of 2.8280(10) Å and 2.784(2) Å and can be best regarded as semi-coordinated to the metal ion. The O1–Cu1–Cl1a angle is 169.31(6)°. The tetrachlorocuprate counter ions, present in the crystal lattice, are hydrogen bonded to two dinuclear units, resulting in a 2D network (Table 5.3).

$[Cu_2(H_2py2th1as)_2Cl_2](ClO_4)_4 \cdot 6CH_3OH$ (2)

A representation of the crystal structure of complex **2** is shown in Figure 5.3. Selected bond lengths and bond angles are given in Table 5.2.

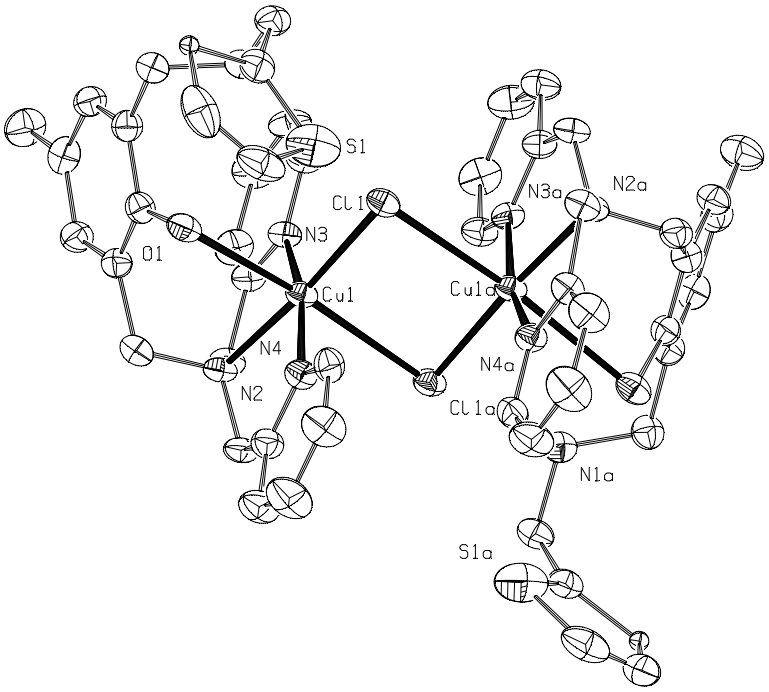

Figure 5.3. ORTEP projection of the complex cation $[Cu_2(H_2py2th1as)_2Cl_2]^{4+}$ in **2**. Hydrogen atoms, non-coordinated perchlorate anions and solvent molecules are omitted for clarity.

Table 5.2. Selected bond lengths and bond angles for $[Cu_2(H_2py2th1as)_2Cl_2](ClO_4)_4 \cdot 6CH_3OH$ (**2**)

Bond lengths (Å)			
Cu1…Cu1a	3.5252(14)		
Cu1 - Cl1	2.2663(17)	Cu1 - N4	1.982(4)
Cu1 - N2	2.034(4)	Cu1 - Cl1a	2.8579(17)
Cu1 - N3	1.996(4)	Cu1 - O1	2.758(4)
Bond angles (°)			
Cl1 - Cu1 - O1	85.44(10)	Cu1 - Cl1 - Cu1a	86.12(6)
Cl1 - Cu1 - N2	174.76(15)	O1 - Cu1 - Cl1a	168.61(10)
Cl1 - Cu1 - N3	95.77(13)	N2 - Cu1 - N3	83.18(17)
Cl1 - Cu1 - N4	99.14(13)	N2 - Cu1 - N4	82.03(17)
Cl1 - Cu1 - Cl1a	93.85(6)	N2 - Cu1 - Cl1a	91.31(14)
O1 - Cu1 - N2	89.69(16)	N3 - Cu1 - N4	165.08(18)
O1 - Cu1 - N3	100.31(16)	N3 - Cu1 - Cl1a	91.07(14)
O1 - Cu1 - N4	81.56(16)	N4 - Cu1 - Cl1a	87.34(14)

Table 5.3. Hydrogen bond interactions in the complexes **1** and **2**.

	Donor - H....Acceptor	*D – H (Å)*	*H...A (Å)*	*D...A (Å)*	*D - H...A (°)*
$[Cu_2(H_2py2th1as)_2Cl_2](CuCl_4)_2$	O1 - H1...Cl2	0.8402	2.2527	3.035(2)	155.10
	N4 - H4a...Cl4	0.9197	2.2838	3.132(3)	153.09
	N4 - H4b...Cl1	0.9206	2.6649	3.320(3)	128.83
	N4 - H4b...O1	0.9206	2.2483	2.929(3)	130.24
$[Cu_2(H_2py2th1as)_2Cl_2](ClO_4)_4 \cdot 6CH_3OH$	O1 - H1...O10	0.8199	1.8568	2.652(7)	163.06
	N1 - H1a…O11	0.8997	1.8278	2.712(7)	167
	N1 - H1b…Cl1	0.9008	2.5757	3.356(5)	145.38
	N1 - H1b…O1	0.9008	2.3088	2.917(6)	124.71
	O10 - H10…O2	0.8191	2.5113	2.784(8)	100.84
	O11 - H11a…O12	0.8188	2.2674	2.734(9)	116.58
	O12 - H12…O5	0.821	2.506	2.895(10)	110.25
	O12 - H12a…O2	0.821	2.5692	2.973(10)	117.75

The complex crystallizes in the space group *C2/c*. The molecular structure of the complex cation is analogous to the one of **1**. Thus, the copper ion is coordinated by three nitrogen atoms N2, N3 and N4 at an average distance of 2.0 Å and a chloride atom Cl1 at a somewhat longer distance of 2.2663(17) Å, which occupy the equatorial

positions of a distorted octahedron. The coordination sphere is completed by O1 and Cl1a which are weakly bound on the Jahn-Teller axis (the Cu1–Cl1a and the Cu1–O1 bond lengths are 2.8579(17) Å and 2.758(4) Å, respectively). The distance between the two doubly bridged copper ions of the two mononuclear units is 3.5252(14) Å, and the O1–Cu1–Cl1a angle is 168.61(10)°. Besides non-coordinated perchlorate anions, six methanol molecules per dimeric unit are present in the crystal lattice, taking part in the formation of an intricate hydrogen bonding network, which is described in Section 5.2.5 (see also Table 5.3).

5.2.4 Physical Characterization

The diffuse reflectance spectrum of **2** (solid state) is characterized by two peaks at 335 nm and 647 nm, whereas in the solid-state spectrum of **1**, one additional peak at 416 nm with a shoulder at 459 nm can be found (Figure 5.4). The latter peak is most likely caused by the presence of the tetrachlorocuprate anions. Indeed, earlier reports on tetrachlorocuprate complexes describe the presence of an intensive charge transfer band at *ca.* 350-400 nm in the UV-Vis spectra. The peak at 647 nm corresponds to d-d transitions of the Cu^{II} ions, whereas the peak at 335 nm is assigned to the charge transfer band from the chloride ions to the copper centers within the complex cation.

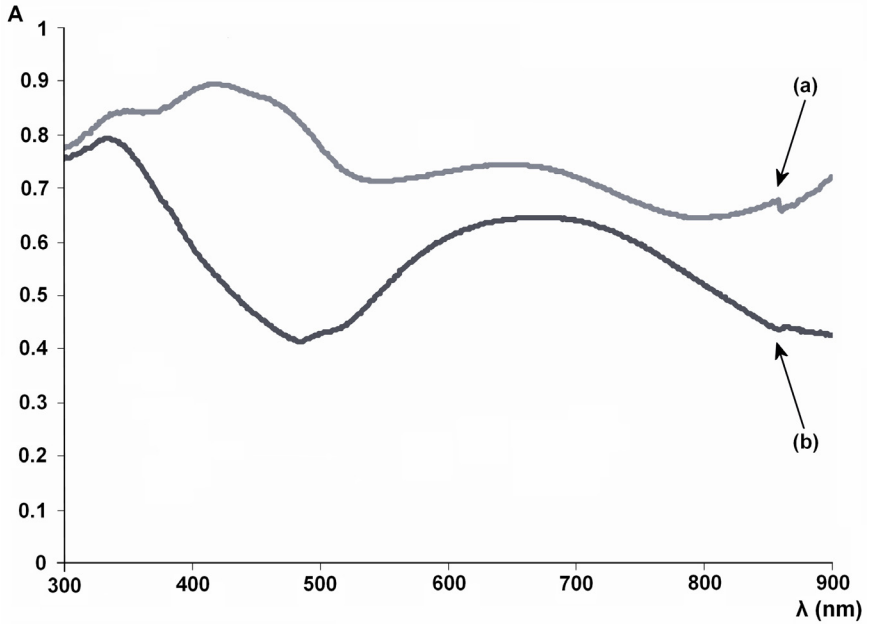

Figure 5.4. Diffuse reflectance ligand field spectra of **1** (a) and **2** (b).

In methanol solution, the UV-Vis spectrum of **2** is characterized by two very weak absorptions at 690 nm (ε = 80 M^{-1} cm^{-1}) and at 480 nm (ε = 80 M^{-1} cm^{-1}). The first one corresponds to the d-d transitions of the Cu^{II} ions, whereas the second is tentatively assigned to the charge transfer band due to the solvation of the metal centers by methanol. The UV-Vis spectrum of **1** in methanol looks very similar, with the d-d

absorption at 700 nm (ε = 160 M^{-1} cm^{-1}) and a broad peak at 450 nm with a shoulder at higher wavelength (ε = 160 M^{-1} cm^{-1}), probably originating from the methanol-solvated tetrachlorocuprate(II) ions.

The EPR spectra of both complexes have been recorded in solid state and in methanol glass at 77 K. The solid-state spectrum of **1** is characterized by one very broad isotropic signal centered at g = 2.14, whereas the spectrum of **2** exhibits an ill-resolved axial signal with $g_{//}$ = 2.30 and $g_{\perp}$ = 2.06.

It is very interesting to compare the solution EPR spectra of **1** and **2** (Figure 5.5, left). The spectrum of **2** exhibits an axial character with $g_{//}$ = 2.25, $g_{\perp}$ = 2.02 and $A_{//}$ = 183×10^{-4} cm^{-1}. Three out of the four lines of the ^{63,65}Cu hyperfine splitting are easily observed, whereas the fourth one is hidden in the $g_{\perp}$ region. The data obtained clearly indicate the dissociation of the dinuclear unit in solution, producing two mononuclear species.

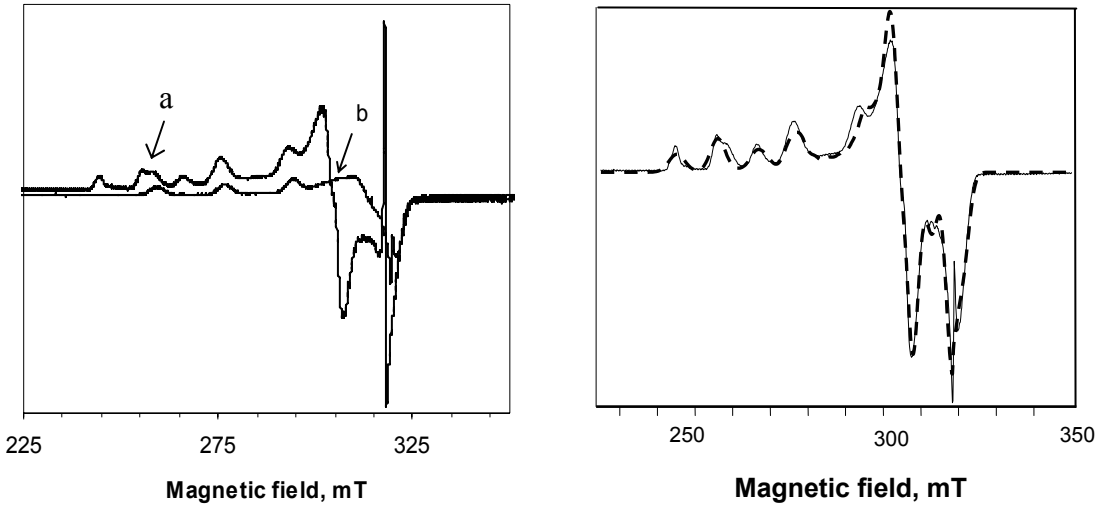

Figure 5.5. Left: frozen methanol EPR spectra of **1** (a) and **2** (b). Right: experimental (frozen methanol glass, solid line) and simulated[9] (dashed line) EPR spectra of **1**. A sharp signal in the spectra corresponds to the reference DPPH (g = 2.0036)

The spectrum of **1** displays two sets of axial signals, suggesting the presence of two mononuclear Cu^{II} species in solution: one originating from the dissociation of the dinuclear core, and another originating from the tetrachlorocuprate counter ions. The spectrum has been satisfactory simulated[9] (Figure 5.5, right), considering two non-interacting mononuclear species X and Y, with the following simulating parameters: for X, g_x=2.06, g_y=2.10, g_z=2.25 and A_z = 191×10^{-4} cm^{-1}; for Y, g_x=2.03, g_y=2.12, g_z=2.45, and A_z= 126×10^{-4} cm^{-1}. The parameters for the latter species in fact are very close to the values reported for elongated rhombic octahedral CuO_6 chromophores,[10] which suggest that the tetrachlorocuprate anions are methanolysed in solution, likely forming $[Cu(CH_3OH)_6]^{2+}$ species. The simulating parameters for species X, on the other hand,

are close to those experimentally obtained for compound **2**, confirming that they correspond to the mononuclear $[Cu(H_2py2th1as)Cl]^{2+}$ cation.

The electrochemical behavior of both complexes was investigated in methanolic solutions, with tetra-*n*-butylammonium perchlorate (TBAP) as supporting electrolyte (0.1 M). The potentials were referred to a standard Ag/AgCl + 3M KCl reference electrode. The CV curve for both complex **1** (Figure 5.6 (a)) and **2** (Figure 5.6 (b)) is characterized by a quasi-reversible electrochemical signal at $E_{1/2}$ = -0.10 V. However, an additionnal reversible system is seen on the CV curve of **1** at $E_{1/2}$ = 0.39 V. The RDE voltammetry curve for **1** (Figure 5.6 (a)) shows unambiguously that both systems involve the same number of electrons. Comparison of the electrochemical behavior of **1** and **2** allows to assign the electron transfer at -0.10 V to the complexed Cu^{II}/Cu^{I} redox couple, whereas the additionnal reversible system for **1**, at +0.39 V, corresponds to the methanol-solvated tetrachlorocuprate Cu^{II}/Cu^{I} redox couple. It can be noted that extending the scan below –0.6 V leads to the deposition of Cu^0 onto the electrode surface.

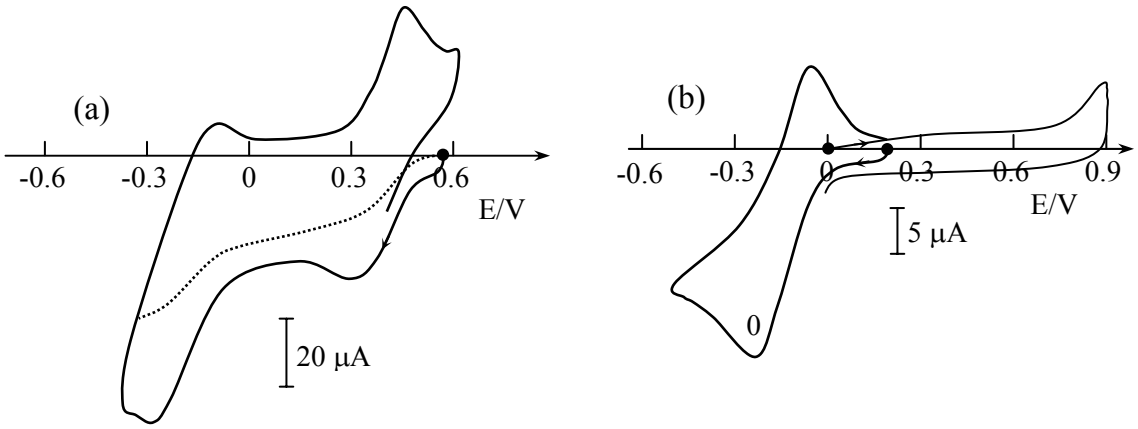

Figure 5.6. (a): Electrochemical curves recorded in a 0.66 mM solution of **1** in MeOH + TBAP 0.1 M on a C disc (∅ = 3 mm); solid line: CV curve, v = 0.1 V s^{-1}; dotted line: RDE curve, N = 600 rpm; V *vs.* standard Ag/AgCl + 3M KCl reference electrode. (b): CV curve of **2** in 0.12 mM in MeOH + NBu_4PF_6 0.1 M, 0.1 V s^{-1}, V *vs.* standard Ag/AgCl + 3M KCl reference electrode.

5.2.5 Counter-ion influence on the crystal packing of 1 and 2

Despite their obvious similarities, it is interesting to compare the details of the structures of the complex cations in **1** and **2**. Both coordination compounds possess several peculiar features (Figure 5.7). First, in both complexes the thiophenyl substituent is not coordinated to the copper ion, similarly to the complexes with the closely related ligand Hpy2th2s, reported in Chapter 4.[7] Second, the phenol (O1) is not deprotonated and thus does not function as a bridging unit between two copper ions. In **1**, the phenolic proton H1 is hydrogen-bonded to the chloride atom Cl2 of a tetrachlorocuprate(II) anion (the O1···Cl2 distance is 3.036(2) Å). Such discrete

chlorocuprate(II) species are known to spontaneously form in solution during the crystallization of copper(II) chloride with neutral amine-based ligands, with the ligand undergoing a protonation.[11] This indeed occurs in the present case, since the secondary amine (N4) bearing the thiophenylmethyl group is protonated and thus not able to coordinate to the copper(II) ion. The resulting ammonium entity is H-bonded to the chloride Cl4 of a tetrachlorocuprate(II) anion (the distance N4···Cl4 is 3.132(3) Å), which is a common characteristic observed in the crystal packing of ammonium halocuprate(II) derivatives,[12,13] and which has been described to be a dominant stabilizing factor. The second ammonium proton, *i.e.* H4B is bonded to the phenolic atom O1, the distance N4···O1 being 2.929(3) Å. As a result, in this network, each dinuclear unit is connected to four neighbors by means of hydrogen bonds, realized between the chloride atoms of the counter-ions and the phenolic and ammonium groups of the complex cation. In addition, the supramolecule is further stabilised via the unusual interactions of the π-clouds of the thiophene rings with the bridging chloride anions (the centroid···Cl distance is 3.64 Å; the angle thiophene plane–centroid–Cl axis is 79.9 º).[14]

On the other hand, in complex **2** the phenol rings and the side-arms holding the thiophene units are positioned differently. Indeed, while the two phenols are *trans* located to each other for **1**, with the *para*-methyl groups pointing in opposite directions (Figure 5.7 (a)), the phenols in **2** can be considered as *cis* located, with the two methyl groups pointing in the same direction (Figure 5.7 (b)). In a similar manner, the thiophenyl moieties are *cis* located as well, preventing the beneficial stabilising π-interactions with the bridging chlorides present in **1**. This significant structural variation is most likely due to the different anions. First, the ratio cation/anion is different for both complexes since the perchlorate ion is monovalent while the tetrachlocuprate ion is divalent. More interestingly, the perchlorate anions are H-bonded to solvent methanol molecules, leading to a completely distinct and intricate hydrogen bonding network, enclosing a large amount of methanol molecules in the crystal lattice (Figure 5.7 (b)). The presence of these solvent entities apparently induces a rotation of the phenol rings through the N1_a–C8_a and C8_a–C2_a axes. Thus, the perchlorate O2 atom is connected to the methanolic proton H10 (the distance O2···O10 is 2.784(8) Å). This methanol is further strongly H-bonded to the proton H1 of the phenol ring (the distance O10···O1 is 2.652(7) Å). The second perchlorate anion is weakly H-bonded to the proton H12A of another methanol molecule (the distance O6···O12 is 3.010(3) Å), and interacts with the sulfur atom S1 of the thiophene (the distance O7···S1 is 3.108(2) Å). Finally, the ammonium proton H1B is connected to the phenolic oxygen atom O1 (the distance N1···O1 is 2.917(6) Å) and the second proton, H1A, is H-bonded to the oxygen atom O11 of a methanol molecule (the distance N1···O11 is 2.712(6) Å). In addition, the methanolic oxygen atom O11 acts as a H donor for a third methanol molecule (the

distance O12···O11 is 2.734(5) Å). The resulting [complex–MeOH–ClO_4^-] H-bonded network connects all dinuclear units to generate a 3D assembly.

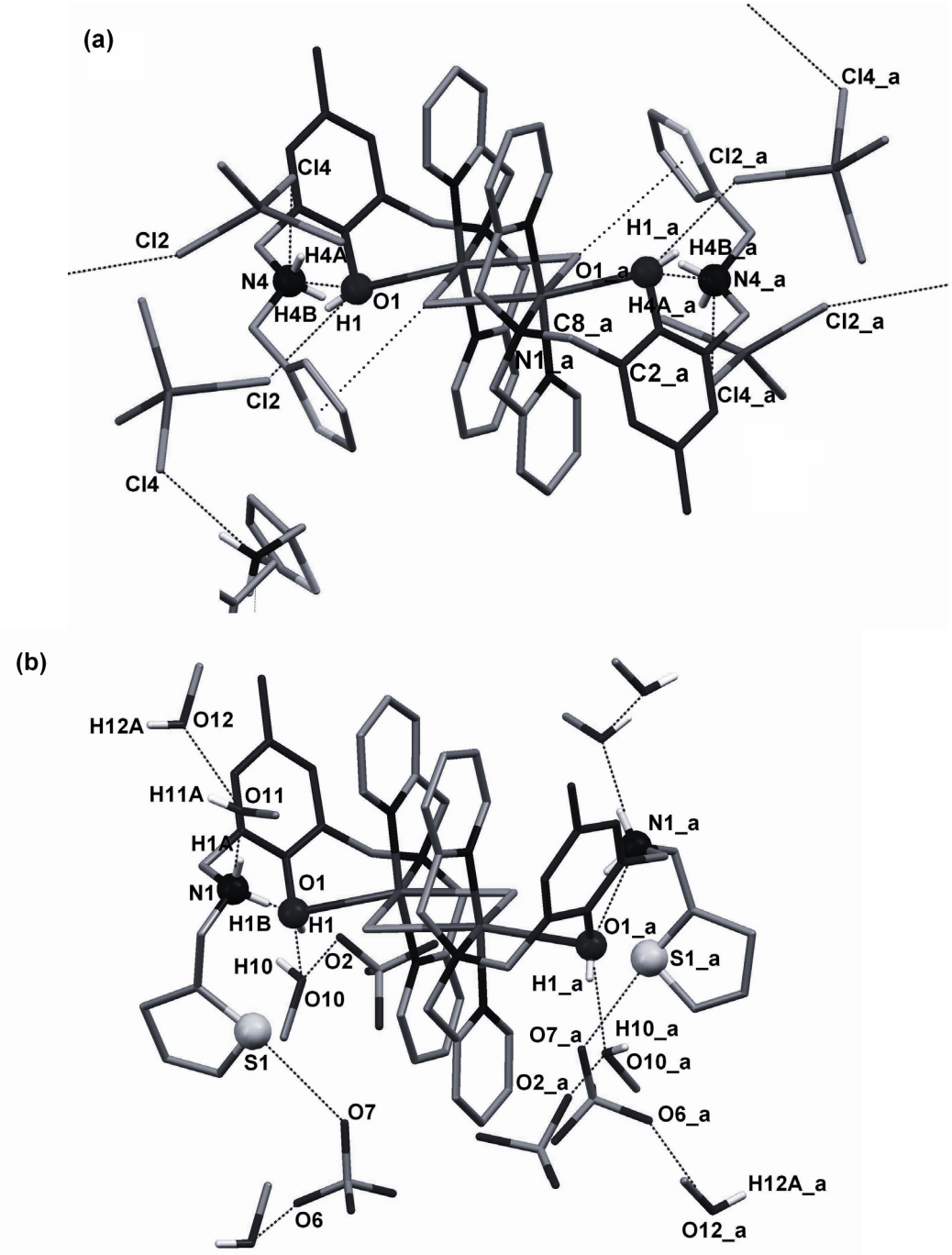

Figure 5.7. Hydrogen-bonding network for complexes **1** (a) and **2** (b).

5.2.6 Catecholase activity studies

Although the ligand Hpy2th1as has been designed to bind two copper(II) ions, resulting in dinuclear complexes, the structures of **1** and **2** are quite different. The unexpected protonation of the secondary amine group prevents it from coordination to

the copper ions; consequently, both complexes are formed by the self-assembly of two mononuclear units, in which a single copper ion is coordinated by a ligand molecule, via the bridging chloride ions. The spectroscopic studies in solution clearly indicated that these dinuclear units fully dissociate into mononuclear species in solution, which in turn makes the complexes in question not very suitable models for the catechol oxidase active site. Unfortunately, the attempts to isolate dinuclear copper(II) complexes with this ligand were unsuccessful.

Nevertheless, the catalytic activity of both complexes towards the oxidation of the model substrate 3,5-di-*tert*-butylcatechol ($DTBCH_2$) has been studied spectrophotometrically in methanolic solution in a dioxygen-saturated atmosphere. Not surprisingly, both complexes do not exhibit catecholase activity, although one equivalent of quinone is produced stoichiometrically upon treating one molar equivalent of **1** with 100 molar equivalents of $DTBCH_2$. This stoichiometric oxidation is obviously caused by the stoichiometric reaction of the methanol-solvated tetrachlorocuprate anions with the substrate.

5.3 Concluding remarks

In summary, a new thiophene-containing phenol-based ligand has been synthesized. Two copper complexes of this N,O,S- ligand have been prepared and fully characterized. Unfortunately, the ligand fails to coordinate two copper(II) ions; instead it binds to only one metal center, generating chloro-bridged dinuclear species. Consequently, the obtained complexes do not bear a large resemblance to the active site of catechol oxidase and do not exhibit catecholase activity. The structural features of both compounds are nevertheless quite interesting. Although the complex cation formulas are identical, the two coordination compounds exhibit significantly different structural arrangements with a distinct ligand conformation, showing the importance of the anion on the crystal packing. The structural difference is obviously due to the counter-ions which are differently charged. Furthermore, the aptitude of the perchlorate anions to form H-bond with less acidic protons, *i.e.* from methanol, contrary to the tetrachlorocuprate(II) ion, which is only capable to act as hydrogen acceptor for more acidic ones, *i.e.* from phenol or ammonium H donors, results in completely distinct supramolecular interactions. For instance, the thiophene ring is involved in uncommon anion-π interactions in **1**, while it acts as H bond acceptor in **2.**

5.4 Experimental Section

5.4.1 Materials and Methods

All starting materials were commercially available and used as purchased. 5-methylsalicylaldehyde was purchased from Fluka, 2-thiophenylmethylamine from Acros, and di-(2-picolyl)amine from Aldrich. 3-chloro-5-methylsalicylaldehyde was

prepared according to the procedure described by Lock.[15] The synthesis of 3-[*N,N*-bis(2-pyridylmethyl)aminomethyl]-5-methylsalicylaldehyde is described in Chapter 2.[6] The NMR spectra were recorded on a JEOL FX-200 (200 MHz) FT-NMR spectrometer. The ligand field spectra of the solids (300-2000 cm^{-1}, diffuse reflectance) were taken on a Perkin-Elmer 330 spectrophotometer equipped with a data station. Electrospray mass spectra (ESI-MS) in methanol solutions were recorded on a Thermo Finnigan AQA apparatus. X-band electron paramagnetic resonance (EPR) measurements were performed at 77 K in the solid state or in a frozen methanol solution on a Jeol RE2x electron spin resonance spectrometer, using DPPH ($g = 2.0036$) as a standard. The electrochemical behavior of the complexes was investigated in a 0.1 M solution of tetra-*n*-butylammonium perchlorate (TBAP) in methanol using a EGG 273 potentionstat coupled with a Kipp&Zonen x-y recorder, or an Autolab PGstat10 potentiostat controlled by GPES4 software. The experiments were performed at room temperature in a three-compartment cell. Potentials are referred to a standard Ag/AgCl reference electrode. The working electrode was polished with 1 μm diamond paste prior to each recording.

5.4.2 Ligand synthesis

2-[*N,N*-bis(2-pyridylmethyl)aminomethyl]-4-methyl-6-[2-thiophenylmethyl)aminomethyl] phenol (Hpy2th1as): A solution of 2-thiophenylmethylamine (0.245 g, 2.25 mmol) in 50 ml of dry methanol was slowly added to a solution of 3-[*N,N*-bis(2-pyridylmethyl)aminomethyl]-5-methylsalicylaldehyde (0.75 g, 2.15 mmol) in 250 ml of dry methanol under argon. After the addition was complete, the resulting bright yellow solution was heated for two hours at 50 ºC. The successful formation of the imine derivative was verified by NMR spectroscopy. After cooling to room temperature, a three-fold excess of sodium borohydride (0.244 g, 6.8 mmol) was added and the reaction mixture was refluxed for 2.5 hours. After evaporation of the solvent under reduced pressure, the resulting oil was dissolved in 50 ml of acidified water (pH = 1). The aqueous phase was washed with dichloromethane (2×50 ml) and subsequently basified using a concentrated aqueous solution of ammonia. The aqueous phase was extracted with dichloromethane (2×50 ml). The separated organic phase was dried over sodium sulfate, filtered, and the solvent was evaporated under reduced pressure. Pure ligand Hpy2th1as was obtained as a clear yellow oil. Yield: 0.88 g, 2.0 mmol (95%). ^{1}H NMR ($CDCl_3$, 200 MHz, ppm): δ = 2.24 (s, 3H, C$\underline{H}_3$), 3.76 (s, 2H, C$\underline{H}_2$N), 3.86 (s, 4H, C$\underline{H}_2$), 3.91 (s, 2H, C$\underline{H}_2$NH), 3.98 (s, 2H, NHC$\underline{H}_2$), 6.83 (s, 1H, 5'-thiophene ring), 6.92 (m, 3H, 3'-thiophene ring, 3'- + 5'-phenol ring), 7.19 (t, 2H, 5'-pyridine rings), 7.35 (d, 2H, 3'-pyridine rings), 7.60 (t, 2H, 4'-pyridine rings), 8.53 (d, 2H, 6'-pyridine rings).

5.4.3 Syntheses of the coordination compounds

$[Cu_2(H_2py2th1as)_2Cl_2](CuCl_4)_2$ (1): A solution of Hpy2th1as (0.111 g, 0.25 mmol) in 5 ml of methanol was added to 5 ml of a methanolic solution of copper chloride (0.085 g, 0.50 mmol). Diffusion of diethyl ether resulted in the precipitation of the complex as a green powder. Yield: 97 mg (49%). Single crystals were obtained by slow diffusion of diethyl ether into a 0.01 M solution of the complex. Elemental analysis, % found (calc.) for $[Cu_2(H_2py2th1as)Cl_2](CuCl_4)_2$. ($=C_{52}H_{58}Cl_{10}Cu_4N_8O_2S_2$): C, 41.62 (41.64), H, 4.26 (3.90), N, 7.46 (7.47), S, 3.55 (4.28). ESI-MS: m/z 542 ($[Cu(H_2py2th1as)Cl]^+$). IR, cm^{-1}: 2998 (C-H stretching, 1610 ($C=N_{arom.}$ and $C=C_{arom.}$ stretching).

$[Cu_2(H_2py2th1as)_2Cl_2](ClO_4)_4 \cdot 6CH_3OH$ (2): Hpy2th1as (0.031 g, 0.08 mmol) and copper perchlorate (0.030 g, 0.08 mmol) were dissolved in methanol (4 ml). 12 mg (0.2 mmol) of $NH_2OH \cdot HCl$ were subsequently added. Slow diffusion of diethyl ether into the resulting solution led to the formation of blue and green crystals. These crystals were re-dissolved in methanol and the addition of diethyl ether immediately yielded a green crystalline precipitate of **1**. After rapid filtration, the resulting blue solution was slowly evaporated, producing light blue crystals of **2**. Yield: 12 mg, 0.007 mmol (9%). The complex partially loses non-coordinated solvent molecules, when separated from the mother liquid. Elemental analysis, % found (calc.) for $[Cu_2(H_2py2th1as)_2Cl_2](ClO_4)_4 \cdot 3CH_3OH$ ($= C_{55}H_{70}Cl_6Cu_2N_8O_{21}S_2$): C, 40.78 (41.73), H, 4.78 (4.46), N, 7.52 (7.08), S, 3.78 (4.05). ESI-MS: m/z 542 ($[Cu(H_2py2th1as)Cl]^+$). IR, cm^{-1}: 3056 (C-H stretching), 1612 ($C=C_{arom.}$ and $C=N_{arom.}$ stretching), 1098, 1049 (ClO_4^- anions).

5.4.4 X-ray crystallographic measurements

$[Cu_2(H_2py2th1as)_2Cl_2](CuCl_4)_2$ (1): A single crystal of $[Cu_2(H_2py2th1as)_2Cl_2](CuCl_4)_2$ (**1**) was mounted at 100 K on a Bruker AXS SMART 6000 diffractometer, equipped with Cu-Kα radiation (λ = 1.54178 Å). $C_{52}H_{58}Cl_{10}Cu_4N_8O_2S_2$, Fw = 1499.90, a = 12.137(2) Å, b = 11.985(2) Å, c = 20.656(4) Å, β = 96.69(3)°, Z = 2, V = 2984(2) $Å^3$, $\rho_{calcd.}$ = 1.669 $g \cdot cm^{-3}$, μ = 6.764 mm^{-1}, absorption correction with SADABS,[16] monoclinic, space group $P2_1/n$ (no. 14), 17214 reflections collected, 5553 independent reflections (R_{int} = 0.0308). The structure was solved by direct methods and refined using the SHELX program package.[17,18] All hydrogen atoms were placed on idealized positions riding on their carrier atoms with isotropic displacement parameters. The final cycle of full-matrix least-squares refinement, including 354 parameters, converted into R_1 = 0.0352 (R_1 = 0.0430 all dat and wR_2 = 0.1172 (wR_2 = 0.1207 all data) with a maximum (minimum) residual electron density of 1.277 (-0.695) $e \cdot Å^3$.

$[Cu_2(H_2py2th1as)_2Cl_2](ClO_4)_4 \cdot 6CH_3OH$ (2): A single crystal of $[Cu_2(H_2py2th1as)_2Cl_2](ClO_4)_4 \cdot 6CH_3OH$ (**2**) was mounted at 293 K on a Bruker AXS SMART 6000 diffractometer, equipped with Cu-Kα radiation (λ = 1.54178 Å). $C_{58}H_{82}Cl_6Cu_2N_8O_{24}S_2$, M = 1679.26, a = 19.693(4) Å, b = 13.376(3) Å, c = 27.401(5) Å, β = 96.69(3)°, Z = 4, V = 7169(3) $Å^3$, $\rho_{calcd.}$ = 1.556 $g \cdot cm^{-3}$, μ = 4.032 mm^{-1}, absorption correction with SADABS,[16] monoclinic, space group *C2/c* (no. 15), 20413 reflections collected, 6673 independent reflections (R_{int} = 0.0520). The structure was solved by direct methods and refined using the SHELX program package.[17,18] All hydrogen atoms were placed on idealized positions riding on their carrier atoms with isotropic displacement parameters. The carbon C11 of the thiophene ring was defined isotropically. The final cycle of full-matrix least-squares refinement, including 424 parameters, converted into R_1 = 0.0761 (R_1 = 0.1086 all data) and wR_2 = 0.2221 (wR_2 = 0.2382 all data) with a maximum (minimum) residual electron density of 1.808 (-0.889) $e \cdot Å^3$.

5.5 References

(1) Torelli, S.; Belle, C.; Hamman, S.; Pierre, J. L.; Saint-Aman, E. *Inorg. Chem.* **2002**, *41*, 3983-3989.
(2) Torelli, S.; Belle, C.; Gautier-Luneau, I.; Pierre, J. L.; Saint-Aman, E.; Latour, J. M.; Le Pape, L.; Luneau, D. *Inorg. Chem.* **2000**, *39*, 3526-3536.
(3) Merkel, M.; Möller, N.; Piacenza, M.; Grimme, S.; Rompel, A.; Krebs, B. *Chem. Eur. J.* **2005**, *11*, 1201-1209.
(4) Reim, J.; Krebs, B. *J. Chem. Soc., Dalton Trans.* **1997**, 3793-3804.
(5) Klabunde, T.; Eicken, C.; Sacchettini, J. C.; Krebs, B. *Nat. Struct. Biol.* **1998**, *5*, 1084-1090.
(6) Koval, I. A.; Pursche, D.; Stassen, A. F.; Gamez, P.; Krebs, B.; Reedijk, J. *Eur. J. Inorg. Chem.* **2003**, 1669-1674.
(7) Koval, I. A.; Huisman, M.; Stassen, A. F.; Gamez, P.; Roubeau, O.; Belle, C.; Pierre, J. L.; Saint-Aman, E.; Luken, M.; Krebs, B.; Lutz, M.; Spek, A. L.; Reedijk, J. *Eur. J. Inorg. Chem.* **2004**, 4036-4045.
(8) Koval, I. A.; Huisman, M.; Stassen, A. F.; Gamez, P.; Lutz, M.; Spek, A. L.; Reedijk, J. *Eur. J. Inorg. Chem.* **2004**, 591-600.
(9) Neese, F.; *The program EPR, a modeling approach, Version 1.0*. University of Konstanz, 1993
(10) Glowiak, T.; Podgorska, I. *Inorg. Chim. Acta* **1986**, *125*, 83-88.
(11) Smith, D. W. *Coord. Chem. Rev.* **1976**, *21*, 93-158.
(12) Weselucha-Birczynska, A.; Oleksyn, B. J.; Hoffmann, S. K.; Sliwinski, J.; Borzecka-Prokop, B.; Goslar, J.; Hilczer, W. *Inorg. Chem.* **2001**, *40*, 4526-4533.
(13) Willet, R. D.; Place, H.; Middleton, M. *J. Am. Chem. Soc.* **1988**, *110*, 8639-8650.
(14) Damodharan, L.; Pattabhi, V.; Behera, M.; Kotha, S. *J. Mol. Struct.* **2004**, *705*, 101-106.
(15) Lock, G. *Chem. Ber.* **1930**, *63*, 551-559.
(16) Sheldrick, G. M.; *SADABS*. University of Göttingen, Germany, 2003
(17) Sheldrick, G. M.; *SHELXL-97, Program for the refinement of crystal structures*. University of Göttingen, Germany, 1997
(18) Sheldrick, G. M.; *SHELXTL PLUS*. University of Göttingen, Germany, 1990

6 | Proton NMR spectroscopy and magnetic properties of a solution-stable dicopper(II) complex bearing a single μ-hydroxo bridge.[†]

The reaction of copper(II) perchlorate with the macrocyclic ligand [22]py4pz (9,22-bis(2-pyridylmethyl)-1,4,9,14,17,22,27,28,29,30-decaazapentacyclo-[22.2.1.1^{4,7}.1^{11,14}.1^{17,20}]triacontane-5,7(28),11(29),12,18,20(30),24(27),25-octaene) in the presence of base leads to the formation of a dinuclear complex [Cu_2([22]py4pz)(μ-OH)](ClO_4)$_3$·H_2O, in which two copper ions are bridged by a single μ-hydroxo bridge. Each copper ion is further surrounded by four nitrogen atoms of the ligand. The μ-hydroxo bridge mediates a strong antiferromagnetic coupling ($2J$ = -691(35) cm^{-1}) between the metal centers, leading to relatively sharp and well-resolved resonances in the ^{1}H NMR spectrum of the complex in solution. In this chapter, the crystal structure, the magnetic properties and the full assignment of the hyperfine-shifted resonances in the NMR spectrum of the complex, as well as the determination of the exchange coupling constant in solution through temperature-dependent NMR studies, are reported.

[†]This chapter is based on: Koval, I. A., van der Schilden, K., Schuitema, A. M., Gamez, P., Belle, C., Pierre, J.-L., Luken, M., Krebs, B., Roubeau, O., Reedijk, J., Inorg. Chem., 2005, 44, 4372-4382

6.1 Introduction

As can be concluded from Chapter 4, one of the factors strongly influencing catecholase activity of dicopper(II) complexes is the bridging ligand between the metal centers. As discussed in Chapter 1, many authors have pointed out that *i.e.* hydroxo-bridged dicopper(II) complexes exhibit catecholase activity, partially due to the ability of the hydroxide anion to facilitate the deprotonation of catechol and thus promote its binding to the copper(II) ions.[1-4] On the other hand, the presence of strongly binding ligands, *e.g.* halogen atoms, prevents their displacement by the incoming catecholate and thus hampers the catalytic cycle.[5]

Consequently, a new dinuclear copper(II) complex $[Cu_2([22]py4pz)(\mu\text{-}OH)](ClO_4)_3{\cdot}H_2O$ (**1**) with the macrocyclic ligand [22]py4pz (Figure 6.1) has been prepared and structurally characterized.[6] This ligand has been designed earlier to model the active site of the structurally related type-3 copper protein hemocyanin.[6,7] It is able to keep two copper ions in a close proximity and to provide each of them with four nitrogen donor atoms from pyridine and pyrazole rings and the tertiary amine groups. In dicopper(II) complex **1** two copper ions are kept together by the macrocyclic moiety, each copper ion being surrounded by four nitrogen donor atoms from the ligand. In addition, the copper(II) ions are bridged by a single hydroxo bridge. The structure of the complex is thus fairly similar to the *met* form of the active site of catechol oxidase.[8] Considering proton NMR as a powerful spectroscopic tool to study paramagnetic copper(II) complexes in solution, the magnetic properties, as well as ^1H NMR studies of the paramagnetic complex **1**, have been studied in depth and are reported in this chapter.

6.2 Results and discussion

6.2.1 Synthesis and physical properties of 1

The reaction scheme of the synthesis of the macrocyclic ligand [22]py4pz is depicted in Figure 6.1.[6] The dinuclear complex $[Cu_2([22]py4pz)(\mu\text{-}OH)](ClO_4)_3{\cdot}H_2O$ was prepared by reaction of $Cu(ClO_4)_2{\cdot}6H_2O$ and the ligand [22]py4pz in acetonitrile in the presence of one equivalent of NMe_4OH. Small green crystals of the compound, suitable for X-ray single crystal analysis, were obtained by slow diethyl ether diffusion in an acetonitrile solution of the complex. The complex was found to be moderately soluble in acetonitrile and DMSO, poorly soluble in water, and completely insoluble in other common solvents.

The UV-Vis-NIR spectrum of the complex in CH_3CN solution exhibits two absorption bands at 350 nm (ε = 7176 $M^{-1}cm^{-1}$) and at 821 nm (ε = 336 $M^{-1}cm^{-1}$). The first one corresponds to the charge transfer band from the hydroxo bridge to the copper ions, whereas the second one is assigned to a d-d transition band of Cu^{II} ions. The complex is EPR silent both in the solid state and in acetonitrile solution at 77 K.

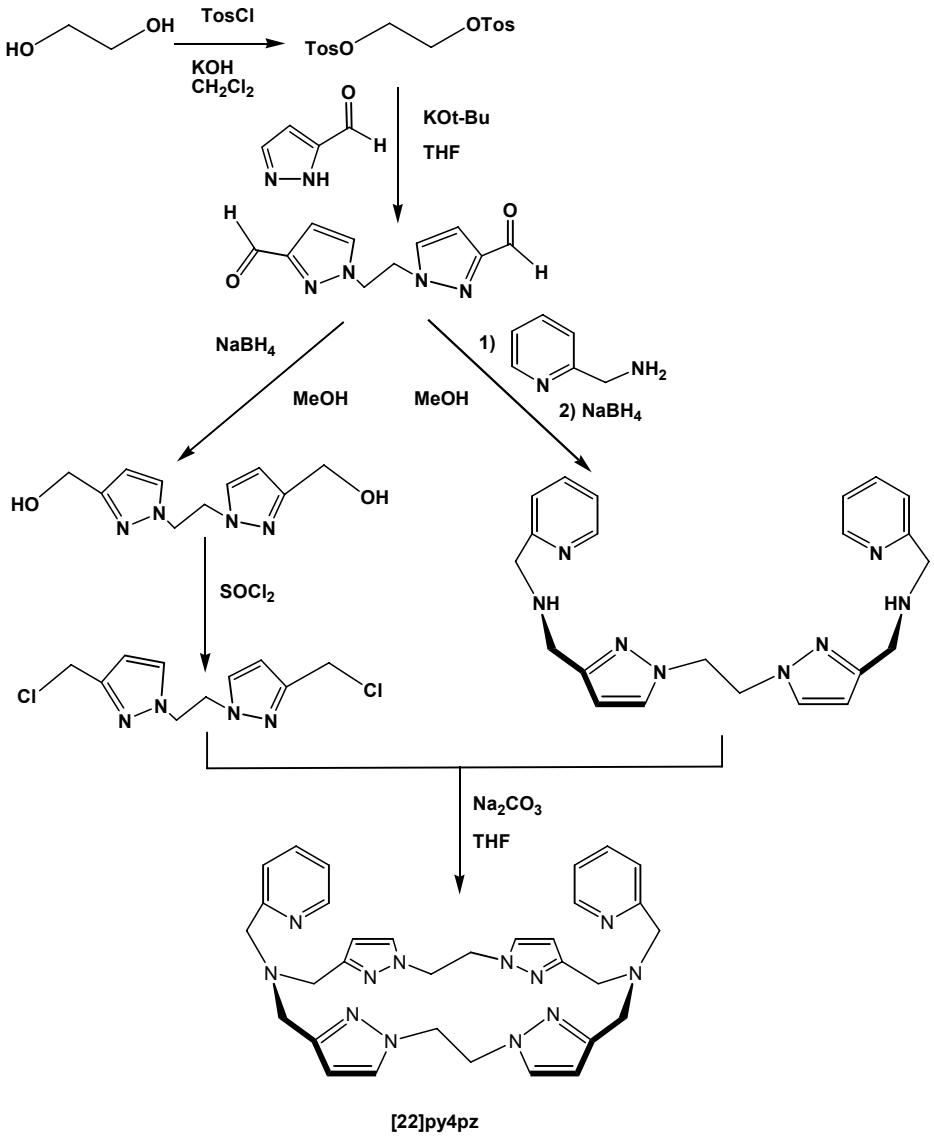

Figure 6.1. The scheme of the synthesis of the macrocyclic ligand [22]py4pz (9,22-bis(2-pyridylmethyl)-1,4,9,14,17,22,27,28,29,30-decaazapentacyclo-[22.2.1.1^{4,7}.1^{11,14}.1^{17,20}]triacontane5,7(28),11(29),12,18,20(30),24(27),25-octaene).[6,7]

6.2.2 Crystal structure description of 1

The ORTEP projection of 1 is depicted in Figure 6.2. Selected bond distances and bond angles are presented in Table 6.1. The Cu^{II} ion is in an N_4O environment, which can be best described as a distorted trigonal bipyramid with a τ value of 0.83 (τ = 1 for the trigonal bipyramidal geometry and 0 for the square pyramidal geometry).[9] The equatorial positions are occupied by the two pyrazole nitrogen atoms, N3 and N10 at distances of, respectively, 2.033(3) Å and 2.072(3) Å, and the pyridine N18 atom at a distance of 2.087(4) Å. The bridging O23 atom at a distance of 1.9215(12) Å and the tertiary amine N15 atom at a distance of 2.065(3) Å are occupying the axial positions. The small N3-Cu1-N15 and N15-Cu1-N10 angles of 80.17(13) and 80.94(13)º,

respectively, are imposed by the three-bond ligand bites. The bridging oxygen atom O23 from the hydroxide anion connects the two central copper atoms Cu1 and Cu1b, whereby the macrocycle adopts a *cis*-(boat)-conformation. The two pyridine groups are located at the same side above the macrocyclic ring and the two Cu^{II} ions lie almost in the plane of the ring with a Cu…Cu distance of 3.7587(11) Å. The Cu-O-Cu angle is 156.0(3) Å.

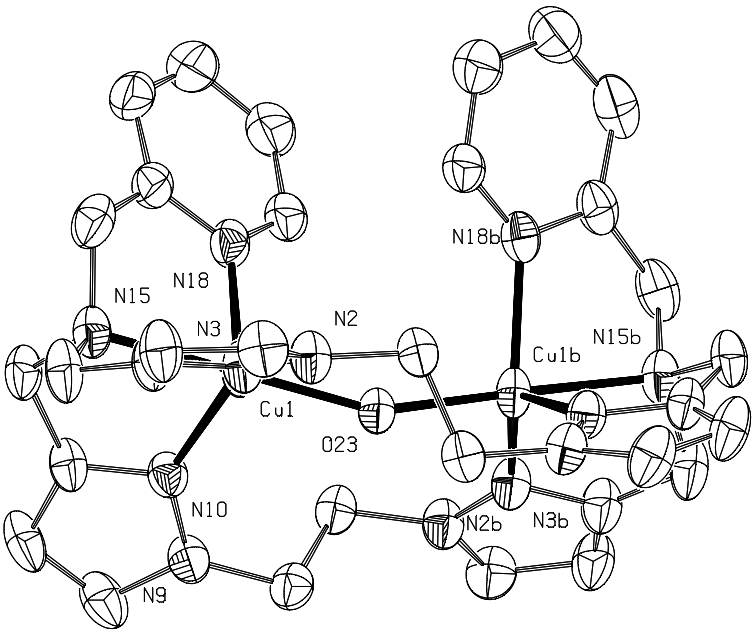

Figure 6.2. ORTEP representation of the complex cation $[Cu_2([22]py4pz)(\mu\text{-}OH)]^{3+}$ (symmetry code: b = -x, y, 1/2-z). Hydrogen atoms are omitted for clarity.

Table 6.1. Selected bond lengths and angles for $[Cu_2([22]py4pz)(\mu\text{-}OH)](ClO_4)_3 \cdot H_2O$ (**1**).

Bond lengths (Å)			
Cu1 - O23	1.9215(12)	Cu2 - N10	2.072(3)
Cu1 - N3	2.033(3)	Cu2 - N18	2.087(4)
Cu1 - N15	2.065(3)		

Bond angles (°)			
O23 - Cu1 - N3	98.55(11)	N15 - Cu1 - N10	80.94(13)
O23 - Cu1 - N15	178.60(14)	O23 - Cu1 - N18	100.85(16)
N3 - Cu1 - N15	80.17(13)	N3 - Cu1 - N18	122.50(14)
O23 - Cu1 - N10	99.49(11)	N15 - Cu1 - N18	80.36(14)
N3 - Cu1 - N10	128.73(13)	N10 - Cu1 - N18	100.38(13)

6.2.3 Magnetic behavior of 1

The temperature dependence of the molar magnetic susceptibility χ_M and its inverse $1/\chi_M$ deduced from measurements at 1000 Oe (0.1 Tesla) are given in Figure 6.3 (left). The molar magnetic susceptibility χ_M of compound **1** at 350 K equals to *ca.*

5×10^{-4} cm^3mol^{-1}, about half of the expected value for two uncoupled $S=1/2$ centres (*ca.* 1×10^{-3} cm^3mol^{-1}), thus indicating a strong antiferromagnetic coupling between the copper(II) ions. Upon lowering the temperature, χ_M further decreases to reach a plateau at *ca.* 1.5×10^{-4} cm^3mol^{-1} below 150 K. At temperatures below 100 K, the behaviour is dominated by a Curie tail, typical of a small paramagnetic impurity, as often found in molecular copper compounds. The presence of a small paramagnetic impurity is confirmed by measurements against the applied field at 5 and 100 K (Figure 6.3, right). To evaluate the strength of the magnetic interaction between the copper(II) ions within the dimeric unit in **1**, the following expression for the susceptibility, based on the Hamiltonian $H = -2J\,S_1S_2$ was thus used (equation 6.1):[10]

(6.1)

$$\chi = (1-p)\frac{2N_A\beta^2g^2}{k_BT\left[3+\exp\left(-\frac{2J}{k_BT}\right)\right]} + p\frac{N_A\beta^2g^2}{2k_BT} + TIP$$

where $2J$ corresponds to the singlet-triplet energy gap, p represents the amount of paramagnetic impurity and TIP a Temperature Independent Paramagnetism term. The fitting was performed fixing g to 2 and the best-fit parameters were then $2J = -691(35)$ cm^{-1}, TIP=$1.0(1)\times10^{-4}$ cm^3mol^{-1} and p=0.63(1)%. The large error bar on $2J$ originates from the lack of data at higher temperatures at which the maximum in χ_M would be observed.

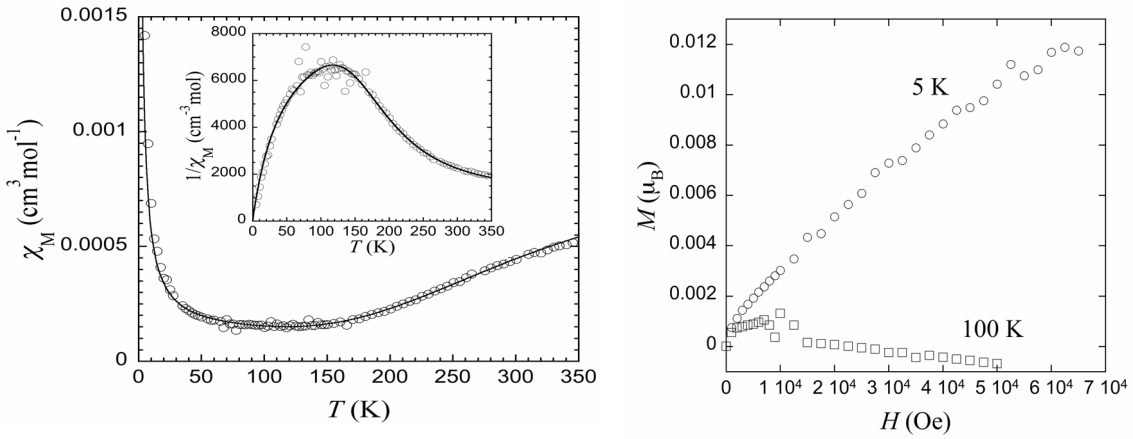

Figure 6.3. Left: magnetic susceptibility data χ and 1/χ *vs.* T for **1** in the temperature range 5-350 K in a 1000 Oe (0.1 Tesla) applied field. The full lines correspond to the best fit to a dimer model (see text). Right: field dependence of the magnetization of **1** at 5 and 100 K, showing the presence of a small paramagnetic impurity, in agreement with the variable-temperature data. The data were corrected for diamagnetism of the sample.

From the magneto-structural viewpoint, dinuclear copper complexes with a single hydroxo bridge are still rare, given the extensive research devoted to copper(II) coordination compounds. In all cases, antiferromagnetic exchange couplings have been observed, the strength of which depends on structural parameters. Attempts to derive

magneto-structural correlations were undertaken recently[11] for monohydroxo-bridged copper(II) ions in a square-planar environment. It was found that the antiferromagnetic exchange coupling increases with the Cu–O–Cu angle. Indeed for such geometry, the σ overlap of the spin-rich $d_{x^2-y^2}$ orbitals increases with Cu–O–Cu angles closer to 180º. In **1**, however, the Cu^{II} ions are in a trigonal bipyramidal environment with the hydroxo bridge in axial position. Furthermore, besides square-pyramidal and trigonal bipyramidal surroundings, monohydroxo-bridged dicopper(II) species are also found in the literature in combination with other bridging ligands, and with tetrahedral, square pyramidal, or octahedral environments, various types of distortions, and different coordination site for the hydroxo bridge. Therefore, the reported magneto-structural data for dinuclear compounds in which the Cu^{II} ions are only bridged by one hydroxo group, and for which the geometry around the Cu^{II} ions can be reasonably described by a type of coordination sphere, have been gathered in Table 6.2 and Figures 6.4 and 6.5. Cases for which the spin density at the hydroxo coordination site is expected to be negligible, *e.g.* for the hydroxo-bridging group in axial position in a square-pyramidal geometry, have been excluded.

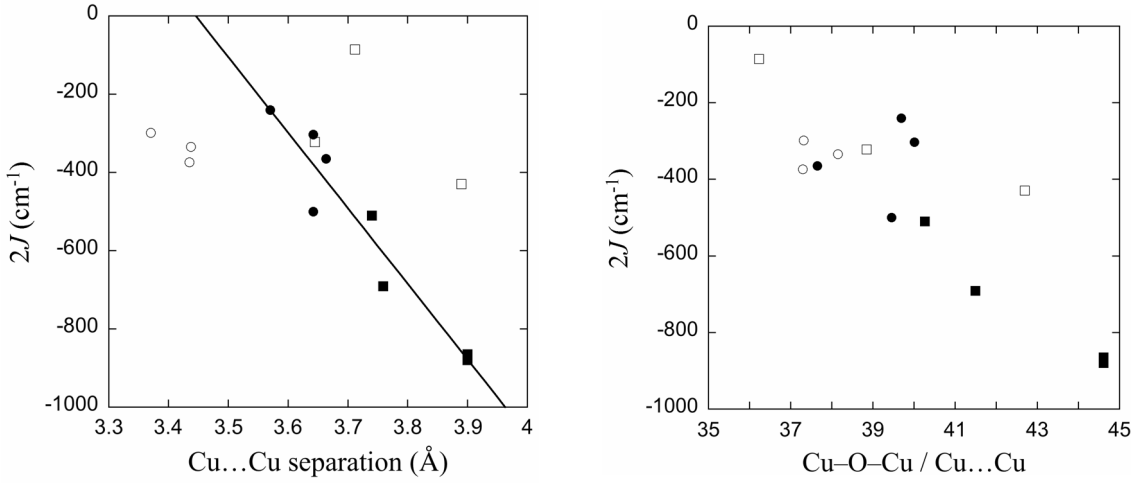

Figure 6.4. Correlation of the singlet-triplet energy gap 2*J* in monohydroxo-bridged dicopper(II) complexes with the Cu…Cu separation (left), and with the ratio Cu–O–Cu angle over Cu…Cu separation (right). Empty circles represent the square planar geometry, full circles the square pyramidal geometry with OH group in the equatorial position, full squares the trigonal bipyramid geometry with OH group in the axial position and empty squares the trigonal bipyramid geometry with OH group in the equatorial position. The full line is a linear fit (Eq. $-2J = 6653.8 - 1931.3 \times$Cu…Cu) of the data concerning compounds with the trigonal bipyramid geometry and the hydroxo bridge in the axial position and the square pyramidal geometry with the hydroxo bridge in the equatorial position.

Table 6.2. Magneto-structural data of relevant dicopper(II) complexes with a single hydroxo bridge. 2*J* represents here the singlet-triplet energy gap. SPl = square planar, Spy = square pyramidal with OH^- in the equatorial position, TBPax = trigonal bipyramid with OH^- in the axial position, TPBeq = distorted trigonal bipyramid with OH^- in the equatorial position. H_2L^1 = 2,6-bis[N-(phenyl)carbamoyl]pyridine, L^2 = tetraimine Schiff base of tris(2-aminoethyl)amine and 2,5-diformylfuran, L^3 = 1,4,7,13,16,19-hexaaza-10,22-dioxatetracosane, L^4 = octaamine from BH_4^- reduction of the Schiff base of tris(2-aminoethyl)amine and 2,5-diformylfuran, L^5 = 1,1,2,2-tetrakis(2-pyridyl)ethylene, dpm = di(2-pyridyl)methane, L^6 = Schiff base of 2,6-diacetylpyridine and 3,6-dioxaoctane-1,8-diamine, dien = diethylenetriamine, terpy = 2,2',6',2''-terpyridine, L^7 = partially hydrolyzed Schiff base of 2,6-diacetylpyridine and tris(2-aminoethyl)amine, tpmc = 1,4,8,11-tetrakis(2-pyridylmethyl)-1,4,8,11-tetraazacyclotetradecane

Geometry type	*Formula*	*Cu…Cu (Å)*	*Cu–O–Cu (°)*	*Cu–O–Cu / Cu…Cu*	*2J (cm^{-1})*	*Ref.*
TBPeq	$[Cu_2(bpy)_4(OH)](ClO_4)_3$	3.645	141.60	38.85	-322	Haddad. 1981[12]
SPl	$Na[Cu_2(L^1)_2(OH)]\cdot 2H_2O$	3.437	131.11	38.15	–334	Patra, 2000[11]
SPl	$K[Cu_2(L^1)_2(OH)]\cdot 2H_2O$	3.370	125.74	37.31	–298	Patra, 2000[11]
TBPax	$[Cu_2(L^2)(OH)](ClO_4)_3\cdot 1.5H_2O$	3.740	150.60	40.27	–510	Adams, 1996[13]
TBPax	$[Cu_2([22]py4pz)OH](ClO_4)_3\cdot H_2O$	3.757	155.97	41.49	–691	This thesis
SPy	$[Cu_2(L^3)(OH)(ClO_4)](ClO_4)_2\cdot CHCl_3$	3.642	143.7	39.46	–500	Coughlin, 1981[14]
TBPax	$[Cu_2(L^4)(OH)](CF_3SO_3)_3$	3.90	174.0	44.61	–865	Lu, 1994[15]
TBPax	$[Cu_2(L^4)(OH)](CF_3SO_3)_3\cdot H_2O$	3.90	174.0	44.61	–880	Harding, 1993[16]
SPy	$[Cu_2(L^5)(dpm)(OH)](ClO_4)_3\cdot 2H_2O$	3.663	137.9	37.65	–365	Spodine, 1991[17]
SPy	$[Cu_2(L^6)(OH)](ClO_4)_2\cdot H_2O$	3.57	141.7	39.69	–240	Drew, 1981[18]
SPl	$[Cu_2(dien)_2(ClO_4)_3(OH)]$	3.435	128.1	37.29	–374	Castro, 1990[19]
SPy	$[Cu_2(terpy)_2(H_2O)(ClO_4)_3(OH)]$	3.642	145.7	40.05	–303	Folgado, 1989[20]
TBPeq	$[Cu_2(L^7)(OH)](CF_3SO_3)(BPh_4)_2$	3.89	166.1	42.70	–430	Harding, 1995[21]
TBPeq	$[Cu_2(tpmc)(OH)](ClO_4)_3\cdot 2H_2O$	3.712	134.5	36.23	–86	Asato, 1989[22]

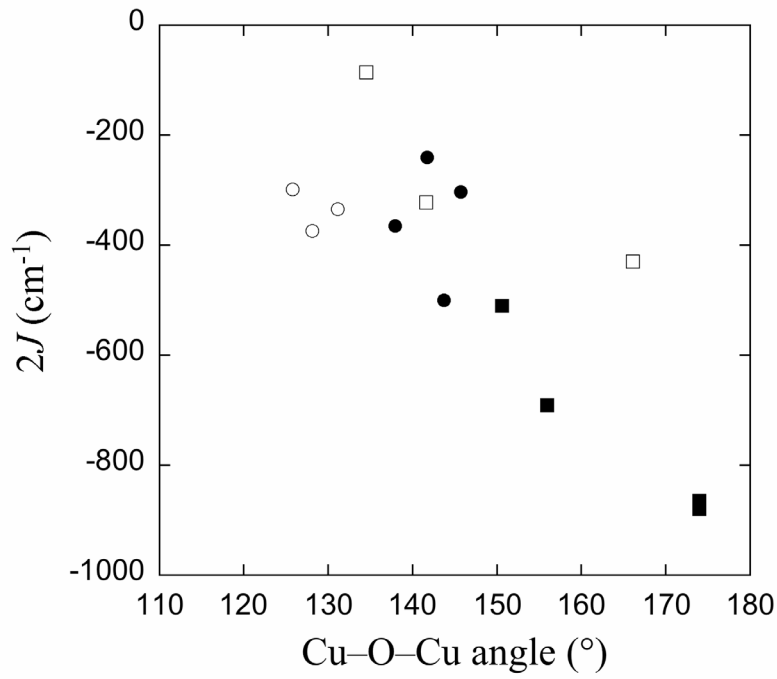

Figure 6.5. Correlation of the singlet-triplet energy gap 2*J* in mono-hydroxo-bridged dicopper(II) complexes with the Cu–O–Cu angle, (empty circles) square planar geometry, (full circles) square pyramidal geometry with OH group in equatorial position, (full squares) trigonal bipyramid geometry with OH group in axial position and (empty squares) trigonal bipyramid geometry with OH group in equatorial position.

A common general trend is observed with the singlet-triplet energy gap increasing with longer Cu…Cu separations, wider Cu–O–Cu angles and higher Cu–O–Cu/ Cu…Cu ratios. These structural parameters are obviously interdependent. For the three geometries considered, the increase in singlet-triplet energy gap in fact corresponds to a variation of the structural parameters towards situations for which the overlap between the magnetic orbitals (d_{z^2} in trigonal bipyramid, $d_{x^2-y^2}$ in square planar and square pyramid) and the hydroxo O 2p orbital is the most efficient, close to linearity. The antiferromagnetic σ-superexchange pathway through the hydroxo bridge is then the most efficient, yielding virtually diamagnetic complexes.

In addition, there is a good linear correlation between the Cu…Cu separation and the singlet-triplet energy gap among compounds having the trigonal bipyramid geometry and the hydroxo bridge in axial position and square pyramidal geometry with the hydroxo bridge in equatorial position (see Figure 6.4, left). It has to be noted that for such a monoatomic single bridge, only a small dependence on the actual Cu^{II} coordination environment can be expected, if the bridging atom lies in a spin-rich position. The correlation found here is of relevance for the characterization of mimics for dinuclear copper centres in biological systems.

6.2.4 ^{1}H NMR assignment strategy for 1

6.2.4.1 ^{1}H NMR, 2D COSY NMR and T_1 measurements

^{1}H NMR spectroscopy has only relatively recently emerged as a useful tool in studying the structural and magnetic properties of Cu^{II} coordination compounds in solution.[23-25] The slow electronic relaxation of Cu^{II} ions usually results in large line widths and poor resolution of the spectra, which makes their interpretation very difficult, if not impossible. However, if two antiferromagnetically coupled copper(II) ions are present in a complex, the situation is different. In antiferromagnetically coupled dicopper(II) systems, the ground state is a diamagnetic (S = 0) singlet. The energy separation between the ground state and the paramagnetic (S = 1) excited triplet state, which increases with the strength of the antiferromagnetic coupling, may lead to relatively sharp resonances, facilitating the spectra interpretation.[26]

In the present case, a very strong ($2J$ = -691(35) cm^{-1}) antiferromagnetic coupling between the copper(II) centers in **1** results in relatively sharp resonances with rather small hyperfine shifts, observed in a range of -50 to +30 ppm.

At room temperature, only 7 well-resolved signals are found in the region of 0-200 ppm in the ^{1}H NMR spectrum of **1** (Figure 6.6). One additional weak signal is observed at -48 ppm (Figure 6.7, left). The temperature-variable 1D spectra, recorded in the temperature interval 233-353 K (Figure 6.7, the data recorded above 293 K are not shown), reveal that the signal observed at 8.6 ppm at RT results from coincidental degeneracy of two resonances. Furthermore, two very broad signals at *ca.* 25 and 20 ppm become clearly visible at 233 K. In total, 11 resonances are thus observed in the whole spectral window (Figure 6.7), which implies the presence of an additional (pseudo-)symmetry plane in the cationic species next to the C_2 symmetry axis, observed in the crystal structure of **1**. One can imagine it connecting two tripodal nitrogen atoms, passing through both copper centers and with two pyridine rings lying virtually in the plane, resulting in the equivalency of all four pyrazole rings, all methylene groups of the ethylene moieties and the methylene N(tripodal)-C<u>H</u>$_2$-pz groups. However, taking into account that the two protons (*e.g.* equatorial *vs.* axial) of the methylene groups are diastereotopic and that these usually experience different hyperfine shifts, 12 resonances are expected for **1** (it should be noted that the protons of the pyridylmethylene moieties are **not** diastereotopic, as they become symmetry-related due to the pseudo symmetry plane). In general, the protons in a close proximity to copper ions experience stronger paramagnetic effects and thus shorter longitudinal relaxation times (T_1) and broader line widths (shorter transverse relaxation times T_2) in comparison to the protons in the periphery.[24] Therefore, as shown previously for paramagnetic Cu^{II} complexes, it is not uncommon for the resonances corresponding to the protons closest to copper to broaden beyond recognition.[27,28] It can be thus tentatively proposed that the resonances corresponding to the methylene protons of the pyridylmethyl moieties, which are the

closest to copper (H16a – Cu 3.050 Å, H16b – Cu 3.728 Å), are too broad to be detected. Another explanation of the observation of only 11 signals instead of 12 would be a coincidental degeneracy of two resonances which can not be resolved at different temperatures due to the line broadness.

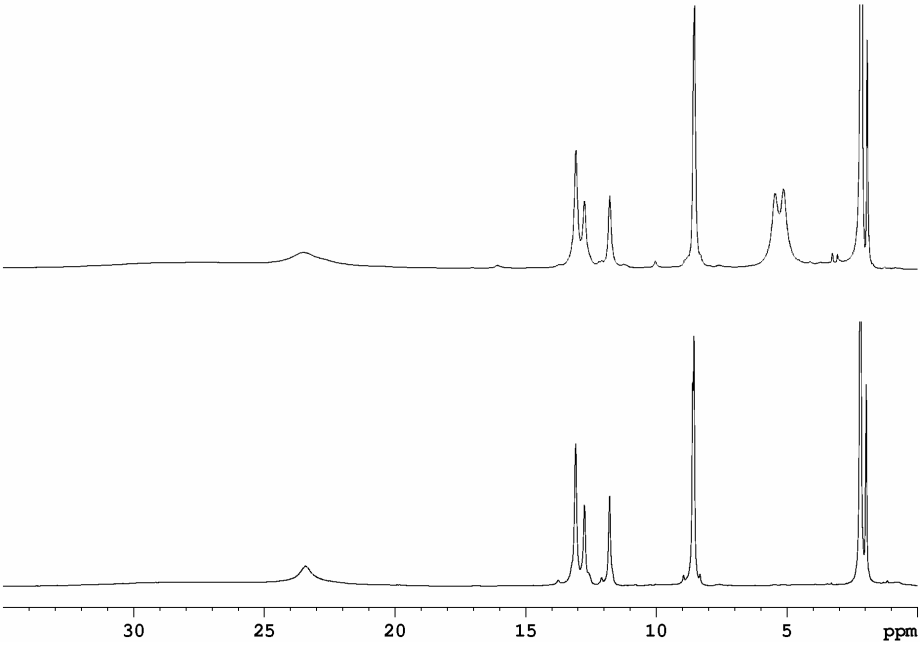

Figure 6.6. Positive range parts of the ^{1}H NMR spectra (300 MHz, CD_3CN) of **1** (top) and **1**-d_8 (the complex in which the protons of the ethylene moieties are substituted with deuterium atoms) (bottom).

The peak at -48 ppm can easily be assigned to the proton of the OH group, as it has an approximate integral intensity of 1 and disappears upon addition of D_2O to the complex solution due to a proton-deuterium exchange. Furthermore, as evidenced from the X-ray structure, the Cu d_z^2 orbital, which contains the unpaired electron, is directed along the Cu-O bond. Therefore, a spin polarization mechanism would cause the μ-hydroxo proton to be shielded and thus upfield shifted, as was previously reported for similar cases.[25] This observation is also consistent with the assignment.

The resonances E, F, G and C have been assigned to the pyridine protons according to their relative integral intensity of 2 (the intensity of C being measured at 233 K, where it appears relatively sharp). The resonances I and J, which overlap at 233 K, integrate as 4:4, as well as the resonances D and H, and the two very broad resonances A and B. However, the integration of the latter two resonances is unfortunately rather ambiguous due to the line broadness, even when measured at 233 K.

Resonances D and H have been assigned to the protons of the pyrazole rings by ^{1}H 2D COSY NMR at 263 K (Figure 6.8). The resonance G shows cross-signals with both resonances E and F, unambiguously ascribing it to the γ-protons of the pyridine rings and the resonances E and F to the *m*-pyridine protons. Resonances I and J, which do not display cross-signals in COSY, have been confirmed to originate from the

diastereotopic ethylene protons by the chemical substitution of the respective protons by deuterium. The signals in question are absent in the spectrum of the deuterated compound (Figure 6.6, bottom).

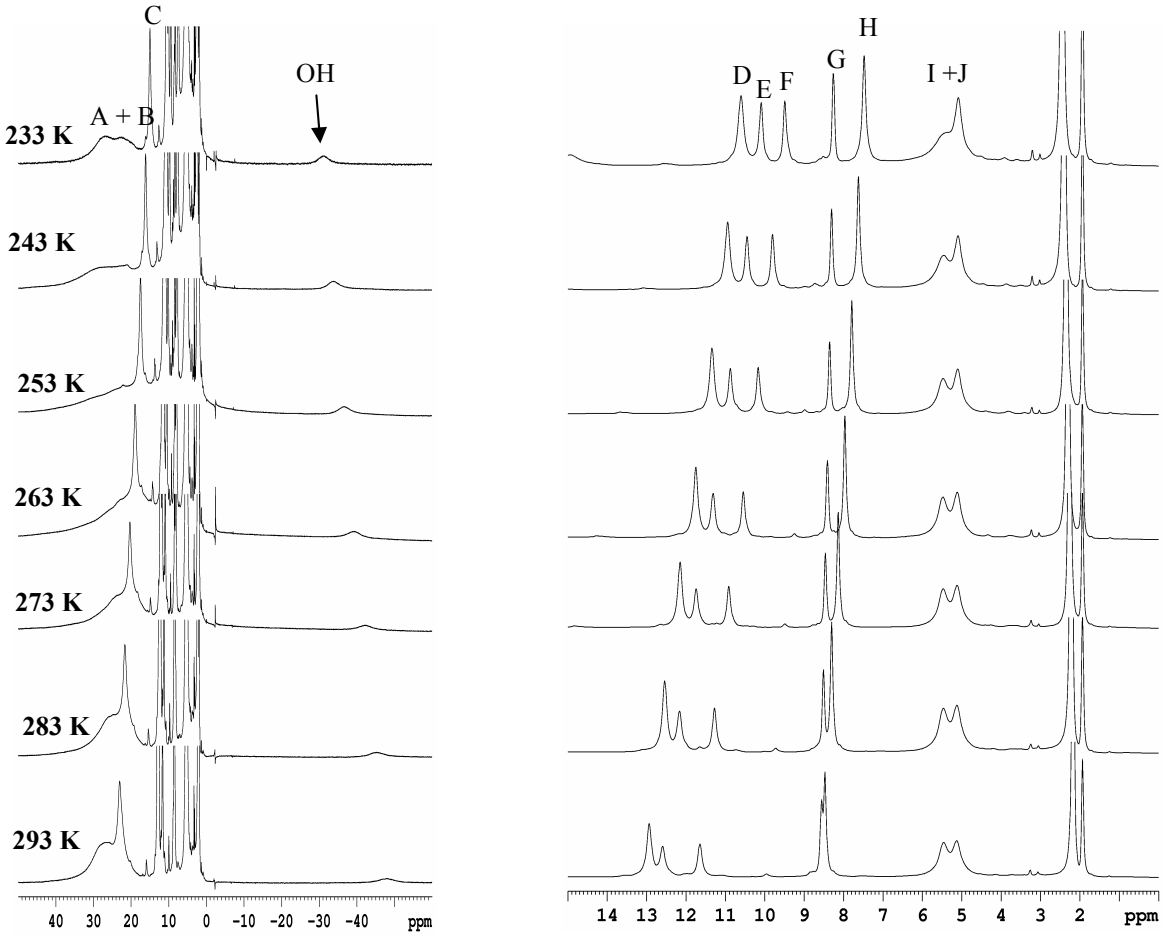

Figure 6.7. The changes in the ^{1}H NMR spectrum (300 MHz, CD_3CN) of **1** in the range 233-293 K. Left: the whole spectrum range (+50 to -60 ppm), enlarged; right: +15 to 0 ppm range.

Careful comparison of the Cu…H contact distances in the crystal structure indicates that the protons H1b and H8b are located significantly closer to Cu^{II} ions than their neighbors H1a and H8a. However, the corresponding resonances I and J are observed very close in the spectrum, which is perhaps caused by a rotational movement of the flexible ethylene groups of the complex cation in solution. The broad resonance A and B with an approximate integral intensity 4 can thus be assigned to the diastereotopic protons of the pyrazolylmethylene moieties, with axial protons experiencing larger hyperfine shifts than equatorial protons.[29] It is believed that the resonance originating from the pyridylmethylene protons, which are closest to copper, is broadened beyond recognition; however, it should emphasized that a possibility of it being hidden under the resonances A and B cannot be ruled out, since the line broadness of the latter resonances makes their integration rather uncertain.

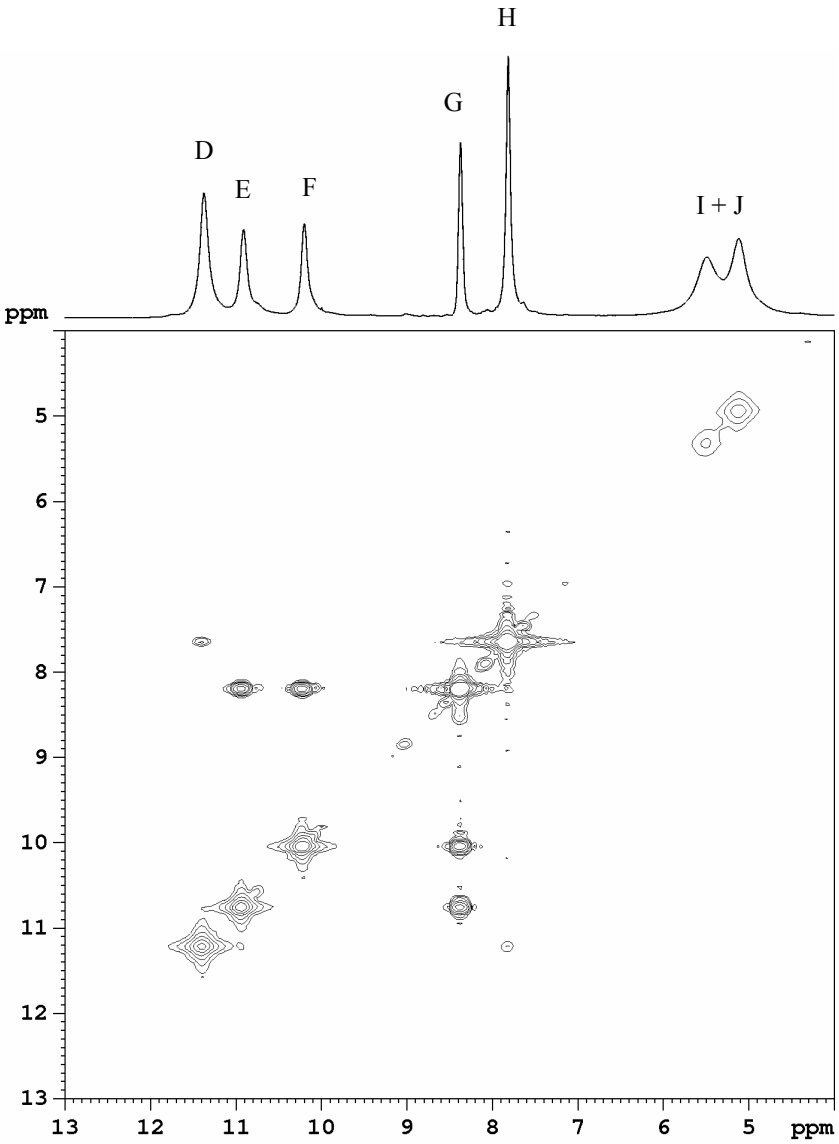

Figure 6.8. 2D COSY spectrum of **1** recorded at 263 K (CD_3CN, 300 MHz), displaying spin-spin connectivities between the resonances D and H, and the resonances E and F and the resonance G.

Further useful information can be obtained from the analysis of the longitudinal relaxation times (T_1). Assuming a predominant dipolar relaxation mechanism as reported by Holz and co-workers[23,25] in spin-coupled dicopper(II) complexes, the Cu…H contact distance *r* should be proportional to $T_1^{1/6}$. Using the equation $r_i = r_{ref}(T_{1i}/T_{1ref})^{1/6}$, in which r_i and T_{1i} are the Cu…H contact distance and the relaxation time of proton *i* and r_{ref} and T_{1ref} are the Cu…H contact distance and the relaxation time of the reference proton, the distances of each proton to the closest Cu^{II} center can be calculated. As a reference proton the γ-proton of the pyridine ring was used, and r_{ref} was taken as an arithmetic average of the Cu…H contact distances of two equivalent γ-protons in the crystal structure. The results are listed in Table 6.3. As can be seen, in general a rather good correlation is observed between the solution-determined Cu…H contact distances and the crystallographic ones, as the discrepancies between the calculated and the observed Cu…H contact distances do not exceed 20%. The differences noted may

originate from slight discrepancies between the solid-state and solution structures, or from electron spin-delocalization and contact interactions within the aromatic rings. However, unfortunately the results do not allow the differentiation between the protons of the aromatic rings, *e.g.* 4' and 5' protons of the pyrazole rings and 3' and 5' protons of the pyridine rings.

Resonance C, which does not show any cross peaks in the 2D COSY spectrum, probably due to its large line width, has been assigned to the 6' pyridine protons by default. The lack of a cross-peak in 2D COSY NMR is not uncommon for α-pyridine protons of paramagnetic Cu^{II} complexes.[23,25,30] The assignment is consistent with its T_1 and T_2 values (T_1 = 6.7 ms, T_2 = 222 Hz at 233 K), and its relatively large downfield shift in comparison to the other pyridine signals, due to its close proximity to the copper(II) ions.

Table 6.3. Longitudinal (T_1) relaxation times and line widths[a] measured at 233 K, and Cu-H distances calculated from the NMR data for **1** and determined from the X-ray structure

Resonance	*T_1, ms*	*Line width, Hz*	*r_{Cu-H}, calc., Å*	*r_{Cu-H}, determ., Å*	*Assignment*[d]
A	5.8	*b*	3.44	3.76	pz–C<u>H</u>$_{2(eq)}$-N
B	4.9	*b*	3.34	3.30	pz-C<u>H</u>$_{2(ax)}$-N
C	6.7	222	3.52	3.20	6'H-py
D	68.0	46	5.18	4.96	4'H-pz
E	58.8	27	5.06	4.90	3'H-py
F	58.8	23	5.06	5.13	5'H-py
G	132.6	13	5.79	5.79	4'H-py
H	67.3	25	5.17	5.17	5'H-pz
I	8.8	~118[c]	3.69	3.36	Pz-$(CH_2)_2$-pz (H1b +H8b)
J	8.8	~77[c]	3.69	4.61	Pz-$(CH_2)_2$-pz (H1a +H8a)

[a] The line widths are full width at half maximum. [b] Not measured because of broadness. [c] Measured at 253 K due to the signals overlapping at 233 K. [d] See also Figure 6.12.

6.2.4.2 1D NOE difference measurements

In the case of paramagnetic metal complexes, the fast nuclear relaxation rates and the relatively small size of the molecules usually prevent the use of NOE techniques. This is caused by the fact that the NOE intensity in paramagnetic molecules is proportional to the rotational correlation time and inversely proportional to the nuclear relaxation rates.[31] Although 1D NMR techniques, like NOE difference spectroscopy were previously successfully applied for the studies of biological proteins, they are scarcely used for the studies of coordination compounds.[32-36] In the present case, the first example of NOE difference experiments being successfully applied on a

paramagnetic Cu^{II} complex, in attempt to achieve a complete assignment of the resonances corresponding to the protons of the aromatic rings is reported.

Irradiation of the resonances I and J at 263 K, corresponding to the protons of the ethylene moieties of the macrocyclic ring, yields in both cases positive NOE's for both resonances D and H (Figure 6.9). The NOE signal of the latter resonances appears to be of higher intensity; therefore it was tentatively assigned it to the 5' protons of the pyrazole rings, which are located closer in space to the protons of the ethylene moieties. The very weak NOE signal of the resonance D is likely to be caused by spin diffusion. However, an absolute discrimination between these two resonances is unfortunately not possible, as the lower intensity of the NOE signal of the resonance D may also be inherent to its large line width.

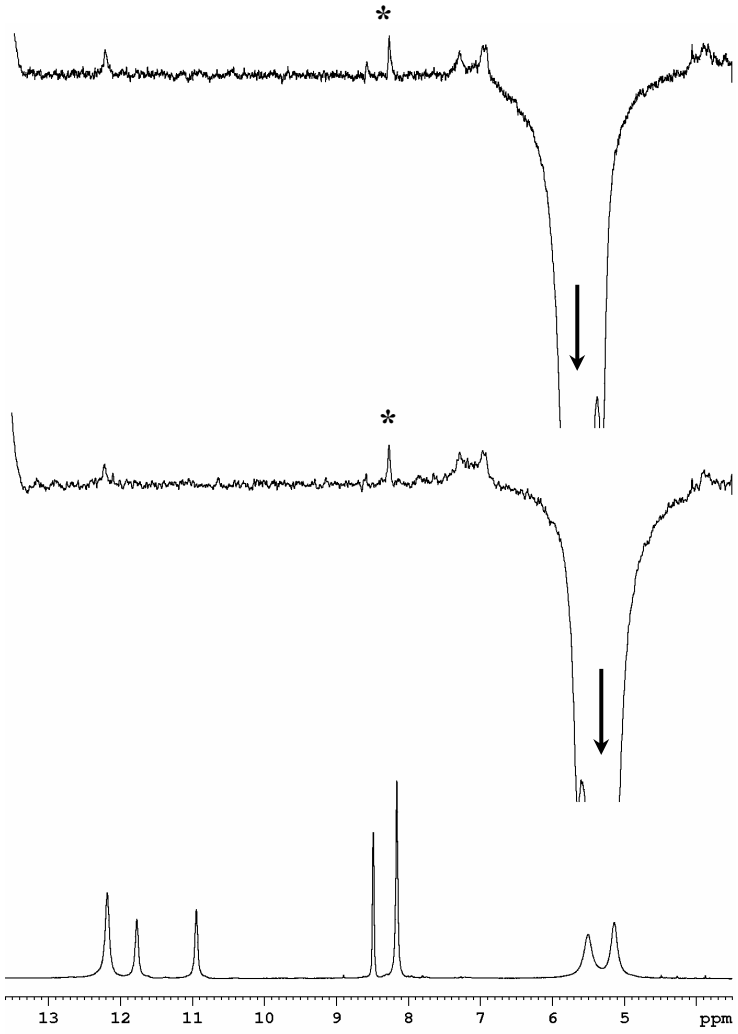

Figure 6.9. NOE difference spectra (CD_3CN, 600 MHz, 263 K), obtained upon irradiation of the resonances I (top) and J (middle). The peak H, which gives a more intense NOE signal, is marked with an asterisk.

It should be mentioned that the NOE connectivities between the pyrazole and ethylene protons are observed only upon irradiation of faster relaxing protons of the ethylene moieties (resonances I and J), but not upon irradiation of slower relaxing

protons of the pyrazole rings (resonances D and H). In the case of the latter protons irradiation, only a positive NOE signal from the neighbor pyrazole proton is observed (Figure 6.10). A similar behavior has been previously reported by Bubacco and co-workers for the Cu^{II} active site of tyrosinase.[37]

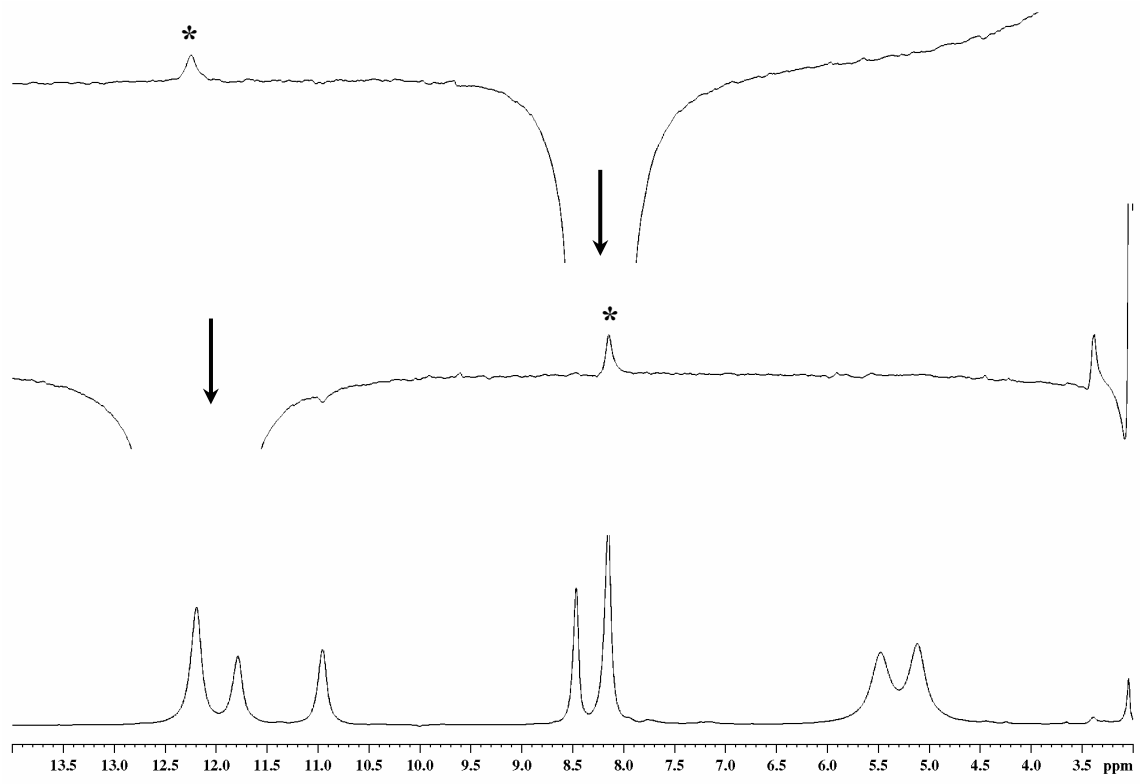

Figure 6.10. NOE difference spectra obtained upon irradiation of the resonances H (top) and D (bottom), corresponding to the pyrazole protons. The neighbor proton of the aromatic ring displays a NOE connectivity to the irradiated signal.

6.2.4.3 Distinguishing between the 3' and 5' protons of the pyridine rings

In the case of the 3' and 5' protons of the pyridine rings, the NOE spectroscopic technique could not be applied, as the only protons closely located to only one of the two considered protons are the protons of the pyridylmethylene moieties and the 6' protons of the pyridine rings. While the protons of the pyridylmethyl moieties are assumed to broaden beyond recognition, the very short T_1 value of the pyridine 6' protons precluded an observation of appreciable NOE connectivities. Therefore, a derivative ligand in which the two 3' protons of the pyridine rings were substituted by methyl groups was prepared. Regretfully, the very light-green compound obtained upon reaction of this ligand with copper(II) perchlorate in the presence of base in acetonitrile, exhibited very broad and poorly resolved resonances in the NMR spectrum in CD_3CN solution. In the UV-Vis spectrum of this solution, the peak at 350 nm, corresponding to the CT band of the bridging OH^- to Cu^{II} ions is absent, suggesting that the hydroxo-bridged complex with the methyl-substituted ligand does not form in acetonitrile.

Fortunately, in D_2O, a reasonably well-resolved NMR spectrum could be recorded, which is shown in Figure 6.11 (bottom). The *in situ* formation of the hydroxo-bridged complex in D_2O was confirmed by UV-Vis and mass spectroscopy (see Experimental part). For comparison, the spectrum of **1** was recorded in water as well (Figure 6.11, top). Although the quality of both spectra is rather poor, not in the least due to a poor solubility of the compounds, the two spectra are very similar. The absence of resonance E in the spectrum of the methylated complex allows its assignment to the 3' protons of the pyridine rings in **1**. Another clear difference between the two spectra is the resolution of the resonances G and H in the spectrum of the complex with the methylated ligand, in contrast to their degeneracy in the spectrum of **1** at RT (Figure 6.11). A very intensive peak of water traces, always present in D_2O, obscures the resonances I and J. A complete assignment of all resonances in ^{1}H NMR spectrum of **1** is shown in Figure 6.12.

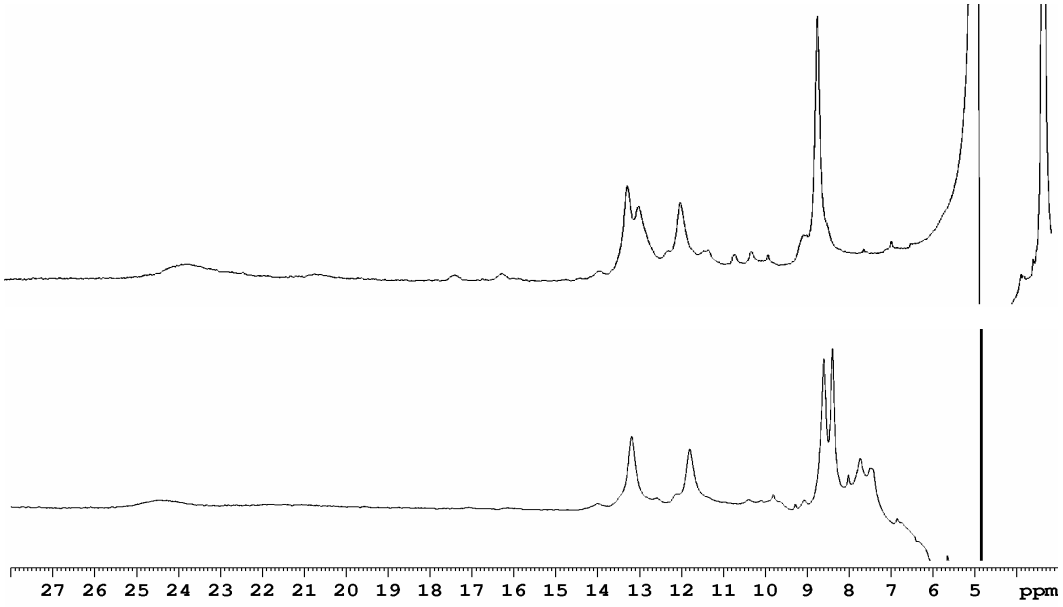

Figure 6.11. The ^{1}H NMR (300 MHz, D_2O) spectra of **1** (top) and **1**-Me_2 (the complex with the macrocyclic ligand containing methyl substituents at the 3' positions of the pyridine rings, *in situ*) (bottom). The measurements were performed with a suppression of H_2O resonance, which causes it being out of phase.

6.2.5 Determination of the antiferromagnetic coupling constant *J* from the temperature-dependent NMR studies on 1

The temperature dependencies of the observed hyperfine-shifted NMR signals of **1** were recorded over the temperature range of 233-353 K. As can be seen from Figure 6.7, the resonances shift downfield with increasing temperature, the complex thus showing an anti-Curie behavior. As shown previously, the type of behavior in the antiferromagnetically coupled Cu^{II} complexes was found to be dependent on the order

of magnitude of the magnetic coupling constant J.[38] The antiferromagnetic coupling creates a dicopper(II) system in which the ground state ($S = 0$) is separated from the first excited ($S = 1$) state by $2J$.[39] A very elegant study reported by Shokhirev and Walker[40] takes into account the temperature-dependent change in the population of the excited state. This approach has been successfully used to evaluate the strength of the spin-coupling interaction for 2Fe-2S clusters and dicopper centers.[41,42] In the present case, the variable temperature data obtained for the hyperfine-shifted signals were simultaneously fitted (Figure 6.13) using the program TDWf, kindly provided by N. Shokirev and A. Walker.[40] The fitting resulted in a $2J$ value of -729(22) cm^{-1}. A relatively large error margin is due to the fitting of a limited temperature range, as dictated by the freezing and boiling temperatures of the solvent. Still, the obtained value is in perfect agreement with the exchange constant obtained from the magnetic susceptibility studies ($2J$ = -691(35) cm^{-1}). This result clearly demonstrates the possibility and power to use NMR spectroscopy to probe the magnetic properties of coordination compounds with unpaired electrons in solution.

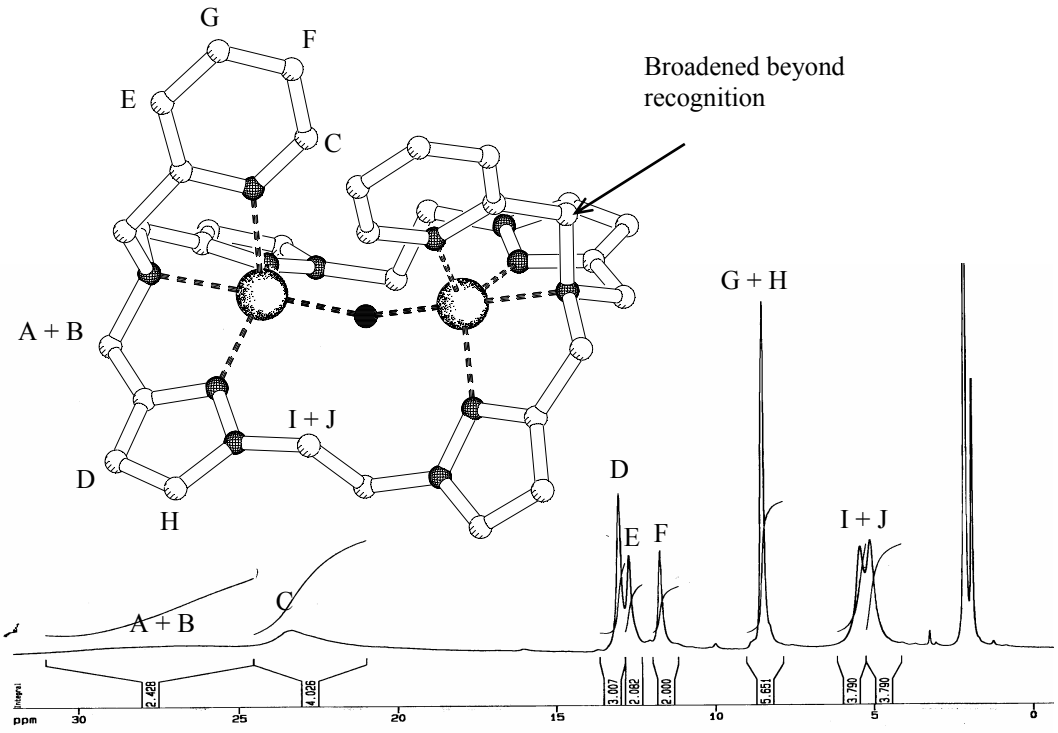

Figure 6.12. An assignment of the resonances in ^{1}H NMR spectrum of **1** (see also Table 6.3).

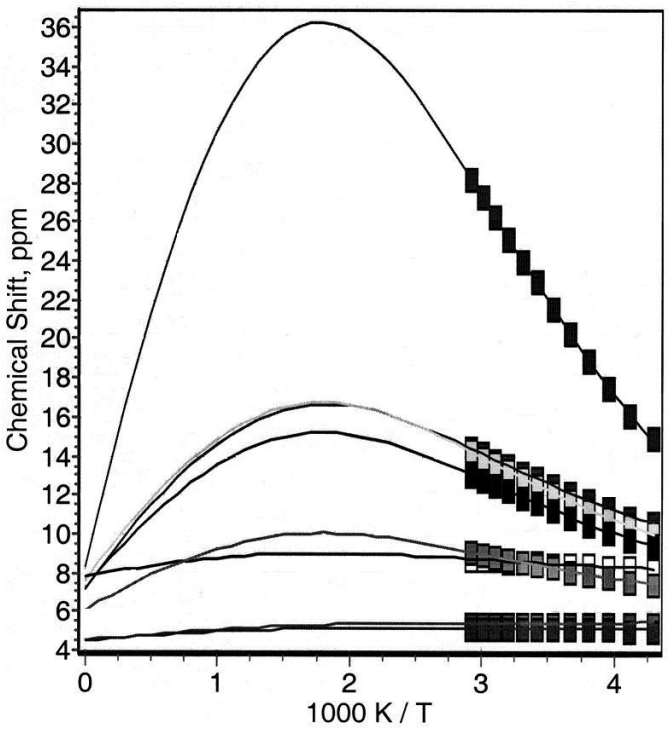

Figure 6.13. Plot of the chemical shifts of **1** in the temperature range of 233-353 K *vs.* the reciprocal temperature (1000 K/T). The simultaneous fitting for eight resonances by the program TDWf[40] results in $2J = -729(22)$ cm^{-1}.

6.3 Concluding remarks

In conclusion, a mono-hydroxo bridge mediates an antiferromagnetic coupling between the metal centers in dinuclear Cu^{II} complexes. The analysis of magneto-structural data for Cu^{II} complexes with a single hydroxo bridge and different coordination geometries around Cu^{II} ions (square-planar, square-pyramidal and trigonal bipyramidal) indicate that in all three cases, a common general trend is present with the strength of antiferromagnetic interaction increasing with longer Cu…Cu separations, wider Cu–O–Cu angles and higher Cu–O–Cu / Cu…Cu ratios.

It can also be concluded that proton NMR spectroscopy is a valuable technique which can be successfully applied on paramagnetic Cu^{II} complexes, provided that a significant antiferromagnetic coupling is present between the metal ions. The presence of strong antiferromagnetic interactions in a molecule overcomes the problem of long electron relaxation of the Cu^{II} ions, leading to shorter longitudinal (T_1) and transversal (T_2) nuclear relaxation times. As a result, commonly used NMR techniques for diamagnetic molecules, like 2D COSY and 1D NOE difference measurements, can also be successfully applied on Cu^{II} complexes. In particular, the latter spectroscopic technique can potentially be a rich source of structural information in solution. Finally, the strength of the magnetic coupling between the metal ions can be determined rather precisely from solution NMR studies. There is little doubt that NMR spectroscopy will

further develop as one of the most successive tools to study the structural and magnetic properties of paramagnetic molecules in solution.

6.4 Experimental Section

6.4.1 Materials and Methods

All starting materials were commercially available and used as purchased, unless stated otherwise. THF and methanol were dried over Na and distilled under Ar prior to use. The macrocyclic ligand [22]py4pz was synthesized by the previously described procedure,[6] according to the reaction scheme shown in Figure 6.1. The deuterated ligand [22]py4pz-d_8 was synthesized following a similar experimental procedure, starting from the commercially available ethylene glycol-d_4 (see below). The infrared spectrum of **1** in the 4000-300 cm^{-1} range was recorded on a Bruker 330V IR spectrophotometer equipped with a Golden Gate Diamond Set. The ligand field spectrum in solution was recorded on a Varian Cary 50 Scan UV-Vis spectrophotometer. Electrospray mass spectra (ESI-MS) in D_2O solutions were recorded on a Thermo Finnigan AQA apparatus. X-band electron paramagnetic resonance (EPR) measurements were performed at 77 K in the solid state on a Jeol RE2x electron spin resonance spectrometer, using DPPH ($g = 2.0036$) as a standard. Bulk magnetization measurements were performed on polycrystalline sample of **1** in the temperature range 5-400 K with a Quantum Design MPMS-5S SQUID magnetometer, in a 0.1 Tesla applied field. The data were corrected for the experimentally determined contribution of the sample holder. Corrections for the diamagnetic response of the complex, as estimated from Pascal's constants, were applied.[43]

6.4.2 ^{1}H NMR spectroscopic studies

The ^{1}H 1D and 2D COSY NMR spectra were recorded on a DPX300 Bruker spectrometer. All chemical shifts were reported with respect to the residual solvent peak. The longitudinal relaxation times (T_1) were determined by standard inversion-recovery experiments, with 2 s relaxation delay and the spectral width of 99.7582 ppm. The COSY spectrum was obtained at 263 K by collecting 1024 F_2×1024 F_1 data points, with a relaxation delay of 0.02 s and the spectral width of 34.0678 ppm. 384 scans were collected. The NOE difference spectra were recorded on a DMX600 Bruker spectrometer. 1D NOE difference experiments were performed by a literature procedure,[44,45] using a frequency list to define irradiation frequencies, alternating on and off resonance every other scan. A WEFT pulse sequence was not applied. The irradiation time was 500 ms. The number of scans during the experiments was 4 k.

6.4.3 Ligand synthesis

1,2-bis-tosylate-ethane-d_4: The compound was synthesized in the same way as its non-deuterated analogue, starting from commercially available ethylene glycol-d_4.[6] Yield: 82.8%. ^{1}H NMR (300 MHz, DMSO, ppm): δ = 7.71 (d, 4H, Ar-(*o*)-H); 7.45 (d, 4H, Ar-(*m*)-H); 2.44 (s, 6H, Ar-CH_3).

1,2-di(3-formyl-1-pyrazolyl)ethane-d_4: The compound was synthesized as a white solid by the same method as its non-deuterated analogue.[6] Yield: 58%. ^{1}H NMR (300 MHz, $CDCl_3$, ppm): δ = 9.97 (s, 2H, C(O)H); 7.08 (d, 2H, 4'pz-H); 6.69 (d, 2H, 5'pz-H).

1,2-di(3-hydroxymethyl-1-pyrazolyl)ethane-d_4: The compound was synthesized by the same method as its non-deuterated analogue and used without purification from borate salts.[6] Yield: not determined (above 100% due to the presence of borate salts). ^{1}H NMR (300 MHz, $CDCl_3$, ppm): δ = 7.13 (d, 2H, 4'pz-H); 6.16 (d, 2H, 5'pz-H); 4.54 (s, 4H, pz-CH_2-OH).

1,2-di(3-chloromethyl-1-pyrazolyl)ethane-d_4: The compound was synthesized according to a slight modification of the procedure reported by Schuitema *et al.*[6] The white solid obtained in the synthesis of 1,2-di(3-hydroxymethyl-1-pyrazolyl)ethane-d_4 was dissolved in 100 ml of thionyl chloride and heated at 50 °C upon stirring for 24 hours. Afterwards, $SOCl_2$ was evaporated under reduced pressure, and the residue was neutralized with saturated aqueous solution of Na_2CO_3. The product was extracted with dichloromethane. The organic phase was dried upon Na_2SO_4, and evaporated under reduced pressure. The product was recrystallized from methanol. Yield: 45% (relative to 1,2-di(3-formyl-1-pyrazolyl)ethane-d_4). ^{1}H NMR (300 MHz, $CDCl_3$, ppm): δ = 6.90 (d, 2H, 4'pz-H); 6.16 (d, 2H, 5'pz-H); 4.59 (s, 4H, pz-CH_2-Cl).

1,2-di-(3'-(2-pyridylmethylamino)-1'-pyrazolyl)ethane-d_4 (py2pz-d_4): The compound was synthesized according to the procedure used for its non-deuterated analogue.[6] Yield: 64%. ^{1}H NMR (300 MHz, $CDCl_3$, ppm): δ = 8.53 (d, 2H, 6'H-py), 7.63 (td, 2H, 4'H-py); 7.34 (d, 2H, 3'H-py); 7.13 (td, 2H, 5'H-py), 6.90 (d, 2H, 5'H-pz); 6.08 (d, 2H, 4'H-pz); 3.95(s, 4H, py-CH_2-N); 3.85 (s, 2H, pz-CH_2-N).

9,22-bis(2-pyridylmethyl)-1,4,9,14,17,22,27,28,29,30-decaazapentacycle [22.2.1.14,7.111,14.117,20]triacontane-5,7(28),11(29),12,18,20(30),24(27),25-octaene ([22]py4pz-d_8): The compound was synthesized according to a slight modification of the procedure earlier reported by Schuitema *et al.*[6] 0.301 g (2.84 mmol) of sodium carbonate and 0.577 g (1.42 mmol) of py2pz-d_4 were suspended in 3000 ml of dry THF. The reaction mixture was cooled to -40 °C, and a solution of 0.374 g (1.42 mmol) of 1,2-di(3'-chloromethylpyrazol-1'-yl)ethane-d_4 in *ca.* 200 ml of THF was added. The reaction mixture was allowed to warm slowly to RT and was then refluxed for 14 days under Ar. After two weeks, the solvent was evaporated, and the residue was redissolved in *ca.* 500 ml of a CH_2Cl_2-water mixture (1:1 v:v). The aqueous phase was acidified

with 35% HCl (till pH = 1) and washed a few times with dichloromethane. Afterwards, the aqueous layer was basified with NH_4OH (pH = 9), and the product was extracted a few times with dichloromethane. The combined organic layers were dried over Na_2SO_4, and the solvent was evaporated. The obtained yellow oil was redissolved in methanol, and the product was precipitated with diethyl ether. Yield: 27%. ^{1}H NMR (300 MHz, $CDCl_3$, ppm): δ = 8.40 (d, 2H, 6'H-py), 7.81 (td, 2H, 4'H-py); 7.64 (d, 2H, 3'H-py); 7.41 (d, 2H, 5'H-pz); 7.25 (td, 2H, 5'H-py); 6.11 (d, 2H, 4'H-pz); 3.56 (s, 4H, py-CH_2-N); 3.36 (s, 2H, pz-CH_2-N).

3-methyl-2-pyridylmethylamine: The compound was synthesized according to a slight modification of the procedure reported earlier by Fos *et al.*[46] 1 g (8.5 mmol) of 2-cyano-3-methylpyridine was dissolved in 200 ml of dry MeOH and hydrogenated with molecular hydrogen in the presence of 1.5 g of 10% Pd on a charcoal. After 6 hours, the charcoal was filtered off, and 4 ml of concentrated HCl was added to the resulting solution. After evaporation, a mixture of white crystals of product and some amount of light yellow oil was obtained. The product was recrystallized from a MeOH-diethyl ether mixture. Yield: 0.70 g (42 %). ^{1}H NMR (MeOD, 300 MHz, ppm): δ = 8.64 (d, 1H, 2'H-py); 8.14 (d, 1H, 4'H-py), 7.69 (dd, 1H, 3'H-py), 4.45 (s, 2H, CH_2py), 2.52 (s, 3H, CH_3).

1,2-di-(3'-(3-methyl-2-pyridylmethylamino)-1'-pyrazolyl)ethane (py2Me$_2$pz): Under an argon atmosphere, 0.38 g (1.78 mmol) of 1,2-di(3-formyl-1-pyrazolyl)ethane and 1.2 ml (4 equivalents) of diisopropylethylamine (DIPEA) were dissolved in 400 ml of dry methanol. A solution of 0.68 g (3.46 mmol) of 3-methylpyridin-2-ylmethylamine in 50 ml of dry MeOH was added dropwise to the reaction mixture. The purity of the imine, which immediately forms *in situ*, was checked by NMR spectroscopy, and its reduction was carried out without isolating the compound. $NaBH_4$ (3 eq/CH=N bond) was added to the solution. After the evolution of gas stopped, the resulting mixture was refluxed for two hours and the solvent was evaporated under reduced pressure. The residue was dissolved in *ca.* 250 ml of a biphasic H_2O-dichloromethane mixture, and the organic layer was separated. After washing the aqueous layer a few more times with dichloromethane, the organic layers were combined, dried over Na_2SO_4 and evaporated. This work-up resulted in the pure product as a light yellow oil. Yield: 0.47 g (61 %). ^{1}H NMR ($CDCl_3$, 300 MHz), ppm: δ = 8.39 (d, 2H, 6'H-py), 7.41 (d, 2H, 4'H-py), 7.06 (dd, 2H, 5'H-py), 6.90 (d, 2H, 3'H-pz), 6.08 (d, 2H, 4'H-pz), 4.47 (s, 4H, pz-(CH_2)$_2$-pz), 3.90 (s, 8H, NH-CH_2-py + NH-CH_2-pz), 2.32 (s, 6H, CH_3-py).

9,22-bis(3-methyl-2-pyridylmethyl)-1,4,9,14,17,22,27,28,29,30-decaazapentacycle[22.2.1.14,7.111,14.117,20]triacontane-5,7(28),11(29),12,18,20(30),24(27),25-octaene ([22]pyMe$_2$4pz): Under an argon atmosphere, 0.343 g (3.24 mmol) of Na_2CO_3 and 0.696 g (1.62 mmol) of py2Me$_2$pz were suspended in 3500 ml of dry THF. *Ca.* 200 ml of CH_3CN was added to ensure the

dissolution of the organic compound. The suspension was cooled down to -20 °C, and a solution of 0.419 g (1.62 mmol) of 1,2-di(3'-chloromethyl-1'-pyrazolyl)ethane in 100 ml of dry THF was added to the reaction mixture. The resulting suspension was allowed to warm slowly to room temperature, and refluxed for two weeks under argon. Afterwards, the solvent was evaporated, and the residue was redissolved in a dichloromethane-water mixture. The organic layer was separated, and the aqueous layer was washed three more times with dichloromethane. The product was extracted by a diluted HCl solution, and the resulting aqueous solution was washed a few more times with dichloromethane. Addition of an ammonium hydroxide solution till pH = 11 resulted in the formation of a white suspension, which was extracted four times with dichloromethane. The resulting organic solution was dried over Na_2SO_4 and evaporated under reduced pressure. The resulting crude product, obtained as a dark-brown oil, was purified by column chromatography on silica, using CH_2Cl_2:MeOH mixture (85:15, v:v) as an eluent. The pure ligand was crystallized from a MeOH/diethyl ether solution and isolated as a white powder. Yield: < 10%. ^{1}H NMR (300 MHz, MeOD, ppm): δ = 8.35 (d, 2H, 6'H-py); 7.68 (d, 2H, 4'H-py); 7.49 (d, 2H, 5'H-pz); 7.29 (d, 2H, 5'H-py); 6.19 (d, 4H, 4'H-pz); 4.57 (s, 16H, pz-(CH_2)$_2$-pz + pz-(CH_2)-N); 3.69 (s, 4H, py-CH_2-N); 2.28 (s, 6H, CH_3-pz)

6.4.4 Syntheses of the coordination compounds

[Cu_2([22]py4pz)(μ-OH)](ClO$_4$)$_3$·H_2O (1): A solution of $Cu(ClO_4)_2·6H_2O$ (74 mg, 0.20 mmol) in *ca.* 2 ml acetonitrile was added to a suspension of [22]py4pz (58 mg, 0.10 mmol) in the same solvent (the free ligand does not dissolve, unless coordinated to the metal ions). To the resulting greenish-blue solution one equivalent of NMe_4OH (20% solution in methanol) was added, which resulted in an immediate color change to clear green. Small amounts of copper hydroxide that may precipitate occasionally were removed by filtration. The resulting clear solution was concentrated to the half of its initial volume. Diethyl ether diffusion led to small green crystals, which were isolated and recrystallized from an acetonitrile/diethyl ether mixture. Single crystals were obtained by slow diffusion of diethyl ether into a diluted acetonitrile solution of **1**. Elemental analysis, % found (calc.) for [Cu_2([22]py4pz)(μ-OH)](ClO$_4$)$_3$·H_2O (=$C_{32}H_{39}Cl_3Cu_2N_{12}O_{14}$): C, 36.6 (36.6), H, 3.7 (3.3), N, 16.0 (15.6). IR (4000-300 cm^{-1}), ν: 3514 (O-H stretching), 3126 (C-H arom. stretching), 1610 (C=N arom. pyridine), 1515 (C=N arom. pyrazole), 1076 (ClO_4^-)

[Cu_2([22]py$Me_2$4pz)(μ-OH)](ClO$_4$)$_3$·H_2O (1-Me_2) (*in situ*): A solution of $Cu(ClO_4)_2·6H_2O$ (7.2 mg, 0.019 mmol) in *ca.* 1 ml acetonitrile was added to a suspension of [22]py$Me_2$4pz (6.0 mg, 0.010 mmol) in the same solvent (the ligand does not dissolve without coordination to metal ions). To the resulting green solution one equivalent of NMe_4OH (20% solution in methanol) was added, which resulted in an immediate color change to greenish-yellow. The resulting solution was concentrated till

the half of its initial volume. Diethyl ether diffusion led to the formation of a very light-green amorphous powder, which was redissolved in D_2O and used for the NMR spectroscopic studies. The *in situ* formation of the hydroxo-bridged complex was confirmed by ESI-MS measurements (D_2O, m/z 529 (1 [22]py$Me_2$4pz + 2 Cu + 1 OH + 3 ClO_4, z = 2; 1078 (1 [22]py$Me_2$4pz + 2Cu + 1 OH + 3 ClO_4 + D_2O, z = 1) and UV-Vis spectroscopy (in D_2O, λ = 350 nm (CT $Cu^{II} \leftarrow$ OH).

Safety Note: Although no problems were encountered during the preparation of perchlorate salts, these compounds are potentially hazardous and should be treated with care.

6.4.5 X-ray crystallographic measurements

X-ray diffraction intensities of **1** were measured on a Bruker AXS Apex diffractometer with graphite monochromator. The structure was solved with direct methods (SHELXS97).[47] The structure refinement was done with SHELXL97[48] against F^2 of all reflections. Molecular illustration, checking for higher symmetry and geometry calculations were performed with the PLATON[49] package. $C_{32}H_{39}Cl_3$ $Cu_2N_{12}O_{14}$, Fw = 1049.19, green block (0.07×0.05×0.04 mm^3), a = 21.826(4) Å, b = 12.189(2) Å, c = 17.687(4) Å, β = 117.47(3)°, Z = 4, V = 4174.9(18) $Å^3$, $\rho_{calcd.}$ = 1.666 $g \cdot cm^{-3}$, μ = 1.291 mm^{-1}, monoclinic, space group *C2/c* (no. 15), 21343 reflections collected, 5187 independent reflections (R_{int} = 0.0540). The final cycle of full-matrix least-squares refinement, including 289 parameters, converged into R_1 = 0.0512 (R_1 = 0.0923 all data) and wR_2 = 0.1344 (wR_2 = 0.1447 all data) with a maximum (minimum) residual electron density of 0.887 (-0.499) $e \cdot Å^3$.

6.5 References

(1) Torelli, S.; Belle, C.; Gautier-Luneau, I.; Pierre, J. L.; Saint-Aman, E.; Latour, J. M.; Le Pape, L.; Luneau, D. *Inorg. Chem.* **2000**, *39*, 3526-3536.
(2) Torelli, S.; Belle, C.; Hamman, S.; Pierre, J. L.; Saint-Aman, E. *Inorg. Chem.* **2002**, *41*, 3983-3989.
(3) Ackermann, J.; Meyer, F.; Kaifer, E.; Pritzkow, H. *Chem. Eur. J.* **2002**, *8*, 247-258.
(4) Mukherjee, J.; Mukherjee, R. *Inorg. Chim. Acta* **2002**, *337*, 429-438.
(5) Koval, I. A.; Huisman, M.; Stassen, A. F.; Gamez, P.; Roubeau, O.; Belle, C.; Pierre, J. L.; Saint-Aman, E.; Luken, M.; Krebs, B.; Lutz, M.; Spek, A. L.; Reedijk, J. *Eur. J. Inorg. Chem.* **2004**, 4036-4045.
(6) Schuitema, A. M.; Aubel, P. G.; Koval, I. A.; Engelen, M.; Driessen, W. L.; Reedijk, J.; Lutz, M.; Spek, A. L. *Inorg. Chim. Acta* **2003**, *355*, 374-385.
(7) Schuitema, A. M. Ph.D. thesis, Leiden University, 2004.
(8) Klabunde, T.; Eicken, C.; Sacchettini, J. C.; Krebs, B. *Nat. Struct. Biol.* **1998**, *5*, 1084-1090.
(9) Addison, A. W.; Rao, T. N.; Reedijk, J.; van Rijn, J.; Verschoor, G. C. *J. Chem. Soc., Dalton Trans.* **1984**, 1349-1356.
(10) Kahn, O. *Molecular Magnetism*; Wiley-VCH: New York, 1993.
(11) Patra, A. K.; Ray, M.; Mukherjee, R. *Polyhedron* **2000**, *19*, 1423-1428.
(12) Haddad, M. S.; Wilson, S. R.; Hodgson, D. J.; Hendrickson, D. N. *J. Am. Chem. Soc.* **1981**, *103*, 384-391.
(13) Adams, H.; Bailey, N. A.; Collinson, S. R.; Fenton, D. E.; Haring, C. J.; Kitchen, S. J. *Inorg. Chim. Acta* **1996**, *246*, 81-88.
(14) Coughlin, P. K.; Lippard, S. J. *J. Am. Chem. Soc.* **1981**, *103*, 3228-3229.

(15) Lu, Q.; Latour, J.-M.; Harding, C. J.; Martin, N.; Marrs, D. J.; McKee, V.; Nelson, J. *J. Chem . Soc., Dalton Trans.* **1994**, 1471-1478.
(16) Harding, C. J.; McKee, V.; Nelson, J.; Lu, Q. *J. Chem. Soc., Chem. Commun.* **1993**, 1768-1769.
(17) Spodine, E.; Manzur, J.; Garland, M. T.; Kiwi, M.; Peña, O.; Grandjean, D.; Poupet, L. *J. Chem. Soc., Dalton Trans.* **1991**, 365-369.
(18) Drew, M. G. B.; McCann, M.; Martin-Nelson, M. *J. Chem. Soc., Dalton Trans.* **1981**, 1868-1878.
(19) Castro, I.; Faus, J.; Julve, M.; Lloret, F.; Verdaguer, M.; Kahn, O.; Jeannin, S.; Jeannin, Y.; Vaisserman, J. *J. Chem. Soc., Dalton Trans.* **1990**, 2207-2212.
(20) Foldago, J. V.; Coronado, E.; Beltran-Porter, D.; Rojo, T.; Fuertes, J. *J. Chem. Soc., Dalton Trans.* **1989**, 237-241.
(21) Harding, C. J.; Lu, Q.; Malone, J. F.; Marrs, D. J.; Martin, N.; McKee, V.; Nelson, J. *J. Chem. Soc., Dalton Trans.* **1995**, 1739-1747.
(22) Asato, E.; Toftlund, H.; Kida, S.; Mikuriya, M.; Murray, K. S. *Inorg. Chim. Acta* **1989**, *165*, 207-214.
(23) Holz, R. C.; Brink, J. M. *Inorg. Chem.* **1994**, *33*, 4609-4610.
(24) Murthy, N. N.; Karlin, K. D.; Bertini, I.; Luchinat, C. *J. Am. Chem. Soc.* **1997**, *119*, 2156-2162.
(25) Brink, J. M.; Rose, R. A.; Holz, R. C. *Inorg. Chem.* **1996**, *35*, 2878-2885.
(26) Banci, L.; Bertini, I.; Luchinat, C. *Struct. Bonding* **1990**, *72*, 113-135.
(27) Satcher, J. H. J.; Balch, A. L. *Inorg. Chem.* **1995**, *34*, 3371-3373.
(28) Aromi, G.; Gamez, P.; Kooijman, H.; Spek, A. L.; Driessen, W. L.; Reedijk, J. *Eur. J. Inorg. Chem.* **2003**, 1394-1400.
(29) Belle, C.; Bougault, C.; Averbuch, M.-T.; Durif, A.; Pierre, J. L.; Latour, J. M.; Le Pape, L. *J. Am. Chem. Soc.* **2001**, *123*, 8053-8066.
(30) Lubben, M.; Hage, R.; Meetsma, A.; Bijma, K.; Feringa, B. L. *Inorg. Chem.* **1995**, *34*, 2217-2224.
(31) Bertini, I.; Luchinat, C. *NMR of Paramagnetic Molecules in Biological Systems*; Benjamin/Cummings: Menlo Park, CA, 1986.
(32) Epperson, J. D.; Ming, L.-J.; Woosley, B. D.; Baker, G. R.; Newkome, G. R. *Inorg. Chem.* **1999**, *38*, 4498-4502.
(33) Epperson, J. D.; Ming, L.-J.; Baker, G. R.; Newkome, G. R. *J. Am. Chem. Soc.* **2001**, *123*, 8583-8592.
(34) Dolores Santana, M.; Rufete, A.; Sanchez, G.; Garcia, G.; Lopez, G.; Casabo, J.; Molins, E.; Miravitlles, C. *Inorg. Chim. Acta* **1997**, *255*, 21-27.
(35) Momot, K. I.; Walker, F. A. *J. Phys. Chem. A* **1997**, *101*, 9207-9216.
(36) Lisowski, J.; Latos-Grazynski, L.; Szterenberg, L. *Inorg. Chem.* **1992**, *31*, 1933-1940.
(37) Bubacco, L.; Saldago, J.; Tepper, A. W. J. W.; Vijgenboom, E.; Canters, G. W. *FEBS Letters* **1999**, *442*, 215-220.
(38) Holz, R. C.; Brink, J. M.; Rose, R. A. *J. Magn. Res. A* **1996**, *119*, 125-128.
(39) Holz, R. C.; Alvarez, M. L.; Zumft, W. G.; Dooley, D. M. *Biochemistry* **1999**, *38*, 11164-11171.
(40) Shokhirev, N. V.; Walker, F. A. *J. Phys. Chem.* **1995**, *99*, 17795-17804.
(41) Holz, R. C.; Bennett, B.; Chen, G.; Ming, L.-J. *J. Am. Chem. Soc.* **1998**, *120*, 6329-6335.
(42) Holz, R. C.; Small, F. J.; Ensign, S. A. *Biochemistry* **1997**, *36*, 14690-14696.
(43) Kolthoff, I. M.; Elving, P. J. *Treatise on Analytical Chemistry*; Interscience Encyclopedia, Inc.: New York, 1963.
(44) Dugad, L. B.; La Mar, G. N. *Biochemistry* **1990**, *29*, 2263-2271.
(45) Banci, L.; Bertini, I.; Luchinat, C.; Piccioli, M.; Scozzafava, A.; Turano, P. *Inorg. Chem.* **1989**, *28*, 4650-4656.
(46) Fos, E.; Bosca, F.; Mauleon, D.; Carganico, G. *J. Heterocyclic Chem.* **1993**, *30*, 473-476.
(47) Sheldrick, G. M.; *SHELXS-97, Program for crystal structure solution*. University of Göttingen, Germany, 1997
(48) Sheldrick, G. M.; *SHELXL-97, Program for the refinement of crystal structures*. University of Göttingen, Germany, 1997
(49) Spek, A. L. *J. Appl. Cryst.* **2003**, *36*, 7-13.

7 | Catecholase activity of a μ-hydroxo-dicopper(II) macrocyclic complex: structures, intermediates and reaction mechanism[†]

This chapter reports the catecholase activity of the dicopper(II) complex $[Cu_2([22]py4pz)(\mu\text{-}OH)](ClO_4)_3 \cdot H_2O$ (**1**), as well as the syntheses and characterization of its reduced dicopper(I) analogue $[Cu_2([22]py4pz)](ClO_4)_2 \cdot 2CH_3OH$ (**2**) and the trans-μ-1,2-peroxo-dicopper(II) adduct **3** ([22]py4pz = (9,22-bis(2-pyridylmethyl)-1,4,9,14,17,22,27,28,29,30-decaazapentacyclo-[22.2.1.1^{4,7}.1^{11,14}.1^{17,20}]triacontane-5,7(28),11(29),12,18,20(30),24(27),25-octaene). These three compounds represent models of the three states of the catechol oxidase active site: *met*, *deoxy* (reduced) and *oxy*. The dicopper(II) complex **1** catalyzes the oxidation of catechol model substrates in aerobic conditions, while in the absence of dioxygen a stoichiometric oxidation takes place, leading to the formation of quinone and the dicopper(I) complex. The catalytic reaction follows a Michaelis-Menten behavior. The dicopper(I) complex binds dioxygen at low temperature, forming a trans-μ-1,2-peroxo-dicopper adduct, which has been characterized by UV-Vis and resonance Raman spectroscopy, and electrochemically. This peroxo complex stoichiometrically oxidizes a second molecule of catechol in the absence of dioxygen. A catalytic mechanism of catechol oxidation by **1** has been proposed, and its relevance to the mechanisms earlier proposed for the natural enzyme and other copper complexes is discussed.

[†]This chapter is based on: Koval, I. A., Belle, C., Selmeczi, K., Philouze, C., Saint-Aman, E., Schuitema, A. M., Gamez, P., Pierre, J.-L., Reedijk, J., J. Biol. Inorg. Chem., 2005, 10, 739-750

7.1 Introduction

As discussed in Chapter 1, despite the large number of model complexes reported in the literature,[1-14] the mechanism of the catechol oxidation by the natural enzyme and by the model complexes still remains far from clear. In Chapter 6, the structure of dicopper(II) complex **1** with a macrocyclic ligand [22]py4pz (Scheme 7.1) with a single hydroxo bridge between the copper centers,[15] which is fairly similar to the *met* form of the active site of catechol oxidase, has been reported. Consequently, in order to investigate catechol oxidation mechanism by **1**, its interaction with catechol model substrates in aerobic and anaerobic conditions has been examined, and the results are presented in the present chapter. The structure and the properties of the dicopper(I) complex $[Cu_2([22]py4pz)](ClO_4)_2{\cdot}2CH_3OH$ (**2**), the dioxygen binding by this complex, leading to a trans-μ-1,2-peroxo-dicopper adduct **3,** and the interaction of the latter species with phenol and catechol substrates are also discussed. Based on the results, a mechanism for the catechol oxidation by **1** is proposed, which closely resembles the earlier one proposed by Krebs and co-workers[16] for the natural enzyme, shedding a new light on the oxidation of phenol and catechol substrates by peroxo-dicopper species.

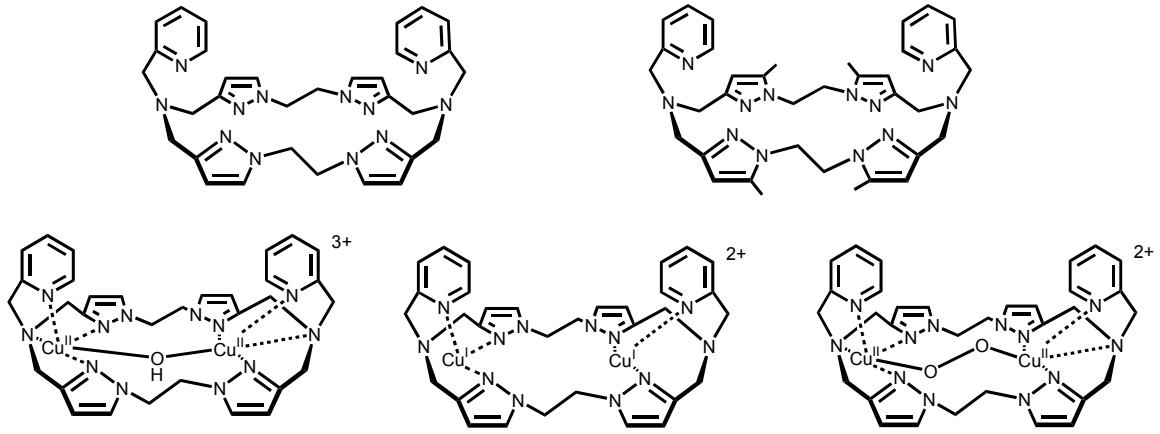

Scheme 7.1. Schematic representations of the ligand [22]py4pz (left, top), its methyl-substituted analog Me[22]py4pz (right, top),[17] the complex cation $[Cu_2([22]py4pz)(\mu\text{-}OH)]^{3+}$ ($\mathbf{1}^{3+}$, left, bottom), the complex cation $[Cu_2([22]py4pz)]^{2+}$ ($\mathbf{2}^{2+}$, middle, bottom) and trans-μ-1,2-peroxo-dicopper adduct $[Cu_2([22]py4pz)(\mu\text{-}O_2)]^{2+}$ ($\mathbf{3}^{2+}$, right, bottom).

7.2 Results and Discussion

7.2.1 Synthesis of the ligand, 1 and 2

The synthesis of the macrocyclic ligand [22]py4pz and the hydroxo-bridged dicopper(II) complex **1** are outlined in Chapter 6. The dicopper(I) complex **2** has been synthesized by reacting $Cu(CH_3CN)_4(ClO_4)$ with [22]py4pz in methanol in dry glove box atmosphere. The diffusion of diethyl ether into the colorless solution, containing two molar equivalents of $Cu(CH_3CN)_4(ClO_4)$ and one equivalent of the ligand, led to the appearance of the small colorless crystals of the product.

7.2.2 Crystal structure description

$[Cu_2([22]py4pz)(\mu\text{-}OH)](ClO_4)_3]\cdot H_2O$ (1)

The crystal structure of **1** has been described in detail in Chapter 6;[15] for clarity it will be very briefly described here. The molecular plot of the complex cation is shown in Figure 6.2 (see Chapter 6). The Cu^{II} ions are in an N_4O environment, which can be best described as distorted trigonal bipyramid ($\tau = 0.83$; $\tau = 0$ for the regular square pyramid and 1 for the regular trigonal bipyramid geometry[18]). The oxygen atom O23 of the hydroxo group bridges two copper ions, occupying the axial position in their coordination spheres and keeping them on a distance of 3.7587(11) Å. The Cu-O-Cu angle is 156.0(3)°.

$[Cu_2([22]py4pz)](ClO_4)_2\cdot 2CH_3OH$ (2)

The molecular structure of **2** is presented in Figure 7.1. Selected bond lengths and angles are given in Table 7.1.

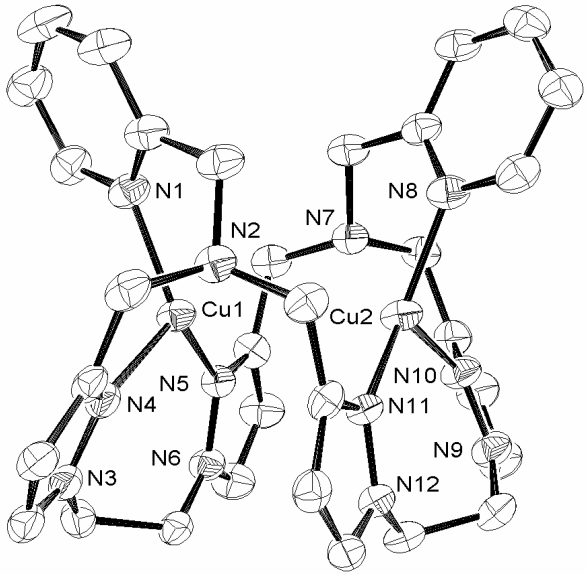

Figure 7.1. ORTEP representation of the complex cation $[Cu_2([22]py4pz)]^{2+}$. Hydrogen atoms are omitted for clarity.

The macrocyclic ligand adopts a saddle-shaped structure with a roof closed by the two pyridines. The complex cation encloses two copper(I) ions at a distance of 3.3922(7) Å, which is shorter than the intermetallic distance in **1**. The Cu1 and Cu2 cations are surrounded by the nitrogen atom of the pyridine ring (N1 and N8 respectively) at an average distance of 2.008 Å and the nitrogen atoms of two pyrazole rings (N4, N5 and N10, N11, respectively) at distances of 2.014(3) (Cu1) or 2.024(3) Å (Cu2) and 1.958(3) (Cu1) or 1.953(3) Å (Cu2), respectively. The tripodal nitrogen atoms (N2 and N7) are located at longer distances of 2.383(4) and 2.407(3) Å. The N-

Cu-N angles around both metal ions range between 76° and 143°. The coordination mode of both copper ions should thus be regarded as trigonal planar rather than tetrahedral, the two tripodal nitrogen atoms being considered as non-coordinating. However, the trigonal planar surrounding is distorted, the coordination angles deviating from the value of 120° expected for a regular trigonal planar geometry. When the oxidation state of a bound metal cation is known unambiguously, the bond valence sum calculation (BVS) can be used to confirm the coordination number.[19] In the present case the value calculated gives a BVS of 1.067 in agreement with a tricoordinated Cu^{I} ion.

Table 7.1. Selected bond lengths and bond angles for $[Cu_2([22]py4pz)](ClO_4)_2 \cdot 2CH_3OH$ (**2**)

Bond distances (Å)			
Cu1 - N1	2.008(3)	Cu2 - N10	2.024(3)
Cu1 - N4	2.014(3)	Cu2 - N11	1.953(3)
Cu1 - N5	1.958(3)	Cu2 - N8	2.008(4)
Cu1 - N2	2.383(4)	Cu2 - N7	2.407(3)
Bond angles (°)			
N1 - Cu1 - N4	112.0(1)	N8 - Cu2 - N10	111.9(1)
N1 - Cu1 - N5	129.7(1)	N8 - Cu2 - N11	130.3(1)
N4 – Cu1 – N5	107.7(1)	N10 – Cu2 – N11	108.1(1)
N5 - Cu1 - N2	143.4(1)	N8 - Cu2 - N7	76.3(1)
N1 - Cu1 - N2	76.6(1)	N10 - Cu2 - N7	77.4(1)
N4 - Cu1 - N2	76.6(1)	N11 - Cu2 - N7	141.8(1)

7.2.3 Formation of trans-*μ*-1,2-peroxo-dicopper(II) complex (3)

Upon dioxygen addition to a solution of **2** in acetonitrile at -40 °C, the UV-Vis spectra of the resulting dark purple solution display two absorption bands at 523 nm (ε = 4320 $M^{-1} \cdot cm^{-1}$) and 617 nm (ε = 2212 $M^{-1} \cdot cm^{-1}$), ascribed respectively to $\pi_\sigma^* \rightarrow$d and $\pi_v^* \rightarrow$d peroxo to Cu^{II} CT transitions,[20,21] which develop almost instantaneously (Figure 7.2, left). The resonance Raman spectrum of the final product **3** (*in situ* formed in acetonitrile) is characterized by two peaks besides the peaks from the solvent (Figure 7.2, right, curve A). The first peak at 510 cm^{-1} was assigned to a ν(Cu-O) stretching, while the second one, at 840 cm^{-1}, corresponds to an intra-peroxide ν(O-O) stretching. These UV-Vis and Raman spectroscopic characteristics are typical for trans-*μ*-1,2-peroxo-dicopper species and suggest that dioxygen is bound to both copper(II) ions in a symmetric end-on fashion,[22] similarly to the earlier reported dicopper-peroxo complex with the macrocyclic ligand Me[22]py4pz (Scheme 7.1),[17] which only differs from the ligand [22]py4pz by the presence of methyl substituents on the pyrazole rings. Numerous studies on the formation of trans-*μ*-1,2-peroxo-dicopper complexes indicate

that oxygenation of the corresponding dicopper(I) complex usually proceeds via formation of an intermediate copper(II)-superoxo Cu-$O_2^{\bullet-}$-species, characterized by an intensive absorption band at *ca.* 410 nm (ε = 3000-8000 $M^{-1}\cdot cm^{-1}$),[22] however, this species has not been observed upon dioxygen addition to **2**.

The formed trans-μ-1,2-peroxo-dicopper(II) complex **3** is stable for *ca.* 3 hours in acetonitrile solution at -40 °C, but less stable than the trans-μ-1,2-peroxo-dicopper(II) complex with Me[22]py4pz, the methyl substituents in the latter ligand apparently sterically protecting the highly reactive peroxo core. Its decomposition leads to the formation of a light-green solution, characterized by a strong absorption band at 350 nm (ε *ca.* 10000 $M^{-1}\cdot cm^{-1}$). This spectrum is consistent with the formation of the μ-hydroxo-bridged dicopper(II) complex **1**.[15,23] This species was further confirmed by ESI-MS studies (m/z 465, z = 2), corresponding to $[[Cu_2([22]py4pz)(\mu\text{-}OH)(CH_3CN)_2(H_2O)]ClO_4]^{2+}$, the isotopic distribution pattern being consistent with the theoretically expected one. As for $[Cu_2(Me[22]py4pz)(\mu\text{-}O_2)]^{2+}$, the dioxygen binding was found to be irreversible, as the absorption of the peaks at 523 and 617 nm did neither diminish upon purging the solution with argon for a few hours, nor by evaporation of the solvent under reduced pressure.

A test assaying the dihydrogen peroxide produced by the addition of an excess of trifluoroacetic acid to the oxygenated solution in acetone at -60 °C, indicated that H_2O_2 was formed in 92% yield, considering a $2Cu{:}1O_2$ stoichiometry.[24]

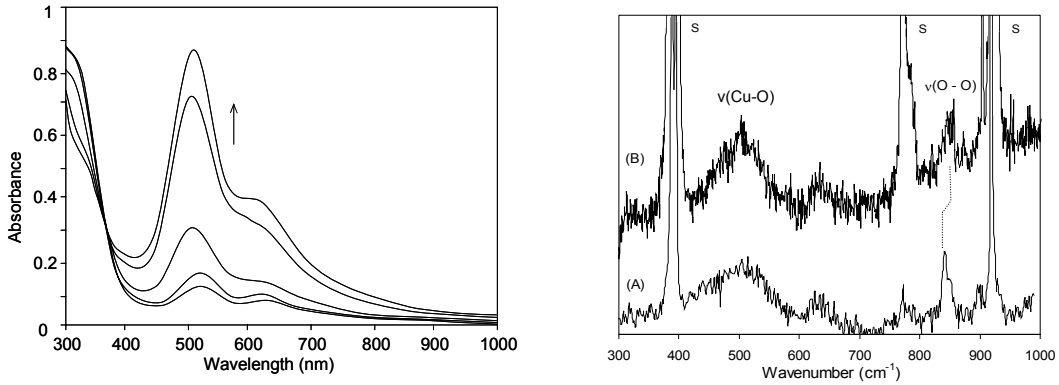

Figure 7.2. Left: changes in the UV-Vis spectrum upon bubbling dioxygen into a 2.5×10^{-4} M solution of **2** (-40 °C, CH_3CN, spectra recorded every 0.2 min). Right: resonance Raman spectrum of **3** (*in situ*, CH_3CN, curve A) and **4** (*in situ*, **3** + 1 eq. 3-FC, CH_3CN, curve B, see Section 7.2.9 for further details), excitation wavelength 514.532 nm; the peaks marked "s" originate from solvent.

7.2.4 General properties of the compounds

The magneto-chemical properties and the NMR spectra of complex **1** have been discussed in Chapter 6.[15] The compound exhibits a very strong antiferromagnetic coupling ($2J$ = -691(35) cm^{-1}) between the copper ions, leading to an EPR-silent complex in both the solid state and in a frozen acetonitrile solution. The complex was found to be moderately soluble in acetonitrile and DMSO, poorly soluble in water, and

completely insoluble in other common solvents. The UV-Vis-NIR spectrum of the complex in CH_3CN solution exhibits two absorption bands at 350 nm (ε = 7176 $M^{-1}\cdot cm^{-1}$) and at 821 nm (ε = 336 $M^{-1}\cdot cm^{-1}$). The first one corresponds to the charge transfer band from the hydroxo bridge to the copper ions, whereas the second one is assigned to the d-d transition band of the Cu^{II} ions.

Complex **2** was found to be moderately soluble in acetonitrile and methanol and very air- and moisture-sensitive. Therefore, it could only be stored in the inert atmosphere of a dry glove box. Its NMR spectrum is characterized by relatively sharp peaks at room temperature and indicates a symmetric structure of the compound in solution.

7.2.5 Acid-base properties of 1

The acid-base properties of **1** have been first studied by spectrophotometric titration of a solution of **1** in a DMSO/water mixture (1:9) with 0.01 M solutions of NaOH and $HClO_4$. A DMSO/water mixture has been used due to the very poor solubility of **1** in pure water. The ionic strength was maintained constant with a 0.01 M solution of $NaNO_3$ (aq) (sodium perchlorate could not be used, as the complex precipitates in the presence of an excess of perchlorate ions in this solvent).

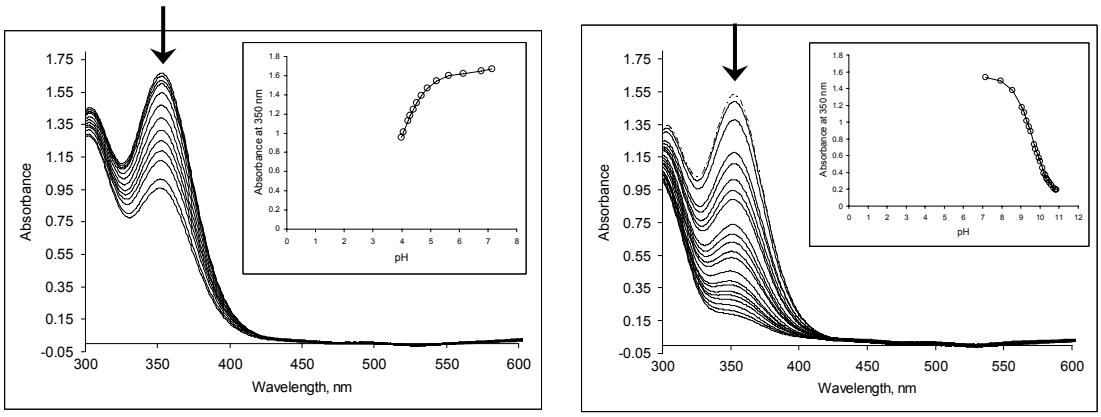

Figure 7.3. Changes in the UV-Vis spectrum of **1** upon titration with $HClO_4$ (left, pH range 7.1 – 4.0) and NaOH (right, pH range 7.1 – 10.9). The insert shows the decrease in absorption of the LMCT band at 350 nm *vs.* pH of the solution.

The titration of **1** by $HClO_4$ results in the progressive diminishing of the CT band at 350 nm till its disappearance at pH 3 (Figure 7.3, left). This process is reversible upon addition of NaOH. A plot of the absorbance *vs.* pH indicates that the protonation process has an apparent pK_1 of 4.0 (±0.05). Similarly, the titration of **1** with NaOH leads to the decrease of the CT band at 350 nm till its complete disappearance at pH 11, with an apparent pK_2 of 9.5 (±0.07) (Figure 7.3, right), and 97% of its initial absorption is restored upon addition of $HClO_4$. No isosbestic points were observed. Thus, the initial structure of **1** is preserved in a limited pH range (pH 5 – 8) and undergoes protonation or deprotonation at higher and lower pH; however, the process is reversible upon restoration of pH to neutral values. This has been further studied from an NMR titration

in a DMSO-d_6/D_2O (1:9) mixture. The NMR resonances of **1** broaden upon addition of either CF_3COOD or NaOD, and their intensity progressively decreases, without any new resonances appearing in the spectrum. The latter results suggest that at higher and lower pH, a dissociation of the hydroxo bridge takes place, leading to the decrease of the antiferromagnetic coupling between the copper(II) centers and signals broadening, and possibly with a subsequent ligand protonation at low pH values.

7.2.6 Electrochemical studies of 1, 2 and 3

The electrochemical behavior of complexes **1** and **2** and the trans-μ-1,2-peroxo adduct **3** (*in situ*) has been investigated by cyclic voltammetry (CV) and rotating disk electrode voltammetry (RDE) in acetonitrile solution, with tetra-*n*-butylammonium perchlorate (TBAP) as supporting electrolyte (0.1 M). The potentials are referred to an Ag/10 mM $AgNO_3$ + CH_3CN + 0.1 M TBAP reference electrode.

The CV curve of complex **1** is characterized by three successive electrochemical signals (Figure 7.4, left) at E_{pc} = -0.43, -0.80 and -1.20 V, respectively. Coulometric titration allows to attribute these systems to the complexed $Cu^{II,II}{}_2/Cu^{II,I}{}_2$, $Cu^{II,I}{}_2/Cu^{I,I}{}_2$ redox couples and finally to the formation of Cu^0 onto the electrode surface. The first system is quasi-reversible, whereas the second one is irreversible. As previously described,[25] OH^- bridges have a poor ability to bind Cu^I centers and tend to dissociate upon copper reduction, causing the irreversibility of the electrochemical system. These results have been confirmed by rotating disk electrode (RDE) voltammetry experiments (Figure 7.4, right) with two well-behaved cathodic waves at $E_{1/2}$ = -0.45 V and -1.20 V. The third cathodic wave at $E_{1/2}$ = -0.80 V could not be observed due to an adsorption phenomenon.

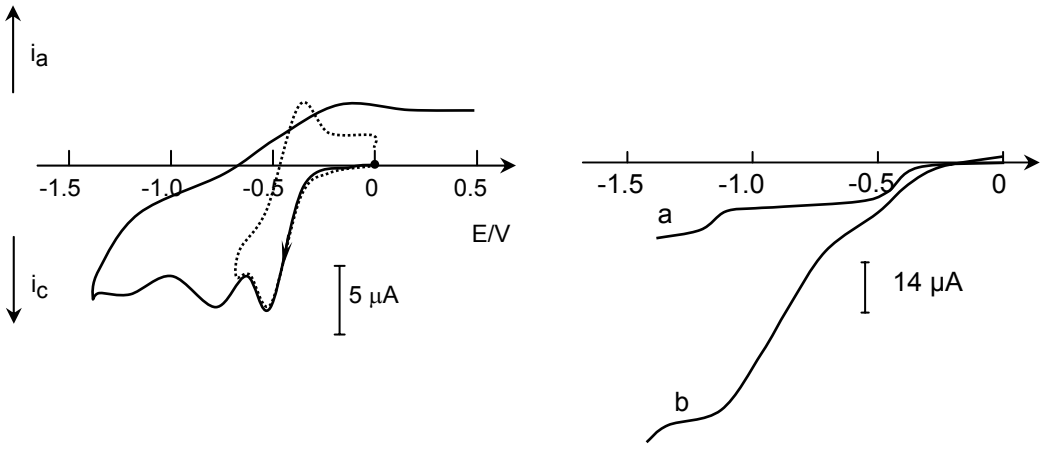

Figure 7.4. Left: CV curves recorded in a 1 mM solution of **1** in CH_3CN + 0.1 M TBAP on a Pt disc (∅ = 5 mm), v = 0.1 $V{\cdot}s^{-1}$. Right: RDE curves of **1** (curve a) and **1** in the presence of 10 molar equivalents of $DTBCH_2$ (curve b, see Section 7.2.8 for further details), N = 600 rpm; v = 0.01 $V{\cdot}s^{-1}$; V *vs.* Ag/10 mM $AgNO_3$ + CH_3CN + 0.1 M TBAP.

The anodic part of the CV curve for **2** (Figure 7.5, left) is characterized by one fully irreversible broad electrochemical signal at E_{pa} = +0.18 V, likely resulting from the overlapping of two successive oxidation waves corresponding to the complexed $Cu^{I,I}{}_2/Cu^{II,I}{}_2$ and $Cu^{II,I}{}_2/Cu^{II,II}{}_2$ redox couples. On the reverse scan, a quasi-reversible one-electron reduction peak at $E_{1/2}$ = -0.43 V is observed, which corresponds to the one-electron reduction of the complex **1**, formed upon oxidation of **2**.

The CV curve of **3** (*in situ*), recorded at -40 °C, displays one ill-behaved irreversible reduction wave at E_{pc} = -0.64 V (Figure 7.5, right, curve a). The reduction of molecular dioxygen, present in solution, is observed at -1.0 V, precluding the observation of other cathodic waves.

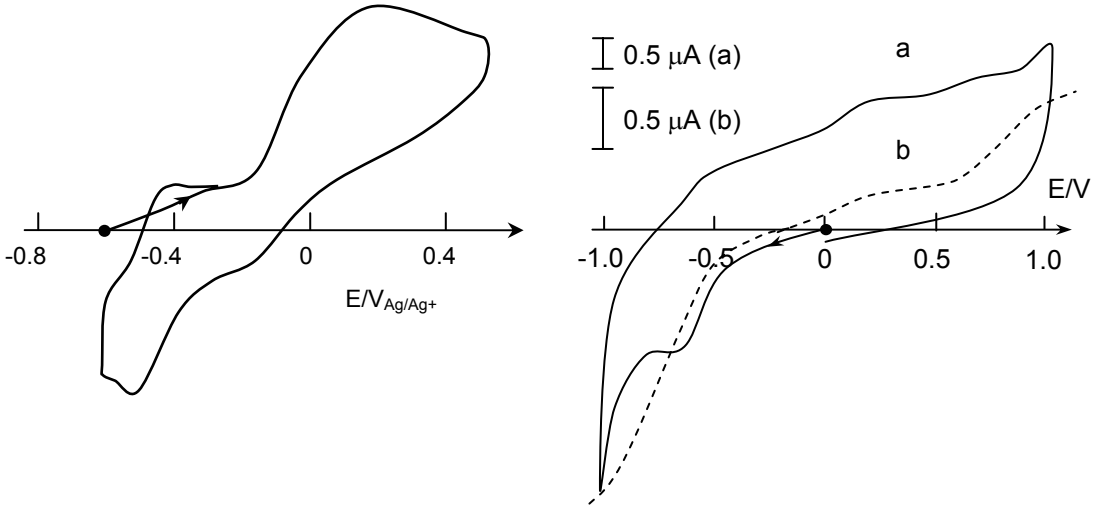

Figure 7.5. Left: CV curve recorded in a 1 mM solution of **2** in CH_3CN + 0.1 M TBAP on a Pt disc (∅ = 5 mm), v = 0.1 $V{\cdot}s^{-1}$. Right: voltammetric curve in CH_3CN + 0.1 M TBAP of the peroxo-dicopper complex **3** (*in situ*, $2.5{\times}10^{-4}$ M, CH_3CN, -40 °C). (a) CV curve 0.1 $V{\cdot}s^{-1}$ (b) (dotted line) RDE 6000 rpm. E *vs.* Ag/10 mM $AgNO_3$ + 0.1 M TBAP in CH_3CN.

Two weak irreversible electrochemical waves at E_{pa} = 0.10 V and 0.58 V are observed in the positive range of potentials. The cathodic RDE voltammogram displays one wave at $E_{1/2}$ = -0.70 V, while on the anodic part of the RDE voltammogram, two successive oxidation waves can be found (Figure 7.5, right, curve b). The first anodic wave at $E_{1/2}$ = 0.06 V is of very low intensity and may correspond to the oxidation of a by-product, likely the starting Cu^{I} complex, present in a very small amount in solution. No electrochemical properties of trans-μ-1,2-peroxo-dicopper complexes have been previously reported, although Karlin and co-workers have very recently reported the CV curves of two μ-η^2:η^2 peroxo-dicopper(II) complexes.[26] However, based on the electrochemical data earlier reported for peroxo-bridged dinuclear cobalt complexes,[27,28] the irreversible cathodic wave has been assigned to the two-electron reduction of the Cu^{II} centers, resulting in the formation of unstable dicopper(I)-peroxo species, which quickly decompose. The main anodic wave was attributed to the one-electron oxidation

of the peroxo moiety, leading to the formation of the dicopper(II)-superoxo species, which is usually observed as an intermediate in the formation of trans-μ-1,2-peroxo-dicopper complexes. The assignment is fully consistent with the height of the RDE cathodic wave being twice the height of the second RDE anodic wave.

7.2.7 Catecholase activity of 1

The catalytic activity of **1** in the oxidation of commonly used model substrate 3,5-di-*tert*-butylcatechol ($DTBCH_2$) has been studied in acetonitrile saturated in dioxygen by monitoring the development of the UV-Vis band at 400 nm, corresponding to the absorption of the produced quinone (ε = 1900 $M^{-1}\cdot cm^{-1}$). Upon treating a 0.25 mM solution of the complex with 100 equivalents of $DTBCH_2$, a turnover number of 36 has been determined after one hour. The reaction follows a Michaelis-Menten behavior. The reaction rate in acetonitrile has been determined from the slope of trace at 400 nm in the first 20 minutes of the reaction, and a Lineweaver-Burk treatment gave V_{max} = 1.3×10^{-6} $M\cdot s^{-1}$ and K_M = 4.9 mM (Figure 7.6).

The utilization of other catechols with higher oxidation potentials, such as 3-fluorocatechol (3-FC), 3-nitrocatechol and tetrachlorocatechol showed that **1** catalyzes the oxidation of 3-FC, but fails to oxidize the latter two substrates. The catalytic reaction in the case of 3-FC proceeds, however, very slowly (*e.g.* one equivalent of quinone was formed after 20 min of reaction), which makes a more detailed kinetic analysis dispensable.

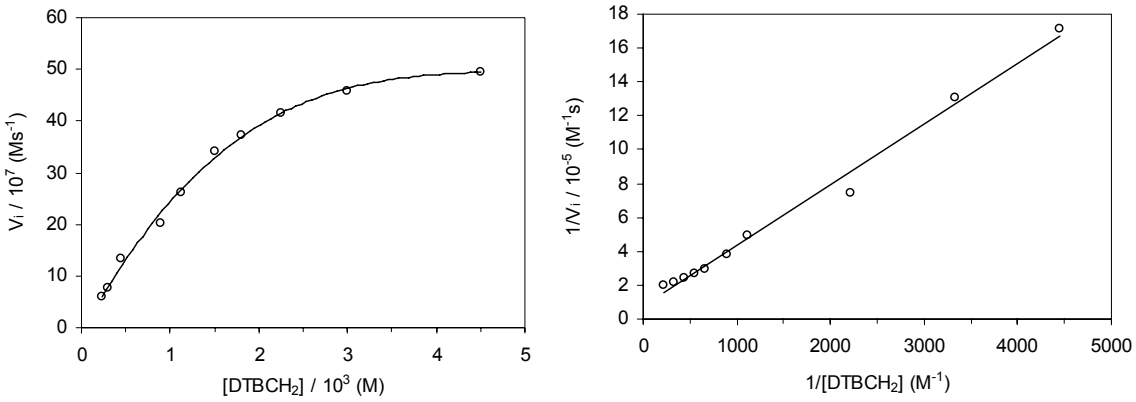

Figure 7.6. Plot of the initial reaction rates determined from the slope of trace at 400 nm in the first 20 minutes *vs.* substrate concentration, indicating substrate saturation behavior (left), and reciprocal Lineweaver-Burk plot (right).

7.2.8 Interaction of 1 with catechol substrates in anaerobic conditions

As shown previously by Krebs and co-workers,[29] the natural *met* form of catechol oxidase reacts with one equivalent of catechol stoichiometrically in anaerobic conditions, producing one equivalent of the corresponding quinone. A stoichiometric

oxidation of catechol has also been proposed or observed as a first step in the catalytic oxidation of catechols by copper(II) complexes.[6,12,30-32] Therefore the interaction of **1** with two model substrates, $DTBCH_2$ and 3-FC, has been investigated. The interaction of **1** with $DTBCH_2$ was evaluated by means of UV-Vis spectroscopy and electrochemically and its interaction with 3-FC from ^{19}F NMR spectroscopy experiments.

Upon addition of $DTBCH_2$ to 0.25 mM solution of **1** in acetonitrile under anaerobic conditions, one equivalent of the corresponding quinone is produced in a fast stoichiometric reaction along with the reduced species **2** (Figure 7.7). This can be evidenced from the disappearance of the CT band at 350 nm and the d-d band of the Cu^{II} ions, and the appearance of a new band at 400 nm, characteristic of the formed quinone. Two isosbestic points at 398 and 600 nm indicate the presence of two absorbing species in solution. As the reaction proceeds too fast to obtain the reliable values of the initial reaction rates, no detailed kinetic analysis could be performed. It is however obvious that the rates increase with the increase in the substrate concentration. The formation of DTBQ upon anaerobic interaction of **1** with $DTBCH_2$ has also been confirmed electrochemically. The addition of an excess of $DTBCH_2$ to a solution of **1** in acetonitrile leads to the development of a new RDE wave at $E_{1/2}$ = -0.88 V, corresponding to the two-electron reduction of the formed DTBQ (Figure 7.4, right, curve b).

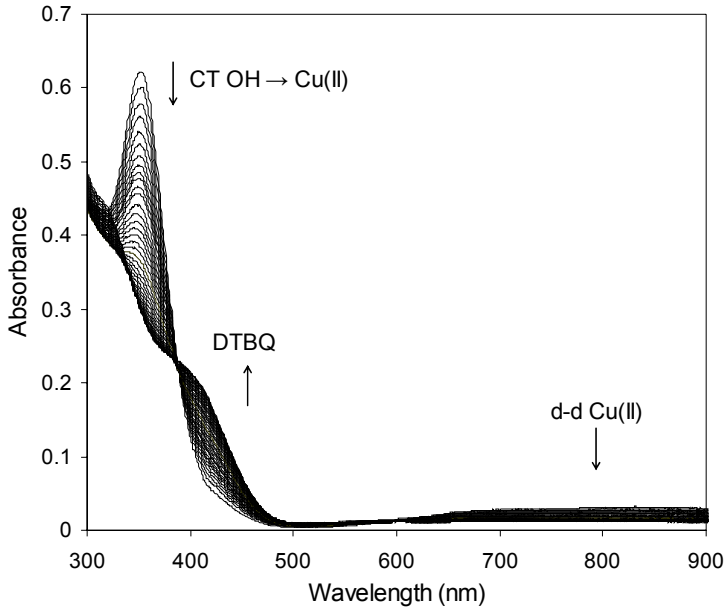

Figure 7.7. Changes in the UV-Vis spectra of **1** (CH_3CN, 2.5×10^{-4} M, dry glove box) upon addition of 3 molar equivalents of $DTBCH_2$ (spectra recorded every 5 seconds, l = 0.5 cm).

The anaerobic interaction of **1** with 3-FC, followed by UV-Vis spectroscopy, also revealed the formation of a very small amount of *o*-quinone. It appears to be much more difficult to oxidize 3-FC, which is in agreement with its higher oxidation potential in comparison with $DTBCH_2$. In fact, even in the presence of a large excess (60 molar

equivalents) of 3-FC, less than one equivalent of quinone was produced. The most direct proof of the quinone formation was obtained by means of ^{19}F NMR spectroscopy. Pure 3-FC exhibits one peak at 26.28 ppm in the ^{19}F NMR spectrum and the gradual addition of 3-FC to a solution of **1** in anaerobic conditions gives rise to a single new peak at 40.14 ppm, corresponding to the 3-fluoroquinone. The intensity of this peak was found to increase significantly in time upon addition of dioxygen, with a concomitant diminution of the original 3-FC peak. It has to be mentioned that no other peaks due to potential reaction intermediates, could be detected in the spectrum.

7.2.9 Interaction of 3 with catechol and phenolic substrates

Relatively few examples of the interaction of peroxo-dicopper(II) species with catechol substrates are described in the literature. Kitajima *et al.* reported the oxidative C-C coupling of $DTBCH_2$ by a μ-η^2:η^2 peroxo complex, resulting in the formation of diphenoquinones.[33] Interestingly, no formation of *o*-benzoquinone was observed, unless exogenous dioxygen was introduced into the reaction mixture. Casella and co-workers reported a stoichiometric oxidation of $DTBCH_2$ to DTBQ by a μ-η^2:η^2 peroxo-dicopper complex.[34] The same type of reactivity was observed by Stack and co-workers for a bis-μ-oxo-dicopper core.[35] The oxidation of $DTBCH_2$ by μ-η^2:η^2-peroxo and bis-μ-oxo-dicopper complexes was also reported by Tolman and co-workers[36] with isolation of mononuclear copper(II)-semiquinonate complexes as a sole product of the reaction, the (per)oxo-dicopper species being generated by reaction of two essentially mononuclear Cu^I molecules with dioxygen. Rockcliffe and Martell also reported a number of examples of the stoichiometric oxidation of catechols to the respective quinones or dicarboxylic acids involving various dicopper-dioxygen complexes.[31,37-39] Unfortunately, these authors did not provide detailed information concerning the structure of the peroxo species. Although the end-on dioxygen-binding mode was proposed based on the results of molecular modeling,[40] the UV-Vis spectroscopic data,[38,40] reported by the authors, as well as the overall reactivity of the described peroxo species[39,41] suggest that dioxygen is bound in the μ-η^2:η^2 mode. However, the oxidation of catechols by end-on peroxo-dicopper complexes has not been reported before, although the deprotonation of tetrachlorocatechol upon reaction with end-on trans-μ-1,2-peroxo-dicopper species has been evidenced by Comba and co-workers.[5,42]

The anaerobic interaction of **3** (*in situ*) with catechol has been studied spectrophotometrically at -40 °C in acetonitrile solution. The changes in the UV-Vis spectrum upon addition of one equivalent of catechol to a 0.25 mM solution of **3** are shown in Figure 7.8 (left). The disappearance of the peaks at 523 nm and 617 nm along with the development of the absorbance at 400 nm corresponds to the stoichiometric oxidation of the catechol substrate by **3**, leading to DTBQ (dotted line, Figure 7.8, left). The bubbling of dioxygen through the solution after completion of the reaction resulted in only a slight increase of the absorptions at 523 nm and 617 nm, indicating that the

trans-μ-1,2-peroxo core could not be restored. This suggests that the copper(II) ions are not reduced upon interaction with the substrate; thus, the oxidation of the substrate is likely to be performed by the peroxo moiety. Upon addition of an excess of $DTBCH_2$ to **3** in the presence of dioxygen, a catalytic oxidation of catechol takes place.

The mechanism of the catechol oxidation by **3** is of interest. Taking into account the basic nature of the end-on peroxo moiety, it can be proposed that in the first place the catechol acts as an acid toward **3**. This assumption is also supported by the earlier reports on the observed deprotonation of catechols and phenols after reaction with trans-μ-1,2-peroxo-dicopper cores.[5,42] Therefore the interaction of **3** with the deuterated analogue of $DTBCH_2$, in which the protons of the phenol groups are substituted with deuterium ($DTBCD_2$), has been studied. As can be seen from Figure 7.8 (left), the oxidation process clearly proceeds in two steps. First, the characteristic absorbencies of the peroxo-dicopper(II) species at 523 nm and 617 nm gradually disappears along with the appearance of the new peak at 342 nm. The isosbestic point at 440 nm indicates the presence of two species in solution. Second, the peak at 400 nm develops, indicating the formation of one equivalent of the quinone. The apparent reaction rate constant of the first process k^1_{obs} is 0.04 s^{-1} for $DTBCD_2$, whereas for non-deuterated $DTBCH_2$ the reaction is too fast to allow the determination of the reaction rate constant. For the second process, the reaction rate constant k^2_{obs} of 0.11 s^{-1} could be determined for both non-deuterated and deuterated substrate. Thus, on the second step of the reaction, no kinetic isotopic effect is observed, whereas a proton is obviously transferred on the first step. It can thus be proposed that initially the protonation of the peroxo core occurs along with the binding of the deprotonated substrate to the metal center, resulting in the formation of a ternary complex of a formal composition [Cu_2([22]py4pz)(O-O-H)-substrate]. The second step involves the oxidation of the bound catecholate by the peroxide moiety, which is thus independent on the proton/deuterium exchange. The interaction of **3** with the less reactive 3-fluorocatechol, the utilization of which stabilizes the formed hydroperoxo-dicopper(II)-substrate intermediate (**4**), has also been studied. The product **4**, formed upon treatment of **3** with one molar equivalent of 3-FC in acetonitrile, is characterized by the peak at 342 nm (ε =3960 $M^{-1}\cdot cm^{-1}$) in the UV-Vis spectrum and remains stable for at least 15 minutes at -40 °C. Its resonance Raman spectrum is characterized by the peak at 851 cm^{-1}, corresponding to a ν(O-O) stretching (Figure 7.2, right, curve B). The protonation thus increases the frequency of the O-O stretching in comparison to the original peroxo-dicopper(II) complex **3**, similarly to earlier reported results by Solomon *et al.*[43] The UV-Vis and resonance Raman spectroscopic characteristics of **4** are very close to the values earlier reported for other μ-1,1-hydroperoxo-copper(II) complexes;[44] furthermore, similarly to such complexes,[45] species **4** is EPR-silent. Thus, based on the spectroscopic data, the formation of μ-1,1-hydroperoxo-dicopper(II) intermediate upon reaction of **3** with catechol can be tentatively suggested. It should be noted that the formation of a hydroperoxo

intermediate has also been evidenced by Karlin *et al.*[24] in the reaction of trans-μ-1,2-peroxo-dicopper complexes with 2,4-di-*tert*-butylphenol.

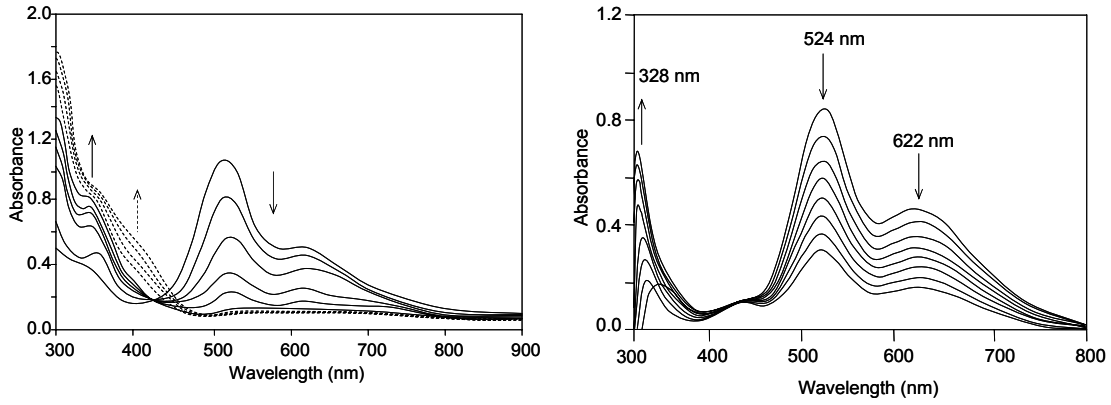

Figure 7.8. Left: changes in the UV-Vis spectrum upon addition of one equivalent of $DTBCD_2$ to a solution of **3** in anaerobic conditions (*in situ*, CH_3CN, 2.5×10^{-4} M, -40 °C). Solid lines: the spectra recorded each 0.2 min after $DTBCD_2$ addition to **3**. The dotted lines correspond to the gradual formation of one equivalent of DTBQ. For clarity, only the spectra recorded after 3.0, 6.0, 11.0 and 16.0 minutes are shown. Right: changes in the UV-Vis spectrum of **3** upon addition of one equivalent of sodium 4-carbomethoxyphenolate (2.5×10^{-4} M, acetone, -60 °C).

The interaction of **3** with sodium 4-carbomethoxyphenolate (a commonly used phenolic substrate) does not result in the hydroxylation of the aromatic ring (monophenolase activity). Earlier, Karlin and co-workers have pointed out the differences in reactivities between trans-μ-1,2-peroxo and μ-η^2:η^2 peroxo complexes.[24] While the former complexes are basic/nucleophlic in nature, the latter complexes display electrophilic properties. Recently, an electrophilic aromatic substitution mechanism has been proposed for the hydroxylation of phenols to the respective catechols by μ-η^2:η^2 peroxo complexes.[46] It includes a rate-determining electrophilic attack of the μ-η^2:η^2 peroxo core, while the oxygenation of the substrate (C-O bond formation) happens simultaneously with the O-O bond cleavage of the peroxo intermediate. Thus, the inability of **3** to hydroxylate a phenol substrate agrees with its nucleophilic character and is consistent with the earlier proposed mechanism of the phenolase activity of peroxo-dicopper complexes. The binding of the phenolate to the metal centers could, however, be confirmed, as the peroxo absorptions in the UV-Vis spectrum decreased with the addition of phenolate (Figure 7.8, right) and could not be restored upon purging the reaction mixture with pure dioxygen. At the same time, the peak at 328 nm gradually develops in the spectrum, which probably corresponds to the CT band from the coordinated phenolate to the copper(II) ions, as it is consistent with the spectroscopic characteristics observed for the reaction of dicopper(II) complexes with kojic acid,[47] and for copper(I)-phenolate adducts.[48]

7.2.10 Mechanistic considerations

On the basis of the results described above, a mechanism for the catechol oxidation by **1**, as depicted in Figure 7.9, can be proposed.

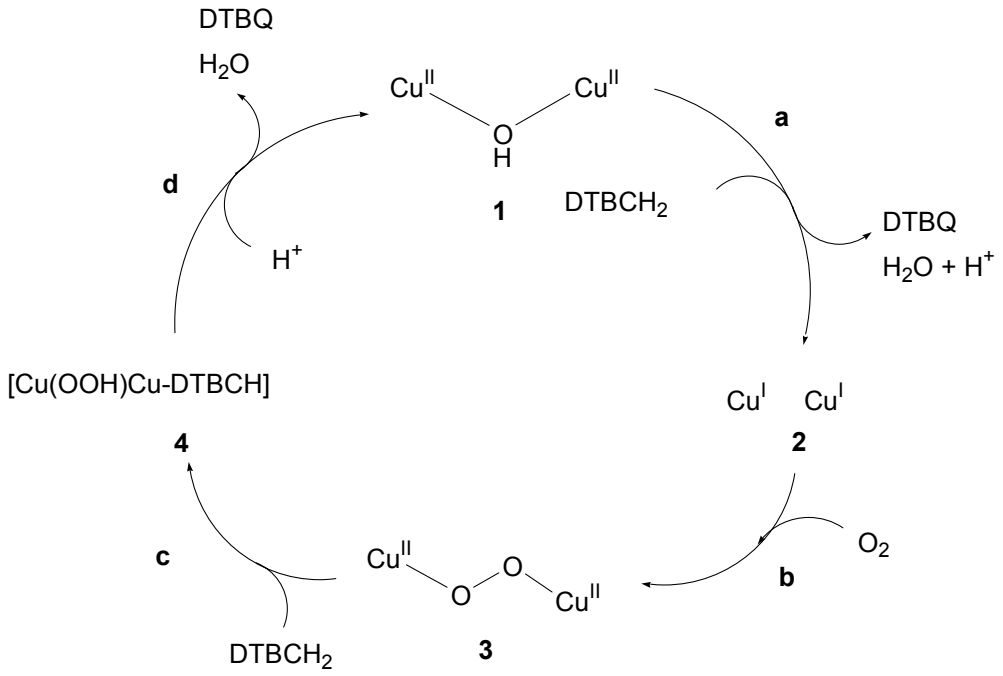

Figure 7.9. Proposed mechanism for the oxidation of 3,5-di-*tert*-butylcatechol by **1**. The complexes **1** and **2** are characterized crystallographically, the peroxo-dicopper(II) intermediate **3** is characterized by UV-Vis and resonance Raman spectroscopy.

In the first stage of the reaction, a stoichiometric oxidation of catechol by **1** takes place (step **a**, Figure 7.9). This step does not require the presence of dioxygen. At the second stage, the dicopper(I) complex **2**, which is formed upon $DTBCH_2$ oxidation by **1**, reacts with dioxygen to form the trans-μ-1,2-peroxo-dicopper(II) species **3** (step **b**). This species oxidizes a second equivalent of catechol in stoichiometric reaction through a two-electron transfer from the catechol to the peroxide moiety. The reaction proceeds in two steps: the proton transfer from the substrate to the nucleophilic peroxo core (step **c**), and the oxidation of the bound catecholate (step **d**). As suggested earlier by Casella *et al.*,[47] the steps **b**-**d** appear to determine the overall catalytic efficiency of **1**, as step **a** is too fast to be considered as a rate-determining step. After the quinone molecule is released, the complex **1** is regenerated, and the catalytic cycle can continue, as shown in Figure 7.9. Two equivalents of quinone are thus generated per one catalytic cycle. This mechanism is in fact very similar to the mechanisms earlier proposed by Rockcliffe *et al.*[31] and Casella and co-workers[49] for dinuclear Cu^{II} complexes, and by Krebs and co-workers for catechol oxidase.[29,50] Two major differences between the present mechanism and those earlier described should though be pointed out. The first one is the structure of the peroxo-dicopper intermediate. Whereas the formation of a μ-η^2:η^2 peroxo-dicopper intermediate was shown for catechol oxidase,[50,51] Casella and co-workers reported the

formation of either μ-η^2:η^2 peroxo or μ-oxo-dicopper species upon reaction of dicopper(I) species with dioxygen, dependent on the ligand structure.[6,34] In the present case, however, dioxygen is clearly bound in a trans-μ-1,2 fashion. The second difference concerns the actual mechanism of catechol oxidation by peroxo-dicopper species. Whereas Krebs and co-workers have proposed the simultaneous binding of dioxygen and the substrate to the deoxy form of catechol oxidase prior to the quinone formation,[29,50] a two-step oxidation mechanism of the substrate by the formed peroxo-dicopper(II) core with the formation of the hydroperoxo-dicopper intermediate takes place in the present case.

In conclusion, a mechanism for the catechol oxidation by the dicopper(II) complex bearing a hydroxide bridge between the metal ions is proposed, with the adequate characterization of the reduced dicopper(I) complex and dicopper(II)-dioxygen adduct. The proposed mechanism closely resembles the earlier mechanism published by Krebs and co-workers of catechol oxidation by the natural enzyme, although the binding mode of the substrate to the dicopper centers unfortunately remains unclear.[29] It should be noted that in this chapter the first example of catechol oxidation by a trans-μ-1,2-peroxo-dicopper species is reported. Remarkably, this species is able to oxidize catechols (catecholase activity), but is not able to perform the hydroxylation of the *o*-position of phenols (tyrosinase activity). Although the formation of μ-η^2:η^2 peroxo species has been evidenced by the treatment of catechol oxidase (*met* form) isolated from *Lycopus europaeus* and *Populus nigra* with H_2O_2, and trans-μ-1,2-peroxo intermediates have never been observed in the natural systems, it is interesting to note that the difference in behavior towards phenol and catechol substrates can in fact be dependent on the structure of the copper-dioxygen adduct. Furthermore, Karlin and co-workers have reported a very rapid conversion of a trans-μ-1,2-peroxo-dicopper intermediate into a μ-η^2:η^2 final species, and suggested that the "end-on" species may initially form upon dioxygen binding by the type-3 copper proteins, due to the long distance between the metal ions in the reduced dicopper(I) core, which may rapidly interconvert into "side-on" species.[52] It is thus fascinating to notice the possible existence of end-on peroxo-dicopper moieties in living systems and the possibility that the reactivity towards different substrates can be tuned by the type of dicopper-dioxygen adduct. Although these assumptions are largely speculative in natural enzymes, future studies on dicopper-dioxygen model systems and their reactivity would be very beneficial in order to shed light on the interpretation of the mechanisms of monophenolase and diphenolase activity by type-3 copper proteins.

7.3 Experimental Section

7.3.1 Materials and Methods

All starting materials were commercially available and used as purchased, unless stated otherwise. The macrocyclic ligand [22]py4pz and [Cu_2([22]py4pz)(μ-

OH)]$(ClO_4)_3 \cdot H_2O$ (**1**) were synthesized as previously described [15,53] (see also Chapter 6). The ligand field spectra in solution were recorded on a Varian Cary 50 Scan UV-Vis spectrophotometer (l = 1 cm), and on a Zeiss MCS500 Diode-Array Spectrometer (l = 0.5 cm). X-band electron paramagnetic resonance (EPR) measurements were performed at 100 K on 1 mM frozen solutions in acetonitrile on a Bruker ESP 300E spectrometer operating at 9.4 GHz (X-band). Resonance Raman spectra were recorded on a Dilor XY multichanel spectrometer. The sample was kept in acetonitrile at -70 °C. As excitation source a coherent Ar laser (514.532 nm) was used. The spectra were run with a laser power of 30 mW and an acquisition time of 2×1800 s. ^1H and ^{19}F NMR spectra were recorded on a Bruker Avance 300 spectrometer at 25 °C. Chemical shifts were referenced to CD_3CN as internal reference and to C_6F_6 as external reference, respectively. The deprotonation constants of **1** were determined spectrophotometrically at 25 °C in a 2.5×10^{-4} M solution in a DMSO:H_2O mixture (1:9), monitoring the UV-vis band at 350 nm, and using the method of Schwarzenbach.[54] The ionic strength was maintained constant with a 0.01 M solution of $NaNO_3$. The electrochemical behavior of the complexes was investigated in a 0.1 M solution of tetra-*n*-butylammonium perchlorate (TBAP) in acetonitrile using a EGG 273 potentionstat coupled with a Kipp&Zonen x-y recorder. The experiments were performed at room temperature in a three-compartment cell. Potentials are referred to an Ag/10 mM $AgNO_3$ + CH_3CN + 0.1 M TBAP reference electrode. The working electrode was a platinum disk of 5 mm diameter for the cyclic voltammetry (CV, 0.1 $V \cdot s^{-1}$) experiments or 3 mm diameter for the rotating disk electrode (RDE, 600 rpm) voltammetry experiments. The working electrode was polished with 1 μm diamond paste prior to each recording.

7.3.2 Syntheses of coordination compounds

$[Cu_2([22]py4pz)](ClO4)_2 \cdot 2CH_3OH$ (2): In a glove box, a solution of $[Cu(CH_3CN)_4]ClO_4$ (65 mg, 0.20 mmol) in 2 ml of dry methanol was added to a suspension of [22]py4pz (58 mg, 0.10 mmol) in the same solvent. The diffusion of diethyl ether into the resulting solution led to the appearance of small pale yellow crystals, suitable for X-ray diffraction analysis. They were found to be very sensitive to air and moisture and could be stored only in an inert atmosphere. ^1H-NMR (CD_3CN, 300 MHz, ppm): 8.57 (d, 2H, 6'H-py, J = 5.1 Hz), 7.86 (td, 2H, 4'H-py, J = 7.7 Hz, J = 1.7 Hz), 7.45 (s, 4H, 5'H-pz, broad), 7.39 (m, 8H, 3'H-py +5'H-py), 6.14 (s, 4H, 4'H-pz, broad), 4.61 (s, 8H, pz-CH_2-CH_2-pz, broad), 3.79 (s, 4H, N-CH_2-py, broad), 3.66 (s, 8H, N-CH_2-pz, broad). ESI-MS, *m/z*: z = 2, $[Cu_2([22]py4pz)]^{2+}$ = 358.

Trans-μ-1,2-peroxo-dicopper complex 3 derived from 2: Trans-μ-1,2-peroxo-dicopper complex **3** was prepared *in situ* upon bubbling dioxygen into a preliminary cooled to -40 °C 2.5×10^{-4} M solution of $[Cu_2([22]py4pz)](ClO_4)_2$ (**2**) in acetonitrile. UV-Vis (CH_3CN): λ/nm (ε/$M^{-1} \cdot cm^{-1}$): 523 (4320), 617 (2212). Resonance Raman (CH_3CN, -70 °C): 840 cm^{-1} (O-O stretching), 510 cm^{-1} (Cu-O stretching).

7.3.3 Catecholase activity studies

The catecholase activity of **1** was evaluated by reaction with 3,5-di-*tert*-butylcatechol ($DTBCH_2$) at 25 ºC. The absorption at 400 nm, characteristic of the formed quinone, 3,5-di-*tert*-butyl-*o*-benzoquinone (DTBQ), was measured as a function of time. The experiments were run in acetonitrile saturated with dioxygen. The kinetic parameters were determined for 4.5×10^{-5} M solutions of the complex and 0.225–4.5 mM solutions of the substrate. In a typical catalytic experiment, 3 ml of a solution of **1** were placed in a 1 cm path-length cell, and the solution was saturated with dioxygen. Afterwards 75 µl of the substrate solution were added. After thorough stirring, the changes in UV-Vis spectra were recorded during 30 min.

The interaction of **3** with $DTBCH_2$, spectrophotometrically monitored, was carried out under argon at -40 °C in acetonitrile by adding 25 µl of a 0.4 M solution of $DTBCH_2$ (10 µmol) to 40 ml of a 2.5×10^{-4} M solution of **3** (10 µmol), prepared *in situ*. The phenol oxidation experiments (tyrosinase activity) were carried out by adding a solution of sodium 4-carbomethoxyphenolate (two or more equivalents) in dry acetone to a cooled to -60 ˚C solution of either **3** or **2** (0.1-0.3 mM, both compounds prepared *in situ*), in dry dichloromethane, acetone or acetonitrile.[47,48,55] Dioxygen bubbling through the solution was continued (in case of **2**, dioxygen was introduced into the solution immediately after the substrate was added), and the reaction mixture was stirred at low temperature in dioxygen-saturated atmosphere. After at least four hours a sample (1 ml) was withdrawn from the reaction mixture and immediately quenched with H_2SO_4. After evaporation of the solvent, 1 ml of H_2O was added, and the resulting solution was analyzed by HPLC, using a Supelco LC18 semipreparative column (250×10 mm). Elution was carried out at 5 ml·min^{-1} starting with water containing 0.1% trifluoroacetic acid for 4 min, followed by a linear gradient from 0% to 100% acetonitrile containing 0.1% trifluoroacetic acid during 20 min. Spectrophotometric detection of the HPLC elution profile in the range 200-650 nm was performed with a Jasco MD-1510 diode array instrument.[56]

7.3.4 X-ray Crystallographic Measurements

The crystal of **2** was mounted on a Enraf-Nonius Kappa CCD diffractometer using a graphite monochromator (λ (Mo K_α): 0.71073 Å). The structure was solved by direct methods and refined using the TEXSAN software.[57] Empirical formula: $[Cu_2C_{32}H_{37}N_{12}]\cdot(ClO_4)_2\cdot(CH_3OH)_2$, Fw = 978.79, colorless block (0.25 mm×0.20 mm×0.18 mm), monoclinic, space group *P21/n*, a = 13.416(4) Å, b = 20.491(20) Å, c = 15.013(5) Å, $\alpha = \gamma = 90°$, β = 98.48(4)°, V = 4082(4) Å^3, Z = 4, $\rho_{calc.}$ = 1.593 g·cm^{-3}, μ = 1.244 mm^{-1}. A total of 52771 reflections, of which 11173 were independent [R(int) = 0.07176], were collected in the range $3 \leq 2\theta \leq 30°$. All non-hydrogen atoms were refined with anisotropic thermal parameters. Hydrogen atoms were generated in

idealized positions, riding on the carrier atoms, with isotropic thermal parameters. Final cycle refinement converged to $R(F) = 0.0675$ and $wR2 = 0.10965$.

Crystallographic data (without structure factors) for the structure of **2** have been deposited with the Cambridge Crystallographic Data Centre as supplementary publication no. CCDC-269469. Copies of the data can be obtained free of charge from the CCDC (12 Union Road, Cambridge CB2 1EZ, UK; tel: (+44) 1223-336-408; fax: (+44) 1223-336-003; e-mail: deposit@ccdc.cam.ac.uk).

7.4 References

(1) Selmeczi, K.; Reglier, M.; Speier, G.; Peintler, G. *React. Kinet. Catal. Lett.* **2004**, *81*, 143-151.
(2) Selmeczi, K.; Reglier, M.; Giorgi, M.; Speier, G. *Coord. Chem. Rev.* **2003**, *245*, 191-201.
(3) Gao, J.; Reibenspies, J. H.; Martell, A. E. *Inorg. Chim. Acta* **2003**, *346*, 67-75.
(4) Ackermann, J.; Meyer, F.; Kaifer, E.; Pritzkow, H. *Chem. Eur. J.* **2002**, *8*, 247-258.
(5) Börzel, H.; Comba, P.; Pritzkow, H. *Chem. Commun.* **2001**, 97-98.
(6) Granata, A.; Monzani, E.; Casella, L. *J. Biol. Inorg. Chem.* **2004**, *9*, 903-913.
(7) Louloudi, M.; Mitopoulou, K.; Evaggelou, E.; Deligiannakis, Y.; Hadjiliadis, N. *J. Mol. Cat. A* **2003**, *198*, 231-240.
(8) Merkel, M.; Möller, N.; Piacenza, M.; Grimme, S.; Rompel, A.; Krebs, B. *Chem. Eur. J.* **2005**, *11*, 1201-1209.
(9) Mukherjee, J.; Mukherjee, R. *Inorg. Chim. Acta* **2002**, *337*, 429-438.
(10) Monzani, E.; Battaini, G.; Perotti, A.; Casella, L.; Gullotti, M.; Santagostini, L.; Nardin, G.; Randaccio, L.; Geremia, S.; Zanello, P.; Opromolla, G. *Inorg. Chem.* **1999**, *38*, 5359-5369.
(11) Monzani, E.; Quinti, L.; Perotti, A.; Casella, L.; Gulotti, M.; Randaccio, L.; Geremia, S.; Nardin, G.; Faleschini, P.; Tabbi, G. *Inorg. Chem.* **1998**, *37*, 553-562.
(12) Than, R.; Feldmann, A. A.; Krebs, B. *Coord. Chem. Rev.* **1999**, *182*, 211-241.
(13) Torelli, S.; Belle, C.; Gautier-Luneau, I.; Pierre, J. L.; Saint-Aman, E.; Latour, J. M.; Le Pape, L.; Luneau, D. *Inorg. Chem.* **2000**, *39*, 3526-3536.
(14) Torelli, S.; Belle, C.; Hamman, S.; Pierre, J. L.; Saint-Aman, E. *Inorg. Chem.* **2002**, *41*, 3983-3989.
(15) Koval, I. A.; van der Schilden, K.; Schuitema, A. M.; Gamez, P.; Belle, C.; Pierre, J.-L.; Luken, M.; Krebs, B.; Roubeau, O.; Reedijk, J. *Inorg. Chem.* **2005**, *44*, 4372-4382.
(16) Gerdemann, C.; Eicken, C.; Krebs, B. *Acc. Chem. Res.* **2002**, *35*, 183-191.
(17) Bol, J. E.; Driessen, W. L.; Ho, R. Y. N.; Maase, B.; Que, L.; Reedijk, J. *Angew. Chem. Int. Ed. Engl.* **1997**, *36*, 998-1000.
(18) Addison, A. W.; Rao, T. N.; Reedijk, J.; van Rijn, J.; Verschoor, G. C. *J. Chem. Soc., Dalton Trans.* **1984**, 1349-1356.
(19) Liu, W.; Thorp, H. H. *Inorg. Chem.* **1993**, *32*, 4102-4105.
(20) Baldwin, M. J.; Ross, P. K.; Pate, J. E.; Tyeklár, Z.; Karlin, K. D.; Solomon, E. I. *J. Am. Chem. Soc.* **1991**, *113*, 8671-8679.
(21) Solomon, E. I.; Tuczek, F.; Root, D. E.; Brown, C. A. *Chem. Rev.* **1994**, *94*, 827-856.
(22) Mirica, L. M.; Ottenwaelder, X.; Stack, T. D. P. *Chem. Rev.* **2004**, *104*, 1013-1045.
(23) Gamez, P.; Koval, I. A.; Reedijk, J. *Dalton Trans.* **2004**, 4079-4088.
(24) Paul, P. P.; Tyeklár, Z.; Jacobson, R. R.; Karlin, K. D. *J. Am. Chem. Soc.* **1991**, *113*, 5322-5332.
(25) Reim, J.; Krebs, B. *J. Chem. Soc., Dalton Trans.* **1997**, 3793-3804.
(26) Shearer, J.; Zhang, C. X.; Zakharov, L. N.; Rheingold, A. L.; Karlin, K. D. *J. Am. Chem. Soc.* **2005**, *127*, 5469-5483.
(27) Ghiladi, M.; Gomez, J. T.; Hazell, A.; Lumtscher, J.; McKenzie, C. J. *Dalton Trans.* **2003**, 1320-1325.
(28) Harris, W. R.; McLendon, G. L.; Martell, A. E.; Bess, R. C.; Mason, M. *Inorg. Chem.* **1980**, *19*, 21-26.
(29) Eicken, C.; Krebs, B.; Sacchettini, J. C. *Curr. Opin. Struct. Biol.* **1999**, *9*, 677-683.
(30) Gupta, M.; Mathur, P.; Butcher, R. J. *Inorg. Chem.* **2001**, *40*, 878-885.
(31) Rockcliffe, D. A.; Martell, A. E. *J. Mol. Catal. A* **1995**, *99*, 101-114.
(32) Chyn, J.-P.; Urbach, F. L. *Inorg. Chim. Acta* **1991**, *189*, 157-163.
(33) Kitajima, N.; Koda, T.; Iwata, Y.; Moro-oka, Y. *J. Am. Chem. Soc.* **1990**, *112*, 8833-8839.
(34) Santagostini, L.; Gulotti, M.; Monzani, E.; Casella, L.; Dillinger, R.; Tuczek, F. *Chem. Eur. J.* **2000**, *6*, 519-522.

(35) Mahadevan, V.; Dubois, L.; Hedman, B.; Hodgson, K. O.; Stack, T. D. *J. Am. Chem. Soc.* **1999**, *121*, 5583-5584.
(36) Berreau, L. M.; Mahapatra, S.; Halfen, J. A.; Houser, R. P.; Young, V. G.; Tolman, W. B. *Angew. Chem. Int. Ed. Engl.* **1999**, *38*, 207-210.
(37) Rockcliffe, D. A.; Martell, A. E. *J. Chem. Soc., Chem. Commun.* **1992**, 1758-1760.
(38) Rockcliffe, D. A.; Martell, A. E.; Reibenspies, J. H. *J. Chem. Soc., Dalton Trans.* **1996**, 167-175.
(39) Rockcliffe, D. A.; Martell, A. E. *J. Mol. Cat. A* **1996**, *106*, 211-221.
(40) Rockcliffe, D. A.; Martell, A. E. *J. Mol. Catal. A* **1995**, *99*, 87-99.
(41) Rockcliffe, D. A.; Martell, A. E. *Inorg. Chem.* **1993**, *32*, 3143-3152.
(42) Börzel, H.; Comba, P.; Hagen, K. S.; Kerscher, M.; Pritzkow, H.; Schatz, E.; Schindler, S.; Walter, O. *Inorg. Chem.* **2002**, *41*, 5440-5452.
(43) Root, D. E.; Mahroof-Tahir, M.; Karlin, K. D.; Solomon, E. I. *Inorg. Chem.* **1998**, *37*, 4838-4848.
(44) Itoh, K.; Hayashi, H.; Furutachi, H.; Mathumoto, T.; Nagamoto, S.; Tosha, T.; Terada, S.; Fujinami, S.; Suzuki, F.; Kitagawa, T. *J. Am. Chem. Soc.* **2005**, *127*, 5212-5223, and references therein.
(45) Karlin, K. D.; Ghosh, P.; Cruse, R. W.; Meyer, G. J.; Farooq, A.; Gultneh, Y.; Jacobson, R. R.; Blackburn, N. J.; Strange, R. W.; Zubieta, J. *J. Am. Chem. Soc.* **1988**, *110*, 6769-6780.
(46) Itoh, S.; Kumei, H.; Taki, M.; Nagamoto, S.; Kitagawa, T.; Fukuzumi, S. *J. Am. Chem. Soc.* **2001**, *123*, 6708-6709.
(47) Battaini, G.; Monzani, E.; Casella, L.; Santagostini, L.; Pagliarin, R. *J. Biol. Inorg. Chem.* **2000**, *5*, 262-268.
(48) Casella, L.; Monzani, E.; Gulotti, M.; Cavagnino, D.; Cerina, G.; Santagostini, L.; Ugo, R. *Inorg. Chem.* **1996**, *35*, 7516-7525.
(49) Martell, A. E.; Motekaitis, R. J.; Menif, R.; Rockcliffe, D. A.; Llobet, A. *J. Mol. Cat. A* **1997**, *117*, 205-213.
(50) Klabunde, T.; Eicken, C.; Sacchettini, J. C.; Krebs, B. *Nat. Struct. Biol.* **1998**, *5*, 1084-1090.
(51) Rompel, A.; Fischer, H.; Meiwes, D.; Buldt Karentsopoulos, K.; Dillinger, R.; Tuczek, F.; Witzel, H.; Krebs, B. *J. Biol. Inorg. Chem.* **1999**, *4*, 56-63.
(52) Jung, B.; Karlin, K. D.; Zuberbühler, A. D. *J. Am. Chem. Soc.* **1996**, *118*, 3763-3764.
(53) Schuitema, A. M.; Aubel, P. G.; Koval, I. A.; Engelen, M.; Driessen, W. L.; Reedijk, J.; Lutz, M.; Spek, A. L. *Inorg. Chim. Acta* **2003**, *355*, 374-385.
(54) Schwarzenbach, G.; Schwarzenbach, K. *Helv. Chim. Acta* **1963**, *46*, 1390-1400.
(55) Schuitema, A. M. Ph.D. thesis, Leiden University, 2004.
(56) Battaini, G.; De Carolis, M.; Monzani, E.; Tuczek, F.; Casella, L. *Chem. Commun.* **2003**, 726-727.
(57) *TEXSAN, Single-Crystal Structure Analysis Software*. Molecular Structure Corporation: The Woodlands, TX, 1995

8 | Catecholase activity of a copper(II) complex with the macrocyclic ligand [22]pr4pz: unraveling catalytic mechanisms[†]

In this chapter the structure, properties and a mechanism for the catecholase activity of a tetranuclear carbonato-bridged copper(II) cluster with the macrocyclic ligand [22]pr4pz (9,22-dipropyl-1,4,9,14,17,22,27,28,29,30-decaazapentacyclo-[22.2.1.1^{4,7}.1^{11,14}.1^{17,20}]triacontane-5,7(28),11(29),12,18,20(30),24(27),25-octaene) are reported. In this complex, two copper ions within a macrocyclic unit are bridged by a carbonate anion, which further connects two macrocyclic units together. The tetranuclear complex was found to be the major compound present in solution at high concentration levels, but its dissociation into two dinuclear units occurs upon dilution. The dinuclear complex catalyzes the oxidation of 3,5-di-*tert*-butylcatechol to the respective quinone in methanol by two different pathways, one proceeding via the formation of semiquinone species with the subsequent production of dihydrogen peroxide as a by-product, and another proceeding via the two-electron reduction of the dicopper(II) center by the substrate, with two molecules of quinone and one molecule of water generated per one catalytic cycle. The occurrence of the first pathway was, however, found to cease shortly after the beginning of the catalytic reaction. The influence of hydrogen peroxide and di-*tert*-butyl-*o*-benzoquinone on the catalytic mechanism has been investigated. The crystal structures of the free ligand and the reduced dicopper(I) complex, as well as the electrochemical properties of both the Cu^{II} and the Cu^{I} complexes are also reported.

[†]This chapter is based on: Koval, I. A.; Selmeczi, K.; Belle, C.; Philouze, C.; Saint-Aman, E.; Gautier-Luneau, I.; Schuitema, A. M.; van Vliet, M.; Gamez, P.; Roubeau, O.; Lüken, M.; Krebs, B.; Lutz, M.; Spek, A. L.; Pierre, J.–L.; Reedijk, J., Chem. Eur. J., submitted for publication

8.1 Introduction

In Chapter 7, the mechanism of catechol oxidation by a μ-hydroxo-dicopper(II) complex with the macrocyclic ligand [22]py4pz (Scheme 7.1, Chapter 7) has been discussed.[1] This dinucleating ligand provides two N_4 donor sets for the metal coordination. In the present chapter, the studies on the catecholase activity of the copper(II) complex with the related macrocyclic ligand [22]pr4pz (Figure 8.1) are presented. Instead of two pyridine-containing pendant arms, present in the ligand [22]py4pz, this ligand contains two propyl residues, thus providing two N_3 donor sets for the metal coordination, and mimicking the active site of the natural enzyme even more closely.

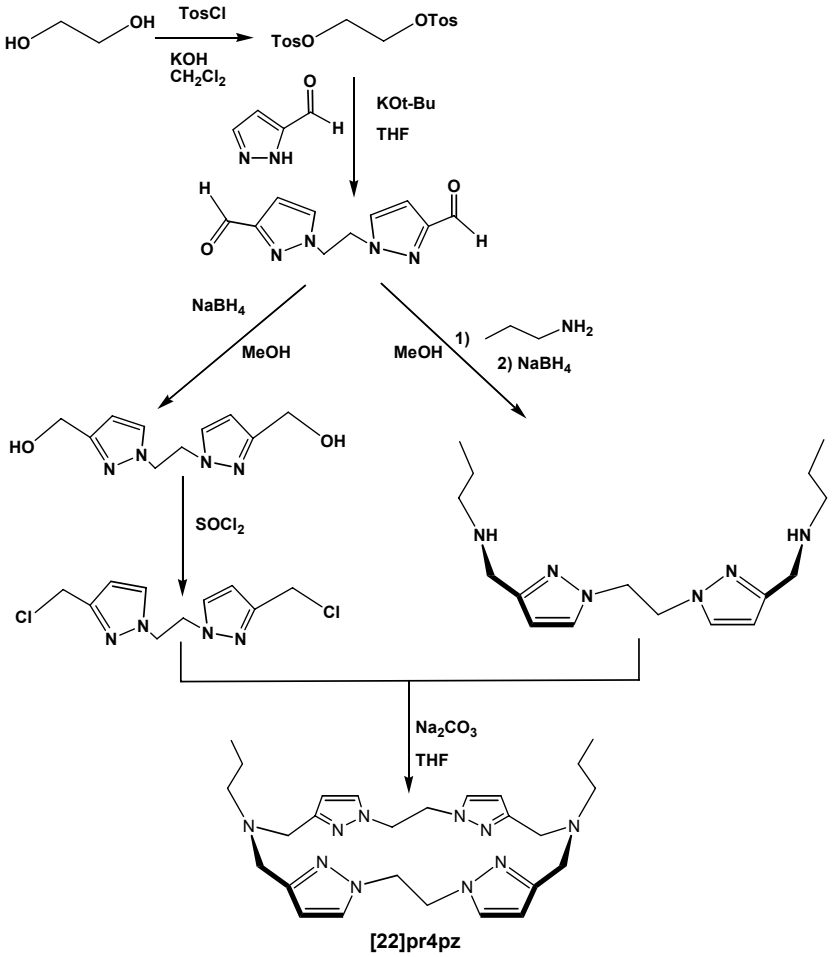

Figure 8.1. The reaction scheme of the synthesis of the macrocyclic ligand [22]pr4pz

In the isolated copper(II) complex with [22]pr4pz, the two metal ions within a macrocyclic unit are bridged by a carbonate anion, and two copper ions of two different macrocyclic units are further doubly bridged by two oxygen atoms of two carbonates, resulting in a tetranuclear structure in the solid state. In this chapter the crystal structures of the bis(perchlorate) salt of the macrocyclic ligand $[H_2[22]pr4pz](ClO_4)_2$,

the tetracopper(II) complex of the composition $[Cu_2([22]pr4pz)(CO_3)(H_2O)]_2(CF_3SO_3)_4 \cdot 2CH_3CN \cdot 4H_2O$ and its reduced dicopper(I) analogue $[Cu_2([22]pr4pz)(CH_3CN)_2](ClO_4)_2$, the kinetic studies on the catechol oxidation by the copper(II) complex and the anaerobic studies on its interaction with catechol are reported, and the catalytic reaction mechanism is discussed.

8.2 Results and Discussions

8.2.1 Synthesis of coordination compounds

The schematic representation of the synthesis of the macrocyclic ligand [22]pr4pz ((9,22-dipropyl-1,4,9,14,17,22,27,28,29,30-decaazapentacyclo-$[22.2.1.1^{4,7}.1^{11,14}.1^{17,20}]$triacontane-5,7(28),11(29),12,18,20(30),24(27),25-octaene) is depicted in Figure 8.1. This ligand has been designed earlier to model the active site of the structurally related type-3 copper protein hemocyanin.[2,3] The macrocyclic cavity comprises four pyrazolyl moieties and two nitrogen atoms of tertiary amine groups, providing two N_3 donor sets for the coordination of the metal ions. Diethyl ether diffusion in an acetonitrile solution, containing two molar equivalents of copper(II) triflate, one molar equivalent of the ligand and one molar equivalent of sodium carbonate, results in the formation of small blue crystals of the copper(II) complex. The X-ray structure determination (see below) revealed that it can be described as a tetranuclear complex of the formula $(\mathbf{1})_2(CF_3SO_3)_4 \cdot 2CH_3CN \cdot 4H_2O$, where $\mathbf{1}^{2+}$ corresponds to the dicopper unit $[Cu_2([22]pr4pz)(CO_3)(H_2O)]^{2+}$. The copper(I) complex was isolated by reacting two molar equivalents of Cu^I as a tetrakis(acetonitrile) complex with a solution of the ligand in methanol. The solid complex which precipitated upon addition of diethyl ether is the dinuclear Cu^I complex, denoted $\mathbf{2}(ClO_4)_2$, where $\mathbf{2}^{2+}$ corresponds to $[Cu_2([22]pr4pz)(CH_3CN)_2]^{2+}$.

8.2.2 Crystal structures description

$[H_2[22]pr4pz](ClO_4)_2$

An ORTEP projection of the bis(perchlorate) salt of the ligand is shown in Figure 8.2. The cationic ligand is located on an exact, crystallographic inversion center. The ligand adopts an *anti*-(chair) conformation, with two propyl groups located on opposite sides of the macrocyclic ring plane. Both symmetry-related tertiary amine nitrogen atoms (N27 and N27') are protonated, leading to a doubly charged cation, the positive charge being compensated by two perchlorate anions. The protonated N-H moiety acts as a donor of an intermolecular bifurcated hydrogen bond with two perchlorate oxygen atoms as acceptors; the angles at the hydrogen atom sum up to 359(4)° (Table 8.1). Due to the inversion center in the ligand the ring N21-N22 and its symmetry related N21'-N22' are arranged in a parallel fashion; the centroid-centroid

distance is 4.4089(18) Å and the parallel distance between the two planes of the aromatic rings is only 3.211 Å, indicating the presence of π stacking. The angle between the centroid-centroid vector and the normal to the aromatic ring plane is 43.25°.

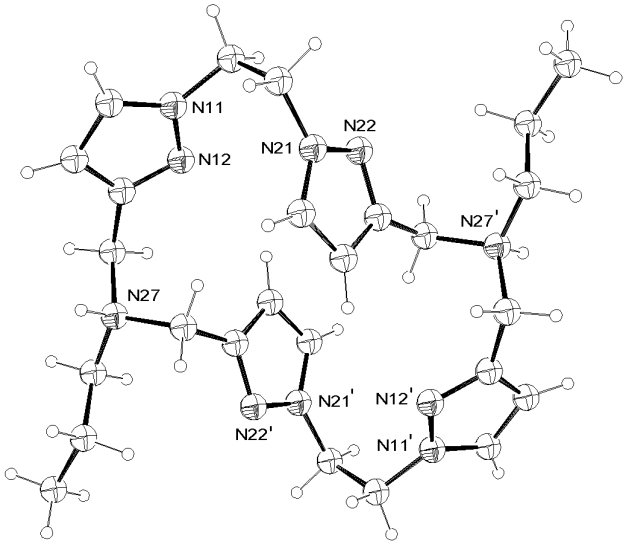

Figure 8.2. ORTEP projection of the cation $[H_2[22]pr4pz]^{2+}$. The perchlorate anions have been omitted for clarity. Symmetry operation ': 1-x, 1-y, 1-z.

Table 8.1. Bifurcated hydrogen bond for $[H_2[22]pr4pz](ClO_4)_2$

Donor - H....Acceptor	*D – H (Å)*	*H...A (Å)*	*D...A (Å)*	*D - H...A (º)*
N27 - H27…O3	0.92(3)	2.52(3)	3.233(3)	135(2)
N27 - H27...O3^{i}	0.92(3)	2.25(3)	3.063(3)	147(2)

Symmetry operation: i = 1-x, -y, 1-z; angle O1...H27...O1^{i}: 77.2(10)°

$[Cu_2([22]pr4pz)(CO_3)(H_2O)]_2(CF_3SO_3)_4 \cdot 2CH_3CN \cdot 4H_2O$

The molecular structure of the isolated solid complex consists of a tetracopper complex cation $[Cu_2([22]pr4pz)(CO_3)(H_2O)]_2^{4+}$ ($(\mathbf{1})_2^{4+}$), four counter ions $CF_3SO_3^-$, two non-coordinated acetonitrile molecules and four non-coordinated water molecules. An ORTEP projection of the structure of the cation $(\mathbf{1})_2^{4+}$ is shown in Figure 8.3 (top), selected bond lengths and angles are reported in Table 8.2. The cation contains four copper(II) centers, two macrocyclic ligands, two coordinated carbonates and two coordinated water molecules. In contrast to the structure of the protonated ligand, [22]pr4pz adopts a *syn*-(boat) conformation, with two propyl residues located on the same side of the macrocyclic ring plane. Each macrocyclic unit encloses two copper(II) ions (Cu1 and Cu2, and Cu1' and Cu2'), which are bridged by a carbonate anion (the Cu1…Cu2 or Cu1'…Cu2' intra-macrocyclic distance is 4.5427(18) Å). Two bridging oxygen atoms O51 and O51' from two different carbonate molecules connect the two central copper atoms Cu1 and Cu1' to form a centrosymmetric four-membered ring,

resulting in the Cu1…Cu1' inter-macrocyclic distance of 3.281(2) Å. Each carbonate ion is thus bound in a *syn, syn-anti* fashion, *e.g.* one of the oxygen atoms of the carbonate anion (O51 and O51') is bridging the coppers Cu1 and Cu1' of two different macrocyclic rings, whereas another oxygen atom (O52 and O52') binds to another copper ion (Cu2, Cu2' respectively).

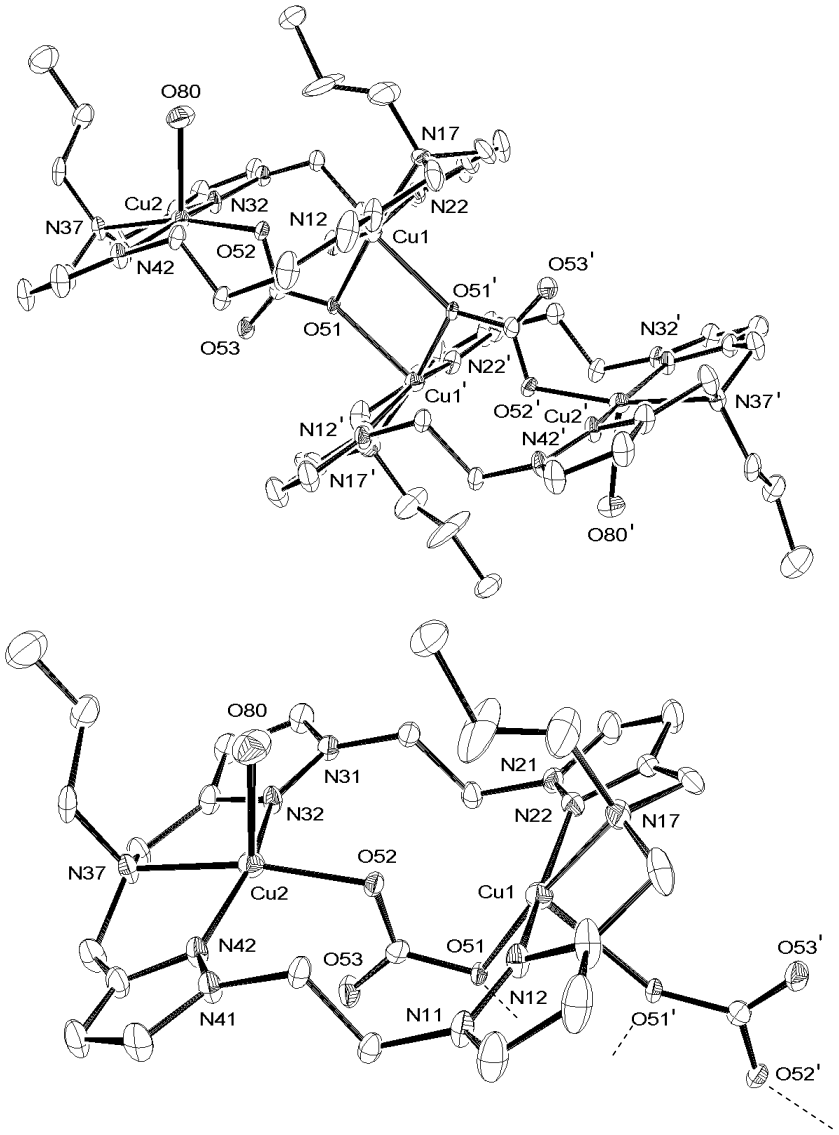

Figure 8.3. ORTEP projection of the tetranuclear cation $[Cu_2([22]pr4pz)(CO_3)(H_2O)]_2^{4+}$ ($(\mathbf{1})_2^{4+}$) (top) and ORTEP projection of half of the tetranuclear cation ($\mathbf{1}^{2+}$) (bottom). Hydrogen atoms and solvent molecules are omitted for clarity. Symmetry operation ': 2-x, y, 0.5-z.

The coordination sphere around the Cu1 ion can be described as a weakly distorted square pyramid ($\tau = 0.23$),[4] with the atoms N12, N17, N22 and O51 occupying the basal plane and the oxygen atom O51' at a distance of 2.330(3) Å occupying the apical position (Figure 8.3, bottom). All copper-nitrogen distances are approximately equal (the average Cu1–N distance is 2.03 Å), whereas the O51 atom is located at a somewhat shorter distance of 1.926(3) Å. The oxygen atom O52 from a bridging

carbonate anion is located at a distance of 2.595(3) Å; however, the very small O52–Cu1–O51a angle of 135.17(11)° suggests that the Cu1 coordination sphere should be considered as a square pyramidal rather than octahedral. Similarly, the coordination geometry around the Cu2 ion can also be best described as a weakly distorted square pyramid ($\tau = 0.1$),[4] in which the basal plane is occupied by the nitrogen atoms N32, N37 and N42 at an average distance of 2.02 Å, and the oxygen atom O52 at the distance of 1.957(3) Å. The axial position is occupied by the oxygen O80 atom from a coordinated water molecule at a distance of 2.267 (4) Å. The oxygen atom O53 is also located in a close proximity of the Cu2 ion (the Cu2-O53 distance is 2.709(4) Å) and could be considered as (semi-)coordinated; however, the very small O80–Cu2–O53 angle of 142.09(14)° does not permit the Cu2 coordination sphere being described as an octahedron.

The crystal packing was found to be uneventful, with only van der Waals interactions realized in the crystal lattice.

Table 8.2. Selected bond lengths and angles for $[Cu_2([22]pr4pz)(CO_3)(H_2O)]_2(CF_3SO_3)_4 \cdot 2CH_3CN \cdot 4H_2O$

Bond lengths (Å)			
Cu1…Cu1'	3.281(2)	Cu1…Cu2	4.5427(18)
Cu1 – O51	1.926(3)	Cu2 – O52	1.957(3)
Cu1 – O51'	2.330(3)	Cu2 – O80	2.267(4)
Cu1 – N12	2.030(5)	Cu2 – N32	1.989(5)
Cu1 – N17	2.025(4)	Cu2 – N37	2.087(4)
Cu1 – N22	2.028(5)	Cu2 – N42	1.998(5)

Bond angles (°)			
O51 – Cu1 – N12	99.94(15)	O52 – Cu2 – O80	87.38(15)
O51 – Cu1 – N17	174.55(16)	O52 – Cu2 – N32	97.65(14)
O51 – Cu1 – N22	99.54(15)	O52 – Cu2 – N37	166.99(15)
O51 – Cu1 – O51'	79.47(13)	O52 – Cu2 – N42	96.75(14)
N12 – Cu1 – N17	80.9(2)	O80 – Cu2 – N32	96.99(16)
N12 – Cu1 – N22	160.18(16)	O80 – Cu2 – N37	105.60(16)
N12 – Cu1 – O51'	92.46(14)	O80 – Cu2 – N42	96.00(16)
N17 – Cu1 – N22	80.0(2)	N32 – Cu2 – N37	81.92(17)
N17 – Cu1 – O51'	95.13(14)	N32 – Cu2 – N42	160.99(16)
N22 – Cu1 – O51'	94.69(14)	N37 – Cu2 – N42	81.25(17)

Symmetry operation: ' = 2-x, y, 1/2-z

$[Cu_2([22]pr4pz)(CH_3CN)_2](ClO_4)_2$

An ORTEP projection of the complex cation $\mathbf{2}^{2+}$ is shown in Figure 8.4. Selected bond lengths and angles are presented in Table 8.3.

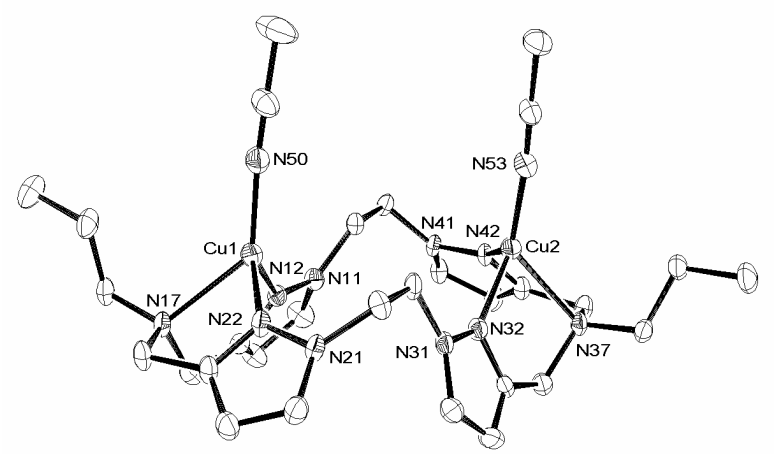

Figure 8.4. ORTEP projection of the complex cation $[Cu_2([22]pr4pz)(CH_3CN)_2]^{2+}$ ($\mathbf{2}^{2+}$). Hydrogen atoms are omitted for clarity.

Table 8.3. Selected bond lengths and bond angles for $[Cu_2([22]pr4pz)(CH_3CN)_2](ClO_4)_2$ ($\mathbf{2}(ClO_4)_2$).

Bond distances (Å)			
Cu1…Cu2	5.547(2)		
Cu1 – N12	2.028(2)	Cu2 – N32	2.055(2)
Cu1 – N17	2.292(2)	Cu2 – N37	2.277(2)
Cu1 – N22	2.063(2)	Cu2 – N42	2.085(2)
Cu1 – N50	1.897(2)	Cu2 – N53	1.903(2)

Bond angles (°)			
N12 – Cu1 – N17	79.47(8)	N32 – Cu2 – N37	79.64(7)
N12 – Cu1 – N22	112.09(8)	N32 – Cu2 – N42	110.05(8)
N12 – Cu1 – N50	121.36(9)	N32 – Cu2 – N53	123.26(9)
N17 – Cu1 – N22	78.20(8)	N37 – Cu2 – N42	78.06(8)
N17 – Cu1 – N50	131.82(8)	N37 – Cu2 – N53	132.19(8)
N22 – Cu1 – N50	121.24(9)	N42 – Cu2 – N53	120.69(9)

Similarly to the structure of the earlier reported dicopper(I) complex with the related macrocyclic ligand [22]py4pz, the macrocyclic ligand adopts a saddle-shaped conformation.[1] However, in [22]py4pz complex the tertiary nitrogen atoms of the ligand fail to bind to the metal ions, resulting in distorted trigonal surroundings for both copper(I) ions. In $\mathbf{2}(ClO_4)_2$, on the contrary, both copper ions are tetracoordinated and have a distorted tetrahedral surrounding, with three positions in the coordination sphere being occupied by the nitrogen donor atoms from the ligand (N12, N17, N22 and N32,

N37, N42) and one by the nitrogen atom of an acetonitrile molecule (N50 and N53). The tripodal nitrogen donor atoms N17 and N37 are located at somewhat longer distances (2.292(2) Å and 2.277(2) Å, respectively) than the nitrogen atoms of the pyrazolyl rings of the ligand (the average Cu1-$N_{pyrazole}$ distance is 2.05 Å, the average Cu2-$N_{pyrazole}$ distance is 2.07 Å). The nitrogen atoms N50 and N53 of the acetonitrile molecules are located, on the contrary, at shorter distances of 1.897(2) Å and 1.903(2) Å, respectively. The N–Cu–N angles for both copper(I) ions vary in quite a large range, *viz.* from 78 to 132°, indicating a significant distortion of the coordination sphere from a regular tetrahedral geometry. The distance between the two copper(I) ions is very large, *viz.* 5.547(2) Å.

8.2.3 Solution stability of $(\mathbf{1})_2(CF_3SO_3)_4{\cdot}2CH_3CN{\cdot}4H_2O$

ESI-MS spectra of $(\mathbf{1})_2(CF_3SO_3)_4{\cdot}2CH_3CN{\cdot}4H_2O$, recorded in a methanol solution (0.2 mM), are characterized by two peaks at *m/z* = 827 and *m/z* = 1801, which correspond to the monocharged dinuclear $\{[Cu_2([22]pr4pz)(CO_3)](CF_3SO_3)\}^+$ and the tetranuclear $\{[Cu_2([22]pr4pz)(CO_3)]_2(CF_3SO_3)_3\}^+$ cation moieties, respectively, and are in agreement with the theoretical isotopic patterns. The tetranuclear copper(II) core stability in methanol solution and its dependence on the concentration was studied by EPR spectroscopy. The EPR spectrum of the solid sample of $(\mathbf{1})_2(CF_3SO_3)_4{\cdot}2CH_3CN{\cdot}4H_2O$ recorded at 13 K is dominated by a strong isotropic signal (g = 2.14), which is characteristic for copper(II) ions experiencing short-range metal-metal exchange interactions, leading to exchange narrowing. The spectrum of $(\mathbf{1})_2(CF_3SO_3)_4{\cdot}2CH_3CN{\cdot}4H_2O$, recorded in KBr matrix (1%), exhibits identical features (Figure 8.5, left, dotted line). The spectrum of a 14 mM solution of the complex in methanol (for simplicity, the complex concentration is calculated based on the molecular weight of the dinuclear species $[Cu_2([22]pr4pz)(CO_3)(H_2O)](CF_3SO_3)_2{\cdot}CH_3CN{\cdot}2H_2O$) also contains a strong isotropic signal with the same g-value; however, the typical features of a triplet spectrum, characteristic for the dinuclear copper(II) species, are also observed (Figure 8.5, left). Upon further dilution, the relative intensity of the isotropic signal gradually diminishes, until at a 0.5 mM concentration a typical triplet spectrum is finally observed. The isotropic signal, observed in the solid state, is likely to be caused by the copper-copper interactions within the tetranuclear core, which are also dominating in a concentrated (14 mM) solution. However, upon dilution, the dissociation of the tetranuclear cluster into two dinuclear species $\mathbf{1}^{2+}$ leads to a typical triplet dicopper(II) spectrum, which gradually increases in relative intensity on the expense of the original isotropic signal.

EPR studies have also been performed in a frozen solution of acetonitrile. The spectrum practically does not change upon dilution, with the strong isotropic signal remaining dominant in the spectrum (0.4–2 mM, Figure 8.5, right), suggesting that the tetranuclear core remains largely intact in this solvent.

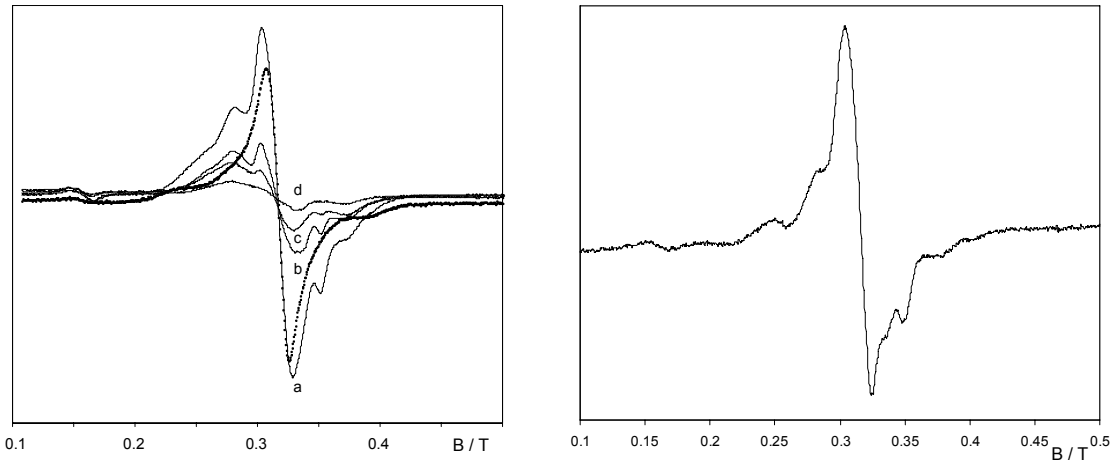

Figure 8.5. Left: Dotted line: EPR spectrum of $(\mathbf{1})_2(CF_3SO_3)_4{\cdot}2CH_3CN{\cdot}4H_2O$ in the solid state (1% in KBr matrix); solid lines: changes in the EPR spectrum of $(\mathbf{1})_2(CF_3SO_3)_4{\cdot}2CH_3CN{\cdot}4H_2O$ in methanol solution upon dilution (a: 14 mM, b: 2 mM, c: 1 mM, d: 0.5 mM) at 13.3 K. Right: EPR spectrum of $(\mathbf{1})_2(CF_3SO_3)_4{\cdot}2CH_3CN{\cdot}4H_2O$ in acetonitrile (2 mM) at 13 K.

8.2.4 Electrochemical properties of $(\mathbf{1})_2(CF_3SO_3)_4{\cdot}2CH_3CN{\cdot}4H_2O$ and $\mathbf{2}(ClO_4)_2$

The electrochemical properties of the complexes were studied by cyclic voltammetry (CV) in methanol and in acetonitrile, using tetrabutylammonium triflate as a supporting electrolyte in case of $\mathbf{1}^{2+}$ ($N\textit{n}Bu_4ClO_4$ could not be used, as the complex precipitates as a perchlorate salt) and tetrabutylammonium perchlorate in case of $\mathbf{2}^{2+}$. The potentials were referred to Ag/10 mM $AgNO_3$ in acetonitrile. In the negative range of potentials, the CV curve of $\mathbf{1}^{2+}$ in MeOH (0.63 mM) is characterized by one irreversible electrochemical signal at E_{pc} = -0.62 V (Figure 8.6, left). Coulometric titrations indicate that this peak corresponds to a one-electron transfer per copper center, resulting in the formation of Cu^I species, its re-oxidation being seen on the reverse scan as an irreversible peak at E_{pa} = 0.14 V. Apparently, the mixed-valenced $Cu^{II}Cu^I$ species is not formed and cannot be isolated, the copper centers in $\mathbf{1}^{2+}$ being electrochemically equivalent. This result was further confirmed following the changes in the EPR spectrum upon electrochemical reduction of the complex $\mathbf{1}^{2+}$. Since the typical triplet dicopper(II) spectrum was still observed after one electron transfer per dinuclear entity (Figure 8.7), - only its intensity is decreased by a factor 2, - it is concluded that no mixed-valenced species could be formed. The CV curve of $(\mathbf{1})_2(CF_3SO_3)_4{\cdot}2CH_3CN{\cdot}4H_2O$ in acetonitrile looks rather similar to that in methanol, with E_{pc} = -0.72 V and E_{pa} = 0.18 V. As the tetranuclear core is largely preserved in the latter solvent, whereas in methanol, the complex is mainly present in its dissociated form at the concentration level (0.63 mM) used for electrochemical studies, it can be concluded that the dissociation of the dimacrocyclic unit into two dinuclear fragments does not significantly influence the metal reduction potentials.

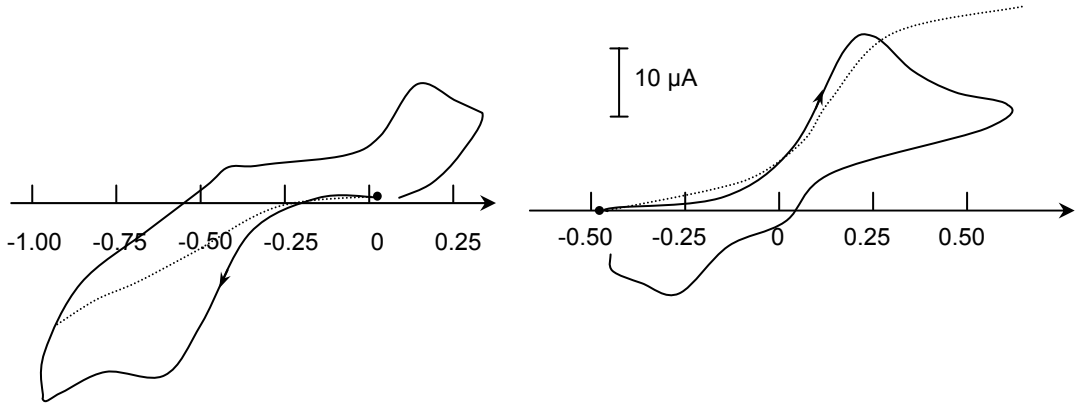

Figure 8.6. Left: electrochemical curves of $\mathbf{1}^{2+}$, recorded in MeOH + 0.1 M N*n*Bu$_4$CF$_3$SO$_3$ on a C disc (∅ = 3 mm); solid line: CV curve, 0.63 mM solution, 0.1 V·s^{-1}, 2 µÅ·cm^{-1}; dotted line: RDE curve, 0.35 mM, 0.01 V·s^{-1}, 5 µÅ·cm^{-1}, N = 600 rpm. Right: Electrochemical curves of $\mathbf{2}^{2+}$, recorded in MeOH + 0.1 M N*n*Bu$_4$ClO$_4$ on a C disc (∅ = 3 mm); solid line: CV curve, 1 mM solution, 0.1 V·s^{-1}; dotted line: RDE curve, 0.65 mM, 0.01 V·s^{-1}, N = 600 rpm.

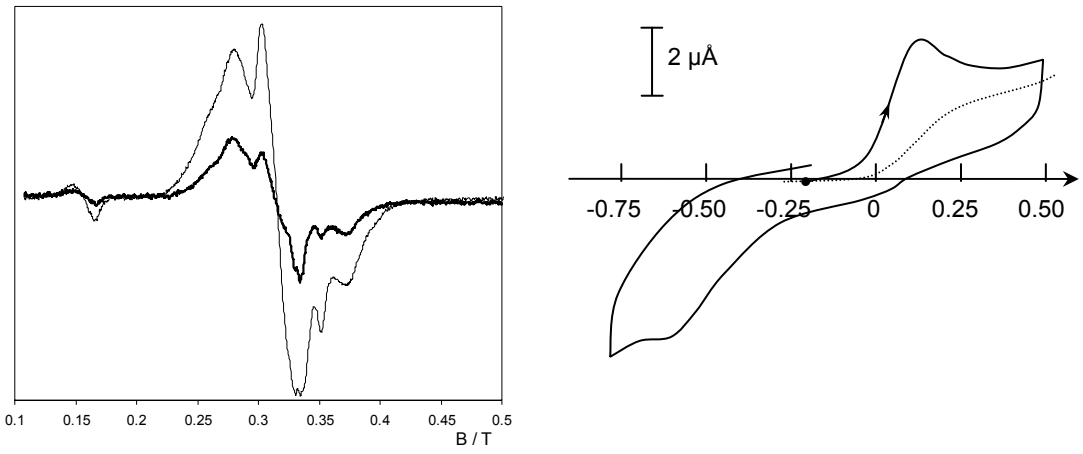

Figure 8.7. Left: Changes in the EPR spectrum at 13 K of $\mathbf{1}^{2+}$ (1 mM solution in MeOH) upon electrolysis. The solid line corresponds to the original spectrum, the bold line corresponds to the spectrum recorded after one-electron reduction. Right: Electrochemical curves of $\mathbf{1}^{2+}$ (1 mM, MeOH + 0.1 M N*n*Bu$_4$CF$_3$SO$_3$, a C disc (∅ = 3 mm)) after one-electron reduction; solid line: CV curve, 0.1 V·s^{-1}, dotted line: RDE curve, 0.01 V·s^{-1}, N = 600 rpm.

The CV curve of $\mathbf{2}^{2+}$ in methanol is characterized by one broad electrochemical signal at E_{pa} = 0.22 V, *i.e.* at a potential close to the one (0.14 V) observed for the Cu^{I} species electrogenerated from $\mathbf{1}^{2+}$ (Figure 8.6, right). This small difference accounts likely for small discrepancy in the coordination spheres around the copper(I) center between the two complexes, *e.g.* caused by the initial presence of coordinated water molecules in $\mathbf{1}^{2+}$ and acetonitrile molecule in $\mathbf{2}^{2+}$ or the carbonate bridge in the copper

coordination sphere in $\mathbf{1}^{2+}$ (the carbonate bridge, however, is expected to dissociate upon electrochemical reduction due to its poor ability to bridge two copper(I) centers). Coulometric titration shows that this anodic process corresponds to a one electron transfer per copper center leading to Cu^{II} species. The reduction of the electrogenerated two-electron oxidized species from $\mathbf{2}^{2+}$ is seen on the CV curve, during the reverse scan, as two ill-resolved peaks at E_{pc1} = 0.03 V and E_{pc2} = -0.45 V, suggesting the presence of two different electrogenerated Cu^{II} species, likely accounting for different re-coordinations with solvent molecules.

8.2.5 Magnetic properties of $(\mathbf{1})_2(CF_3SO_3)_4 \cdot 2CH_3CN \cdot 4H_2O$

The thermal dependence of the complex χT (where χ is the magnetic susceptibility per Cu_2 formula unit) is plotted in Figure 8.8. χT gradually increases upon lowering the temperature from 0.84 $cm^3 \cdot mol^{-1} \cdot K$ at 300 K to reach a maximum around 0.95 $cm^3 \cdot mol^{-1} \cdot K$ at 15 K. A decrease is then observed down to 0.81 $cm^3 \cdot mol^{-1} \cdot K$ at 5 K. Values at high temperatures are in agreement with two uncoupled spin 1/2 centers (*e.g.* 0.75 $cm^3 \cdot mol^{-1} \cdot K$ for g = 2), while the increase observed is the signature of intramolecular ferromagnetic interactions. The full Hamiltonian describing the pairwise interactions among the Cu^{II} ions in $(\mathbf{1})_2(CF_3SO_3)_4 \cdot 2CH_3CN \cdot 4H_2O$, can be expressed by equation 8.1:

$$H = -2J_1\left(S_1 \cdot S_2 + S_{1'} \cdot S_{2'}\right) - 2J_2\left(S_1 \cdot S_{1'}\right) - 2J_3\left(S_1 \cdot S_{2'} + S_{1'} \cdot S_2\right) - 2J_4\left(S_2 \cdot S_{2'}\right) \quad (8.1)$$

where the structural numbering scheme has been kept. The energy levels and their spin quantum numbers were derived previously.[5] Testing the influence of each interaction parameter on the quality of the fit, J_4 was found to be of no influence, while J_3 was found to be undetermined when allowed to vary freely together with J_2. Indeed, although it was observed in a specific case,[5] a significant coupling between fourth neighbouring spins (J_4) is unlikely. On the other hand, given the low spin density in the axial position for a close to square-pyramidal coordination environment, the central coupling pathway through the two oxygen atoms respectively in axial and equatorial positions (J_2) can be expected to be more significant than that through the carbonato bridge with again one axial and one equatorial oxygen atom (J_3). Thus, and in light of these magneto-structural considerations, J_3 and J_4 were fixed to 0. Then the best fit parameters were J_1/k_B = 11.4(5) K, J_2/k_B = –3.49(4) K and g = 2.10(1), with a Temperature Independent Paramagnetism term at TIP = $6.6(3) \times 10^{-4}$ $cm^3 \cdot mol^{-1}$. It should be noted that a small negative value of J_3 (< 1 K) is likely, but could not be determined with accuracy, given its interdependence with J_2, and its small influence on the quality of the fit. The resulting low-lying states are then a singlet ground state with a triplet state and a quintuplet state at respectively *ca.* 1.4 K and 5.4 K above it. The ferromagnetic coupling propagated through the *syn*, *syn* carbonato bridge is in agreement with previous observations in dinuclear[6] and trinuclear[7,8] compounds with a

syn-syn bridging coordination mode. On the other hand, because of the low spin density in axial d_{z^2} orbital, only a weak antiferromagnetic interaction, such as that found for J_2, can be expected from the orbital overlap through the asymmetric di-μ-$O_{carbonate}$ bridge.

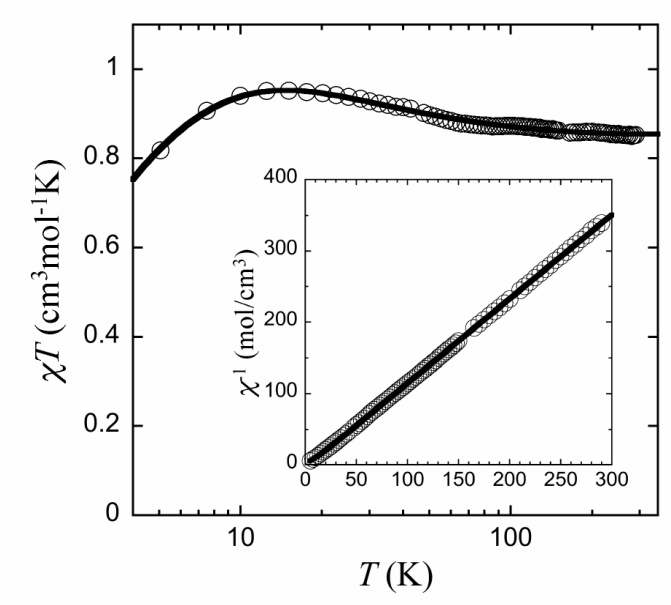

Figure 8.8. Semi-logarithmic plot of χT *vs.* T for $(\mathbf{1})_2(CF_3SO_3)_4{\cdot}2CH_3CN{\cdot}4H_2O$ under a 0.1 T applied field, where χ is the magnetic susceptibility per Cu_2 formula unit. The inset shows the thermal dependence of the inverse magnetic susceptibility. Full lines represent the best fit obtained with a tetranuclear model (see text for further details).

8.2.6 Catecholase activity of $(\mathbf{1})_2(CF_3SO_3)_4{\cdot}2CH_3CN{\cdot}4H_2O$

8.2.6.1 Kinetic studies

The catalytic oxidation of the model substrate $DTBCH_2$ (3,5-di-*tert*-butylcatechol) by $(\mathbf{1})_2(CF_3SO_3)_4{\cdot}2CH_3CN{\cdot}4H_2O$ was evaluated spectrophotometrically in dioxygen-saturated methanol by monitoring the increase in absorbance at 400 nm, corresponding to the formation of the quinone product DTBQ (3,5-di-*tert*-butyl-*o*-benzoquinone). The initial reaction rates were determined from the slope of the trace at 400 nm during the first 0.7 minutes of the reaction, when the absorption at 400 nm increases linearly. Because the concentration of the complex, used for the catecholase activity studies, was 2×10^{-5} M, the active species can be regarded as dinuclear.

The $DTBCH_2$ oxidation rate was found to be strongly dependent on the substrate concentration. The rate-determining step was found to change with the substrate to complex ratio. Thus, at low substrate to complex ratios (< 12:1, $[\mathbf{1}^{2+}] = 2\times10^{-5}$ M), the reaction shows Michaelis-Menten behavior (Figure 8.9, right). The Lineweaver-Burk treatment gives K_M = 0.176 mM and $V_{max} = 2.47\times10^{-6}$ M·s^{-1}. This behavior indicates the presence of equilibrium in the rate-determining step. At high substrate to complex ratios

(up to 200:1), the reaction rate depends linearly on the $DTBCH_2$ concentration, with the 1st order rate constant $k_1 = 2\times10^{-4}$ s^{-1} ($R^2 = 0.9986$, Figure 8.9, left).

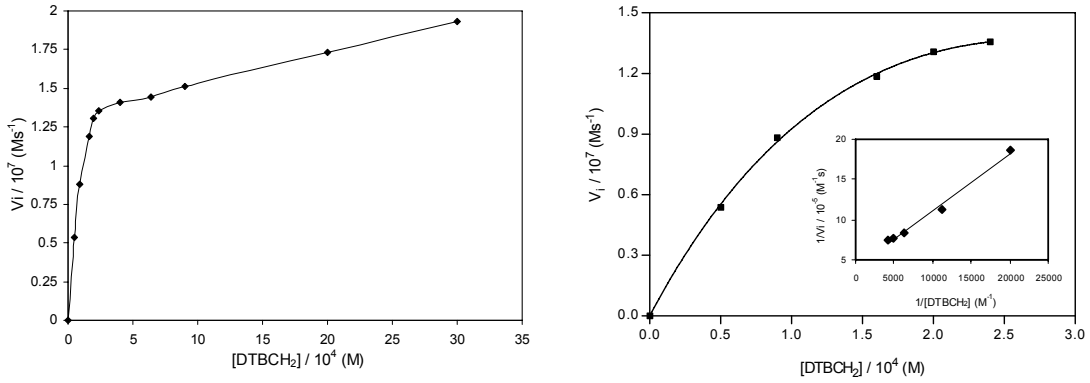

Figure 8.9. Left: the dependence of the initial reaction rates on catechol concentration, as determined from the slope of trace at 400 nm in the first 0.7 min of the catalytic reaction. Right: the dependence of the initial reaction rates on catechol concentration for substrate to catalyst ratios below 12:1 ([$\mathbf{1}^{2+}$] = 2×10^{-5} M), the insert shows the reciprocal Lineweaver-Burk plot ($R^2 = 0.9932$).

A linear dependence on the complex concentration in the whole concentration range at all substrate to complex ratios was found (Figure 8.10).

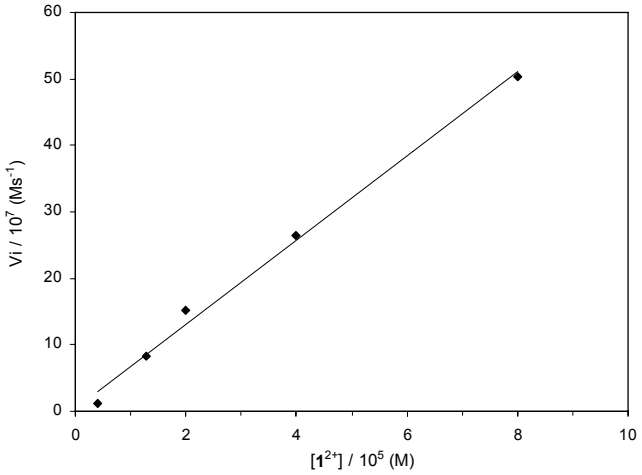

Figure 8.10. Dependence of the initial reaction rates on the concentration of $\mathbf{1}^{2+}$ in the catalytic oxidation of $DTBCH_2$ in methanol solution ([$DTBCH_2$] = 1 mM, $k_2 = 0.063$ s^{-1}, $R^2 = 0.9945$).

The catalytic reaction is finished within a few minutes at low catechol to complex ratios, whereas at high catechol to complex ratios, no full conversion of $DTBCH_2$ could be achieved, not even after 24 hours. To evaluate whether the reaction rate may be influenced by the formed product DTBQ, the kinetic studies in the presence of variable amounts of added quinone were performed. DTBQ was indeed found to have a strong inhibiting effect on the catalytic process, as can be seen from Figure 8.11. For instance, the initial reaction rate was found to decrease to 50% of its initial value in the presence of *ca.* 5 molar equivalents of DTBQ. This inhibiting effect was observed both at low (10:1) and high (50:1) catechol to complex ratios ([$\mathbf{1}^{2+}$] = 2×10^{-5} M).

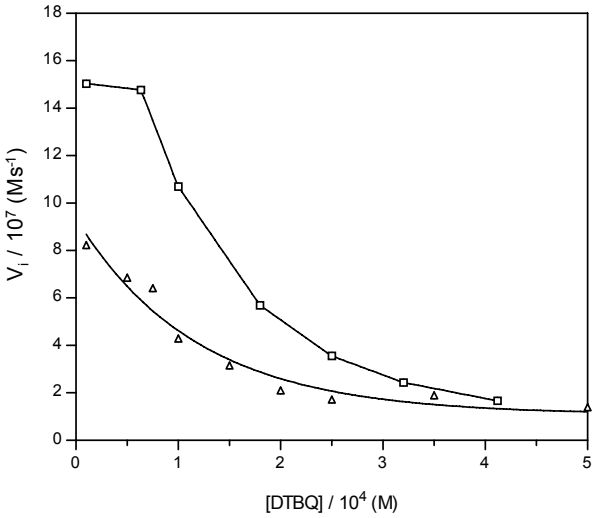

Figure 8.11. Dependence of the initial reaction rates on the concentration of DTBQ at low (Δ, 10:1) and high (□, 50:1) $DTBCH_2$ to complex ratios ([$\mathbf{1}^{2+}$] = 2×10^{-5} M).

Interestingly, $(\mathbf{1})_2^{4+}$ does not exhibit catecholase activity in acetonitrile. Instead, only one equivalent of quinone is formed stoichiometrically. The plot of the initial reaction rates *vs.* catechol concentration indicates a substrate saturation behavior (Figure 8.12, left). The reciprocal Lineweaver-Burk plot (Figure 8.12, right) gives K_M = 0.42 mM and $V_{max} = 5\times10^{-7}$ $M^{-1}\cdot s^{-1}$.

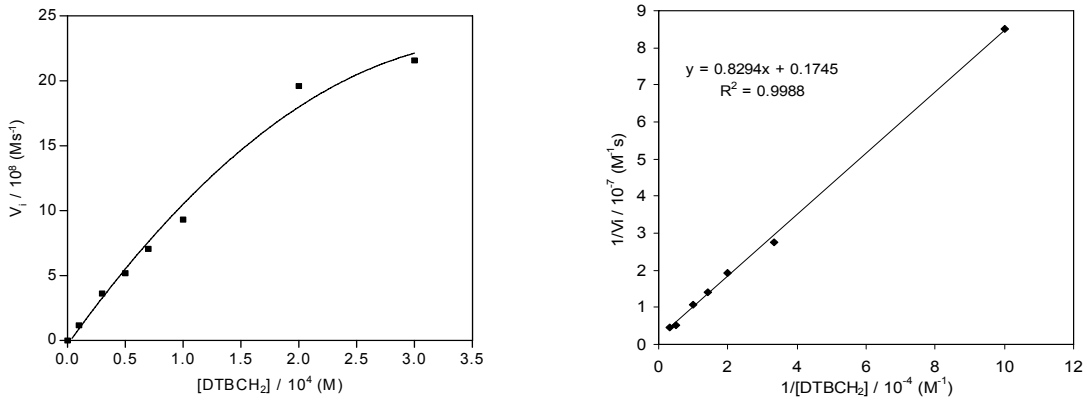

Figure 8.12. The dependence of the initial reaction rates on catechol concentration for the stoichiometric quinone formation in CH_3CN (left) and the reciprocal Lineweaver-Burk plot (right). [complex] = 2×10^{-5} M (the concentration calculated based on the molecular weight of the dinuclear species $[Cu_2([22]pr4pz)(CO_3)(H_2O)]\cdot CH_3CN\cdot 2H_2O$).

8.2.6.2 Formation of H_2O_2 and its influence on the reaction

The reduction of dioxygen to dihydrogen peroxide upon catechol oxidation by copper(II) complexes has been previously established only in a few cases.[9-12] The formation of H_2O_2 in the course of the catalytic reaction has been studied for two different catechol to complex ratios (10:1 and 50:1, [$\mathbf{1}^{2+}$] = 2×10^{-5} M). In both cases,

dihydrogen peroxide was formed at the initial stage of the reaction, and its formation was found to practically stop after a few minutes, although the oxidation of $DTBCH_2$ was still continuing (Figure 8.13). This suggests that two different mechanisms may be operating during the catalytic oxidation of $DTBCH_2$ by $\mathbf{1}^{2+}$: one, in which dioxygen undergoes a two-electron reduction to dihydrogen peroxide, and a second mechanism, in which it is converted into water upon four-electron reduction.

In order to evaluate the influence of dihydrogen peroxide on the catalytic reaction, catalytic studies were performed in the presence of variable amounts of H_2O_2. The plot of the initial reaction rates *vs.* dihydrogen peroxide concentrations is depicted in Figure 8.14. As can be seen, at low H_2O_2 concentrations its presence has virtually no influence on the reaction rates. At higher concentrations (above 20 molar equivalents of H_2O_2 per one mole of the complex), it accelerates the reaction rate. However, the concentration of dihydrogen peroxide, formed during the reaction, does not reach this level (Figure 8.13).

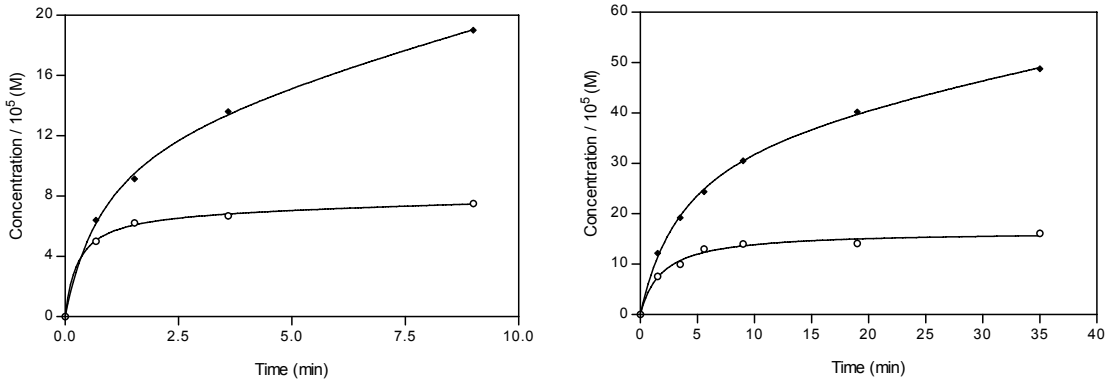

Figure 8.13. The course of DTBQ (◆) and H_2O_2 (○) formation during the catalytic reaction at low (10:1, left) and high (50:1, right) substrate to catalyst ratios ([$\mathbf{1}^{2+}$] = 2×10^{-5} M).

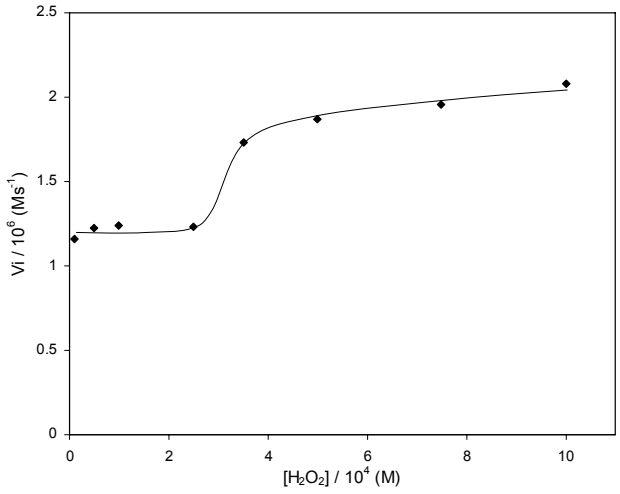

Figure 8.14. Dependence of the initial reaction rates in the catalytic oxidation of $DTBCH_2$ by $\mathbf{1}^{2+}$ in MeOH on the dihydrogen peroxide concentration. The initial concentration of $DTBCH_2$ is 1 mM, the concentration of $\mathbf{1}^{2+}$ is 2×10^{-5} M.

8.2.6.3 Anaerobic interaction of 1^{2+} and 2^{2+} with $DTBCH_2$ and DTBQ

As shown previously by Krebs and co-authors,[13] the catalytic cycle of catechol oxidase starts with the native *met* state of the enzyme, which reacts stoichiometrically with catechol, producing one equivalent of the quinone and leading to the dicopper(I) (*deoxy*) form. The anaerobic interaction of $\mathbf{1}^{2+}$ with $DTBCH_2$ has been studied spectrophotometrically. Upon addition of one molar equivalent of $DTBCH_2$ to a 0.5 mM solution of $\mathbf{1}^{2+}$ in methanol, two new absorptions at 389 nm (ε = 2920 $M^{-1}\cdot cm^{-1}$) and 760 nm (ε = 359 $M^{-1}\cdot cm^{-1}$) gradually develop in the spectrum (Figure 8.15, left). Both bands are characteristic of the formation of the semiquinone radical[14] and suggest that $\mathbf{1}^{2+}$ reacts with $DTBCH_2$, while undergoing a one-electron reduction, leading to the formation of mixed-valenced $Cu^{II}Cu^{I}$-semiquinone species (DTSQ). The rate constant k_3 of this process is 1.8×10^{-3} $M^{-1}\cdot s^{-1}$. The addition of an excess of $DTBCH_2$ (up to five molar equivalents) has no influence on the spectrum. The formed semiquinone species is stable for at least 24 hours under anaerobic conditions.

These results were further confirmed by EPR spectroscopy (Figure 8.15, right). The EPR spectrum of a 1 mM frozen solution in MeOH of $\mathbf{1}^{2+}$ in the presence of one molar equivalent of $DTBCH_2$ is characterized by a typical axial signal of mononuclear Cu^{II} species ($g_{//}$ = 2.23, $A_{//} = 175\times10^{-4}$ cm^{-1}, $g\perp$ = 2.04) and a sharp signal centered at g = 2.00 corresponding to an organic radical. The results explicitly show the absence of interaction between the two metal centers, indicating the presence of discrete Cu^{II} and Cu^{I} ions within the complex, and the absence of interaction between the semiquinone radical and the Cu^{II} ion.

The electrochemical behavior of the mixed-valenced $Cu^{II}Cu^{I}$-semiquinone species has been also examined. The CV curve, recorded in a 0.5 mM methanolic solution of $\mathbf{1}^{2+}$ in the presence of one molar equivalent of $DTBCH_2$, is characterized in the negative region of potentials by a quasi-reversible electrochemical signal at $E_{1/2}$ = -0.34 V (Figure 8.16), which is followed at lower potential by the copper(0) deposition onto the electrode surface. Based on earlier reported electrochemical properties of the semiquinone species,[15,16] this signal has been assigned to the one-electron reduction of the semiquinone radical. However, a close examination of this signal shows that it displays a shoulder suggesting the presence of two overlapping electrochemical systems. It is likely that the reduction process of the Cu^{II} center in the mixed-valenced $Cu^{II}Cu^{I}$-semiquinone species is hidden underneath the electrochemical response of the semiquinone moiety. In the positive range of potentials, the electrochemical curve is characterized by two ill-resolved oxidation waves at E_{pa} = 0.12 V and E_{pa} = 0.42 V (Figure 8.16), associated with the electrochemical responses of the $Cu^{II}Cu^{I}$ / $Cu^{II}Cu^{II}$ redox couple and the one-electron oxidation of the semiquinone radical.

It is interesting to note that mixed-valenced $Cu^{II}Cu^{I}$ species forms readily upon anaerobic reaction of $\mathbf{1}^{2+}$ with $DTBCH_2$, whereas they could not be generated

electrochemically. These results suggest an asymmetric binding of the substrate to only one of the two copper centers of the dinuclear subunit $\mathbf{1}^{2+}$ prior to the redox reaction, leading to the differentiation of the two metal centers. This in turn results in their different reduction potentials, allowing the subsequent formation of the mixed-valenced dicopper core.

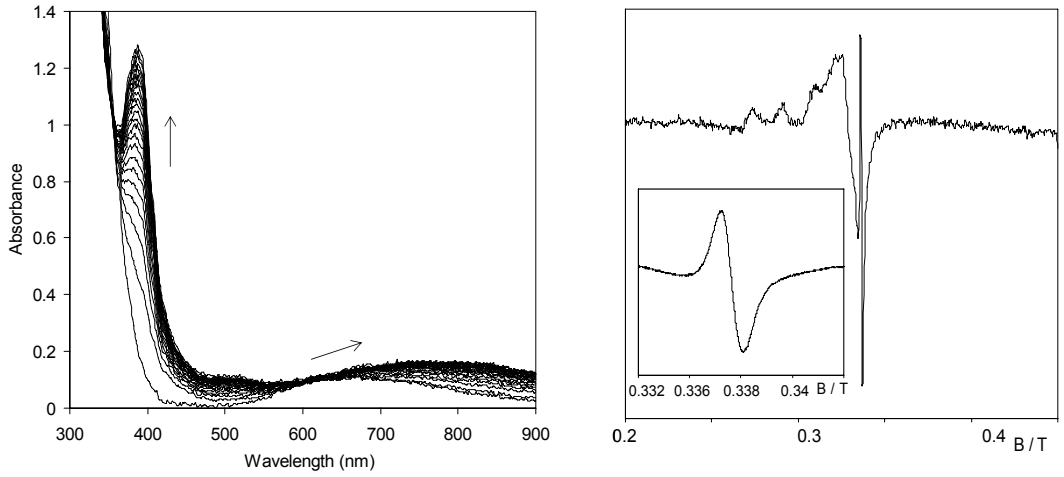

Figure 8.15. Left: changes in the UV-Vis spectrum upon addition of 1 eq. $DTBCH_2$ to a methanolic solution of $\mathbf{1}^{2+}$ (0.5 mM) in anaerobic conditions at 100 K. Right: the EPR-spectrum of the resulting mixed-valenced $Cu^{II}Cu^{I}$-semiquinonate species in anaerobic conditions (1 mM solution of $\mathbf{1}^{2+}$ in methanol, 100 K). Insert: the enlarged signal of the semiquinone radical.

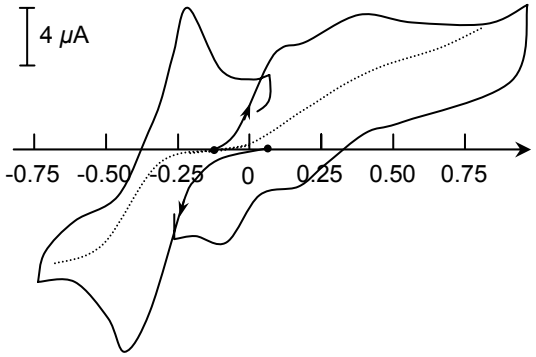

Figure 8.16. Electrochemical curves of $\mathbf{1}^{2+}$ (0.5 mM) in the presence of one equivalent of $DTBCH_2$, recorded in MeOH + 0.1 M $N\mathit{n}Bu_4CF_3SO_3$ on a C disc (∅ = 3 mm). Solid line: CV curves, 0.1 $V{\cdot}s^{-1}$; dotted line: RDE curves, 0.01 $V{\cdot}s^{-1}$, N = 600 rpm.

The mixed-valence $Cu^{II}Cu^{I}$-semiquinone species was also found to form upon treating the solution of the dicopper(I) complex $\mathbf{2}^{2+}$ (0.5 mM) with one molar equivalent of DTBQ under anaerobic conditions. In contrast to the slow reaction of $\mathbf{1}^{2+}$ with $DTBCH_2$, upon reaction of $\mathbf{2}^{2+}$ with the quinone the redox process occurs immediately, precluding the determination of the reaction rate constant. Upon exposing the resulting solution to dioxygen, the characteristic bands of semiquinone at 389 nm and 760 nm

gradually diminish, with an isosbestic point at 460 nm, indicating its oxidation by dioxygen. Accordingly, the radical signal in the EPR spectrum disappears, and an increase of the absorption at 400 nm in the UV-Vis spectrum indicates the formation of the quinone. The iodometric H_2O_2 assay test in the presence of lactoperoxidase indicates that this process is accompanied by the formation of one equivalent of dihydrogen peroxide as a side product.

8.2.6.4 Mechanisms *vs.* a coordination mode of the substrate

Based on the results reported above it is possible to suggest the mechanism of catechol oxidation by $\mathbf{1}^{2+}$, as depicted in Figure 8.17. The catalytic cycle starts with the anaerobic oxidation of $DTBCH_2$ by $\mathbf{1}^{2+}$; however, in contrast to the natural enzyme behavior,[13,17] only one electron is transferred in the stoichiometric reaction between the complex and the substrate, leading to the formation of the mixed-valenced $Cu^{II}Cu^{I}$-semiquinone species. This observation is rather interesting, as the formation of a semiquinone radical as an intermediate species in catechol oxidation has been earlier proposed and/or observed in only a few cases.[10,14,18,19] In most cases, such species was formed upon reaction of catechol with mononuclear[19] or dinuclear[10] Cu^{II} complexes generated by self-assembly of two mononuclear units. In the present case, however, $\mathbf{1}^{2+}$ is essentially dinuclear in solution; nevertheless, the second copper(II) ion does not participate in the redox process, playing solely a structural role.

The formed semiquinone radical is further oxidized by dioxygen, as was confirmed by UV-Vis and EPR spectroscopy. According to the earlier mechanistic reports of Kaizer *et al.*[19] and Kodera *et al.*,[10] dioxygen can bind to the Cu^{I} ion forming a Cu^{II}-superoxo species, with the consequent one-electron oxidation of the semiquinone radical leading to the release of quinone and hydrogen peroxide (Figure 8.17, cycle A). However, in the course of the catalytic oxidation of $DTBCH_2$ by $\mathbf{1}^{2+}$ the concentration of H_2O_2 stops increasing after a few minutes, indicating that, most likely, a different mechanism is operating at later stages of the reaction. A proposal about H_2O_2 being consumed in the course of the reaction, as suggested by some authors,[20] does not seem plausible in this case, as the results of kinetic measurements indicate that its presence has virtually no influence on the catalytic cycle, except at unrealistically high concentrations levels, which are never reached during the reaction. Another reason to suggest a different mechanistic pathway operating at later stages of the catalytic oxidation is the inhibiting effect of DTBQ, indicating that the formed quinone does not simply accumulate in the reaction mixture, but obviously also participates in the catalytic process. This effect cannot be explained based on the simple oxidation scheme via the semiquinone formation (cycle A in Figure 8.17).

Consequently, it can be proposed that at later stages of the catalytic reaction, the oxidation of $DTBCH_2$ proceeds by a "classic" mechanism, proposed by Krebs *et al.*[17] and Casella *et al.*,[21,22] involving a stoichiometric reaction between the dicopper(II)

species and the substrate, leading to the reduced dicopper(I) species. The oxidation of the second equivalent of the substrate by a peroxo-dicopper(II) adduct, formed upon dioxygen binding to the dicopper(I) intermediate, results in the formation the second molecule of quinone and water as a by-product (Figure 8.17, cycle B). The inhibiting effect of DTBQ on the catalytic cycle can then be rationalized considering its very fast reaction with the reduced dicopper(I) species (which is the only intermediate species able to react with the quinone), leading to semiquinone formation (Figure 8.17). Thus, at high concentrations, DTBQ competes with dioxygen in the reoxidation of $\mathbf{2}^{2+}$, resulting in the mixed-valenced $Cu^{II}Cu^{I}$ semiquinone species, which is then subsequently oxidized in the less efficient cycle A. Consequently, the concentration of quinone increases more slowly, as only one molecule of DTBQ is produced in cycle A, contrary to cycle B.

On the other hand, when present in high concentration (Figure 8.14), H_2O_2 can compete with dioxygen in the reoxidation of the dicopper(I) complex to the dicopper(II) state, therefore the increase in its concentration results in its progressive involvement as copper(I) oxidant. The increase of the reaction rates in this case can be explained by a change in the rate-determining step of the reaction, as previously proposed by Casella and co-workers.[21]

The change of the catalytic mechanism in the course of the reaction can be explained by proposing that the different mechanistic pathways are directly related to the binding mode of the substrate to the dicopper(II) core. The latter has often been debated in the literature in the past years.[23-27] Up till now, different examples of substrate coordination modes to dicopper(II) complexes have been reported.[23-25] Although the first example of a dicopper(II)-catecholate adduct, crystallized by Karlin,[23] showed the catecholate to be coordinated as a bridging didentate ligand to both dicopper(II) centers, later reports from Casella[24] and Meyer[25] argued for an asymmetric binding of catechol to only one of the two available copper(II) ions in a η^2 fashion, possibly with one of the two oxygen atoms being involved in a weak interaction with either an adjacent copper(II) ion, or in hydrogen bonding. This apparent contradiction can be rationalized by considering that the binding mode of the substrate is to a large extent determined by the distance between the two copper centers and their accessibility. Thus, the short metal-metal distance promotes a binding of the catecholate in a didentate bridging fashion (*e.g.* in the dicopper(II)-catecholate adduct reported by Karlin[23] two metal ions are kept at a distance of 3.248 Å), whereas in case of long metal-metal separation, a binding of the substrate to only one of the two metal centers occurs. Consequently, in the first case, only one electron can be transferred from the substrate to the metal center, resulting in the semiquinone formation, the subsequent oxidation of which proceeds by the mechanism proposed by Kodera[10] (Figure 8.17, cycle A). In the case of a didentate bridging coordination, both copper ions are reduced in the stoichiometric reaction with the substrate, leading to the quinone formation and the reduced dicopper(I) species, and

the catalytic reaction further proceeds via the mechanism suggested by Krebs *et al.*[17] for the natural enzyme (Figure 8.17, cycle B).

The long Cu1…Cu2 separation (4.5427(18) Å) observed for two copper ions in the macrocyclic unit in $\mathbf{1}^{2+}$ prohibits the substrate binding in a bridging didentate fashion, thus favoring the binding of catechol to only one metal center with semiquinone formation. However, it is liable that in the course of the catalytic reaction the original dicopper(II) core undergoes substantial modification, as the carbonate bridge is likely to be cleaved by the incoming catecholate, as proposed in Figure 8.17. Earlier studies on other dicopper complexes with structurally related macrocyclic ligands[2,28] indicate that the macrocyclic cavity has a sufficient flexibility to bring two copper ions on a short distance, required for a didentate bridging coordination mode of catechol. As a result, in the absence of the rigid carbonate bridge the substrate can bind to both copper(II) ions in a bridging fashion, pushing the catalytic reaction towards the cycle B, whereas the relative influence of mechanistic pathway A becomes negligible after a few minutes of the reaction.

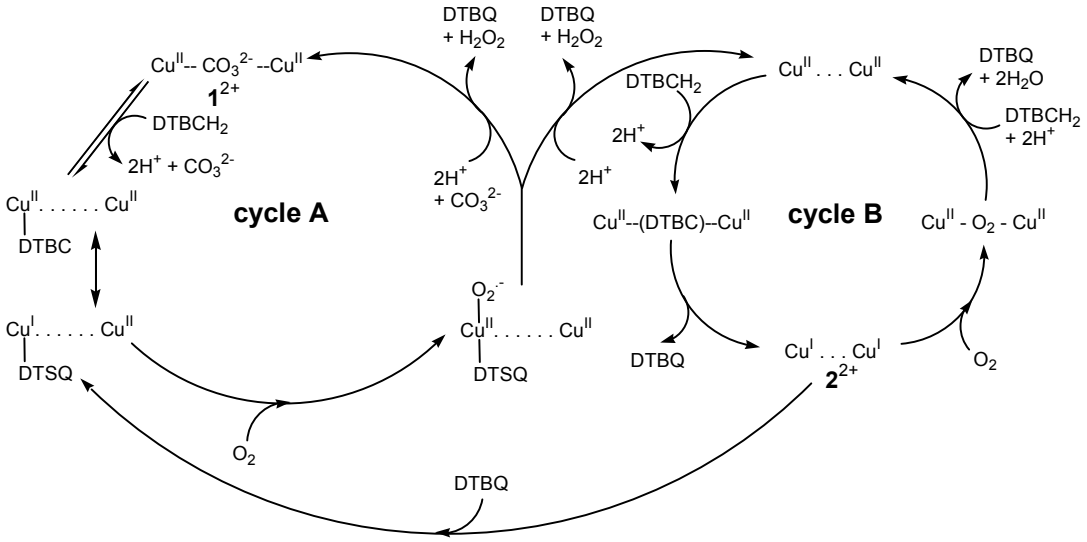

Figure 8.17. The proposed mechanism for the catalytic catechol oxidation by $\mathbf{1}^{2+}$.

8.3 Concluding remarks

It is very interesting to compare the catalytic behavior of $\mathbf{1}^{2+}$ with earlier reported examples of synthetic models of catechol oxidase. The metal-metal distance in the dicopper(II) core of $\mathbf{1}^{2+}$ exceeds 4.5 Å and is thus much longer than the usual range found in catalytically active copper(II) compounds (2.9-3.5 Å). However, $\mathbf{1}^{2+}$ still exhibits catecholase activity, proving that a large copper-copper separation does not inhibit the catalytic properties. Furthermore, the results give an answer to the question, whether the binding of the substrate to the dicopper core includes a bridging catecholate coordinated to the two copper ions[29] rather than a monodentate coordination to only one

metal center,[13] demonstrating that in fact both options are possible. It is also clear that different binding modes of the substrate to a dicopper(II) core result in completely different mechanisms of catechol oxidation by dicopper(II) complexes; furthermore, in case of sufficiently flexible ligands, both mechanistic pathways can be realized.

In addition, a possible mechanism for the formation of dihydrogen peroxide is now established. Previously, it has been suggested that the formation of dihydrogen peroxide is the result of either the protonation of the peroxo-dicopper intermediate, or its reaction with catechol, leading to the formation of the reduced dicopper(I) species along with H_2O_2.[22,25,30] However, no actual proof that either of these pathways indeed takes place has been reported, although the formation of dihydrogen peroxide upon treating trans-μ-1,2-peroxo-dicopper(II) species with a strong acid is well-known.[31,32] Consequently, it can be assumed that dihydrogen peroxide is formed as a by-product during the oxidation of the semiquinone intermediate with dioxygen, when the metal-metal distance within a dicopper(II) complex is too long to allow the binding of the substrate in a didentate bridging fashion. Indeed, Meyer and co-workers reported a recovery of 58% to 71% of dihydrogen peroxide for a series of dicopper(II) complexes,[25] for which an asymmetric coordination mode of a non-reactive catechol to only one of the copper(II) centers has been clearly established. In addition, two other crystallographically characterized dicopper(II) complexes with essentially dinucleating ligands, for which the reduction mode of dioxygen to dihydrogen peroxide has been definitely established, also possess a large metal-metal separation (3.7 Å and 7.8 Å).[12]

It thus appears that the mechanism of catechol oxidation by the model compounds is very intricate, which obviously explains often contradictory literature reports on the catalytic behavior of copper(II) complexes. It is also very interesting to note that some authors have recently reported the formation of dihydrogen peroxide,[33] as well as semiquinone radicals,[34] during the catalytic oxidation of DOPA by the structurally related enzyme tyrosinase in haemolymph of some insects. Although it appears that neither of these species has ever been observed during the substrate oxidation by catechol oxidase, the question about the possibility of two different catechol oxidation pathways for the natural enzyme, as found for model compounds, still needs to be answered.

8.4 Experimental Section

8.4.1 Materials and Methods

All starting materials were commercially available and used as purchased, unless stated otherwise. The macrocyclic ligand [22]pr4pz was synthesized as previously described.[2] The single crystals of $[H_2[22]pr4pz](ClO_4)_2$ suitable for X-ray crystal structure determination were obtained by diethyl ether diffusion into a methanol solution containing one equivalent of [22]pr4pz and two equivalents of perchloric acid.

The ligand field spectra in solution were recorded on a Varian Cary 50 Scan UV-Vis spectrophotometer and on a Zeiss MCS500 Diode-Array Spectrometer (l = 0.5 cm). X-band electron paramagnetic resonance (EPR) measurements were performed on a Bruker ESP 300E spectrometer equipped with a Bruker nitrogen flow cryostat, or on a Bruker EMX spectrometer equipped with an ESR 900 helium flow cryostat (Oxford Instruments). The electrochemical behavior of the complexes was investigated in a 0.1 M solution of tetra-*n*-butylammonium perchlorate (TBAP) or tetra-*n*-butylammonium triflate in methanol using a EGG 273 potentionstat coupled with a Kipp&Zonen x-y recorder. The experiments were performed at room temperature in a three-compartment cell. Potentials are referred to an Ag/10 mM $AgNO_3$ + CH_3CN + 0.1 M TBAP reference electrode. The working electrode was a platinum disk of 5 mm diameter. The working electrode was polished with 1 μm diamond paste prior to each recording. C, H, N, S determinations were performed on a Perkin Elmer 2400 Series II analyzer. ESI-mass spectra in methanol or acetonitrile were recorded on a Bruker Esquire 300 apparatus.

8.4.2 Synthesis of the coordination compounds

$[Cu_2([22]pr4pz)(CO_3)(H_2O)]_2(CF_3SO_3)_4{\cdot}2CH_3CN{\cdot}4H_2O$ ($(1)_2(CF_3SO_3)_4{\cdot}2CH_3CN{\cdot}4H_2O$): Copper(II) triflate (36.9 mg, 0.10 mmol) was dissolved in 5 ml of acetonitrile, and the resulting solution was added to a suspension of the ligand [22]pz4pz (25 mg, 0.05 mmol) in the same solvent (the ligand does not dissolve, unless coordinated to the metal ions). To the resulting clear blue solution, a solution of anhydrous Na_2CO_3 (5.4 mg, 0.05 mmol) in a minimal amount of water was added. The small amount of precipitate, most likely basic copper carbonate, which may form, was filtered off. Diethyl ether diffusion into the resulting greenish-blue solution led to the appearance of small blue crystals which were found to be of a sufficient quality for X-ray single crystal structure determination. Elemental analysis, found (calc.) for $[Cu_2([22]pr4pz)(CO_3)(H_2O)]_2(CF_3SO_3)_4{\cdot}2CH_3CN{\cdot}4H_2O$ (=$C_{62}H_{94}N_{22}O_{24}F_{12}S_4Cu_4$): C, 35.1 (34.8); H, 4.6 (4.4); N, 14.4 (14.4). ESI-MS, CH_3OH: *m/z*: z = 1, 1801 $[[Cu_2([22]pr4pz)(CO_3)]_2(CF_3SO_3)_3]^+$, z = 2, 827 $[[Cu_2([22]pr4pz)_2(CO_3)](CF_3SO_3)]^{2+}$.

$[Cu_2([22]pr4pz)(CH_3CN)_2](ClO_4)_2$ ($2(ClO_4)_2$): In a glove box, a solution of $[Cu(CH_3CN)_4]ClO_4$ (13.1 mg, 0.04 mmol) in 2 ml of dry methanol was added to a solution of [22]py4pz (9.8 mg, 0.02 mmol) in the same solvent. The diffusion of diethyl ether into the resulting solution led to the appearance of very small colorless crystals, suitable for X-ray diffraction analysis. The complex is easily oxidized and can only be stored in a dry glove box atmosphere. ^{1}H NMR (CD_3OD, 300 MHz, 25 ºC, TMS, ppm): δ = 7.72 (d, ^{3}J(H,H) = 2 Hz, 4H, 5'H-pz), 6.32 (d, ^{3}J(H,H) = 2 Hz, 4H, 4'H-pz), 4.87 (s, 8H, pz-(CH_2)$_2$-pz), 3.65 (s, 4H, N-CH_2-pz), 2.65 (t, ^{3}J(H,H) = 8 Hz, 4H, N-CH_2-C_2H_5), 1.50 (m, 4H, N-CH_2-CH_2-CH_3), 0.86 (t, ^{3}J(H,H) = 7 Hz, 6H, N-C_2H_5-CH_3) ppm. ESI-MS (CH_3CN) *m/z*: z = 1, $[[Cu_2([22]py4pz)]ClO_4]^+$ = 717.

8.4.3 Catecholase activity studies

The catecholase activity of $\mathbf{1}^{2+}$ was evaluated by reaction with 3,5-di-*tert*-butylcatechol at 25 ºC in methanol. The absorption at 400 nm (ε = 1400 $M^{-1}\cdot cm^{-1}$), characteristic of the formed quinone, was measured as a function of time. The experiments were run under a 1 atm of dioxygen. The kinetic parameters were determined for 2×10^{-5} M solutions of the complex (for simplicity, the complex concentration has been calculated based on the molecular weight of the dinuclear species $[Cu_2([22]pr4pz)(CO_3)(H_2O)](CF_3SO_3)_2\cdot CH_3CN\cdot 2H_2O$) and 0.05-3 mM solutions of the substrate. In a typical catalytic experiment, 2.5 ml of the solution of $\mathbf{1}^{2+}$ were placed in a 1 cm path-length cell, and the solution was saturated with dioxygen. Afterwards, 75 μl of the solution of substrate were added. After thorough shaking, the changes in UV-Vis spectra were recorded during 30 min.

8.4.4 Effect of dihydrogen peroxide on the kinetics of $DTBCH_2$ oxidation

The effect of dihydrogen peroxide on the reaction rates was studied in dioxygen-saturated methanol by varying the concentration of H_2O_2 in the range of 0.01–1 mM at constant concentrations of the complex (2×10^{-5} M) and $DTBCH_2$ (1 mM).

8.4.5 Effect of DTBQ on the kinetics of $DTBCH_2$ oxidation

The effect of DTBQ on the reaction rates was studied in dioxygen-saturated methanol by varying the concentration of DTBQ in the range of 0.01–0.412 mM at constant concentrations of the complex and $DTBCH_2$. The concentration of $\mathbf{1}^{2+}$ was 2×10^{-5} M, the concentration of $DTBCH_2$ 0.2 mM and 1 mM.

8.4.6 Detection of dihydrogen peroxide in the catalytic $DTBCH_2$ oxidation

The presence of dihydrogen peroxide in the reaction mixture was analyzed using the iodometric assay based on I_3^-, which has a characteristic absorption band at 353 nm (ε = 26000 $M^{-1}\cdot cm^{-1}$ in water). The oxidation reaction of $DTBCH_2$ by $\mathbf{1}^{2+}$ was carried out as described in the kinetic experiment. When the formation of quinone reached a desired value at 400 nm the solution was acidified with H_2SO_4 to pH 2 to stop the reaction. 3 ml of water was added and the reaction mixture was then extracted two times with CH_2Cl_2 to remove the formed DTBQ. To a 2 ml aliquot of the aqueous layer 1 ml of a KI solution (0.3 M) was added with a catalytic amount of lactoperoxidase to accelerate the formation of I_3^-. Blank experiments were performed under identical conditions in the presence of DTBQ and $\mathbf{1}^{2+}$, but only minor formation of I_3^- was observed.

8.4.7 X-ray crystallographic studies

X-ray intensities of $[H_2[22]pr4pz](ClO_4)_2$ were measured on Nonius KappaCCD diffractometer with rotating anode and graphite monochromator (λ = 0.71073 Å). The structure was solved with direct methods (SHELXS97[35]) and refined with SHELXL97[36] against F^2 of all reflections. $[C_{26}H_{40}N_{10}](ClO_4)_2$, Fw = 691.58, colorless/yellowish block (0.09×0.18×0.27 mm^3), monoclinic, space group *P2₁/c* (no. 14), a = 8.0611(14) Å, b = 11.660(2) Å, c = 17.306(3) Å, $\alpha = \gamma = 90°$, β = 96.557(16)°, V = 1615.9(5) $Å^3$, Z = 2, $\rho_{calc.}$ = 1.421 $g \cdot cm^{-3}$, μ = 0.264 mm^{-1}. A total of 23591 reflections, of which 3002 were independent [R(int) = 0.063], were collected in the range $2.1 \leq 2\theta \leq 25.5°$.Non-hydrogen atoms were refined freely with anisotropic displacement parameters. All hydrogen atoms were located in the difference Fourier map. The N-H hydrogen atom was refined freely with isotropic displacement parameters; C-H hydrogen atoms were refined with a riding model. Geometry calculations and checking for higher symmetry were performed with the PLATON package.[37]

X-ray intensities of compound $(\mathbf{1})_2(CF_3SO_3)_4 \cdot 2CH_3CN \cdot 4H_2O$ were measured on a Bruker AXS Apex diffractometer with a graphite monochromator. The structure was solved with direct methods (SHELXS97)[35] and the refinement was performed with SHELXL97[36] against F^2 of all reflections. Molecular illustrations, checking for higher symmetry and geometry calculations were performed with the PLATON package.[37] The entries for formula weight, density, F(000) and μ of complex are based on the formula $C_{54}H_{76}Cu_4N_{20}O_8(CF_3O_3S)_4 \cdot 2(C_2N) \cdot 4(O)$, which does not contain the hydrogen atoms of the solvent molecules. Fw = 2123.85, blue block (0.25×0.40×0.21 mm^3), monoclinic, space group *P21/n*, a = 18.716(5) Å, b = 15.043(5) Å, c = 32.110(5) Å, $\alpha = \gamma = 90°$, β = 103.118(5)°, V = 8804(4) $Å^3$, Z = 4, $\rho_{calc.}$ = 1.602 $g \cdot cm^{-3}$, μ = 1.156 mm^{-1}. A total of 25022 reflections, of which 8021 were independent [R(int) = 0.177], were collected in the range $1.3 \leq 2\theta \leq 25.9°$. The hydrogen atoms of the complex cation were calculated on idealized positions using a riding model with isotropic displacement parameters. The hydrogen atoms of the co-crystallized solvent molecules were not calculated. All non-hydrogen atoms were refined anisotropically. Final cycle refinement converged to R(F) = 0.0705 and *wR2* = 0.2007 (all reflections).

Due to sensitivity of $\mathbf{2}(ClO_4)_2$ towards dioxygen, the crystal was dropped into grease and then quickly frozen at 150 K on the Bruker AXS-Enraf-Nonius Kappa-CCD diffractometer using a graphite monochromator (λ (MoKα) : 0.71073Å). The crystal was twinned and the two components were separated using the EvalCCD software package with the following twin law [1 -0.65 -0.32, 0 -1 0, 0 0 -1] corresponding to a two fold axis along the [1 0 0] direction. The structure was solved by direct methods and refined by full matrix least-squares, based on F^2 from the HKLF5 file using the SHELXL97 software[36] through the WinGX program.[38] The fractional contributions of two domains were refined and are 0.737(1), 0.263(1). $[C_{30}H_{44}N_{12}Cu_2]Cl_2O_8$, Fw =

898.75, colorless block (0.50×0.32×0.16 mm^3), triclinic, space group $P\overline{1}$ (no. 2), a = 11.079(3) Å, b = 11.825(4) Å, c = 17.329(5) Å, α = 87.10(2)°, β = 74.92(2)°, γ = 68.81(2)°, V = 2041.5(11) $Å^3$, Z = 2, $\rho_{calc.}$ = 1.462 $g \cdot cm^{-3}$, μ = 1.233 mm^{-1}. A total of 38986 reflections, of which 10797 were independent, were collected in the range $1.22 \leq 2\theta \leq 30.11°$. All non-hydrogen atoms were refined with anisotropic thermal parameters. Hydrogen atoms were generated in idealized positions, riding on the carrier atoms, with isotropic thermal parameters. Final cycle refinement converged to $R(F) = 0.0591$ and $wR2 = 0.1632$ (all reflections).

8.5 References

(1) Koval, I. A.; Belle, C.; Selmeczi, K.; Philouze, C.; Saint-Aman, E.; Schuitema, A. M.; Gamez, P.; Pierre, J.-L.; Reedijk, J. *J. Biol. Inorg. Chem.* **2005**, *10*, 739-750.
(2) Schuitema, A. M.; Aubel, P. G.; Koval, I. A.; Engelen, M.; Driessen, W. L.; Reedijk, J.; Lutz, M.; Spek, A. L. *Inorg. Chim. Acta* **2003**, *355*, 374-385.
(3) Schuitema, A. M. Ph.D. thesis, Leiden University, 2004.
(4) Addison, A. W.; Rao, T. N.; Reedijk, J.; van Rijn, J.; Verschoor, G. C. *J. Chem. Soc., Dalton Trans.* **1984**, 1349-1356.
(5) Chiari, B.; Piovesana, O.; Tarantelli, T.; Zanazzi, P. F. *Inorg. Chem.* **1993**, *32*, 4834-4838.
(6) van den Brenk, A. L.; Byriel, K. A.; Fairlie, D. P.; Gahan, L. R.; Hanson, G. R.; Hawkins, C. J.; Jones, A.; Kennard, C. H. L.; Moubaraki, B.; Murray, K. S. *Inorg. Chem.* **1994**, *33*, 3549-3557.
(7) van Albada, G. A.; Mutikainen, I.; Roubeau, O.; Turpeinen, U.; Reedijk, J. *Inorg. Chim. Acta* **2002**, *331*, 208-215.
(8) van Albada, G. A.; Mutikainen, I.; Roubeau, O. S.; Turpeinen, U.; Reedijk, J. *Eur. J. Inorg. Chem.* **2000**, 2179-2184.
(9) Chyn, J.-P.; Urbach, F. L. *Inorg. Chim. Acta* **1991**, *189*, 157-163.
(10) Kodera, M.; Kawata, T.; Kano, K.; Tachi, Y.; Itoh, S.; Kojo, S. *Bull. Chem. Soc. Jpn.* **2003**, *76*, 1957-1964.
(11) Balla, J.; Kiss, T.; Jameson, R. F. *Inorg. Chem.* **1992**, *31*, 58-62.
(12) Selmeczi, K.; Reglier, M.; Giorgi, M.; Speier, G. *Coord. Chem. Rev.* **2003**, *245*, 191-201.
(13) Eicken, C.; Krebs, B.; Sacchettini, J. C. *Curr. Opin. Struct. Biol.* **1999**, *9*, 677-683.
(14) Thompson, J. S.; Calabrese, J. C. *Inorg. Chem.* **1985**, *24*, 3167-3171.
(15) Benelli, C.; Dei, A.; Gatteschi, D.; Pardi, L. *Inorg. Chem.* **1990**, *29*, 3409-3415.
(16) Stallings, M. D.; Morrison, M. M.; Sawyer, D. T. *Inorg. Chem.* **1981**, *20*, 2655-2660.
(17) Klabunde, T.; Eicken, C.; Sacchettini, J. C.; Krebs, B. *Nat. Struct. Biol.* **1998**, *5*, 1084-1090.
(18) Thompson, J. S.; Calabrese, J. C. *J. Am. Chem. Soc.* **1986**, *108*, 1903-1907.
(19) Kaizer, J.; Pap, J.; Speier, G.; Parkanyi, L.; Korecz, L.; Rockenbauer, A. *J. Inorg. Biochem.* **2002**, *91*, 190-198.
(20) Neves, A.; Rossi, L. M.; Bortoluzzi, A. J.; Szpoganicz, B.; Wiezbicki, C.; Schwingel, E.; Haase, W.; Ostrovsky, S. *Inorg. Chem.* **2002**, *41*, 1788-1794.
(21) Monzani, E.; Quinti, L.; Perotti, A.; Casella, L.; Gulotti, M.; Randaccio, L.; Geremia, S.; Nardin, G.; Faleschini, P.; Tabbi, G. *Inorg. Chem.* **1998**, *37*, 553-562.
(22) Monzani, E.; Battaini, G.; Perotti, A.; Casella, L.; Gullotti, M.; Santagostini, L.; Nardin, G.; Randaccio, L.; Geremia, S.; Zanello, P.; Opromolla, G. *Inorg. Chem.* **1999**, *38*, 5359-5369.
(23) Karlin, K. D.; Gultneh, Y.; Nicholson, T.; Zubieta, J. *Inorg. Chem.* **1985**, *24*, 3725-3727.
(24) Plenge, T.; Dillinger, R.; Santagostini, L.; Casella, L.; Tuczek, F. *Z. Anorg. Allg. Chem.* **2003**, *629*, 2258-2265.
(25) Ackermann, J.; Meyer, F.; Kaifer, E.; Pritzkow, H. *Chem. Eur. J.* **2002**, *8*, 247-258.
(26) Börzel, H.; Comba, P.; Pritzkow, H. *Chem. Commun.* **2001**, 97-98.
(27) Torelli, S.; Belle, C.; Hamman, S.; Pierre, J. L.; Saint-Aman, E. *Inorg. Chem.* **2002**, *41*, 3983-3989.
(28) Koval, I. A.; van der Schilden, K.; Schuitema, A. M.; Gamez, P.; Belle, C.; Pierre, J.-L.; Luken, M.; Krebs, B.; Roubeau, O.; Reedijk, J. *Inorg. Chem.* **2005**, *44*, 4372-4382.
(29) Solomon, E. I.; Sundaram, U. M.; Machonkin, T. E. *Chem. Rev.* **1996**, *96*, 2563-2605.
(30) Monzani, E.; Casella, L.; Zoppellaro, G.; Gullotti, M.; Pagliarin, R.; Bonomo, R.; Tabbi, G.; Nardin, G.; Randaccio, L. *Inorg. Chim. Acta* **1998**, *282*, 180-192.

(31) Karlin, K. D.; Ghosh, P.; Cruse, R. W.; Meyer, G. J.; Farooq, A.; Gultneh, Y.; Jacobson, R. R.; Blackburn, N. J.; Strange, R. W.; Zubieta, J. *J. Am. Chem. Soc.* **1988**, *110*, 6769-6780.
(32) Paul, P. P.; Tyeklár, Z.; Jacobson, R. R.; Karlin, K. D. *J. Am. Chem. Soc.* **1991**, *113*, 5322-5332.
(33) Komarov, D. A.; Slepneva, I. A.; Glupov, V. V.; Khramtsov, V. V. *Free Radic. Res.* **2005**, *39*, 853-858.
(34) Slepneva, I. A.; Komarov, D. A.; Glupov, V. V.; Serebrov, V. V.; Khramtsov, V. V. *Biochem. Biophys. Res. Commun.* **2003**, *300*, 188-191.
(35) Sheldrick, G. M.; *SHELXS-97, Program for crystal structure solution*. University of Göttingen, Germany, 1997
(36) Sheldrick, G. M.; *SHELXL-97, Program for the refinement of crystal structures*. University of Göttingen, Germany, 1997
(37) Spek, A. L. *J. Appl. Cryst.* **2003**, *36*, 7-13.
(38) Farrugia, L. J. *J. Appl. Cryst.* **1999**, *32*, 837-838.

9 Summary, general discussion and outlook

9.1 General

The research described in this thesis deals with the synthesis of copper(II) complexes which can be regarded as model compounds of the active site of catechol oxidase, and with the mechanism of the catalytic oxidation of catechol mediated by these compounds. Catechol oxidase is a type-3 copper enzyme usually encountered in plants and in some crustaceans, which catalyzes a conversion of a wide range of *o*-diphenols (catechols) to the respective *o*-benzoquinones. These highly reactive compounds subsequently auto-polymerize, resulting in the formation of a dark pigment melanin, which is thought to protect a damaged tissue from pathogens.

In Chapter 1 a general overview of the model compounds of catechol oxidase, reported in the literature, is given, and the different approaches used by various authors to study the mechanism of the catalytic reaction are discussed. The general overview of the recognized types of copper proteins and the detailed description of the crystal structure of catechol oxidase, as well as the proposed mechanisms of the enzymatic cycle are also presented in this chapter.

Chapters 2, 4 and 5 deal with the preparation of novel dinucleating phenol-based ligands, designed to mimic certain peculiar features of the active site of the enzyme, *e.g.* the asymmetric surroundings of the two copper ions and the unusual thioether bond in a close proximity to one of the metal centers. The structures and properties of the Cu^{II} complexes with these ligands are also reported in these chapters. In Chapter 3 the structures, spectroscopic and magnetic properties of several Cu^{II}, Mn^{II} and Co^{II} complexes with the phenol-based ligand Hpy2ald, containing pyridine and formyl functions, which has been prepared as an intermediate synthon in the preparation of asymmetric phenol-based ligands, are presented.

In Chapters 6-8 the structures of Cu^{II} and Cu^{I} complexes with two N-donor macrocyclic ligands [22]py4pz and [22]pr4pz, which provide respectively two N_4 and two N_3 donor sets for the metal coordination are presented, and the mechanisms of the catechol oxidation by the copper(II) complexes with these ligands are discussed. Chapter 6 also describes detailed paramagnetic ^1H NMR spectroscopic studies on the hydroxo-bridged dicopper(II) complex with the macrocyclic ligand [22]py4pz.

9.2 Cu^{II}, Co^{II} and Mn^{II} complexes with the phenol-based ligands

The ability of dinucleating phenol-based ligands to bind simultaneously two metal centers, keeping them in a close proximity thanks to the presence of a bridging phenolate group, gave rise to an extensive utilization of in this class of ligands to model bimetallic biosites.[1-7] In this thesis, the syntheses of four novel phenol-based ligands (Figure 9.1) are reported, and the structures and properties of seven Cu^{II}, two Co^{II} and two Mn^{II} complexes with these ligands are discussed.

In Chapter 2 the synthesis of the dinucleating phenol-based ligand Hpy3asym (Figure 9.1, a), which was designed to mimic the asymmetric surrounding of the two copper ions in the active site of catechol oxidase, are reported. This ligand contains one tridentate and one didentate arm attached to the 2 and 6 positions of the phenolic ring in order to achieve a coordination number asymmetry in its dicopper(II) complexes. The developed strategy for the synthesis of this ligand can also be successfully applied to generate other asymmetric phenol-based ligands, as discussed elsewhere.[8]

A dinuclear copper(II) nitrate complex with Hpy3asym $[Cu_2(py3asym)(H_2O)_{1.5}(NO_3)_{2.5}](NO_3)_{0.5}$ shows a donor-atom asymmetry that consists of a N_3O_3 donor set for the Cu1 ion and a N_2O_4 donor set for the Cu2 ion. Both Cu^{II} ions adopt a distorted octahedral surrounding, completed by the donor atoms of the solvent molecules and the nitrate counter ions, besides the donor atoms provided by the ligand. The absence of an exogenous bridging ligand in this complex results in a relatively long metal-metal separation of 3.9003 Å.

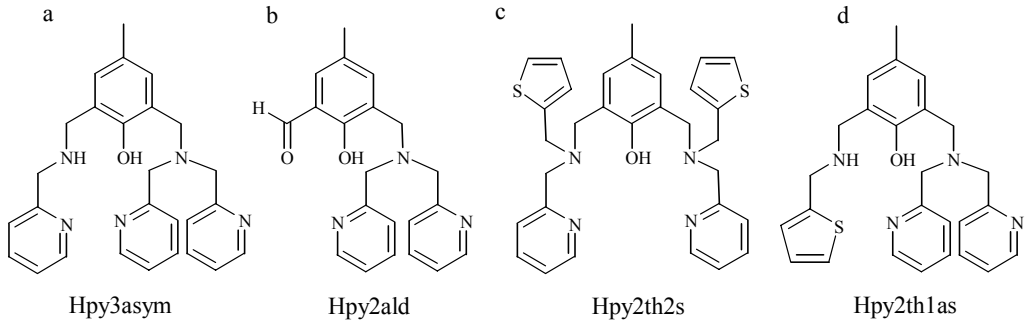

Figure 9.1. Schematic representation of the prepared phenol-based ligands.

Chapter 3 reports the structures and properties of six novel complexes of Cu^{II}, Co^{II} and Mn^{II} with the phenol-based ligand Hpy2ald (Figure 9.1, b), containing a tridentate pyridine-containing arm and a formyl group in two *ortho* positions with respect to the phenol group of the aromatic ring. Due to the presence of a weak donor formyl group in the ligand, the structures of the resulting complexes were found to depend strongly on the donor properties of the counter ions. Thus, the use of metal salts with weakly coordinating anions like perchlorate and tetrafluoroborate (*i.e.* $Co(ClO_4)_2{\cdot}6H_2O$, $Co(BF_4)_2{\cdot}6H_2O$ and $Mn(ClO_4)_2{\cdot}6H_2O$) leads to the formation of

dinuclear complexes with a metal to ligand ratio of 2:2, in which two metal ions are doubly bridged by two oxygen atoms of the deprotonated phenol groups of two different ligands. The metal ions have a distorted octahedral (Co^{II}) or trigonal prismatic (Mn^{II}) surrounding, with the remaining positions in the coordination sphere being occupied by three nitrogen donor atoms of one ligand and the oxygen atom of the formyl group of another ligand. The obtained complexes are thus structurally related to the nickel(II) complexes earlier reported by Adams[9] resulting from the hydrolysis of the imine arm of the original dinucleating phenol-based ligands during their reaction with Ni^{II} salts.

The presence of stronger donors, such as nitrate, bromide or chloride, prevents the coordination of the weaker donor formyl group, resulting in metal complexes of quite different structures. Thus, the reaction of manganese(II) chloride and copper(II) bromide with Hpy2ald leads to the isolation of the complexes $[Mn(Hpy2ald)Cl_2]$ and $[Cu(Hpy2ald)Br_2]\cdot 0.5H_2O$. In these complexes, the phenol group of the ligand remains protonated, failing to bridge two metal ions and instead being semi-coordinated to only one of them. The coordination environment around the metal center in both complexes is a distorted octahedron, constituted by three nitrogen donor atoms from the pendant arm of the ligand, two halogen anions and a loosely bound oxygen atom of the phenol group. The reaction of copper(II) nitrate with the ligand results in the formation of the complex $[Cu_2(py2ald)(\mu\text{-}NO_3)(NO_3)_2]\cdot CH_3CN$ with a metal to ligand ratio of 2:1. Two copper ions in the complex are bridged by the oxygen atom of the deprotonated phenol group and one of the nitrate counter ions. One of the two copper(II) ions has an almost ideal square pyramidal N_3O_2 surrounding, whereas the second shows a distorted octahedral O_6 surrounding, in which only one of the oxygen atoms is provided by the ligand, whereas the other five originate from three nitrate counter ions. Similarly to the copper(II) bromide and manganese(II) chloride complexes, the formyl group of the ligand remains uncoordinated to the metal centers.

In Chapter 4 the preparation of the symmetric phenol-based ligand Hpy2th2s (Figure 9.1, c) containing pyridine and thiophene functions is described. This ligand was designed to mimic the presence of the unusual thioether bond at the active site of catechol oxidase, resulting in the presence of a non-coordinated sulfur atom in the close proximity of one of the metal centers. In the case of Hpy2th2s, the very weak donor properties of the thiophene sulfur atoms prevent their coordination to the copper ions. Two copper(II) complexes with this ligand have been prepared and structurally, spectroscopically and magnetically characterized, *viz.* $[Cu_2(py2th2s)(\mu\text{-}Cl)Cl_2]$ and $[Cu_2(py2th2s)(\mu\text{-}Br)Br_2]$. In these complexes, both copper(II) ions are pentacoordinated and doubly bridged by the oxygen atom of the deprotonated phenol group and a halogen anion. The remaining positions in the metal coordination sphere are occupied by two nitrogen atoms provided by the pendant arms of the ligand and the remaining halogen atom. The magnetic susceptibility studies indicate a moderate antiferromagnetic coupling between the copper(II) ions in both complexes. The complexes do not exhibit

catecholase activity, most likely owing to the presence of the strongly coordinated halogen anions as bridging ligands between the metal centers. The studies on the interaction of these complexes with the model substrate tetrachlorocatechol (TCC) indicate that the bridging ligands indeed cannot be replaced by the incoming catecholate, although in the case of the chloride complex, one of the apical halogen anions undergoes a substitution with TCC. These results emphasize the importance of the bridging ligands on the catecholase activity of the dicopper(II) complexes, as the ability of these ligands to be displaced by the substrate is one of the crucial demands for the catalytic activity.

In Chapter 5, the synthesis of the asymmetric phenol-based ligand Hpy2th1as (Figure 9.1, d), containing a thiophene ring on one of the pendant arms, is reported. Two copper(II) complexes with this ligand, *viz.* $[Cu_2(H_2py2th1as)Cl_2](CuCl_4)_2$ and $[Cu_2(H_2py2th1as)Cl_2](ClO_4)_4 \cdot 6CH_3OH$, have been isolated and structurally characterized. The structures of the complex cations in the two complexes are very similar. Surprisingly, the secondary amine atom of one of the pendant arms undergoes a protonation during the crystallization with copper(II) salts, which prevents it from binding to the metal centers. Furthermore, the phenol group of the ligand remains protonated, similarly to the copper(II) bromide and manganese(II) chloride complexes with the ligand Hpy2ald. As a result, the metal to ligand ratio in the complexes is 2:2, with two metal ions being doubly bridged by two chloride anions. The thiophene rings remain uncoordinated; however, in the tetrachlorocuprate(II) complex they are involved in unusual stabilizing π-stacking interactions with the bridging chloride anions. Despite the large similarities between the two compounds, the major difference being different counter ions, the two coordination compounds exhibit significantly different structural arrangements, showing the important influence of the anion on the crystal packing.

The dimeric core in both complexes dissociates in solution, resulting in the mononuclear $[Cu(H_2py2th1as)Cl]^{2+}$ species. The complexes do not exhibit catecholase activity, although one equivalent of quinone is formed as a result of a stoichiometric reaction between 3,5-di-*tert*-butylcatechol ($DTBCH_2$) and the copper(II) tetrachlorocuprate complex. The absence of catalytic activity is, however, not surprising, since the complexes are essentially mononuclear in solution, which makes them less suitable models of the dinuclear active site of catechol oxidase.

9.3 Cu^{II} and Cu^{I} complexes with dinucleating macrocyclic ligands: structures and properties

Chapters 2, 4 and 5 of this thesis are devoted to the design of new phenol-based ligands in order to mimic the coordination surroundings of the metal centers in the active site of catechol oxidase. Nevertheless, these ligands have a few shortcomings, such as the presence of a phenol group, which, although beneficial in keeping two metal

ions at a short distance from each other, provides an additional oxygen donor atom for the metal coordination spheres. Because the presence of a single hydroxide ligand between the copper(II) centers was proposed for the natural enzyme,[10] the presence of an additional bridging group is therefore superfluous. Furthermore, the poor ability of the phenolate group to bridge two copper(I) centers makes the isolation of the reduced dicopper(I) complexes with such ligands nearly impossible, and it appears that dinuclear Cu^{I} complexes containing bridging phenolate groups have never been structurally characterized.

In addition, the preparation of metal complexes with phenol-based ligands requires a careful control of the pH of the solution, as an unexpected protonation of the pendant arms of the ligands may possibly occur, yielding complexes with unpredictable structural features.

Therefore in Chapters 6-8 the attention has been turned to the synthesis and characterization of dicopper(II) and dicopper(I) complexes with dinucleating macrocyclic ligands [22]py4pz and [22]pr4pz, which are shown in Figure 9.2. These ligands have been designed earlier to mimic the coordination surroundings of the copper centers in the active site of the structurally related type-3 copper protein hemocyanin.[11,12]

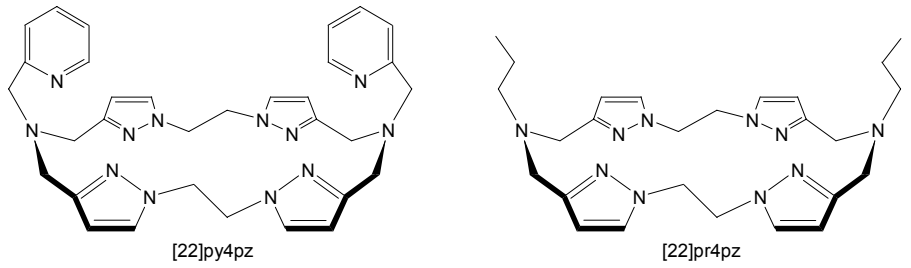

Figure 9.2. Schematic representation of the macrocyclic ligands [22]py4pz and [22]pr4pz.

In Chapter 6 the synthesis, spectroscopic and magnetic properties of the hydroxo-bridged dicopper(II) complex $[Cu_2([22]py4pz)(\mu\text{-}OH)](ClO_4)_3 \cdot H_2O$, as well as the paramagnetic ^1H NMR studies on this complex, are presented. The copper(II) ions in the complex are in a distorted trigonal bipyramidal surrounding, constituted by four nitrogen atoms of the ligand and the oxygen atom of the bridging hydroxide anion, with the oxygen atom and the nitrogen atom of the tertiary amine group of the ligand occupying the apical positions. A large Cu-O-Cu angle of 156.0(3)° results in a very strong antiferromagnetic coupling ($2J$ = -691(35) cm^{-1}) between the two metal ions, allowing the solution study of the complex by ^1H NMR spectroscopy. The complex shows an anti-Curie type behavior, with resonances in the spectrum shifting downfield when increasing the temperature. A complete assignment of the hyperfine-shifted signals was achieved by applying ^1H 1D NOE difference and 2D COSY NMR spectroscopy, through the determination of the relaxation times and by a selective chemical substitution. Temperature-dependent NMR studies were also used for an independent determination of the antiferromagnetic coupling constant $2J$ in solution,

and the obtained value was found to be in a very good agreement with the one obtained from the solid-state magnetic susceptibility measurements.

In Chapter 7 the 3D structure and properties of the dicopper(I) complex with [22]py4pz, *viz.* $[Cu_2([22]py4pz)](ClO_4)_2 \cdot 2CH_3OH$ are reported. The Cu^I ions in this complex are tricoordinated with a distorted trigonal surrounding, the nitrogen atoms of the tertiary amine groups remaining uncoordinated. At low temperature (-40 °C) in acetonitrile, the complex reacts with dioxygen, leading to the formation of a trans-μ-1,2-peroxo-dicopper(II) complex, which has been characterized by UV-Vis and resonance Raman spectroscopic techniques.

In Chapter 8 the structures and properties of the copper(II) and copper(I) complexes with the macrocyclic ligand [22]pr4pz are presented. The copper(II) complex exhibits a tetranuclear structure in the solid state, with one macrocyclic unit accommodating two metal ions, bridged by a carbonate anion. Two oxygen atoms of two carbonate anions then doubly bridge two copper centers of two different macrocyclic units, resulting in the complex $[Cu_2([22]pr4pz)(CO_3)(H_2O)]_2(CF_3SO_3)_4 \cdot 2CH_2CN \cdot 4H_2O$. The copper(II) ions have a distorted square-pyramidal environment, with a long intra-macrocyclic copper-copper distance of 4.5427(18) Å. In a diluted methanol solution, the tetranuclear structure dissociates into two dinuclear units, although at high concentrations it is preserved in solution. The magnetic susceptibility studies indicate that a ferromagnetic coupling is realized between the two Cu^{II} ions of one macrocyclic unit through the *syn, syn*-carbonato bridge, while a very weak antiferromagnetic coupling occurs between two copper(II) ions of two different macrocyclic units through the asymmetric di-μ-$O_{carbonate}$ bridge. The dicopper(I) complex $[Cu_2([22]pr4pz)(CH_3CN)_2](ClO_4)_2$ contains two tetracoordinated Cu^I ions, coordinated by three nitrogen donor atoms from the ligand and a nitrogen atom of a coordinated acetonitrile molecule.

9.4 Catecholase activity of Cu^{II} complexes with macrocyclic ligands: mechanisms of the catalytic reaction

The dinuclear complex $[Cu_2([22]py4pz)(\mu\text{-}OH)](ClO_4)_3 \cdot H_2O$ can be regarded as a satisfactory structural model of the active site of catechol oxidase. In particular, the presence of a single hydroxide bridge between the metal centers is an important structural feature of the natural enzyme. As hydroxo-bridged compounds have been previously reported as successful functional models of catechol oxidase, the catecholase activity of the complex has been investigated. The complex indeed catalytically oxidizes $DTBCH_2$ in acetonitrile, the catalytic reaction showing a Michaelis-Menten behavior with $V_{max} = 1.3 \times 10^{-6}$ M·s^{-1} and $K_M = 4.9$ mM.

It is even more important to appraise the mechanism of the substrate oxidation by model complexes in order to understand the mechanism of action of the natural enzyme. Consequently, the mechanism of $DTBCH_2$ oxidation by this complex was investigated by studying separately every step of the catalytic cycle. On the first stage, the stoichiometric reaction of the complex and the substrate in anaerobic conditions leads to the release of one molar equivalent of quinone and the generation of reduced dicopper(I) species. Dioxygen binding to the latter complex results in the formation of a trans-μ-1,2-peroxo-dicopper(II) adduct, which oxidizes a second molecule of catechol, leading to the restoration of the original hydroxo-bridged dicopper(II) core. This reaction was found to proceed in two successive steps: initially, a proton transfer from the substrate to the peroxo core leads to the formation of a highly reactive intermediate, which was assumed to be a hydroperoxo-dicopper(II) species on the basis of the resonance Raman, UV-Vis and EPR spectroscopy. Secondly, the bound catecholate is oxidized by the hydroperoxo moiety, which is accompanied by the reduction of the peroxide to water. The general mechanism of the catalytic reaction closely resembles the mechanism for catechol oxidase earlier proposed by Krebs;[10] however, the structure of the peroxo-dicopper(II) intermediate species most likely differs, as a μ-η^2:η^2 peroxo-dicopper intermediate has been proposed for the natural enzyme. This is also the first example of catechol oxidation by trans-μ-1,2-peroxo-dicopper(II) species.

It is also interesting to note that while trans-μ-1,2-peroxo-dicopper(II) species oxidize catechol to the corresponding quinone (catecholase activity), they do not perform the hydroxylation of the *o*-position of a phenol ring (monophenolase activity), in contrast to μ-η^2:η^2 peroxo-dicopper(II) species. The ability to hydroxylate the *o*-position of phenolic substrates prior to the oxidation of the resulting catechols into quinones is also a major difference between catechol oxidase and a structurally related type-3 copper enzyme tyrosinase. As the exact structure of tyrosinase remains unknown, no acceptable explanation for this difference in behavior of the two enzymes is available; however, it is tempting to speculate that this difference can be caused by the different structures of the peroxo-dicopper(II) intermediates formed in the catalytic reaction.

In Chapter 8 the mechanism of the catecholase activity of the dinuclear copper(II) species $[Cu_2([22]pr4pz)(CO_3)(H_2O)]^{2+}$in methanol is discussed. During the first few minutes of the catalytic reaction, the substrate oxidation is accompanied by the formation of dihydrogen peroxide, which, however, quickly cedes. The anaerobic interaction of the complex with catechol indicates that instead of a two-electron reduction of the dicopper(II) core, leading to the quinone and the dicopper(I) species formation, only one electron is transferred in the stoichiometric reaction, resulting in the formation of the mixed-valence $Cu^{II}Cu^{I}$- semiquinone species. The oxidation of the latter species by dioxygen leads to the formation of one molar equivalent of quinone and one molar equivalent of dihydrogen peroxide. Thus, the complex initially behaves

as a mononuclear copper(II) species, with only one copper ion participating in the redox process, whereas another plays solely a structural role. This is likely to be caused by the long copper-copper separation within a macrocyclic unit, which makes the simultaneous binding of catechol in a didentate bridging fashion to both copper(II) ions impossible.

However, the dihydrogen peroxide formation stops after a few minutes, suggesting that a different mechanism takes place at later stages of the catalytic reaction, most likely similar to the mechanism proposed by Krebs and co-workers for the natural enzyme.[10] This assumption is also confirmed by the inhibiting influence of the oxidation product DTBQ on the catalytic reaction, indicating that it does not simply accumulate in the reaction mixture, but also participates in the catalytic process. As DTBQ is able to react very quickly with the reduced dicopper(I) species, reoxidizing it to the mixed-valence $Cu^{II}Cu^{I}$-semiquinone species, this is a probable cause of its inhibiting behavior. The formation of dicopper(I) species can in turn be only explained by the mechanistic pathway proposed by Krebs and co-workers.[10] Thus, two different mechanistic pathways are realized in this case, proving that the catechol oxidation by model copper(II) complexes can be a very intricate process. The findings also explain the mechanism of dihydrogen peroxide formation as a by-product of catechol oxidation and indicate that the copper-copper distance plays a substantial role in the catalytic mechanism: a short distance enables a binding of catechol in a didentate bridging fashion, resulting in its further oxidation by the mechanism, similar to that observed for $[Cu_2([22]py4pz)(\mu\text{-}OH)](ClO_4)_3 \cdot H_2O$, whereas a long distance results in the binding of catechol to only one of the copper(II) centers with the formation of the semiquinone intermediate and subsequent reduction of dioxygen to dihydrogen peroxide.

9.5 Future outlook

In conclusion, the mechanism of catechol oxidation by model compounds appears to be very intricate, which obviously explains often contradictory literature reports on the catecholase activity of copper complexes. It should also be added that the investigations carried out by different research groups on the structure and function of catechol oxidase is a perfect example of the essential strategy adopted by the chemist of the 21st century. Indeed, such studies inevitably bring in distinct but complementary disciplines of contemporary chemistry, *i.e.* biochemistry, synthetic and inorganic chemistry, and spectroscopy. It is also evident that research on model compounds of natural enzymes is very inspiring for the development of novel bio-inspired efficient catalysts for oxidation reactions. The design of environmentally benign and clear processes for industrial applications is essential for a sustainable development of industrial chemistry. Therefore one should look at how Nature performs bio-transformations in order to find alternatives to the current environmentally unfriendly procedures. In this context, studies of enzymatic syntheses like the one achieved by

catechol oxidase are crucial since effective, selective, and ecologically friendly catalysts may be produced via a biomimetic approach.

As very promising results have been achieved with copper complexes with macrocyclic ligands, future investigations with these compounds are highly desired. In particular, further studies on the influence of the metal-metal distance on the catalytic behavior would be very beneficial to confirm the hypothesis about it being a crucial factor defining the whole catalytic mechanism. It should also be noted that very recently,[13] the monohydroxo-bridged dicopper(II) complex with the macrocyclic ligand [22]pr4pz has been isolated, the structure of which is shown in Figure 9.3. In this complex, two copper(II) ions are kept at a shorter distance of 3.8207(15) Å, comparable with the copper-copper distance in the complex $[Cu_2([22]py4pz)(\mu\text{-}OH)](ClO_4)_3 \cdot H_2O$. The coordination spheres of the metal ions in the complex also strongly resemble the active site of catechol oxidase, as each copper(II) ion is coordinated by three nitrogen donor atoms of the ligand; the loosely bound perchlorate anions are expected to dissociate in solution and be replaced by solvent molecules. It is very interesting to study the mechanism of the catecholase activity of this complex and to compare it with the mechanism of the catalytic reaction for its carbonate-bridged analogue, as well with the mechanism found for the hydroxo-bridged complex with the related macrocyclic ligand [22]pr4pz.

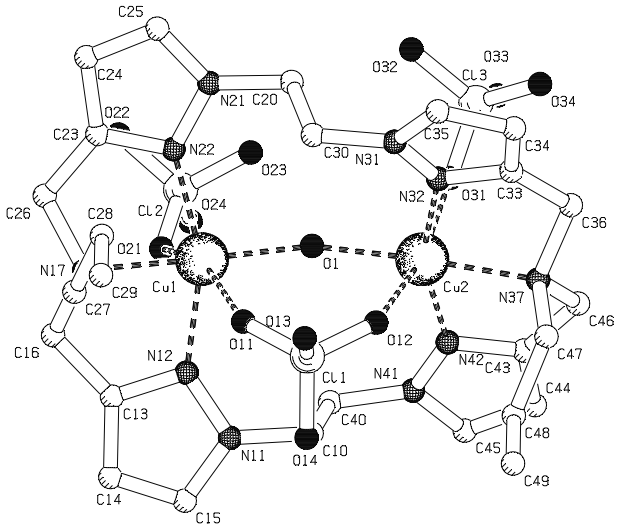

Figure 9.3. Platon[14] projection of the crystal structure of the complex $[Cu_2([22]pr4pz)(\mu\text{-}OH)(ClO_4)_3]$. Hydrogen atoms are omitted for clarity.

Furthermore, it is very appealing to study dioxygen binding by the dicopper(I) complex with [22]pr4pz, since it has been shown that the utilization of ligands with N_3 donor sets generally leads to the formation of $\mu\text{-}\eta^2\text{:}\eta^2$ peroxo-dicopper species, while trans-μ-1,2-peroxo-dicopper(II) complexes are usually obtained upon dioxygen binding to copper(I) complexes with N_4 ligands.[15] As $\mu\text{-}\eta^2\text{:}\eta^2$ peroxo-dicopper complexes are generally known to be able to perform the hydroxylation of the *o*-position of phenolic

substrates, it would be beneficial to study the reactivity of such species with respect to the modeling of the catalytic activities of both tyrosinase and catechol oxidase.

The oxidation of the mixed-valence $Cu^{II}Cu^{I}$-semiquinone species by dioxygen also deserves additional attention. As discussed in Chapter 8, this mechanism implies the formation of intermediate Cu^{II}-superoxide species, the spectroscopic characterization of which would undoubtedly be a highly interesting and challenging task.

The synthesis of copper(II) complexes with phenol-based ligands also has a significant potential interest. Despite certain shortcomings of these ligands, as outlined above, they are very easy to prepare, in contrast to the macrocyclic ligands. It is also relatively easy to synthesize structurally related ligands with only small variations, which would allow to study in detail the influence of certain factors (electron-donating or electron-withdrawing properties, steric hindrance etc.) on the catalytic behavior of the respective copper complexes. It is also very interesting to isolate dicopper(II) complexes, holding an additional exogenous hydroxide bridge between the metal centers, with such ligands. Unfortunately, the attempts to prepare such complexes with the ligands reported in Chapters 2-5 were futile; therefore new ligands can be designed for this purpose. One of such ligands, designed to provide both a coordination number asymmetry and the presence of non-coordinated sulfur atom in a close proximity of one of the copper centers, is depicted in Figure 9.4.

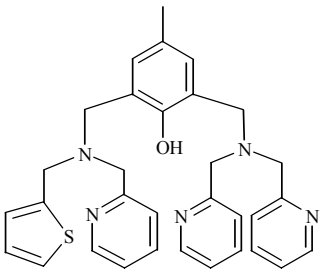

Figure 9.4. Schematic representation of the phenol-based ligand designed to mimic two peculiar features of catechol oxidase: the presence of non-coordinating sulfur atom in a close proximity of one of the copper(II) ions and a coordination number asymmetry of two metal ions.

9.6 References

(1) Fenton, D. E. *Inorg. Chem. Comm.* **2002**, *5*, 537-547.
(2) Torelli, S.; Belle, C.; Gautier-Luneau, I.; Pierre, J. L.; Saint-Aman, E.; Latour, J. M.; Le Pape, L.; Luneau, D. *Inorg. Chem.* **2000**, *39*, 3526-3536.
(3) Karlin, K. D.; Hayes, J. C.; Gultneh, Y.; Cruse, R. W.; McKown, J. W.; Hutchinson, J. P.; Zubieta, J. *J. Am. Chem. Soc.* **1984**, *106*, 2121-2128.
(4) Karlin, K. D.; Gultneh, Y.; Nicholson, T.; Zubieta, J. *Inorg. Chem.* **1985**, *24*, 3725-3727.
(5) Torelli, S.; Belle, C.; Hamman, S.; Pierre, J. L.; Saint-Aman, E. *Inorg. Chem.* **2002**, *41*, 3983-3989.
(6) Belle, C.; Beguin, C.; Gautier-Luneau, I.; Hamman, S.; Philouze, C.; Pierre, J. L.; Thomas, F.; Torelli, S.; Saint-Aman, E.; Bonin, M. *Inorg. Chem.* **2002**, 479-491.
(7) Merkel, M.; Möller, N.; Piacenza, M.; Grimme, S.; Rompel, A.; Krebs, B. *Chem. Eur. J.* **2005**, *11*, 1201-1209.
(8) Huisman, M.; Koval, I. A.; Gamez, P.; Reedijk, J. *Inorg. Chim. Acta* **2005**, in press.

(9) Adams, H.; Clunas, S.; Fenton, D. E. *Inorg. Chem. Comm.* **2001**, *4*, 667-670.
(10) Klabunde, T.; Eicken, C.; Sacchettini, J. C.; Krebs, B. *Nat. Struct. Biol.* **1998**, *5*, 1084-1090.
(11) Schuitema, A. M.; Aubel, P. G.; Koval, I. A.; Engelen, M.; Driessen, W. L.; Reedijk, J.; Lutz, M.; Spek, A. L. *Inorg. Chim. Acta* **2003**, *355*, 374-385.
(12) Schuitema, A. M. Ph.D. thesis, Leiden University, 2004.
(13) Selmeczi, K., Koval, I.A. *unpublished results*.
(14) Spek, A. L. *J. Appl. Cryst.* **2003**, *36*, 7-13.
(15) Mirica, L. M.; Ottenwaelder, X.; Stack, T. D. P. *Chem. Rev.* **2004**, *104*, 1013-1045.

Samenvatting

Dit proefschrift behandelt de synthese van koper(II)complexen die beschouwd kunnen worden als modelverbindingen van de active site van catecholoxidase en het mechanisme van de katalytische oxidatie van catechol door deze verbindingen. Catecholoxidase is een type-3 kopereiwit, aanwezig in planten en sommige schaaldieren, dat de oxidatie van verschillende catecholen (*o*-diphenolen) tot de respectievelijke chinonen katalyseert. De chinonen worden vervolgens gepolymeriseerd, wat resulteert in de vorming van het pigment melanine. Deze reactie is bedoeld om beschadigd weefsel tegen veschillende pathogene invloeden te beschermen. Type-3 kopereiwitten, die behalve catecholoxidase ook het eiwit hemocyanine en het enzym tyrosinase bevatten, zijn bekend door hun eigenschappen om moleculaire zuurstof te activeren en zijn toe te passen brengen onder gewone omstandigheden.[1] Vanwege hun mogelijke gebruik als oxidatiekatalysatoren in millieuvriendelijke industriéle processen is de synthese van modellen van deze eiwitten en onderzoek naar de mechanismen van hun katalytische activiteiten een zeer interessant onderwerp.

Hoofdstuk 1 is een algemene beschouwing van de modelverbindingen van catecholoxidase, die in de literatuur gerapporteerd zijn, en de verschillende manieren van diverse auteurs om het mechanisme van de katalytische reactie. Hoofdstuk 2 beschrijft de synthese van het dinucleaire fenolgebaseerde ligand Hpy3asym, dat ontworpen is om de asymmetrische omgeving van de twee koperionen in de active site van catecholoxidase na te bootsen, en het dinucleaire complex ervan $[Cu_2(py3asym)(H_2O)_{1.5}(NO_3)_2]NO_3$. Het ligand bevat een tridentaat en een didentaat arm verbonden met de 2 en 6 posities van de fenolring, om een asymmetrische coördinatienummering te verkrijgen voor de koper(II)complexen ervan. De ontwikkelde strategie voor de synthese van dit ligand kan ook succesvol worden toegepast voor het genereren van andere asymmetrische op fenol gebaseerde liganden.[2]

Hoofdstuk 3 rapporteert over de structuren en eigenschappen van zes nieuwe complexen van Cu^{II}, Co^{II} en Mn^{II} met het op fenol gebaseerde ligand Hpy2ald, dat een tridentaat pyridinebevattende arm heeft op de 2' positie en een formylgroep op de 6' positie van de fenolring. Vanwege de aanwezigheid van een zwak donerende formylgroep in het ligand bleek dat de structuren van de resulterende complexen sterk afhangen van de donoreigenschappen van de tegenionen. Kortom, het gebruik van metaalzouten met zwak-coördinerende anionen zoals perchloraat en tetrafluorboraat leiden tot de vorming van dinucleaire complexen met een metaal-ligandverhouding van 2:2, waarin twee metaalionen dubbel gebrugd zijn door zuurstofatomen van de gedeprotoneerde fenolgroepen van twee verschillende liganden. De aanwezigheid van sterkere donoren, zoals nitraat, bromide of chloride, voorkomt de coördinatie van de zwakker donerende formylgroep, wat resulteert in metaalcomplexen met vrij verschillende structuren, waarbij de formylgroep niet coördineert aan de metaalionen.

Hoofdstuk 4 beschrijft de bereiding van het symmetrische op fenol gebaseerde ligand Hpy2th2s, dat de functionele groepen pyridine en thiofeen bevat. Dit ligand was ontworpen om de aanwezigheid van de ongebruikelijke thioethergroep bij de active site van catecholoxidase na te bootsen, resulterend in de aanwezigheid van een niet-coördinerend zwafeltoom in de nabijheid van de metaalcentra. Twee koper(II)complexen met dit ligand zijn gemaakt en structureel, spectroscopisch en magnetisch gekarakteriseerd: $[Cu_2(py2th2s)Cl_3]$ en $[Cu_2(py2th2s)Br_3]$. In deze kopercomplexen zijn beide koperionen vijfvoudig gecoördineerd en dubbel gebrugd door het zuurstofatoom van de gedeprotoneerde fenolgroep en een halogeen anion. De complexen vertonen geen catecholaseactiviteit, waarschijnlijk vanwege de aanwezigheid van de sterk coördinerende halogeen anionen die bruggend binden tussen de metaalcentra. De onderzoeken naar de interactie van deze complexen met het modelsubstraat tetrachloorcatechol (TCC) wijzen erop dat de bruggende liganden inderdaad niet vervangen kunnen worden door het aanwezige catecholaat, hoewel in het geval van het chloridecomplex één van de apicale halogeen anionen gesubstituteerd wordt door TCC. Deze resultaten benadrukken het belang van de bruggende liganden voor de catecholaseactiviteit van de dikoper(II)complexen, omdat de mogelijkheid van deze liganden om vervangen te worden door het substraat een van de cruciale eisen zijn voor katalytische activiteit.

In hoofdstuk 5 wordt de synthese van het asymmetrische ligand Hpy2th1as (Figuur 9.1, d), met een thiofeenring aan een van de armen, gerapporteerd. Twee koper(II)complexen met dit ligand, $[Cu_2(H_2py2th1as)Cl_2](CuCl_4)_2$ en $[Cu_2(H_2py2th1as)Cl_2](ClO_4)_4 \cdot 6CH_3OH$, zijn geïsoleerd en structureel gekarakteriseerd. Ondanks de grote overeenkomsten tussen de twee verbindingen, het grootste verschil is een ander anion, verschillen de twee coördinatieverbindingen structureel significant. Dit duidt op de belangrijke invloed van het anion op de kristalstapeling.

Hoofdstukken 6–8 behandelen de structuren van Cu^{II} en Cu^{I} complexen met twee N-donor macrocyclische liganden [22]py4pz en [22]pr4pz, die respectievelijk twee N_4 en twee N_3 donor sets verschaffen voor de metaalcoördinatie, en beschrijven het mechanisme van de catecholoxidatie van de koper(II)complexen met deze liganden. Hoofdstuk 6 beschrijft tevens gedetailleerde paramagnetische ^1H NMR spectroscopie-studies van het hydroxygebrugde dikoper(II)complex met het macrocyclische ligand [22]py4pz.

Het mechanisme van de oxidatie van 3,5-di-*tert*-butylcatechool ($DTBCH_2$) door het hydroxygebrugde dikopercomplex $[Cu_2([22]py4pz)(\mu\text{-}OH)](ClO_4)_3 \cdot H_2O$ is onderzocht door het bestuderen van elke afzonderlijke stap in de katalytische cyclus. In de eerste fase leidt de stoichiometrische reactie van het complex en het substraat, in anaerobe condities, tot het loslaten van een equivalent chinon en de vorming van een dikoper(I)complex. Zuurstofbinding aan het laatste complex resulteert in de vorming van een trans-μ-1,2-peroxo-dicopper(II) verbinding dat een tweede catecholmolekuul

oxideert en weer het originele hydroxo-gebrugde dikoper(II)complex vormt. Deze laatste reactie bleek in twee successievelijke stappen te verlopen: Ten eerste leidt een protonverhuizing van het substraat naar de peroxo kern tot de vorming van een zeer reactief intermediair dat, op basis van het Raman, UV-Vis en EPR-spectroscopie, verondersteld wordt een hydroperoxo-dikoper(II) complex te zijn. Ten tweede wordt het gebonden catecholaat geoxideerd door het hydroperoxodeel, gecombineerd met de reductie van het peroxide tot water. Het algemene mechanisme van de katalytische reactie is erg vergelijkbaar met het mechanisme voor catecholoxidase, dat eerder is voorgesteld door Krebs,[3] hoewel de structuur van het peroxo-dikoper(II) intermediair deeltje zeer waarschijnlijk verschilt, omdat een μ-η^2:η^2 peroxo-dikoperintermediair is voorgesteld voor het natuurlijke enzym. Dit is ook het eerste voorbeeld van catecholoxidatie door trans-μ-1,2-peroxo-dikoper(II) deeltjes.

Hoofdstuk 8 behandelt het mechanisme van de catecholaseactiviteit van het dikoper(II)complex $[Cu_2([22]pr4pz)(CO_3)(H_2O)]^{2+}$ in methanol. Gedurende de eerste paar minuten van de katalytische reactie wordt de substraatoxidatie vergezeld door de vorming van waterstofperoxide, hoewel dat snel stopt. De anaerobe interactie van het complex met catechol duidt erop dat in plaats van een twee-elektronreductie van het dikoper(II)kation, dat leidt tot een chinon en een koper(I)complex, slechts één elektron is overgedragen in de stoichiometrische reactie, resulterend in de vorming van het $Cu^{II}Cu^{I}$-semichinondeeltje. De oxidatie van de laatste verbinding door dizuurstof leidt tot de vorming van een molaire equivalent chinon en een molaire equivalent waterstofperoxide. Kortom, het complex gedraagt zich in het begin als een mononucleair koper(II)deeltje, met slechts een koperion deelnemend in het redoxproces, terwijl de andere alleen een structurele rol speelt. Dit wordt waarschijnlijk veroorzaakt door de lange koper-koperafstand in het macrocyclische ligand, dat het simultaan binden van catechol op een didentaatgebrugde wijze aan beide koper(II)ionen onmogelijk maakt.

De vorming van waterstofperoxide stopt echter na een paar minuten, wat suggereert dat een ander mechanisme plaatsvindt in een latere fase van de katalytische reactie, zeer waarschijnlijk vergelijkbaar met het mechanisme dat is voorgesteld door Krebs en medewerkers voor het natuurlijke enzym.[3] Deze aanname wordt ook bevestigd door het onderdrukkende effect van het oxidatieproduct 3,5-di-*tert*-butylbenzochinon (DTBQ) op de katalytische reactie, wat erop duidt dat dit product zich niet gewoon ophoopt in het reactiemengsel, maar ook deelneemt in het katalytische proces. Omdat DTBQ snel kan reageren met het gereduceerde dikoper(I)complex, en dit reoxideert tot het gemengde valentie $Cu^{II}Cu^{I}$-semichinondeeltje, is dit een waarschijnlijke reden van het onderdrukkende gedrag. De vorming van dikoper(I)deeltjes kan op zijn beurt alleen worden verklaard door de mechanistische route die is voorgesteld door Krebs en zijn medewerkers.[3] Kortom, twee verschillende mechanistische routes worden in dit geval gerealiseerd, wat aantoont dat de catecholoxidatie door model koper(II)complexen een

ingewikkeld proces kan zijn. Deze bevindingen verklaren tevens het mechanisme van de vorming van waterstofperoxide als bijproduct van catecholoxidatie en wijzen erop dat de koper-koperafstand een substantiële rol speelt in het katalytische mechanisme: een korte afstand maakt het mogelijk dat catechol bindt op een didentaat bruggende wijze waardoor dit verder kan oxideren via het mechanisme vergelijkbaar met datgene dat is waargenomen voor $[Cu_2([22]py4pz)(\mu\text{-}OH)](ClO_4)_3 \cdot H_2O$, terwijl een lange afstand resulteert dat catechol alleen aan één van de koper(II)ion bindt, met de vroming van het semichinon en een daaropvolgende reductie tot waterstofperoxide.

Referenties

(1) Solomon, E. I.; Sundaram, U. M.; Machonkin, T. E. *Chem. Rev.* **1996**, *96*, 2563-2605.
(2) Huisman, M.; Koval, I. A.; Gamez, P.; Reedijk, J. *Inorg. Chim. Acta* **2005**, in press.
(3) Klabunde, T.; Eicken, C.; Sacchettini, J. C.; Krebs, B. *Nat. Struct. Biol.* **1998**, *5*, 1084-1090.

Короткий зміст

Ця дисертація присвячена синтезу комплексів міді(II), що є моделями активного центру мідьвмісного ензиму типу-3 катехолоксидази, та вивченню механізму каталітичного окислення субстрату (катехолу) цими сполуками. Даний тип протеїнів також включає в себе білок гемоціанін, що є переносчиком кисню у родинах молюсків та клишоногих, та ензим тирозиназу, що каталізує гідроксилювання орто-положення амінокислоти L-тирозину з утворенням сполуки, відомої під назвою L-DOPA, і її подальше окислення до відповідного бензохінону. Ця реакція є критичною стадією в процесі утворення пігменту меланіну, що відповідає за темне забарвлення шкіри та шерстяного покрову у ссавців, і за потемніння пошкоджених тканин при доступі кисню повітря у рослинах.

Катехолоксидаза найчастіше зустрічається в рослинах та деяких молюсках та каталізує окислення великої кількості орто-дифенолів (катехолів) у відповідні бензохінони, що аутополімеризуються з утворенням меланіну. Остання реакція призначена захищати пошкоджені тканини від патогенних впливів. Характерною рисою протеїнів типу-3 є таким чином їх здатність активувати і зв'язувати молекулярний кисень за звичайних умов та, у випадку катехолоксидази та тирозинази, застосовувати його для селективного окислення органічних субстратів. Через цю властивість вивчення структури цих природніх сполук та дослідження загальних принципів їх каталітичної дії є цікавою і важливою темою, завдяки можливому застосуванню синтетичних моделей цих протеїнів у якості промислових каталізаторів в органічних окислювальних процесах.

Кристалічна структура катехолоксидази у декількох формах (*мет*, відновленій (*деоксі*) та у комплексі з інгібітором тіосечовиною) була визначена методом рентгеноструктурного аналізу Кребсом та співробітниками декілька років тому.[1] Активний центр катехолоксидази містить два іони міді, кожний з яких оточений трьома амінокислотними залишками гістидину. У *мет* формі обидва іони міді мають ступінь окислення +2 і знаходяться на короткій відстані (2.9 Å) один від одного завдяки гідроксидному містку між ними. Наявність цього місткового ліганда є також причиною сильної антиферомагнітної взаємодії між двома іонами міді, що в результаті призводить до відсутності сигналу в спектрі електронного парамагнітного резонансу цього ензиму. Ця ознака є загалом характерною рисою спектральних властивостей протеїнів типу-3 в окисленому стані (Cu^{II}). У відновленій *деоксі* формі обидва іони міді мають ступінь окислення +1, та відстань між ними є значно довшою (4.4 Å).

Не зважаючи на те, що структура катехолоксидази відома, точний механізм дії цього ензиму є невизначеним до цього часу. Загальноприйнятий на даний момент механізм, запропонований Кребсом та співробітниками,[1] включає в себе

стехіометричне окислення одної молекули субстрату *мет* формою, та подальше зв'язування молекулярного кисню утвореною *деоксі* формою. Це призводить до утворення пероксо-мідного інтермедіату, що в свою чергу окислює другу молекулу субстрату на наступній стадії ензиматичного циклу з утворенням молекули води як побічного продукту. Проте декілька альтернативних механізмів, заснованих зокрема на вивченні механізмів каталітичної активності модельних сполук,[2,3] та на квантово-механічних обчисленнях,[4] було також запропоновано різними авторами. На даний момент значна увага дослідників привернута зокрема до таких аспектів каталітичного механізму, як спосіб координації субстрату до двоядерного активного центру (містковий, монодентатний, хелатний),[5-7] роль незвичного сірковуглецевого зв'язку у активному центрі ензиму[8] та структура проміжного мідно-кисневого аддукту.[9-11]

В першому розділі цієї дисертації представлений загальний огляд модельних сполук катехолоксидази, описаних в літературі, та розглянуті методи, які використовувалися різними авторами з метою вивчення механізму каталітичної реакції. Другий розділ розглядає синтез фенолвмісного ліганда Hpy3asym, що був синтезований з метою моделювання асиметричного оточення двох іонів міді у активному центрі ензиму, і структуру та властивості двоядерного комплексу $[Cu_2(py3asym)(H_2O)_{1.5}(NO_3)_{2.5}](NO_3)_{0.5}$. Ліганд Hpy3asym містить тридентатний та дводентатний замісники у відповідно 2 та 6 положеннях фенольного кільця і таким чином може потенційно забезпечити асиметрію координаційних чисел двох іонів міді у відповідних двоядерних комплексах. Розроблена стратегія синтезу цього ліганда може бути успішно застосована для синтезу споріднених фенолвмісних лігандів.[12]

Розділ 3 описує структури та власивості шести нових комлексів міді(II), кобальту(II) та мангану(II) з фенолвмісним лігандом Hpy2ald, що містить тридентатний піридинвмісний замісник та альдегідну групу в двох орто-положеннях по відношенню до фенольної групи ароматичного кільця. За рахунок присутності слабкого донора (альдегідної групи) в цьому ліганді структури вищезгаданих комплексів значною мірою залежать від донорних властивостей аніонів. Таким чином, використання солей металів з такими слабко координуючимися аніонами, як перхлорат і тетрафтороборат, призводить до утворення двоядерних комплексів зі співвідношенням металу до ліганду 2:2, у яких два іони металу з'єднані двома містковими кисневими атомами депротонованих фенольних груп двох лігандів. В той же час, присутність сильних донорів на зразок нітрату, броміду або хлориду перешкоджає координації слабкого донора альдегідної групи, що призводить до утворення комплексів з зовсім іншими структурними властивостями, у яких альдегідна група не координована до іону металу.

Розділ 4 описує синтез симетричного фенолвмісного ліганда Hpy2th2s, що містить піридинову та тіофенову функціональні групи. Цей ліганд був синтезований з метою моделювання незвичного сірковуглецевого зв'язку в активному центрі катехолоксидази, що призводить до присутності некоординованого атому сірки поблизу одного з двох атомів міді у активному центрі.[1] Два комплекси міді(II) з цим лігандом $[Cu_2(py2th2s)(\mu\text{-}Cl)Cl_2]$ і $[Cu_2(py2th2s)(\mu\text{-}Br)Br_2]$ були синтезовані та вивчені методом рентгеноструктурного аналізу. Обидва іони міді в цих комплексах пентакоординовані і зв'язані кисневим атомом депротонованої фенольної групи ліганда та іоном галогену. Обидва комплекси не проявляють каталітичних властивостей, що може бути викликано присутністю сильного донора (іону галогена) в якості місткового ліганда між двома іонами металу. Вивчення взаємодії комплексів з модельним субстратом тетрахлорокатехолом у розчині показали, що ці місткові ліганди дійсно не можуть бути заміщеними на субстрат, хоча у випадку хлоридного комплекса один з апікально розташованих іонів хлору заміщується на катехол. Ці результати підкреслюють важливість впливу місткових лігандів на каталітичні властивості двоядерних мідних комплексів, оскільки здатність місткового ліганда заміщуватися на субстрат є однією з необхідних умов для каталітичної активності.

Розділ 5 розглядає синтез асиметричного фенолвмісного ліганда Hpy2th1as, що містить тіофеновий замісник в 6 позиції ароматичного кільця. Два комлекси міді(II) з цим лігандом $[Cu_2(H2py2th1)Cl_2](CuCl_4)_2$ і $[Cu_2(H2py2th1)Cl_2](ClO_4)_4{\cdot}6CH_3OH$ було синтезовано і охарактеризовано методом монокристального рентгеноструктурного аналізу. Не зважаючи на велику подібність цих сполук, основною відмінністю яких є різні аніони, кристалічні упаковки цих комлексів суттєво різняться. Зокрема, нехарактерна π-стекінгова взаємодія між ароматичними кільцями тіофенових замісників та містковими іонами хлору спостерігається в першому з комплексів, в той час як в перхлоратному комплексі тіофенові групи є акцептором водневих зв'язків.

Розділи 6-8 розглядають синтез, структуру та фізико-хімічні властивості комплексів міді(II) і міді(I) з двома азотовмісними макроциклічними лігандами [22]py4pz і [22]pr4pz, що містять відповідно 8 і 6 донорних атомів азоту, і розглядають механізм каталітичного окислення катехолу комплексами міді(II) з цими лігандами. Розділ 6 також описує детальне вивчення парамагнітного двоядерного комплексу міді(II) з гідроксидним містковим лігандом $[Cu_2([22]py4pz)(\mu\text{-}OH)](ClO_4)_3{\cdot}H_2O$ методом протонного ядерного магнітного резонансу, та магнітні і спектральні властивості даної сполуки.

Механізм окислення 3,5-ди-*терт*-бутилкатехолу ($DTBCH_2$), який здебільшого застосовується як модель субстрату в лабораторних дослідженнях, двоядерним мідним комплексом $[Cu_2([22]py4pz)(\mu\text{-}OH)](ClO_4)_3{\cdot}H_2O$ було вивчено

шляхом окремого дослідження кожної стадії каталітичного циклу. На першій стадії стехіометрична реакція комплексу з субстратом, яка не потребує участі кисню, призводить до утворення одного молярного еквіваленту хінону та відновленого двоядерного комплексу міді(I). Цей комплекс було також охарактеризовано методом монокристального рентгеноструктурного аналізу. Реакція останньої сполуки з киснем призводить до утворення транс-μ-1,2-пероксо-мідного аддукту,[13] що окислює другу молекулу катехолу, утворюючи вихідний двоядерний комплекс міді(II) з гідроксидним містком між двома іонами міді. Ця реакція протікає у дві послідовні стадії: спочатку протон однієї з фенольних груп субстрату зв'язується з мідно-кисневим аддуктом, призводячи до утворення дуже активного проміжного комплексу, який на наступній стадії власне окислює субстрат. Вивчення цього проміжного продукту методами Раман, ультрафіолетової та видимої спектроскопії, та методом електронного парамагнітного резонансу дозволило припустити, що він є двоядерним гідропероксидним комплексом міді(II) складу $[Cu_2([22]py4pz)(OOH)]^{3+}$. Окислення молекули субстрату цим інтермедіатом призводить до відновлення гідропероксидної групи до води. Загальний механізм каталітичної реакції таким чином нагадує раніше запропонований Кребсом та співавторами[1] механізм каталітичного циклу катехолоксидази. Основною відмінністю між двома механізмами є структура пероксо-мідного аддукту: в той час як μ-η^2:η^2-пероксо-мідний комплекс був запропонований для ензиму,[1] в даному випадку реакція молекулярного кисню з відновленим комплексом міді(I) призводить до утворення транс-μ-1,2-пероксо-мідного інтермедіату. Даний випадок також є першим прикладом окислення катехолу транс-μ-1,2-пероксо-мідним комплексом.

Розділ 8 розглядає механізм каталітичного окислення катехолу комплексом міді(II) $[Cu_2([22]pr4pz)(CO_3)(H_2O)]_2(CF_3SO_3)_4{\cdot}2CH_3CN{\cdot}4H_2O$ у метанолі. Цей тетраядерний кластер за високої концентрації (>> 14 ммоль/л) є стабільним у розчині, проте дисоціює з утворенням двох двоядерних фрагментів при розведенні. Два іони міді в макроциклічному кільці зв'язані між собою карбонатним містком і розташовані на відстані 4.5427(18) Å один від одного.

Протягом перших хвилин каталітичної реакції окислення субстрату супроводжується утворенням пероксиду водню як побічного продукту, проте зростання концентрації цієї сполуки швидко припиняється. Слід відзначити, що відновлення молекулярного кисню до пероксиду водню у каталітичній реакції було описано в декількох випадках,[2,3,14,15] проте причина цього явища є досі невизначеною. Вивчення стехіометричної взаємодії комплексу з субстратом в анаеробних умовах показало, що на відміну від двоелектронного відновлення двоядерного комплексу міді(II) до відповідного комплексу міді(I), згідно механізму, запропонованого для природнього ензиму,[1] лише один з двох іонів міді(II) у комплексі відновлюється до міді(I). Це призводить до утворення

семіхінонного радикалу та змішановалентного двоядерного комплексу міді(II/I), що було підтверджено методами ЕПР та ультрафіолетової та видимої спектроскопії у розчині. Оскільки лише один з іонів міді зазнає відновлення, подальше окислення реакційної суміші киснем призводить до утворення проміжного супероксидно-мідного аддукту Cu^{II}-$O_2^{\cdot-}$,[13] що окислює семіхінонний радикал з утворенням одного молярного еквіваленту хінону та одного молярного еквіваленту пероксиду водню. Таким чином, не зважаючи на двоядерну структуру комплексу, лише один з двох іонів міді приймає участь у окислювально-відновлюваному процесі, в той час як інший іон відіграє лише структурну роль. Причиною такої незвичної поведінки може бути велика відстань між двома іонами міді (4.5427(18) Å) у комплексі, що перешкоджає одночасній координації субстрату до обох іонів металу і призводить натомість до його звьязування лише з одним з них. В свою чергу, це призводить до відновлення лише одного з двох іонів міді двоядерного каталітичного центру.

Проте, оскільки концентрація пероксиду водню перестає збільшуватися вже через декілька хвилин, можна припустити, що на пізніших стадіях каталітична реакція протікає за іншим механізмом. Ця гіпотеза також підтверджується інгібуючим ефектом продукту реакції, 3,5-ди-*терт*-бутилбензохінону (DTBQ), на каталітичну реакцію, що означає, що дана сполука не просто акумулюється в реакційній суміші, а ще і приймає участь у каталітичному процесі. Дослідження показали, що DTBQ здатний швидко реагувати з двоядерним комплексом міді(I), окислюючи його до змішановалентного комплексу міді(II/I) та семіхінону . Оскільки двоядерний комплекс міді(I) є єдиною сполукою, здатною реагувати з DTBQ, цей факт може служити поясненням інгібуючого впливу хінону на каталітичний процес. В свою чергу, присутність у реакційній суміші двоядерного комплексу міді(I) можна пояснити лише за припущення, що реакція протікає за механізмом, подібним до запропонованого Кребсом та ін.[1] Таким чином, можна зробити висновок, що в даному випадку реакція протікає за двома різними механізмами: 1) через утворення семіхінону і змішановалентного комплексу і утворенням одної молекули продукту за каталітичний цикл, який супроводжується утворенням пероксиду водню як побічного продукту, і 2) через двоелектронне відновлення двоядерного комплексу міді(II) до відповідного комплексу міді(I), із подальшим окисленням катехолу за механізмом, подібним до того, що спостерігався для комплексу $[Cu_2([22]py4pz)(\mu\text{-}OH)](ClO_4)_3\cdot H_2O$. Причиною цього явища може бути зміна координаційного оточення іонів міді, зокрема, дисоціація карбонатного містка, під час каталітичного циклу, що в свою чергу призводить до зменшення відстані між ними. Попередні дослідження двоядерних комплексів міді зі спорідненими макроциклічними лігандами показали, що ліганди цього типу є дуже гнучкими, і відстань між двома іонами металу в їх комплексах може

змінюватися в досить широких межах, зокрема в залежності від наявності між ними місткового ліганда.[16] Зменшення міжіонної відстані в свою чергу робить можливою одночасну координацію субстрату до обох металічних центрів, і відповідно до зміни механізму каталітичної реакції..

Ці результати свідчать, що механізм окислення субстрату модельними сполуками катехолоксидази є досить складним. Очевидно, важливий вплив на механізм каталітичної реакції справляє відстань між двома іонами міді у двоядерному комплексі. Мала відстань сприяє зв'язуванню субстрату з обома іонами міді у вигляді місткового дводентатного ліганда, що в свою чергу дозволяє одночасне відновлення обох іонів міді до ступеню окислення +1. З іншого боку, велика відстань між двома іонами дозволяє зв'язування субстрату лише з одним із двох іонів міді. Подальша каталітична реакція таким чином протікає через утворення семіхіноннного радикалу. Ці результати дозволяють також зробити висновок, що пероксид водню у якості побічного продукту утворюється, коли велика відстань між двома іонами міді у двоядерному комплексі перешкоджає одночасній координації субстрату до обох іонів.

Слід також зазначити, що на даний момент у літературі відсутні дані про можливість утворення пероксиду водню або семіхінону у випадку катехолоксидази, проте деякі автори відзначили утворення обох цих сполук під час каталітичного окислення сполуки L-DOPA спорідненим ензимом тирозиназою в гемолімфі деяких молюсків.[17,18] Таким чином, подальші дослідження мають надати відповідь на питання про можливість протікання каталітичної реакції за обома механізмами, описаними для модельних сполук, у випадку природнього ензиму.

Література

(1) Klabunde, T.; Eicken, C.; Sacchettini, J. C.; Krebs, B. *Nat. Struct. Biol.* **1998**, *5*, 1084-1090.
(2) Kodera, M.; Kawata, T.; Kano, K.; Tachi, Y.; Itoh, S.; Kojo, S. *Bull. Chem. Soc. Jpn.* **2003**, *76*, 1957-1964.
(3) Kaizer, J.; Pap, J.; Speier, G.; Parkanyi, L.; Korecz, L.; Rockenbauer, A. *J. Inorg. Biochem.* **2002**, *91*, 190-198.
(4) Siegbahn, P. E. M. *J. Biol. Inorg. Chem.* **2004**, *9*, 577-590.
(5) Plenge, T.; Dillinger, R.; Santagostini, L.; Casella, L.; Tuczek, F. *Z. Anorg. Allg. Chem.* **2003**, *629*, 2258-2265.
(6) Börzel, H.; Comba, P.; Pritzkow, H. *Chem. Commun.* **2001**, 97-98.
(7) Torelli, S.; Belle, C.; Hamman, S.; Pierre, J. L.; Saint-Aman, E. *Inorg. Chem.* **2002**, *41*, 3983-3989.
(8) Merkel, M.; Möller, N.; Piacenza, M.; Grimme, S.; Rompel, A.; Krebs, B. *Chem. Eur. J.* **2005**, *11*, 1201-1209.
(9) Berreau, L. M.; Mahapatra, S.; Halfen, J. A.; Houser, R. P.; Young, V. G.; Tolman, W. B. *Angew. Chem. Int. Ed. Engl.* **1999**, *38*, 207-210.
(10) Mahadevan, V.; Hou, Z. G.; Cole, A. P.; Root, D. E.; Lal, T. K.; Solomon, E. I.; Stack, T. D. P. *J. Am. Chem. Soc.* **1997**, *119*, 11996-11997.
(11) Santagostini, L.; Gulotti, M.; Monzani, E.; Casella, L.; Dillinger, R.; Tuczek, F. *Chem. Eur. J.* **2000**, *6*, 519-522.
(12) Huisman, M.; Koval, I. A.; Gamez, P.; Reedijk, J. *Inorg. Chim. Acta* **2005**, in press.

(13) Mirica, L. M.; Ottenwaelder, X.; Stack, T. D. P. *Chem. Rev.* **2004**, *104*, 1013-1045.
(14) Ackermann, J.; Meyer, F.; Kaifer, E.; Pritzkow, H. *Chem. Eur. J.* **2002**, *8*, 247-258.
(15) Selmeczi, K.; Reglier, M.; Giorgi, M.; Speier, G. *Coord. Chem. Rev.* **2003**, *245*, 191-201.
(16) Schuitema, A. M.; Aubel, P. G.; Koval, I. A.; Engelen, M.; Driessen, W. L.; Reedijk, J.; Lutz, M.; Spek, A. L. *Inorg. Chim. Acta* **2003**, *355*, 374-385.
(17) Komarov, D. A.; Slepneva, I. A.; Glupov, V. V.; Khramtsov, V. V. *Free Radic. Res.* **2005**, *39*, 853-858.
(18) Slepneva, I. A.; Komarov, D. A.; Glupov, V. V.; Serebrov, V. V.; Khramtsov, V. V. *Biochem. Biophys. Res. Commun.* **2003**, *300*, 188-191.

List of publications

1) Koval, I. A., Yatsimirsky, K. B., Trofimenko, S., Pavlishchuk, V. V., "*Directed synthesis, spectral and magnetochemical characteristics of the new multispin (S=7/2, T = 292 K) trinuclear complex"* Teoreticheskaya i Eksperimentalnaya Khimiya, **1998**, 34, 351-354 (in Russian)

2) Pavlishchuk, V. V., Koval, I. A., Goreshnik, E., Addison, A. W., van Albada, G. A., Reedijk, J., *"The first example of a true "Turnbull's Blue" family compound with trapped iron oxidation states"* Eur. J. Inorg. Chem., **2001**, 297-301

3) Schuitema, A. M., Engelen, M., Koval, I. A., Gorter, S., Driessen, W. L., Reedijk, J., *"New didentate bispyrazole ligands forming uncommon eight-ring chelates with divalent copper, zinc and cobalt"* Inorg. Chim. Acta, **2001**, 324, 57-64

4) Koval, I. A., Schuitema, A. M., Driessen, W. L., Reedijk, J., *"Unprecedented copper(II)-assisted acetal formation of a formyl-substituted bispyrazole. The X-ray structures of copper[1,2-bis(3 '-dimethoxymethylpyrazol-1 '-yl)ethane] dichloride and dibromide"* J. Chem. Soc., Dalton Trans., **2001**, 3663-3667

5) Koval, I. A., Gamez, P., Roubeau, O., Driessen, W. L., Lutz, M., Spek, A. L., Reedijk, J., *"Century-known copper salt Cu(OAc)(OMe) proven to be a unique magnetic lattice composed of tetranuclear copper(II) species with a rare binding mode of the acetate anion"* Inorg. Chem., **2003**, 42, 868-872

6) Koval, I. A., Pursche, D., Stassen, A. F., Gamez, P., Krebs, B., Reedijk, J., **"***The dicopper(II) complex of the novel asymmetric dinucleating ligand Hpy3asym as a structural model of catechol oxidase"* Eur. J. Inorg. Chem., **2003**, 1669-1674

7) Schuitema, A. M., Aubel, P. G., Koval, I. A., Engelen, M., Driessen, W. L., Reedijk, J., Lutz, M., Spek, A. L., *"Dinuclear copper(II) complexes of four new pyrazole-containing macrocyclic ligands are active catalysts in the oxidative coupling of 2,6-dimethylphenol"* Inorg. Chim. Acta, **2003,** 355, 374-385

8) Koval, I. A., Huisman, M., Stassen, A. F., Gamez, P., Lutz, M., Spek, A. L., Pursche, D., Krebs, B., Reedijk, J., *"New dinuclear Co(II) and Mn(II) complexes of the phenol-based compartmental ligand containing formyl and amine functions: structural, spectroscopic and magnetic properties"* Inorg. Chim. Acta, **2004**, 357, 294-300

9) Koval, I. A., Huisman, M., Stassen, A. F., Gamez, P., Lutz, M., Spek, A. L., Reedijk, J., *"Unusual Cu^{II} and Mn^{II} complexes of phenol-based ligands containing amine, pyridine and formyl functions: Unexpected structural features and solution studies"* Eur. J. Inorg. Chem., **2004**, 591-600

10) Song, Y. F., Koval, I. A., Gamez, P., van Albada, G. A., Mutikainen, I., Turpeinen, U., Reedijk, J., *"Solution studies and structure of a dinuclear-based double-stranded helicate of [Cu-2(p-xysal)(2)] (H-2-p-xysal = bis (hydroxylbenzyl)diaminoxylene)"* Polyhedron, **2004**, 1769-1775

11) Gamez, P., Koval, I. A., Reedijk, J., *"Bio-mimicking galactose oxidase and hemocyanin, two dioxygen-processing copper protein"* Dalton Trans., **2004**, 4079-4088

12) Song, Y. F., Massera, C., Quesada, M., Koval, I. A., Gamez, P., Lanfredi, A. M. M., Reedijk, J., *"A new trinuclear linear copper(II) complex: Unusual crystal structure with semi-coordinated thiophene moieties and weak antiferromagnetic coupling through the bridging imidazolate rings"* Eur. J. Inorg. Chem., **2004**, 4566-4571

13) Koval, I. A., Huisman, M., Stassen, A. F., Gamez, P., Roubeau, O., Belle, C., Pierre, J.-L., Saint-Aman, E., Luken, M., Krebs, B., Lutz, M., Spek, A.L., Reedijk, J., *"Dinuclear Cu^{II} complexes with a new phenol-based ligand bearing pyridine and thiophene substituents: Synthesis, characterization and interaction with catechol substrates"*
Eur. J. Inorg. Chem., **2004**, 4036-4046

14) Kozlevčar, B., Golobic, A., Gamez, P., Koval, I. A., Driessen, W. L., Reedijk, J., *"A tridentate bis(pyrazolyl) ligand binds to Cu(II), without using the pyrazole group: a very unusual coordination mode of the ligand Hbdmpb, 1,3-bis(3,5-dimethylpyrazol-1-yl)-2-butanoic acid"* Inorg. Chim. Acta, **2005**, 358, 1135-1140

15) Koval, I. A, van der Schilden, K., Schuitema, A. M., Gamez, P., Belle, C., Pierre, J.-L., Luken, M., Krebs, B., Roubeau, O., Reedijk, J., *"Proton NMR spectroscopy and magnetic properties of a solution-stable dicopper(II) complex bearing a single μ-hydroxo bridge"*
Inorg. Chem., **2005**, 44, 4372-4382

16) Tanase, S., Koval, I. A., Bouwman, E., de Gelder, R., Reedijk, J., *"Ligand conformation enforces trigonal bipyramidal coordination geometry in a new dinuclear bis(pyrazolato)-bridged copper(II) complex: synthesis, crystal structure, and properties of $[Cu_2(Npy_2pz)]_2 \cdot 2CH_3CN$"*
Inorg. Chem., **2005**, 44, 7860-7865

17) Huisman, M., Koval, I. A., Gamez, P., Reedijk, J., "*Thiophene-containing dinucleating ligands for the copper-catalyzed oxidative coupling of 2,6-dimethylphenol"*
Inorg. Chim. Acta, **2005**, in press

18) Koval, I. A., Belle, C., Selmeczi, K., Philouze, C., Saint-Aman, E., Schuitema, A. M., Gamez, P., Pierre, J.-L., Reedijk, J., "*Catecholase activity of a μ-hydroxodicopper(II) macrocyclic complex: structures, intermediates and reaction mechanism"*
J. Biol. Inorg. Chem., **2005**, 10, 739-750

19) Koval, I. A., Sgobba, M., Huisman, M., Lüken, M., Saint-Aman, E., Gamez, P., Krebs, B., Reedijk, J., *"A remarkable anion effect on the crystal packing of two analogous copper complexes from a thiophene-containing phenol-based ligand"*
New J. Chem., submitted

20) Koval, I. A., Selmeczi, K., Belle, C., Philouze, C., Saint-Aman, E., Schuitema, A. M., van Vliet, M., Gamez, P., Roubeau, O., Lüken, M., Krebs, B., Lutz, M., Spek, A. L., Pierre, J.-L., Reedijk, J. "*Catecholase activity of a copper(II) complex with a macrocyclic ligand: unraveling catalytic mechanisms"*
Chem. Eur. J., submitted

21) Koval, I. A., Gamez, P., Belle, C., Selmeczi, K., Reedijk, J., "*Synthetic models of the active site of catechol oxidase: mechanistic studies"*
Chem. Soc. Rev., submitted

Curriculum Vitae

The author of this thesis was born in Kyiv, Ukraine, on 24th October 1979. In 1996, she has graduated from the Technical Lyceum at Kyiv National Technical University, with a major in chemistry and biology. The same year she enrolled as a student at the Chemistry Department at Kyiv National Taras Shevchenko University, from which she obtained her B.Sc. degree (cum laude) in 2000. Her B.Sc. thesis titled "Directed synthesis of ferrocyanide(III)-based polynuclear 3d metal complexes as molecular magnets" was written under supervision of Dr. Vitaly V. Pavlishchuk at the Institute of Physical Chemistry of the National Academy of Science of Ukraine in Kyiv. In June 2000, she has started her M.Sc. studies at Leiden University, The Netherlands, and received her M.Sc. diploma in August 2001, with a M.Sc. thesis "Copper(II) complexes with pyrazole-containing ligands as synthetic models for dinuclear copper-containing proteins" completed under supervision of Dr. Anna M. Schuitema, Dr. Willem L. Driessen and Prof. Dr. Jan Reedijk.

In February 2002, the author has started to work on the Ph.D. thesis in the group of Coordination and Bioinogranic Chemistry (CBAC) at Leiden University, under supervision of Prof. Dr. Jan Reedijk and Dr. Patrick Gamez. In the course of her research, collaboration between CBAC and LEDSS and LEOPR groups at Université J. Fourier, Grenoble, France was initiated. Consequently, the author has visited Université J. Fourier four times in the period of 2003-2005. In 2004, this joined research project has been awarded a collaborative travel grant from the French Ministry of Research and Foreign Affairs (EGIDE) and NWO (Van Gogh Program), allowing visits and exchanges between Leiden and Grenoble.

The results reported in this thesis were presented at various international conferences, such as the 35th and 36th International Conferences on Coordination Chemistry (Heidelberg, Germany, 2002, and Mérida, Mexico, 2004, poster presentations), the 12th International Conference on Bioinorganic Chemistry (Ann Arbor, Michigan, USA, 2005, poster presentation), the 2nd, 4th and 5th Netherlands' Catalysis and Chemistry conferences (Noordwijkerhout, The Netherlands, 2002, 2004 and 2005, poster and oral presentations), HRSMC meeting (Leiden, 2003, oral presentation), NRSC workshop (Amsterdam, The Netherlands, 2004, oral presentation), and a Combined workshop of NIOK and NRCS-Catalysis (Utrecht, The Netherlands, 2005, oral presentation).

Acknowledgement

At the end of this thesis, it is time to thank many people who have contributed greatly to its completion.

First of all I would like to name three people whose expertise, advice and encouragement had a tremendous influence on my work. These are Dr. Catherine Belle, Dr. Katalin Selmeczi and Prof. Dr. Eric Saint-Aman from Université J. Fourier of Grenoble, France. Dear Catherine, Eric and Katalin, I will always treasure the memories of our collaboration and of my visits to Grenoble. Only your attempts to teach me French were less successful. I will miss you a lot!

Next I would like to mention my students. Mieke Huisman was the first of them, and she definitely had "golden fingers" in crystallizations! The number of crystal structures she managed to obtain during her 10 months research project led to five articles and four chapters of this thesis. Mieke, I am still amazed by all you have done! My next two students, Marcel van Vliet and Maila Sgobba, stayed for a shorter time, but they have also contributed to two chapters of this thesis and both got one article based on the results of their work. My last student, Hilda Akhideno, has joined our group when I was already at the end of my Ph.D. studies, but the project she has started can undoubtedly lead to some nice results in the future.

I am also very grateful to Annemarieke Schuitema-Kamans, who was my supervisor during my M.Sc. research project at CBAC. Annemarieke has taught me a great deal of organic synthesis, and her work with macrocyclic ligands has formed a solid basis, on which I could build my own research.

The crystallographers Dr. Martin Lutz of Utrecht University, Dr. Christian Philouze of Université J. Fourier, Grenoble, and Daniel Pursche and Matthias Lüken of Westfälische Wilhelms-Universität Münster have solved the crystal structures, reported in this thesis. My ex-colleagues Arno Stassen and Olivier Roubeau provided a lot of help with the magnetic susceptibility studies. Gé van Albada's advice was of a great value when performing EPR experiments, and Lies Bouwman has taught me the simulation of EPR spectra. 13 K EPR measurements in Grenoble were performed with a kind assistance of Dr. Stéphane Ménage

Of course, I cannot forget to thank Jos van Brussel for elemental analysis measurements, and John van Dijk and Jopie Erkelens-Duijndam for ESI-MS studies! Fons Lefeber and Cees Erkelens were extremely helpful, patiently assisting with paramagnetic NMR studies. The secretaries Yvonne Snellenberg, Ingrid Bekooy and Marianne Kooistra were very effective in arranging all administrative work.

I am also very grateful to my (ex-)colleagues from CBAC, the joined efforts with whom have led to several publications: Karlijn van der Schilden for her input in the paramagnetic NMR studies, Stefania Grecea, Yufei Song and Bojan Kozlevčar. I would also like to mention other members of CBAC with whom I had a pleasure to work for the past years, spend time together at the conferences, or play volleyball at Fridays after a hard working week: Patrick, Meenal, Paul, Manu, Elena, Eva, Christophé, Patricia, Ferry, Joris, and many others.

There is also one person who deserves a great credit for all he did: my first supervisor from Ukraine, Dr. Vitaly V. Pavlishchuk. He is the one who introduced me to the world of scientific research, and influenced greatly my choice of profession.

It is a very special tradition that during your Ph.D. defense, two people stand next to your side: your moral support and reassurance. So I would like to thank two very dear friends, one from Ukraine and one from Holland, Anya Kalayda and Kristel Flinzner, for being my paranymphs.

Finally, I would like to thank people closest to me: my parents, my family in-law, my friends in both Ukraine and Holland, and my husband Peter for their love and support during these years.

Ira